Closing the *In Vitro* / *In Vivo* Gap in Tuberculosis Drug Discovery

BY

GEPING CAI

M.S., Fudan University, Shanghai, China, 2008
B.S., Fudan University, Shanghai, China, 2005

DISSERTATION

Submitted as partial fulfillment of the requirements for the degree of
Doctor of Philosophy in Pharmacognosy
in the Graduate College of the
University of Illinois at Chicago, 2014

CHICAGO, ILLINOIS

DEFENSE COMMITTEE:
Dr. Scott G. Franzblau, Advisor
Dr. Guido F. Pauli, Chair and Advisor
Dr. Birgit U. Jaki
Dr. Sanghyun Cho
Dr. David S. Seigler, University of Illinois at Urbana-Champaign

DEDICATION

To my parents, Huichun Ge and Xilan Cai.

Without their support, this thesis would never have been accomplished.

ACKNOWLEDGEMENTS

The dissertation was only made possible with the help, support and advice from many individuals from ITR and our department. I am indebted to all those who devoted their time and efforts to make my dissertation come to fruition.

First of all, I would like to express my sincerest gratitude to my advisor, Dr. Scott G. Franzblau for his guidance and cares throughout my research. His extensive knowledge, encouraging mentorship, and selfless support helped me harvest invaluable treasures in the "gold mining" of science. In addition, I also would like to give my profound thankfulness to my co-advisor, Dr. Guido F. Pauli for his academic instructions and impartation. His passionate and meticulous attitude toward science, as well as his careful supervision over my studies and research made him an influential paradigm for me to learn from in my future work.

For all the work involved within ITR, I would like to warmly thank Dr. Sanghyun Cho for his extensive guidance in my benchwork including teaching me all the important phenotypic screening techniques and TB-related skills in the Biosafety level-3 setting. I am grateful to Dr. Yuehong Wang for her care and devotion to my research, especially the animal-related work. My thesis would never have been possible without her selfless help. My thanks also go to Dr. Birgit U. Jaki for her guidance and insight in many of my natural product projects, e.g. TBSA determination, TLC-bioautography, as well my lab rotation project on essential oils. I am also grateful to Dr. Farahnaz Movahedzahed for her valuble advice and effort on my molecular biology work. I am thankful to Ms. Baojie Wan for her instructions on my basic lab techniques, and support with routine material ordering. Her work has provided a reality to all my

research. I would like to thank Ms. Lorna Haubrich and Ms. Valsamma Abraham for organizing the institute and guaranteeing that projects run properly. I also would like to thank Dr. Larry L. Klein for sharing his humor, wisdom and experiences in research and science. I thank Ms. Valentina Petukova for sharing her knowledge in synthetic chemistry and her timely help locating the reagents and solvents. I am thankful to senior graduates of ITR, Dr. Yang Song for being a caring elderly sister who offered me precious opinions on my research, and Dr. Changhwa Hwang for being my big brother by supporting me with my assays and sharing experiences in so many different aspects of my projects. My thanks also go to other ITR members, Dr. Hiten Gutka for sharing those interesting stories and opinions with me, Dr. Yongmao Sun for guiding me in the ITR labs during my rotation, Ms. Nan Zhang and Ms. Wei Gao for being good friends and labmates sharing our experiences in ITR from the very beginning, Ms. Hahn Vuong for her collaboration with my high throughput screening efforts and lab logistics, Mr. Jeffrey Anderson for his efforts in providing help with PCR, as well as Mr. David D. Anderson, Surafel Mulugeta, Trinidad Gonzalez, Maxwell Rutter, Hyun-sup Lee, and Ms. Marcelle Hon, Laurina Luo and Noelle Kwan for their friendship.

For my work related to natural product chemistry, I thank Dr. José G. Napolitano for his persistent efforts in obtaining NMR data for my samples and his informative knowledge on structural elucidation, which made possible make great progress on my projects. I also thank Dr. James B. McAlpine for his wisdom, knowledge, and valuable perspectives on my high throughput screening project and his warm hospitality for inviting us to his well-prepared picnics. I also appreciate the advisorship from Dr. J. Brent Friesen in a variety of occasions during my research on chemistry, especially GC-MS and countercurrent chromatography. I

would like to thank Dr. Brian T. Murphy for guiding me through the theories and ideology in actinomycete extract screening and his kind suggestions on structural elucidation. I also thank Dr. Shao-nong Chen for all his timely help and maintenance on lab hardwares and his heartfelt concerns on the progresses of my researches. I also thank Dr. María Florencia Rodríguez-Brasco for her collaboration with my anti-*M. tb* active principle isolation project and her palpable friendliness. I am thankful to Dr. David C. Lankin for obtaining the NMR data and supporting my spectroscopic work. My thanks also go to Dr. Feng Qiu for being an unforgettable friend, roommate and labmate during these years, and Dr. Shi-hui Dong for his collaboration and his friendship. I also thank all other members from Dr. Pauli's lab, such as Dr. Charlotte Simmler, Dr. Edyta Grzelak, Dr. Joo-won Nam, Mr. Rene F. Ramos Alvarenga, Yang Liu, Ms. Rasika Phansalka, Mary Choules, for their friendship and collaboration. I give my special thanks to Dr. Taichi Inui for his suggestions and help with formatting of this dissertation.

I am grateful to Dr. Jimmy Orjala and Dr. George Chlipala for their guidance and orientation through the researches at UIC during my first lab rotation. I thank Dr. Aleksej Krunic for his maintenance of the instruments in the shared labs of the department. I especially want to thank Dr. David Seigler from University of Illinois at Urbana Champaigne for his timely reviews and edits to my dissertation upon emergent changes to the committee.

I would like to give my thanks to Ms. Cece Chau and Dr. Stefan Green at the DNA Services Facility (DNAS) of UIC Research Resources Center (RRC) for guiding me through the usage of the real-time PCR instruments.

Finally, I am indebted to the Department of Medicinal Chemistry and Pharmacognosy for providing the teaching assistantship and tuition waiver for the first three years of my studies,

and the College of Pharmacy for offering me the W.E. van Doren and Myron Goldsmith Scholarships. My gratefulness also goes to Ms. Arletta Harris for her persistent efforts in providing me with the most important and timely help during my researches and studies. The work presented in this dissertation was made possible by the grants from the Pott's Foundation.

-GC

TABLE OF CONTENTS

1. Introduction 1
1.1 Tuberculosis 1
1.1.1 Facts about pandemic tuberculosis 1
1.1.2 TB etiology 2
1.1.3 TB diagnosis and quantification 4
1.2 TB chemotherapy 6
1.2.1 Anti-TB drugs 6
1.2.2 Antimycobacterial natural products 9
1.3 Statement of problem and specific aims 10
2. Quantification of TBSA with GC-MS/MS 14
2.1 Introduction 14
2.2 Materials and methods 16
2.2.1 Sample preparation and TBSA analysis by GC-MS/MS 16
2.2.2 TBSA correlation with CFU *in vitro* 17
2.2.3 Drug inhibition of *M. tb* in axenic medium 18
2.2.4 Growth of *M. tb* Erdman in macrophages 18
2.2.5 Drug inhibition of *M. tb* in macrophages 19
2.2.6 Growth inhibition of *M. tb* in gamma-interferon knock-out (GKO) mice treated with anti-*M. tb* drugs 20
2.3 Results 20
2.3.1 Correlation of TBSA with CFU *in vitro* 20
2.3.2 Dose-dependent inhibition of INH and RMP on *M. tb* growth in bacterial broth 22
2.3.3 Growth and drug-inhibition of *M. tb* in macrophage culture 23
2.3.4 Inhibition of *M. tb* growth in the lungs of gamma-interferon gene knock-out (GKO) mice by anti-*M. tb* drugs 25
2.4 Discussion 28
3. Quantification of TB-specific RNAs with real-time PCR 32
3.1 Introduction 32
3.2 Materials and methods 33
3.2.1 *In vitro* correlation of RNA level with CFU 33

TABLE OF CONTENTS (continued)

3.2.2 *In vitro M. tb* growth in axenic medium 34
3.2.3 Correlation of RNA level with CFU in the presence of mouse lung tissue..... 34
3.2.4 Acute and chronic growth of *M. tb* in infected BALB/c mice 35
3.2.5 Growth inhibition of *M. tb* in gamma-interferon gene knock-out (GKO) and BALB/c mice treated with anti-*M. tb* drugs..... 36
3.2.6 Total RNA extraction..... 37
3.2.7 Reverse transcription and real-time PCR..... 38
3.2.8 Standard curve establishment..... 40
3.2.9 Statistical analysis 40
3.3 Results..... 41
3.3.1 Correlation of RNA copies with CFU *in vitro*..... 41
3.3.2 Correlation of CFU and RNA levels during *in vitro* growth 42
3.3.3 Correlation of RNA copies with CFU in lung tissue-spiked bacterial culture..... 43
3.3.4 Acute and chronic mouse models of *M. tb* infection 44
3.3.5 Inhibition of *M. tb* growth in GKO and BALB/c mice treated with anti-*M. tb* drugs47
3.4 Discussion..... 55
4. Phenotypic screening (Methodology)..... 62
4.1 Percentage inhibition..... 64
4.1.1 Assay plate configuration 64
4.1.2 Z' factor calculation..... 66
4.2 Minimum inhibitory concentrations (MICs) 66
4.2.1 Normoxic condition – microplate Alama Blue assay (MABA)..... 66
4.2.2 Hypoxic condition – low oxygen recovery assay (LORA) 68
4.2.3 Protein MIC shift assay 69
4.2.4 Mono-drug resistant strains and clinical isolates 69
4.2.5 Spectrum of activity (SA)..... 70
4.3 Minimum bactericidal concentration (MBC) 71
4.4 Cytotoxicity test 71
4.5 Selectivity Index (SI)..... 72
4.6 Bioassay-guided fractionation (BGF) 73
5. Bioautography..... 75
5.1 Introduction 75
5.2 Material and methods 80

TABLE OF CONTENTS (continued)

5.2.1 Construction of the bioluminescent *M. tb* strain 80
5.2.2 Working stock preparation 80
5.2.3 Contact bioautography 80
5.2.4 Direct bioautography: dipping the TLC plate into liquid or agar culture broth..... 81
5.2.5 TLC-bioautography with ECUM8412 and E14046 extracts/fractions..... 81
5.3 Results and discussion 82
5.3.1 Rifampin inhibition zone..... 82
5.3.2 Bioautography method..... 83
5.3.3 Bioautography of cyclic peptides..... 84
6. Quantitative purity-activity relationship (qPAR) 88
6.1 Introduction 88
6.2 Example 1: Dereplication of phytols in *Taxillus chinensis* 89
6.2.1 Background 89
6.2.2 Materials and methods..... 90
6.2.3 Results and discussion 92
6.3 Example 2: qPAR of hytramycins in ECUM14046 GE fractions..... 98
7. Discovery of hytramycins, new anti-*M. tb* hexapeptides 99
7.1 Introduction 99
7.2 Experimental section 100
7.2.1 General Experimental Procedures..... 100
7.2.2 Screening and Prioritization..... 101
7.2.3 Marfey's experiments..... 103
7.2.4 Antibacterial activity assays..... 106
7.2.5 qPAR of hytramycins by LC-MS..... 106
7.3 Results and discussion 107
7.3.1 Physicochemical Properties and Masses of the Isolates 108
7.3.2 Structural Elucidation..... 109
7.3.3 Stereochemical Determination..... 124
7.3.4 Antimicrobial Activity..... 127
7.3.5 qPAR of hytramycins in ECUM14046 GE 131
7.3.6 Summary 134
8. Discovery of xylamycins..... 137
8.1 Introduction 137

TABLE OF CONTENTS (continued)

8.2 Materials and methods 138
8.2.1 Culture and Extraction of ECUM8412 E 138
8.2.2 Column Chromatography 138
8.2.3 High Speed Counter Current Chromatography (HSCCC) 139
8.2.4 LC-PDA-MS analysis of HEMWat-0 fractions 140
8.2.5 Preparative HPLC of the HEMWat-0 **B14** fraction 141
8.2.6 Antibacterial activity assays 141
8.3 Results and discussion 142
8.3.1 Physicochemical properties of **B14** 144
8.3.2 Screening, prioritization and fractionation of ECUM8412 E extract 144
8.3.3 Structural elucidation 151
8.3.4 Antimicrobial Activity 167
8.3.5 Summary 170
9. Overall summary 175
9.1 Aim 1: *In vivo* quantification of *M. tb* with GC-MS/MS and real-time PCR methods 175
9.2 Aim 2: *In vitro* screening of anti-*M. tb* constituents 177
9.3 Aim 3: Isolation of hytramycin and xylamycin 179
9.3 Future Perspectives 181
9.3.1 Determination of TBSA in *M. tb* infected mice with GC-MS/MS 181
9.3.2 Quantification of gene markers of *M. tb* infected mice with real-time PCR 183
9.3.3 Assay development with TLC-bioautography 184
9.3.4 Anti-*M. tb* drug discovery from Actinomycete extracts 185
9.4 Overall Conclusions 186
CITED LITERATURE 188
APPENDICES 205
Appendix A 206
Appendix B 220
Appendix C 227
Appendix D 230
Appendix E 233
Appendix F 237
Appendix G 238
VITA 241

LIST OF TABLES

TABLE I CORRELATION OF DRUG CONCENTRATION AND CFU OR TBSA IN MACROPHAGE INFECTION MODEL 25

TABLE II CORRELATION OF DRUG DOSE AND CFU OR TBSA IN GKO MOUSE INFECTION MODEL 27

TABLE III DRUG DOSAGES (mg/kg/DAY) USED TO TREAT INFECTED GKO AND BALB/C MICE 36

TABLE IV SEQUENCES OF PRIMER PAIRS AND *TAQMAN* PROBES USED FOR QUANTIFICATION OF SPECIFIC RNA PRODUCTS 39

TABLE V LINEAR CORRELATION BETWEEN Ct AND LOG_{10}C OF DNA TEMPLATE IN ng/µL.. 40

TABLE VI LINEAR CORRELATIONS BETWEEN LOG_{10}RNA AND LOG_{10}CFU IN BALB/C MOUSE ACUTE AND CHRONIC INFECTION MODELS 47

TABLE VII LINEAR CORRELATIONS IN LOG_{10}RNA-LOG_{10}CFU, LOG_{10}RNA-DOSAGE, AND LOG_{10}CFU-DOSAGE IN GKO MICE 52

TABLE VIII LINEAR CORRELATIONS IN LOG_{10}RNA-LOG_{10}CFU, LOG_{10}RNA-DOSAGE, AND LOG_{10}CFU-DOSAGE IN BALB/C MICE 53

TABLE IX SPECIFICITY OF *fbpB, icl1*, AND 16S rRNA IN MYCOBACTERIAL SPECIES 61

TABLE X STOCK CONCENTRATION OF STANDARD DRUGS FOR MABA AND LORA 68

TABLE XI RETENTION TIME OF THE FDAA DERIVATIVES AND SOURCES OF THE UNDERIVATIZED AMINO ACIDS 105

TABLE XII 1D & 2D ^{1}H AND ^{13}C NMR DATA OF **1** 120

TABLE XIII ^{1}H AND ^{13}C NMR DATA OF **2** 123

TABLE XIV *IN VITRO* ANTI-*M. TB* ACTIVITIES AND CYTOTOXICITY OF **1** AND **2** (µg/mL), IN COMPARISON TO FIVE ANTI-*M. tb* DRUGS 127

TABLE XV MICs OF **1** AND **2** AGAINST STRAINS REPRESENTING MAJOR GLOBAL CLADES OF *M. tb* 129

TABLE XVI MICs OF **1** AND **2** AGAINST MONODRUG-RESISTANT STRAINS OF *M. tb* 129

LIST OF TABLES (continued)

TABLE XVII *IN VITRO* ANTIBACTERIAL SPECTRUM OF ACTIVITY OF **1** AND **2**..... 130

TABLE XVIII EFFECT OF SUPPLEMENTAL SERUM AND ALBUMIN ON NORMOXIC AND HYPOXIC ACTIVITY OF **1** AND **2** 131

TABLE XIX ANTI-*M. tb* ACTIVITY OF SUB-FRACTIONS OF FRACTION S1..... 148

TABLE XX ^{1}H AND ^{13}C NMR DATA OF **B14** IN METHANOL-d_4..... 152

TABLE XXI *IN VITRO* ANTI-*M. tb* ACTIVITIES AND IC_{50} (µg/mL) OF **B14**, IN COMPARISON TO ANTI-*M. tb* DRUGS 167

TABLE XXII *IN VITRO* MACROPHAGE ACTIVITY OF **B14**..... 168

TABLE XXIII MICs OF B14 AGAINST MONODRUG-RESISTANT STRAINS OF *M. tb* 168

TABLE XXIV MICs OF B14 AGAINST STRAINS REPRESENTING MAJOR GLOBAL CLADES OF *M. tb* 168

TABLE XXV *IN VITRO* ANTIBACTERIAL SPECTRUM OF ACTIVITY OF **B14** 170

TABLE XXVI EFFECT OF SUPPLEMENTAL SERUM AND ALBUMIN ON ANTI-*M. tb* ACTIVITY OF **B14** UNDER NORMOXIC CONDITIONS 170

LIST OF FIGURES

Figure 1 Estimated TB incidence rate by countries in 2011 2

Figure 2 Structures of first-line anti-TB drugs and newly emerging anti-TB agents..... 8

Figure 3 The PrOBE approach to lead discovery and the contributions from the present work 12

Figure 4 Structures and putative MS fragmentations of TBSAME and MND-d_3..... 17

Figure 5 Correlation of TBSA and CFU from serially diluted *M. tb* H_{37}Rv from stationary phase culture 21

Figure 6 Growth curves of *M. tb* and TBSA-CFU correlation 21

Figure 7 TBSA and CFU response to INH and RMP *in vitro* 22

Figure 8 *M. tb* Erdman growth inhibition in macrophages..... 25

Figure 9 *M. tb* Erdman growth inhibition in GKO mice..... 27

Figure 10 C_{26}ME response to INH and RMP..... 29

Figure 11 Correlation between $\log_{10}$CFU/mL culture and $\log_{10}$RNA of *fbpB*, *icl1*, and 16S rRNA from real-time PCR analysis in serially diluted bacterial culture media 42

Figure 12 Growth curve in $\log_{10}$CFU/mL culture, and in $\log_{10}$RNA of *fbpB*, *icl1*, and 16S rRNA 43

Figure 13 Linear correlation between $\log_{10}$CFU/mL culture and $\log_{10}$RNA of *fbpB*, *icl1*, and 16S rRNA in serially diluted bacterial culture media spiked with uninfected BALB/c mouse lung tissue..... 44

Figure 14 Growth of *M. tb* in infected BALB/c mice..... 46

Figure 15 Growth inhibition of *M. tb* in infected GKO mice as determined by CFU and transcription levels of the three RNAs..... 49

Figure 16 Growth inhibition of *M. tb* in infected BALB/c mice as determined by CFU and transcription levels of the three RNAs..... 51

Figure 17 Log_{10}CFU enumeration and $\log_{10}$RNA expression of *icl1* in BALB/c mice..... 55

LIST OF FIGURES (continued)

Figure 18 Linear correlation between CFU and *icl1* RNA expression in BALB/c mice 55

Figure 19 Phenotypic screening flow chart 64

Figure 20 Assay plate configuration for percentage inhibition testing 65

Figure 21 Volume (µL) of 7H12 media used for MABA plate configuration..... 67

Figure 22 Fractionation scheme 74

Figure 23 Bioautography methods 78

Figure 24 The *luxABCDE* vector 79

Figure 25 Inhibition zones formed by applying rifampin to the bacterial lawn of *M. tb* $mc^2$7000-*luxABCDE* strain as determined by luminescence..... 82

Figure 26 Bioautography of hytramycins and xylamycins 86

Figure 27 Structure of (*E*)-phytol 93

Figure 28 GC-MS chromatogram of Fr6-3, Fr6-4, and Fr6-5..... 93

Figure 29 GC-MS chromatogram of the CCC "Front", Stationary phase extrusion, fraction Fr6-3, and commercial standard of phytol isomers..... 94

Figure 30 GC-MS chromatogram of 20 CCC sub-fractions, showing (*E*)-phytol, eluted in fractions CCC-14 through CCC-16 at around 24.5 min 94

Figure 31 (A) Weight distribution of CCC fractions, (B) Quantitative PAR presentation of the CCC fractions in MICs of each fraction and the percentage concentration (w/w) of phytol..... 95

Figure 32 Screening of 14046 GE3 from 35,000 actinomycete extracts 102

Figure 33 Preparative HPLC and thin layer chromatogram of the constituents contained in fraction 14646GE3 103

Figure 34 Structures of **1** and **2**..... 107

Figure 35 ^{13}C and DEPT-135 spectra of **1** overlapped (100 MHz, MeOH-d_4)..... 109

Figure 36 ^{1}H NMR expansion spectra of **1** in MeOH-d_4 (400 MHz, Exponential -0.3 Hz, Gaussian 0.5 Hz)..... 110

Figure 37 ^{1}H NMR expansion spectra of **1** in DMSO-d_6 (600 MHz, Exponential -0.3 Hz, Gaussian 0.5 Hz)..... 110

LIST OF FIGURES (continued)

Figure 38 COSY and HMBC spectra highlighting the *N*-methylalanine residue in **1** (400 MHz, DMSO-d_6) 111

Figure 39 COSY and HMBC spectra highlighting the valine residue in **1** (400 MHz, DMSO-d_6) 112

Figure 40 COSY and HMBC spectra highlighting the leucine residue in **1** (400 MHz, DMSO-d_6) 113

Figure 41 COSY and HMBC spectra highlighting the three piperazic acid (Pip) residues in **1** (400 MHz, DMSO-d_6) 114

Figure 42 Semi-selective HMBC spectrum of **1** (600 MHz, DMSO-d_6) 116

Figure 43 ^{1}H NMR spectra of **1** and **2** overlapped (400 MHz, MeOH-d_4) 117

Figure 44 HSQC spectrum of **2**, highlighting the additional methylene from the isoleucine residue which distinguishes **2** from **1**, containing values 118

Figure 45 Key correlations in the 2D-NMR spectra of **1** 118

Figure 46 Comparison of experimental and calculated ^{1}H NMR spectra of **1** 122

Figure 47 LC-MS chromatograms of derivatized **1** and **2** in Marfey's experiment 126

Figure 48 Total ion chromatogram (TIC) of 14046 GE fractions 132

Figure 49 Biochromatogram of 1/MIC of **1** and **2**, and their abundance in the column fractions of 14046 GE 132

Figure 50 Chromatogram of ECUM8412 **B14** fraction showing the elution of compound **B14** with preparative HPLC and TLC of **B14** fraction on silica gel F_{254} developed with $CHCl_3$:MeOH (9:1) 142

Figure 51 Bioassay-guided fraction scheme of ECUM8412 E extract 143

Figure 52 Biochromatogram (mass vs. 1/MIC) of fractions B1 through B17 149

Figure 53 TLC of fractions B1 through B17 on silica gel F_{254} developed with $CHCl_3$:MeOH (9:1) 149

Figure 54 Structure of **B14** showing color coded amino acid residues 151

Figure 55 ^{1}H NMR spectra of **B14** in MeOH-d_4 (600 MHz) 154

Figure 56 ^{1}H NMR expansion (900 MHz) spectrum of **B14** in MeOH-d_4 155

LIST OF FIGURES (continued)

Figure 57 Key correlations in the 2D-NMR spectra of **B14** 156

Figure 58 COSY and HMBC spectra highlighting the alanine (Ala) residue in **B14** (600 MHz, MeOH-d_4) 157

Figure 59 COSY and HMBC spectra highlighting the leucine (Leu) residue in **B14** (600 MHz, MeOH-d_4) 158

Figure 60 COSY and HMBC spectra highlighting the *N*-methyl leucine (*N*MeLeu) residue in **B14** (600 MHz, MeOH-d_4) 159

Figure 61 COSY and HMBC spectra highlighting the cyclized *N*-methyl leucine (c*N*MeLeu) residue in **B14** (600 MHz, MeOH-d_4) 160

Figure 62 COSY and HMBC spectra highlighting the amino hexenoic acid (Hex) residue in **B14** (600 MHz, MeOH-d_4) 161

Figure 63 COSY and HMBC spectra highlighting the nitrotyrosine (NTyr) residue in **B14** (600 MHz, MeOH-d_4) 162

Figure 64 COSY and HMBC spectra highlighting the prenylated tryptophan (pTrp) residue in **B14** (600 MHz, MeOH-d_4) 164

Figure 65 Comparison of experimental and calculated ^{1}H NMR spectra of **B14** 166

Figure 66 Structure of ilamycins A, B1, and B2, highlighting the two variable amino acid residues, AA_1 and AA_2 171

Figure 67 Funnel scheme of summary 176

Figure A-1 Accurate ESI-IT-TOF mass spectra of **1** and **2** 206

Figure A-2 MS/MS spectra and key fragmentation patterns of hytramycin V (**1**) and hytramycin I (**2**) 207

Figure A-3 IR spectra of hytramycin V (**1**) and hytramycin I (**2**) 209

Figure A-4 COSY spectrum of hytramycin V (**1**), (400 MHz, MeOH-d_4) 210

Figure A-5 HSQC spectrum of hytramycin V (**1**) (400 MHz, MeOH-d_4) 211

Figure A-6 HMBC spectrum of hytramycin V (**1**), (400 MHz, MeOH-d_4) 212

Figure A-7 TOCSY spectrum of hytramycin V (**1**) (400 MHz, MeOH-d_4) 213

Figure A-8 NOESY spectrum of hytramycin V (**1**), (400 MHz, MeOH-d_4) 214

LIST OF FIGURES (continued)

Figure A-9 ^{1}H NMR expansion spectra of hytramycin I (**2**), (400 MHz, MeOH-d_4) 215

Figure A-10 COSY spectrum of hytramycin I (**2**), (400 MHz, MeOH-d_4) 216

Figure A-11 HSQC spectrum of hytramycin I (**2**), [400 MHz, MeOH-d_4, vertical axis showing ^{13}C NMR spectrum of hytramycin V (**1**)] 217

Figure A-12 HMBC spectrum of hytramycin I (**2**), [400 MHz, MeOH-d_4, vertical axis showing ^{13}C NMR spectrum of hytramycin V (**1**)] 218

Figure A-13 ^{13}C NMR spectrum of hytramycin I (**2**), (100 MHz, DMSO-d_6) 219

Figure B-1 UV and IR spectra of **B14** (**3**) 220

Figure B-2 Accurate ESI-IT-TOF mass spectra of **B14** (**3**), ($[M+H]^+$) 221

Figure B-3 COSY spectrum of **B14** (**3**) and expansions (600 MHz, MeOH-d_4) 221

Figure B-4 ^{13}C spectrum of **B14** (**3**), (400 MHz, MeOH-d_4) 223

Figure B-5 HSQC spectrum of **B14** (**3**) and expansions (600 MHz, MeOH-d_4) 223

Figure B-6 HMBC spectrum of **B14** (**3**) and expansions (600 MHz, MeOH-d_4) 225

LIST OF EQUATIONS

Equation 1.....40

Equation 2.....41

Equation 3.....65

Equation 4.....66

Equation 5.....72

Equation 6.....91

Equation 7.....96

Equation 8.....133

Equation 9.....133

Equation 10.....133

Equation 11.....133

Equation 12.....133

Equation 13.....133

Equation 14.....133

Equation 15.....133

LIST OF SYMBOLS AND ABBREVIATIONS

$[\alpha]_D$	specific optical rotation
MeCN	acetonitrile
APCI	atmospheric-pressure chemical ionization
ATCC	American Type Culture Collection
ATP	adenosine triphosphate
BALB/c mouse	an albino, laboratory-bred strain of the house mouse
BGF	bioassay-guided fractionation
BSA	bovine serum albumin
calcd	calculated
CAP	capreomycin
CCC	countercurrent chromatography
cDNA	complementary DNA
CFU	colony forming unit
ChMWat	chloroform/methanol/water
CLF	clofazimine
CMC	carboxylmethylcellulose
COSY	correlation spectroscopy
Ct	threshold value
CTRL	control
δ (ppm)	chemical shift (in parts per million downfield from TMS)

DEPT	distortionless enhancement by polarization transfer
D-MEM	Dulbecco's modified eagle media
DMSO	dimethyl sulfoxide
DNA	deoxyribonucleic acid
DNase I	deoxyribonuclease I
DOTS	directly observed treatment, short-course
ECUM	extract collection of useful microorganisms
ELISA	enzyme-linked immunosorbent assay
EMB	ethambutol
Et	ethyl group
EtOAc	ethyl acetate
EtOH	ethanol
FAS	fatty acid synthase
fbp-B	antigen 85B
FBS	fetal bovine serum
FDAA	1-fluoro-2,4-dinitrophenyl-5-L-alanine amide
G.S.S. media	glutamine synthetase system media
GC-MS/MS	gas chromatography-tandem mass spectroscopy
GKO	gamma-interferon gene knock-out
G.U.E.S.S.	generally useful estimation of solvent systems

LIST OF SYMBOLS AND ABBREVIATIONS (continued)

HBSS	Hanks' balanced salt solution
HEMWat	hexane/ethyl acetate/methanol/water
HiFSA	^{1}H iterative full spin analysis
HIV	human immunodeficiency virus
HMBC	heteronuclear multiple-bond correlation spectroscopy
HPLC	high performance liquid chromatography
hr(s)	hour(s)
HR-ESI-MS	high resolution electrospray ionization mass spectrometry
HSCCC	high speed countercurrent chromatograph
HSQC	heteronuclear single-quantum correlation spectroscopy
I.D.	inner diameter
IC_{50}	concentration at half maximal inhibition
ICL	isocitrate lyase
INH	isoniazid
INT	*p*-iodonitrotetrazolium violet
IR	infrared
IS6110	insertion sequence 6110
IT-TOF	ion trap - time of flight
K value	partition coefficient
KM	kanamycin
λ (nm)	wavelength (in nanometers)

L-J medium	Löwenstein-Jensen medium
LogP	Log_{10} of the *n*-octanol/water partition coefficient
LORA	low oxygen recovery assay
LTBI	latent TB infection
M. tb	*Mycobacterium tuberculosis*
MABA	microplate Alamar blue assay
MBC	minimum bactericidal concentration
MDR	multi-drug resistance
Me	methyl group
MeOH	methanol
MET	metronidazole
MGIT	*Mycobacteria* growth indicator tube
MIC	minimum inhibitory concentration
min	minute (time)
MND-d_3	nonadecanoic acid tri-deuterated methyl ester
MOPS	3-(*N*-morpholino)propane-1-sulfonic acid
MOX	moxifloxacin
MTS	3-(4,5-dimethylthiazol-2-yl)-5-(3-carboxymethoxyphenyl)-2-(4-sulfophenyl)-2H-tetrazolium
MTT	methyl thiazolyl tetrazolium
m/z	mass-to-charge ratio

NAAT	nucleic acid amplification tests
NADPH	nicotinamide adenine dinucleotide phosphate
NMR	nuclear magnetic resonance
NOESY	nuclear Overhauser effect spectroscopy
NP	normal phase
NR	non-replicating
NTM	non-tuberculous mycobacteria
OADC	oleic acid, albumin, dextrose, catalase
OD	optical density
PA	PA 824
PAR	purity-activity relationship
PBS	phosphate buffered saline
PCR	polymerase chain reaction
PDA	photodiode array
Φ	diameter
PIM	phosphatidyl-*myo*-inositol mannoside
Pip	piperazic acid
PMS	phenazine methosulfate
PrOBE	Prioritization by Orthogonal Biological Evaluation
PZA	pyrazinamide
QFT-G test	QuantiFERON-TB Gold test

qPAR	quantitative purity-activity relationship
R^2	correlation coefficient
RC	residual complexity
redox	reduction-oxidation
RLU	relative light unit
RMP	rifampin
RPMI	Roswell Park Memorial Institute medium
RNA	ribonucleic acid
RNase	ribonuclease
RP	reverse phase
rpm	revolutions per minute
RT	reverse transcription
SA	spectrum of activity
SD	standard deviation
SDS	sodium dodecyl sulfate
sec	second (time)
SI	selectivity index
SIM	selective ion monitoring
SM	streptomycin
TB	tuberculosis
TBSA	tuberculostearic acid

LIST OF SYMBOLS AND ABBREVIATIONS (continued)

TBSAME	tuberculostearic acid methyl ester
TCM	traditional Chinese medicine
TIC	total ion chromatogram
TLC	thin layer chromatography
TMC207	bedaquiline
TNBT	tetranitro blue tetrazolium
TOCSY	total correlation spectroscopy
TST	tuberculin skin test
UV	ultraviolet
Vero	African green monkey kidney cell line
VLC	vacuum liquid chromatography
WHO	world health organization
XDR	extensively drug-resistant

SUMMARY

This study establishes a new anti-*M. tuberculosis* (*M. tb*) drug lead screening scheme that integrates *in vitro* and *in vivo* methods for early detection of bioactive constituents during the purification of nature-derived extracts.

Two *in vivo M. tb* quantification methods were established: 1) the determination of a *Mycobacterium* genus-specific cell wall fatty acid, tuberculostearic acid, with GC-MS/MS and 2) determination of *M. tb* marker RNAs with real-time PCR. Both are efficient, accurate and relatively inexpensive, and adaptable to *in vitro* and *in vivo M. tb* growth and inhibition monitoring in anti-*M. tb* drug discovery programs. The conventional *in vitro* high-throughput phenotypic screening, the newly designed *M. tb* bioautography on thin layer chromatography plates, as well as the determination of quantitative purity-activity relationship study all aid in exploring and screening for bioactive principles in a crude state.

Two classes of cyclic peptides, hytramycins and a xylamycin, were isolated from the extracts of two different actinomycete strains through bioassay-guided fractionation. The structures were elucidated mainly with LC-MS and 1D/2D-NMR. Both peptides contain unusual amino acid residues in the structural cores, and also exhibit strong anti-*M. tb* activity *in vitro* with unique antimicrobial mechanisms of action.

1. Introduction

1.1 Tuberculosis

1.1.1 Facts about pandemic tuberculosis

Tuberculosis (TB) is a frequently lethal infectious disease caused by *Mycobacterium tuberculosis* (*M. tb*), most common in low- and middle-income countries. It is estimated that approximately one-third of the world's population is infected with *M. tb*, and 10% of these will develop active tuberculosis during their lifetime [1, 2]. The World Health Organization (WHO) estimated that in the year 2012 TB claimed about 1.3 million lives worldwide and 8.6 million new TB cases were detected [3] (**Figure 1**), giving it the distinction of having the highest human mortality of all microbial infections.

People with weakened immune systems have a much greater risk of developing active TB. A person infected with HIV is about 25 times more likely to develop active TB than one not suffering from HIV infection. There were an estimated 1.1 million HIV positive new TB cases globally including 0.32 million deaths in 2012. TB is the leading cause of death among people infected by HIV, accounting for one in four HIV-related deaths [3].

Another important factor in the control of tuberculosis is the prevalence of drug-resistance. There were an estimated 0.45 million multi-drug resistant (MDR) TB cases among notified TB patients with pulmonary TB worldwide in 2012. About 60% of these cases occur in Brazil, the Russian Federation, India, China, and South Africa alone ("BRICS" countries). According to the WHO, reliable data suggest approximately 9% of MDR-TB cases also have resistance to fluoroquinolones and at least one of the anti-*M. tb* injectables (aminoglycosides or

cyclic peptides), termed extensively drug-resistant (XDR) TB. As of October 2012, 84 countries had reported at least one XDR-TB case [3]. XDR-TB has been transmitted to HIV co-infected patients and is associated with high mortality [4, 5]. For the near future, TB will continue to be a major public health threat.

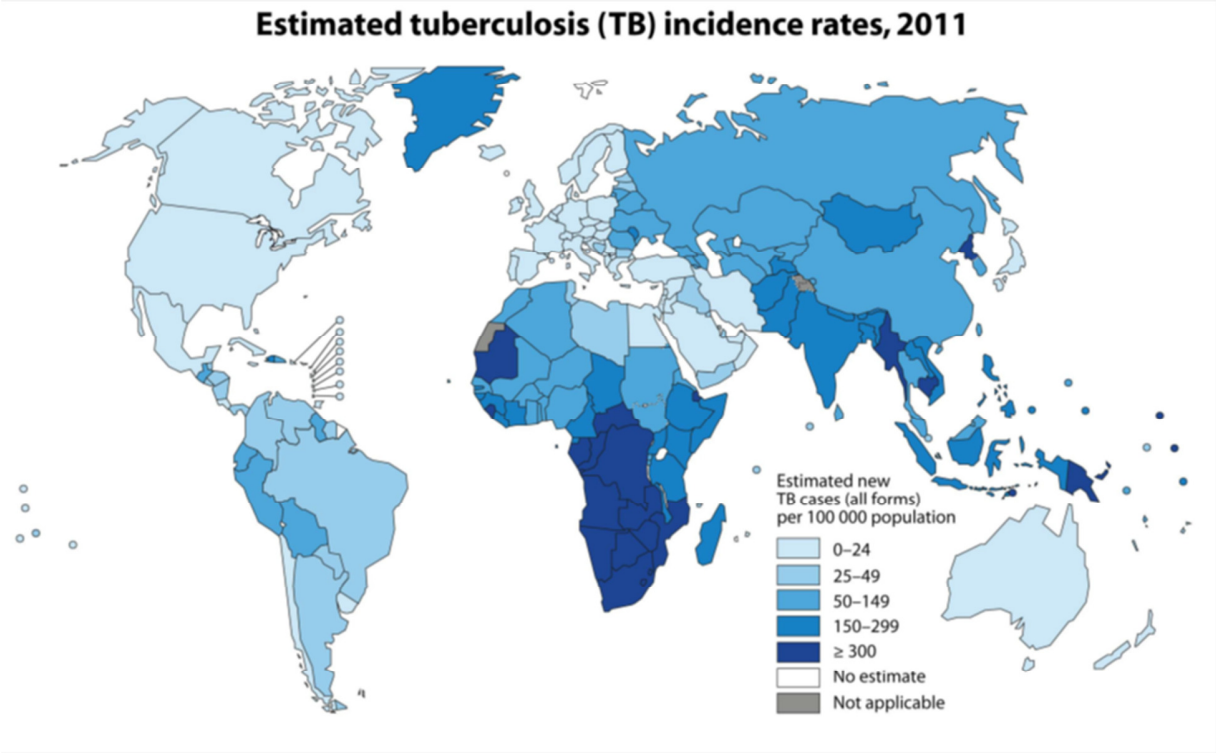

Figure 1. Estimated TB incidence rate by countries in 2011 (Global tuberculosis report 2012, WHO 2012)

1.1.2 TB etiology

Mycobacterium tuberculosis is an aerobic but hypoxia-tolerant, acid-fast bacillus, 2-4 µm in length and 0.2-0.5 µm in width, first discovered in 1882 by Robert Koch. *M. tb* divides every 15-20 hrs, sharing the same slow-growing characteristic as some other bacterial species in the

Mycobacterium genus. This makes effective detection and diagnosis of tuberculosis difficult, especially in children, the immune-deficient, and in latent TB infection (LTBI).

M. tb does not retain crystal violet nor safranin due to the high lipid content in its cell wall, thus it is classified neither as a Gram-positive nor a Gram-negative bacterium with regard to staining properties. In spite of this, *M. tb* is usually categorized as a Gram-positive bacterium on the basis of closer genetic relatedness. Mycobacteria, along with some *Nocardia sp.*, are unique in retaining carbol fuchsin following decolorization with acid-alcohol in the Ziehl-Neelsen staining procedure and so are termed “acid-fast”, a property also conferred by the unique cell wall. The mycobacterial cell wall is a complex combination of lipids and carbohydrates and accounts for 60% of the dry weight of cell mass [6, 7]. Inner layers of the cell wall consist of arabinogalactan and peptidoglycan [8, 9], requiring the organism to synthesize a large quantity of carbohydrates from lipids via gluconeogenesis. The thick waxy outer layer of the cell wall mainly consists of mycolic acids, a group of α-branched β-hydroxylated long chain fatty acids, which build a defensive barrier with extremely low fluidity, conferring low cellular permeability and consequently an intrinsic resistance to antibiotics [10-13]. Outside the cell wall, another capsule layer built from polysaccharides and proteins with traces of lipids render the mycobacterial surface rather hydrophobic, leading to bacterial aggregation or clumping during culturing in liquid media [8, 14].

The transmission of tuberculosis most commonly occurs when *M. tb*, in an aerosol droplet, enters the alveolar passages of exposed hosts. Macrophages, pneumocytes as well as dendritic cells are considered to be involved in the host defense during the early stage of infection [15]. The kernel of infected macrophages constructs the granuloma, i.e., tubercles, a

characteristic which literally defines the disease. No obvious symptoms of disease appear in this phase of an infection, and the host does not transmit the bacteria to others, unless the containment of granuloma tissue fails after a change in immune status of the host. This is commonly caused with increasing age, malnutrition, or HIV co-infection. These factors release the viable infectious bacilli into the airways and permit them to spread further through coughing [16].

Other than active tuberculosis, an infected person can carry the asymptomatic or latent tuberculosis. This situation is mimicked by *in vitro* latency when the available oxygen level drops below about 0.06% saturation, culture turbidity, colony forming units (CFU), and synthesis of DNA starts to slow down or cease [17-19], the concentration of glycine dehydrogenase and isocitrate lyase rise abruptly, and the production of a unique antigen, URB-1, is detected. The non-replicating stage of *M. tb* enables the bacterium to lie dormant in the host for a long period of time, with the capability to revitalize at a later time. All of these facts contribute to the difficulties of tuberculosis detection, treatment, and control.

1.1.3 TB diagnosis and quantification

It has been estimated that an early test with 85% sensitivity and 97% specificity in the diagnosis of TB infection, including active, latent, and drug-resistant strains, could prevent 392,000 deaths annually, accounting for 22% of global TB deaths [20]. However, existing diagnostic tests are still incapable of detecting sputum-smear-negative cases, childhood tuberculosis, and accurate prediction of reactivation of latent tuberculosis [21, 22]. To evaluate the time required to diagnose TB by established methods, chest tomography, microscopy aided by Ziehl-Neelsen staining, and serological identification of TB-specific antibodies can take less

than 2 hrs to accomplish. The disadvantages of these three methods include poor specificity, low resolution between mycobacterial species, and low sensitivity, respectively [22]. Sputum smear microscopy has a particularly low sensitivity for detecting TB among HIV co-infected patients.

Representing recent progresses in rapid and sensitive culture examination of *M. tb*, BACTEC mycobacterial growth indicator tubes (BACTEC 960/MGIT) require a mean detection time of 13.3 days, the radiometric BACTEC 460 system needs 14.8 days, while growth on the Löwenstein-Jensen medium requires 25.6 days. Whereas measurement of CFU on L-J medium still serves as a gold standard, the BACTEC 460 system [23] gives the most accurate counts of viable culture, followed by MGIT [24, 25]. Immunological diagnosis mainly encompasses the tuberculin skin test (TST), the T-SPOT.*TB* assay, and the QuantiFERON-TB Gold (QFT-G) test which measures interferon-γ using an enzyme-linked immunosorbent assay (ELISA) [26, 27]. TST has a major drawback of yielding false positives in individuals with a history of BCG vaccination; T-SPOT.*TB* appears to be more sensitive than either QuantiFERON tests or TST [28, 29].

Nucleic acid amplification tests (NAAT) are highly sensitive molecular techniques for laboratory diagnosis of pulmonary tuberculosis. This test can differentiate *M. tb* from non-tuberculous mycobacteria (NTM). Insertion sequence 6110 (IS6110) has been commonly selected as the amplification target. However, for smear-negative cases, this PCR method may not be consistently accurate [30, 31]. One example of NAAT in clinical use is the commercially available test kit, COBAS® TaqMan® MTB Test, which qualitatively detects *M. tb* in liquefied and concentrated human respiratory specimens.

By far, the most commonly adopted laboratory *M. tb* quantification method for assessing response to inhibitory agents is the agar dilution method, involving serially diluted test samples of extracts, fractions, or compounds of known concentrations added to the molten media in Petri dishes or microplates and allowed to solidify. Then the inoculum is spotted or spread on an agar surface, the plates are incubated, and CFUs enumerated after 18-21 days [32].

Oxidation-reduction indicator dyes, such as the Alamar blue reagent, make the quantification of mycobacteria more rapid, sensitive, and accurate [23, 33]. The blue non-fluorescent reagent turns pink and fluorescent upon reductive reactions with endogenous dehydrogenases in live cells; therefore, bacterial growth can be visualized by the color change and measured by fluorometry. Alternatively, reporter genes have been introduced on plasmids, enabling the bacterial viability to be rapidly determined by measuring the fluorescence or luminescence from the expressed proteins, such as green fluorescent [34, 35] and luciferase proteins [36, 37], e.g. the luminescent *M. tb* H37Rv strain bearing a *luxABCDE* gene.

1.2 TB chemotherapy

1.2.1 Anti-TB drugs

The current first-line treatment for TB is a multiple drug regimen consisting of rifampin (RMP), isoniazid (INH), pyrazinamide (PZA), and ethambutol (EMB) (**Figure 2**), taken for the first two months, then isoniazid and rifampin alone for another four months, in order to achieve high cure rates [38]. There is still a relapse rate of 2 to 3% in patients initially considered to be cured. Second-line anti-*M. tb* drugs, used primarily in cases of drug-resistance, include

aminoglycosides [amikacin (AMK), streptomycin (SM), kanamycin (KM)], thioamides [ethionamide (ETH), prothionamide (PTH)], polypeptides [capreomycin (CAP), viomycin, enviomycin], fluoroquinolones [ciprofloxacin (CIP), levofloxacin (LEV), moxifloxacin (MOX)], cycloserine (CS), and terizidone (TZ). For the treatment of latent TB infection, 6-9 months of monotherapy with INH is considered the gold standard with 93% effectiveness.

In 1990, the WHO established the Directly Observed Treatment--Short-course (DOTS) strategy [39, 40] to better control and treat TB by focusing on the following five elements: (1) political commitment with increased and sustained financing; (2) diagnosis primarily by sputum-smear microscopy among patients; (3) direct observation of standardized treatment; (4) a definite supply of drugs and a management system; and (5) systematic monitoring of cases and treatment outcomes. Properly implemented DOTS treatment has a success rate exceeding 95% and prevents the emergence of further MDR strains of tuberculosis. The WHO extended the DOTS program in 1998 to "DOTS-Plus" to include the treatment of MDR-TB. Implementation of DOTS-Plus requires the capacity to perform drug-susceptibility testing and the availability of second-line anti-*M. tb* agents, in addition to all the requirements for DOTS.

Currently available TB treatment still has some major challenges: long duration and complexity in dosing, strong adverse effects, increasing incidence of MDR and XDR TB, HIV co-infection, and non-adherence in latent TB treatment [41]. Accordingly, there is an urgent need to improve the current treatment regimen and develop new anti-*M. tb* agents. The most recent clinical pipeline of new TB drugs consists of fluoroquinolones (gatifloxacin, moxifloxacin in phase III), nitro-imidazoles [PA 824, delamanid (OPC-67683) in phase II], diarylquinoline [bedaquiline (TMC207) in phase II], sudoterb (LL-3858) in phase II, oxazolidinones (PNU-100480

in phase I), 1,2-ethylenediamine (SQ109 in phase I), AZD 5847 in phase I, as well as increased dosage of rifampin and its analog, rifapentine [41-43] (**Figure 2**). In spite of these emerging therapies, new challenges still hamper the development of anti-*M. tb* drugs, potentially exemplified by the insufficient profit opportunity of the TB drug market for pharmaceutical industries, the unclear mechanisms of TB dormancy, persistence, and drug resistance, and time-consuming clinical testing [41].

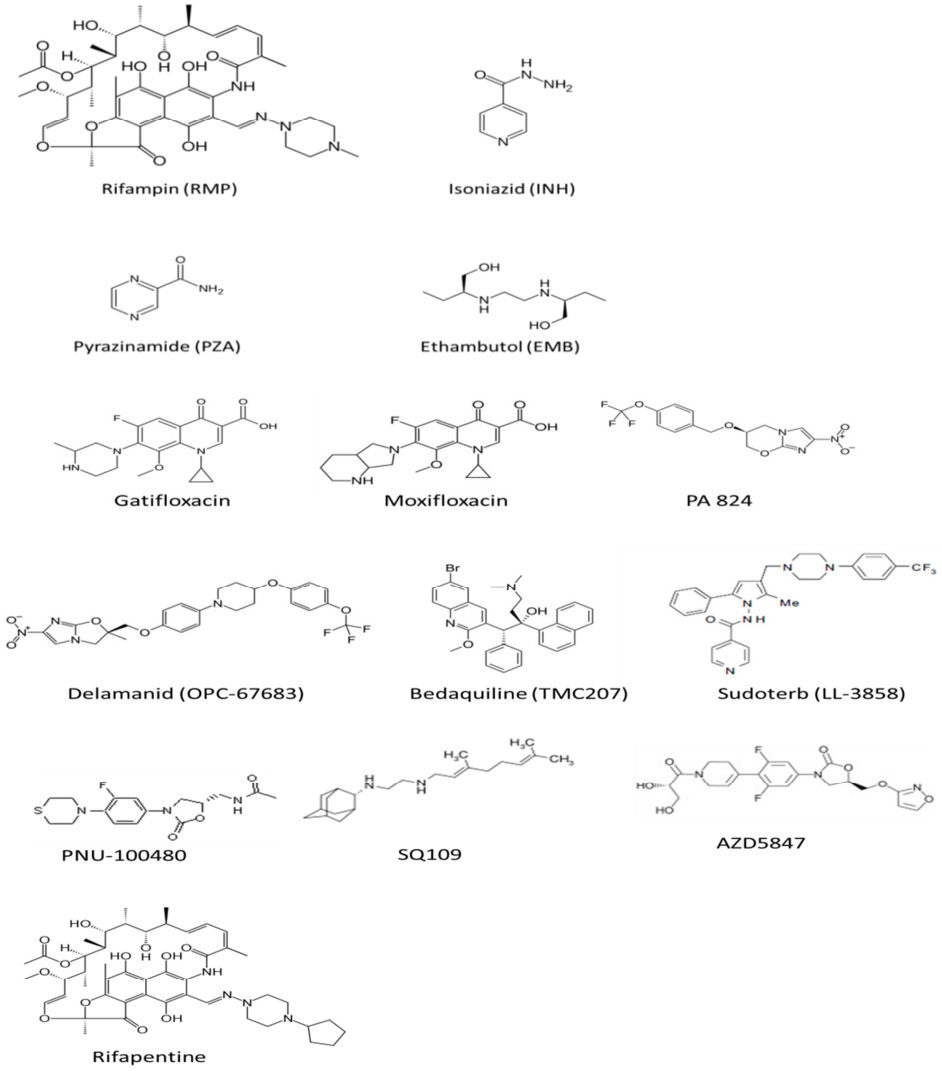

Figure 2. Structures of first-line anti-TB drugs and newly emerging anti-TB agents

1.2.2 Antimycobacterial natural products

Historically, a great number of antimicrobial agents have been discovered from natural resources, including herbal and microorganism extracts. Over 350 plant species from a wide range of families have been recognized as showing antimycobacterial activity [44]. Between 1990 and 2011, nearly 1000 compounds isolated from both terrestrial and marine sources have been reported to exhibit antimycobacterial activity, some having minimum inhibitory concentration (MIC) values of less than 4 μg/mL [45-48]. These compounds belong to a wide range of chemical classes and provide scaffolds for the design and development of new antimycobacterial drugs. However, notable concerns with these compounds still remain in terms of their cytotoxicity toward mammalian cells and the essential lack of *in vivo* efficacy studies.

Actinomycetes in particular have proven to be a rich resource for anti-mycobacterial antibiotic drug discovery. Clinically used anti-*M. tb* drugs from actinomycete sources, mainly exemplified by capreomycin (CAP), cycloserine (CS), kanamycin (KM), neomycin (NEO), rifampin (RMP), and streptomycin (SM), have played important roles in the treatment of tuberculosis. Considering the structural diversity among these chemical classes, there might be a general perception that metabolites from soil and aquatic microorganisms have been completely exploited in recent decades. On the contrary, it can be estimated that only 1-3% of all actinomycete antibiotics have been discovered, and that less than one part in 10^{12} of the earth's soil surface has actually been screened for bioactive actinomycetes [49]. To find the remaining bioactive compounds requires a combination of modern technologies for high-throughput screening, selective procedures to dereplicate the commonly known antibiotics,

methods to enrich rare strains, culturing and harvesting techniques for the uncultured actinomycetes from nature, as well as biosynthetic engineering of the active agents in bacteria [50]. However, the strategies and innovations currently being used to address the discovery of new antibiotics have not translated into success in finding novel structural cores of antibacterial compounds [51, 52].

1.3 Statement of problem and specific aims

Conventional bioassay-guided fractionation (BGF), i.e., purification of individual constituents from a crude extract prioritized by *in vitro* bioactivities, follows empirical streamlines in which *in vivo* assays are usually not carried out until pure compounds with a balance of good activity and low toxicity have been isolated. However, efforts particularly on later rounds of BGF based on *in vitro* assays often turn out to be futile in the end when these elaborately purified fractions exhibit low efficacy due to loss of active constituents, impurities that interfere with activities, i.e., synergy, or poor *in vivo* stability and efficacy. In the present study, a different BGF scheme, Prioritization by Orthogonal Biological Evaluation (PrOBE), is applied (**Figure 3**). This includes *in vivo* efficacy studies by means of the newly established *M. tb* quantification methods for infected mouse tissue samples. Primary fractions are prioritized early based on MICs aided by bioautography of thin layer chromatograms and the determination of quantitative purity-activity relationships (qPAR).

The following five groups of contributions to this broader aim are made in the present study: Two newly developed TB quantification techniques, using GC-MS/MS (A) and real-time PCR (B) techniques, are verified as reliable surrogates for bacterial cell counts in the *in vivo* efficacy studies of the test samples, i.e., extracts, fractions, or pure compounds. Phenotypic

screening (C) involving *in vitro* specificity and selectivity assays with both replicating and dormant *M. tb* strains based on the established MABA and LORA methods provide valuable bioactivity parameters of each test sample. Bioautography (D) greatly facilitates the procedure of identifying and targeting active fractions *in vitro* in very early fractionation steps. Quantitative purity-activity relationship studies, qPAR (E), identify the combinational effects of each constituent on the bioactivity of the isolated fractions, which serves as a tool to dereplicate known compounds, explore minor but active principles, and verify the proven major actives. Overall, with these methods available from both *in vitro* and *in vivo* stages, the efficiency and accuracy of the throughput procedures on anti-*M. tb* natural product screening are considerably elevated. The integration of these methods is introduced in details in "Chapter 4: Phenotypic Screening (Methodology)".

In order to demonstrate feasibility of the PrOBE approach to TB drug discovery, two batches of actinomycete extract libraries were investigated consecutively, screening for novel anti-*M. tb* drug leads with unique mechanisms of action. Structural elucidation by advanced spectroscopic methods together with *in vitro* bioactivity tests of the isolated cyclic peptides, including the use of TLC-bioautography and qPAR methods, led to identification of hytramycins and xylamycin, and aided in determination of the chemical and biological properties of these two potential anti-TB leads.

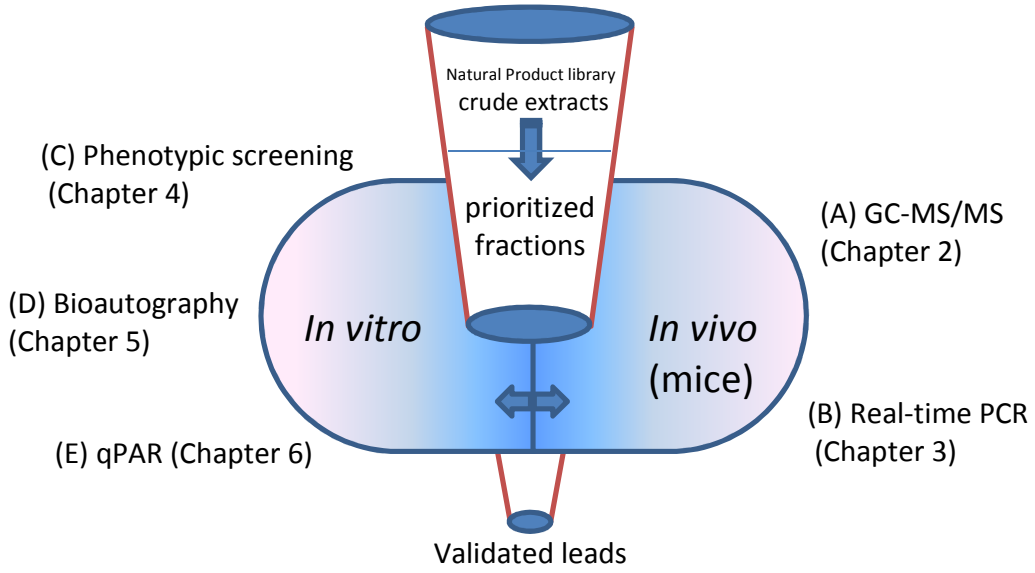

Figure 3. The PrOBE approach to lead discovery and the contributions from the present work

In order to reinforce the establishment of the PrOBE approach, the study implemented the following three main aims:

Specific Aim 1: *In vivo* quantification of *M. tb* with GC-MS/MS and real-time PCR methods

Subaim 1.1 Validation of tuberculostearic acid (TBSA) as a biomarker for *M. tb* quantification by GC-MS/MS

Subaim 1.2 Method establishment of using *M. tb*-specific genes as CFU surrogates for *in vivo M. tb* quantification by real-time PCR

Specific Aim 2: *In vitro* evaluation of anti-*M. tb* fractions using phenotypic screening, bioautography, and qPAR

Subaim 2.1 Isolation of anti-*M. tb* drug leads from actinomycete extracts through phenotypic screening

Subaim 2.2 Early biological assessments of bio-active crude fractions through TLC - bioautography

Subaim 2.3 Determining quantitative purity-activity relationship (qPAR) to rationalize the prioritization of bioactive fractions

Specific Aim 3: Bioassay-guided fractionation (BGF) and isolation of anti-*M. tb* compounds derived from actinomycetes

Subaim 3.1 Isolation of anti-*M. tb* leads from the ECUM 14046 strain

Subaim 3.2 Isolation of anti-*M. tb* leads from the ECUM 8412 strain

2. Quantification of TBSA with GC-MS/MS [1]

2.1 Introduction

In vivo screening to test anti-tuberculosis compounds has long been obstructed by the lack of accurate, efficient, and sensitive surrogate biomarkers for quantification of *M. tb* growth. Quantitative analysis of *M. tb* via the determination of CFU from serially diluted suspensions has always presented difficulties due to 1) the highly hydrophobic mycobacterial cell wall which predisposes individual bacteria to aggregate in aqueous media and 2) the long generation time, requiring 2-3 weeks to visualize colonial growth. The clumping issue is only partially ameliorated through the use of non-ionic surfactants and/or physical dispersion such as vortexing and sonicating. Especially in the initial evaluation of compounds for anti-*M. tb* activity *in vivo* where infection and treatment times can range from weeks to months, the additional time required for CFU determination further decreases the efficiency of hit to lead and lead optimization efforts. Metabolic surrogates employed in axenic culture of *M. tb* (e.g. MIC determination) such as redox dye reduction, fluorescent protein expression and intracellular ATP measurement, lack sensitivity and/or specificity for use in samples containing low numbers of *M. tb* and high numbers of host cells or tissues. Therefore, a simple, rapid and accurate method for quantifying *M. tb* from cell culture and tissue homogenates should facilitate drug discovery efforts for TB.

Tuberculostearic acid (10*R*-methyloctadecanoic acid, TBSA, $C_{19}H_{38}O_2$) is a methyl-branched fatty acid reported as a constituent of the cell wall of the genus *Mycobacterium*,

[1] Contents presented in this chapter has been partially published in: Geping Cai, Guido F. Pauli, Yuehong Wang, Birgit U. Jaki, Scott G. Franzblau. Rapid determination of growth inhibition of *Mycobacterium tuberculosis* by GC-MS/MS quantitation of tuberculostearic acid. *Tuberculosis*. 2013, 93, 322-329 (Appendix G)

including *M. tb* [53-55], and other phylogenetically related organisms within the suborder Corynebacterineae including the genera *Nocardia, Corynebacterium, Gordonia*, and *Turicella* [53, 56, 57]. Compared to mycolic acids which form clusters of high molecular weight homologues, TBSA has a favorable physico-chemical profile with regard to volatility and ionization efficiency, making it a superior analytical target with respect to specificity and throughput. The detection of TBSA in sputum specimens with gas chromatography – mass spectroscopy (GC-MS) has been used for rapidly diagnosing pulmonary *M. tb* infection [58-61]. TBSA was detected in specimens with tuberculous meningitis at concentrations of 25 to 50 fmol (10^{-15} mol) [62]. However, there have been no reports of using TBSA as quantitative biomarker of *M. tb* growth, especially *in vitro* drug-mediated growth inhibition in broth, in macrophage cell models, and in mouse models.

As macrophages are immune effector cells in tuberculosis and as intracellular anti-*M. tb* activity is likely required to observe efficacy in the established mouse models of *M. tb* infection, macrophage culture infection models have been used for the evaluation of established and experimental anti-*M. tb* agents [63, 64]. This infection model was also evaluated as a drug inhibition assay with both TBSA and CFU determination. Since gamma-interferon is a principal mediator of macrophage activation and is essential in resistance to intracellular *M. tb* infection, gamma-interferon knock-out (GKO) mice exhibit more serious tissue necrosis and a more rapid and fatal tuberculosis infection [65, 66]. To date GKO mice have been used in anti-*M. tb* drug efficacy assays with only CFU as bacterial growth indicator [67-69]. In this study, it is demonstrated that TBSA can be used to rapidly quantify *M. tb* in infected macrophage cells

(J774) and GKO mouse lung homogenates in a dose-dependent manner after exposure to various anti-*M. tb* drugs.

2.2 Materials and methods

2.2.1 Sample preparation and TBSA analysis by GC-MS/MS

The TBSA standard was obtained from the Research Institute for Chromatography (Kortrijk, Belgium) and was derivatized to its methyl ester (TBSAME) by a slight modification of the reported methods [70, 71]. In detail, approximately 0.2 mg TBSA was saponified from *M. tb*-containing samples by adding 1 mL of 1.2 M NaOH and MeOH (50%/50%) followed by autoclaving (120 °C for 15 min), and methylated with 2 mL of 6 N HCl and MeOH (54%/46%) in an 80 °C water bath for 10 min followed by quick cooling. The samples were extracted with 1.25 mL of *n*-hexane and methyl *t*-butyl ether (50%/50%), the supernatant was purified by mixing and extracting with 3 mL of 0.3 M NaOH, and then dehydrated with approximately 10 mg anhydrous Na_2SO_4. Then, 95 µL of the purified supernatant was spiked with 5 µL nonadecanoic acid tri-deuterated methyl ester (MND-d_3) in *n*-hexane of known concentration as internal standard. The internal standard was synthesized with nonadecanoic acid (Sigma) and MeOH-d_4 (Sigma) using the same method as TBSA. TBSAME and MND-d_3 elute in the Agilent HP-5ms Capillary GC column (Agilent 19091S-433, 5% phenyl methyl silox, 30 m × 2, I.D. 0.25 mm, film thickness 0.25 µm) at 8.6 min and 9.2 min respectively within a total run of 12.6 min, using a GC temperature ramp starting from 220 °C to 280 °C at a rate of 6 °C/min, then at 50 °C/min to 310 °C and held for 2 min. Both TBSAME and MND-d_3 were fragmented into their qualifiers and quantifiers in an Agilent 7890A GC system linked with an Agilent 7000A triple quadrupole mass

spectrometer. Multiple Reaction Monitoring (MRM) mode was applied with collision energy of 10 eV: *m/z* 312.5 to 143 and to 199 for TBSAME, and *m/z* 315.5 to 104 and to 146 for MND-d_3, as quantifiers and qualifiers for both compounds respectively (**Figure 4**). TBSAME concentrations were calculated with the Agilent Masshunter Quantitative software based on a calibration curve of serially diluted TBSAME standard solutions spiked with MND-d_3.

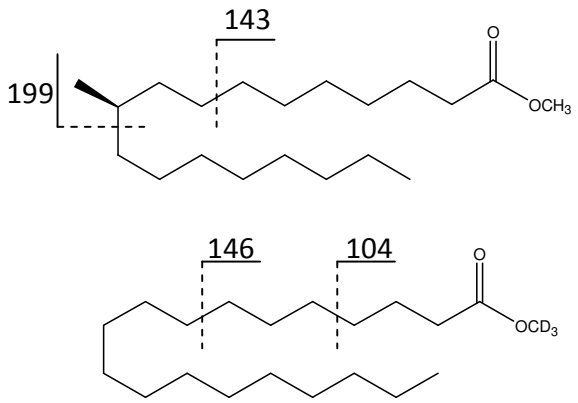

Figure 4. Structures and putative MS fragmentations of TBSAME and MND-d_3

2.2.2 TBSA correlation with CFU *in vitro*

The H_{37}Rv (ATCC 27294) and Erdman (ATCC 35801) strains of *M. tb* were obtained from the American Type Culture Collection (Bethesda, MD). For *in vitro* correlations of TBSA with CFU, cultures were grown in Middlebrook 7H9 broth (BD Biosciences) supplemented with oleic acid, albumin, dextrose, catalase (OADC, Fisher Scientific). To determine the linearity of correlation of TBSA with CFU, stationary phase cultures were harvested after 9 days of incubation. Six 50 mL aliquots of the culture were centrifuged, and the pellets were each re-suspended in 50 mL of PBS buffer solution. For each, five serial dilutions of 1:5 were prepared in PBS. After

removing 100 µL aliquots of each diluted suspension for CFU determination on Middlebrook 7H11 agar (BD Biosciences) with 10% OADC, the remaining 39.9 mL of each sample was centrifuged, and the pellets were processed for TBSA analysis as per the above method for converting the TBSA standard compound to TBSAME. The concentrations of TBSAME from the same gradient were averaged.

To monitor the correlation of TBSA with CFU during growth in axenic medium, one milliliter of 1.7-2 × 10^7 CFU/mL *M. tb* H_{37}Rv or Erdman was inoculated into 300 mL of Middlebrook 7H9 liquid culture media (with 10% OADC). At 48-hr intervals for 14 days, 100 µL aliquots of culture were serially diluted for CFU determination and the remaining 30 mL of sample was processed as above for quantification of TBSA.

2.2.3 Drug inhibition of *M. tb* in axenic medium

M. tb H_{37}Rv was incubated for 7 days in 300 mL of Middlebrook 7H9 with 10% OADC in a 1 L flask with shaking at 120 rpm until early plateau phase was reached as determined by optical density using a Klett-Summerson colorimeter. Individual cultures received isoniazid (INH, Sigma) at 21, 63, and 189 ng/mL or rifampin (RMP, Fisher Bioreagents) at 33, 99, and 296 ng/mL. Three aliquots of 25 mL were removed from each flask before (Day 0) and 7 days after addition of drugs, and each aliquot used for the determination of CFU and for TBSA in the bacterial pellets.

2.2.4 Growth of *M. tb* Erdman in macrophages

Adherent macrophages (J774, 3rd or 4th passage) were cultured in three 6-well plates in 5 mL of Dulbecco's Modified Eagle Media (D-MEM, ATCC, Manassas, VA) supplemented with 10%

fetal bovine serum (FBS, Atlanta biologicals, Lawrenceville, GA) and 200 U/mL polymyxin B (Sigma). Macrophages were exposed to *M. tb* Erdman suspended in D-MEM at a multiplicity of infection of approximately 1 for one hour, and then culture media was separated from the macrophage monolayer on the plate surface. Extracellular *M. tb* was removed by washing the layer of macrophage cells attached to the plate twice with 5 mL of warm Hanks' Balanced Salt Solution (HBSS, Atlanta Biologicals). The washings, combined with the initial 5 mL culture media, were centrifuged at 1485 × g for 10 min at room temperature (Eppendorf centrifuge 5415D, 24-place fixed-angle rotor) and supernatant was discarded. Both the media/wash pellets from the mixture of extracellular *M. tb* and unattached macrophage cells and the adherent layer of macrophages were treated with 1 mL of 0.25% SDS and incubated at 37 °C for 10 min to release intracellular *M. tb*. One-hundred microliters of lysate were used for CFU determination on Middlebrook 7H11 agar plates. Five milliliter warm D-MEM media was added to the remaining wells and two wells of the 6-well plates were processed in the same manner on days 1, 3, 5, 6 and 7 post-infection. In this manner growth curves of *M. tb* were established from both adherent and floating macrophages. After taking aliquots for CFU, lysate and washings on day 5, 6, and 7 were combined and centrifuged and the resulting pellets were used for determination of TBSA.

2.2.5 Drug inhibition of *M. tb* in macrophages

One day after infection, the culture media was replaced with fresh media containing three 4-fold concentrations of anti-*M. tb* drugs in D-MEM; three replicate wells were set up for each drug concentration and for drug-free media controls. The pellets of both floating and adherent macrophages were combined and lysed for CFU determination and then centrifuged

for TBSA analyses. Drug-free controls were harvested on T1, T3, T5 and T7 while drug-treated samples were evaluated only on T7.

2.2.6 Growth inhibition of *M. tb* in gamma-interferon knock-out (GKO) mice treated with anti-*M. tb* drugs

Ninety-two GKO mice (11 weeks old, female, Jackson Laboratory) were infected by aerosolization of 10 mL of a suspension containing 2×10^6 CFU/mL *M. tb* Erdman using an aerosol infection chamber (Glas Col, Terre Haute, IN). Growth was monitored by TBSA and CFU in untreated mice at days 10, 17 and 24 post-infection. Ten days after infection, groups of 5 mice were treated by oral gavage daily for fourteen days with one of three two-fold dosages of RMP, INH, MOX, PA and EMB suspended in 0.5% carboxylmethylcellulose (CMC). All drugs were administered in 200 µL CMC, except for MOX which was delivered in 100 µL, 200 µL and 400 µL of a 1.6 mg/mL stock solution. Two days following the final dose, mice were euthanized, both lungs removed and homogenized in 3 mL of HBSS. After removal of an aliquot for CFU determination, 2.5 mL of lung homogenates were centrifuged and pellets used for TBSA analysis.

2.3 Results

2.3.1 Correlation of TBSA with CFU *in vitro*

There was a linear correlation of $\log_{10}$CFU values with $\log_{10}$TBSA from a serially diluted stationary phase culture of $H_{37}Rv$ (R^2 = 0.9774, **Figure 5**). In growing cultures of both *M. tb* $H_{37}Rv$ and Erdman, TBSA synthesis appears to initially lag behind the increase in CFU, however the overall correlation of these parameters throughout the growth curves of the two strains

were R^2 = 0.9112 and R^2 = 0.9314, respectively (**Figure 6**). No significant differences in growth rate or TBSA concentration were found between *M. tb* H_{37}Rv and Erdman.

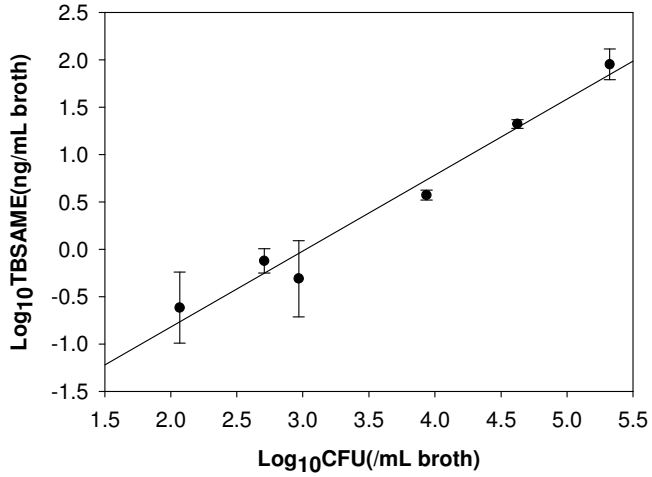

Figure 5. Correlation of TBSA and CFU from serially diluted *M. tb* H_{37}Rv from stationary phase culture. For TBSA, each data point represents the mean of six culture aliquots, each independently serially diluted, and for CFU, each data point represents one aliquot.

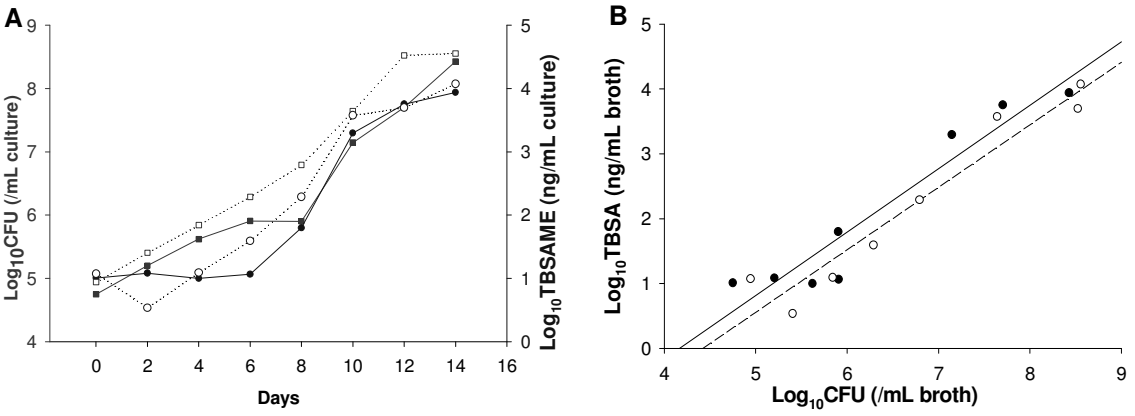

Figure 6. Growth curves of *M. tb* and TBSA-CFU correlation. (**A**) TBSA and CFU during *in vitro* growth of *M. tb* H_{37}Rv and Erdman. Solid line with closed squares: H_{37}Rv CFU; Solid line with closed circles: H_{37}Rv TBSA; Dashed line with open squares: Erdman CFU; Dashed line with open circles: Erdman TBSA; (**B**) Linear correlation of $\log_{10}$TBSA and $\log_{10}$CFU of *M. tb* H_{37}Rv (solid line, closed dots) and Erdman (dashed line, open dots)

2.3.2 Dose-dependent inhibition of INH and RMP on *M. tb* growth in bacterial broth

In axenic medium both INH and RMP effected significant dose-dependent inhibition of TBSA (**Figure 7**) while this marker increased by 35-55 µg/mL in untreated controls over the 7-day incubation period. Despite the reduction in CFU relative to pre-treatment values with the two higher concentrations of INH and all three concentrations of RMP, as expected, the thermally stable TBSA never fell significantly below pre-treatment levels reflecting its nature of a bacteriostatic biomarker. The R^2 values of CFU and TBSA across the concentration ranges were 0.698 for INH and 0.629 for RMP.

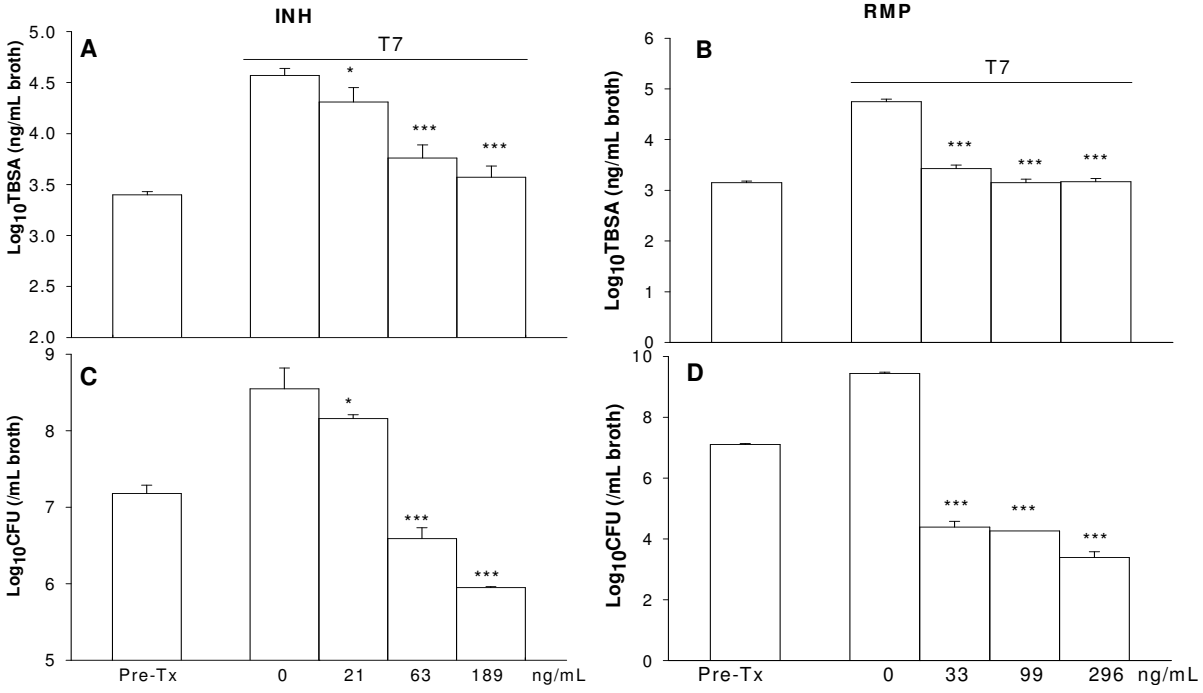

Figure 7. TBSA (A-B) and CFU (C-D) response to INH and RMP *in vitro*. (* 0.01 < p < 0.05; ** 0.005 < p < 0.01; *** p < 0.005 compared with CTRL)

2.3.3 Growth and drug-inhibition of *M. tb* in macrophage culture

Six-well plates were used to obtain sufficient quantities of *M. tb* for TBSA analysis. A preliminary experiment indicated that in such cultures, *M. tb* Erdman within adherent macrophages, increased within one day after infection and greatly decreased after day 3 (data not shown). The number of *M. tb* recovered from floating macrophages increased slowly but continuously starting from the day of infection. Considering both *M. tb* residing within adherent and floating macrophages, the total intracellular *M. tb* titer increased by 0.8 $\log_{10}$CFU over the 7-day incubation.

In a subsequent experiment, untreated intracellular *M. tb* gradually increased throughout the 7 days of culture as indicated by both a 0.22 μg/mL increase in TBSA concentration and a 0.63 $\log_{10}$ increase in CFU. With the exception of the effect of EMB on CFU, all drugs demonstrated a concentration-dependent inhibition of both TBSA and CFU at day 7 ($R^2 > 0.7$ for each readout). Whereas the highest concentrations of INH and RMP appeared bactericidal when assessed by CFU (i.e., values below that observed on day 1), TBSA concentrations never fell below starting levels (**Figure 8**). The correlation between TBSA and CFU during growth in untreated control cultures was better ($R^2 = 0.87$) than when considering both untreated and drug-treated cultures ($R^2 = 0.45$) (**Figure 8C**; **TABLE I**).

A

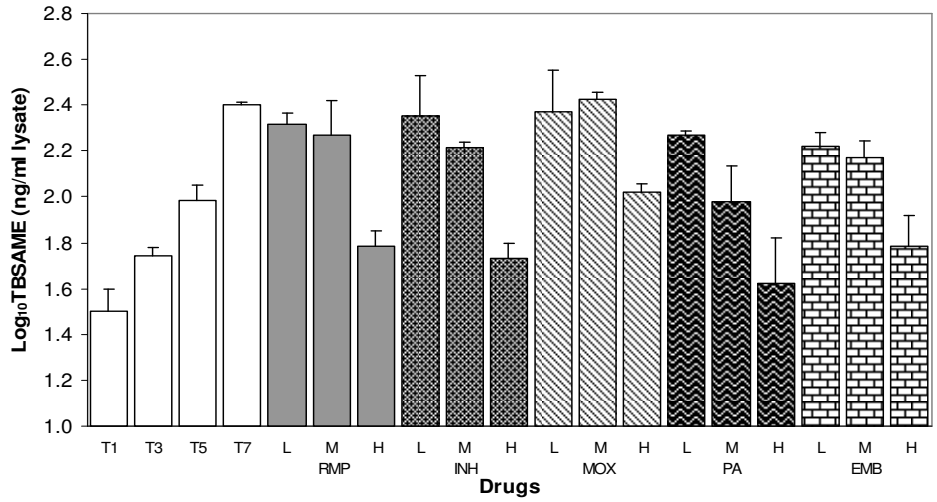
Log10TBSAME (ng/ml lysate)
2.8
2.6
2.4
2.2
2.0
1.8
1.6
1.4
1.2
1.0
T1 T3 T5 T7 L M H L M H L M H L M H L M H L M H
RMP INH MOX PA EMB
Drugs

B

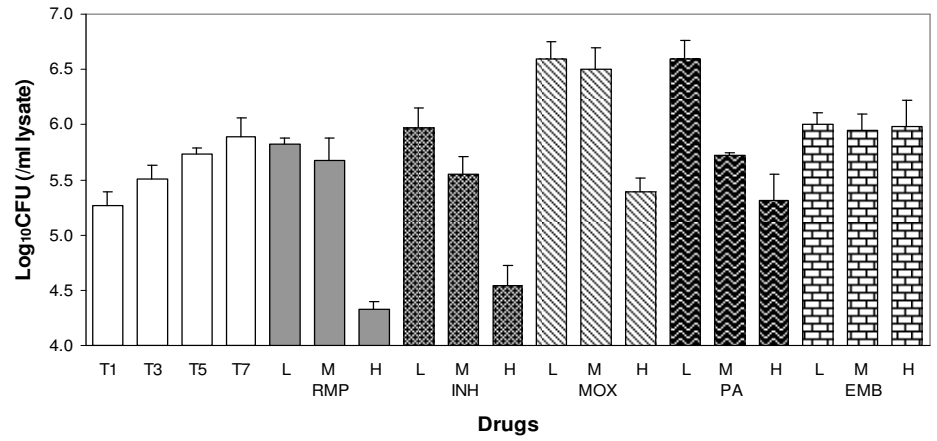
Log10CFU (/ml lysate)
7.0
6.5
6.0
5.5
5.0
4.5
4.0
T1 T3 T5 T7 L M H L M H L M H L M H L M H L M H
RMP INH MOX PA EMB
Drugs

C

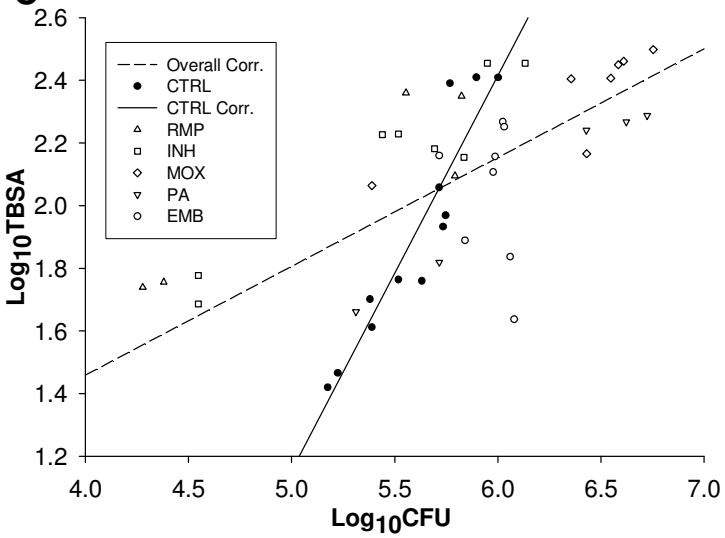
Overall Corr.
CTRL
CTRL Corr.
RMP
INH
MOX
PA
EMB
Log10TBSA
2.6
2.4
2.2
2.0
1.8
1.6
1.4
1.2
4.0 4.5 5.0 5.5 6.0 6.5 7.0
Log10CFU

Figure 8. *M. tb* Erdman growth inhibition in macrophages. (**A-B**) Growth and responses of TBSA and CFU in *M. tb* Erdman-infected macrophages to 7-day drug exposure. The drug concentrations (μg/mL) were: 0.01, 0.04 and 0.16 for RMP and INH, 0.025, 0.1 and 0.4 for moxifloxacin (MOX) and PA 824 (PA), and 0.25, 1.0 and 4.0 for ethambutol (EMB). Each data point represents an individual culture; (**C**) TBSA and CFU correlation for all cultures (dashed line, $y = 0.35x-2.93$, $R^2 = 0.45$) and for only untreated control cultures (solid line, closed circles, $y = 1.26x-8.15$, $R^2 = 0.87$)

TABLE I. CORRELATION OF DRUG CONCENTRATION AND CFU OR TBSA IN MACROPHAGE INFECTION MODEL

Drug	R^2	
	CFU	TBSA
RMP	0.98	0.89
INH	0.96	0.88
MOX	0.90	0.73
PA	0.77	0.77
EMB	0.02	0.86

2.3.4 Inhibition of *M. tb* growth in the lungs of gamma-interferon gene knock-out (GKO) mice by anti-*M. tb* drugs

M. tb in the lungs of untreated GKO mice increased by 5.1 $\log_{10}$CFU from day 3 to day 24 post-infection while TBSA increased by 1.74 μg/mouse from day 10 to day 24 post-infection. TBSA in lung homogenates at day 3 post-infection was still below the limit of detection. All three dosages of the five established and experimental anti-*M. tb* drugs significantly decreased the level of TBSA in lung homogenates after 14 days treatment (except the low dosage of 3.75 mg/kg/day rifampin) compared with untreated mice, and did so in a dose-dependent manner (**Figure 9**).

TBSA correlated well with CFU with an overall R^2 value of 0.733 for all samples and 0.974 for only untreated controls. RMP and MOX demonstrated the most proportional dose-response effects in both TBSA and CFU ($R^2 > 0.8$) (**Figure 9C**; **TABLE II**).

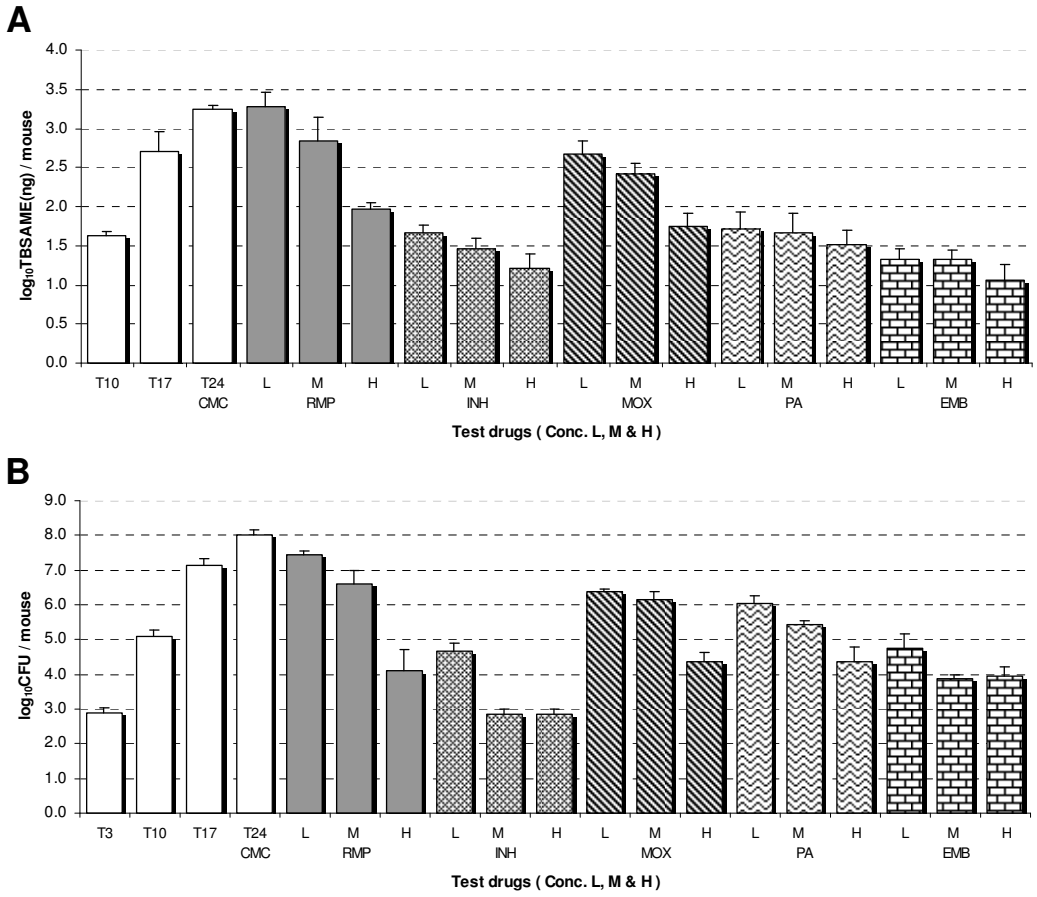

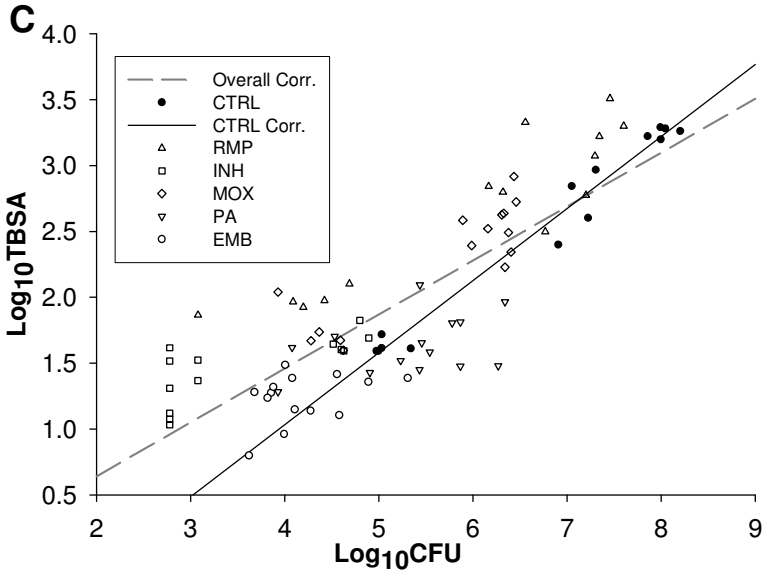

Figure 9. *M. tb* Erdman growth inhibition in GKO mice. Growth and responses (day 24 after infection) of TBSA (**A**) and CFU (**B**) in *M. tb* Erdman-infected GKO mice (combined right and left lung homogenates) after treatment with three dosages of five anti-*M. tb* drugs; Drug dosages (mg/kg/day) used to treat infected GKO mice are (in the order of Low, Medium and High): 3.75, 7.5, 15 for RMP, 6.25, 12.5, 25 for INH, 8, 16, 32 for MOX, 25, 50, 100 for PA, and 100, 200, 400 for EMB in five replicates each dosage; (**C**) Overall correlation of $\log_{10}$CFU with $\log_{10}$TBSA in all samples (dashed line, y = 0.41x-0.18, R^2 = 0.73) and in only untreated control samples (solid line, closed circles, y = 0.55x-1.2, R^2 = 0.97)

TABLE II. CORRELATION OF DRUG DOSE AND CFU OR TBSA IN GKO MOUSE INFECTION MODEL

Drug	R^2	
	CFU	TBSA
RMP	0.92	0.89
INH	0.59	0.68
MOX	0.91	0.88
PA	0.87	0.14
EMB	0.35	0.44

2.4 Discussion

The ability to rapidly and accurately quantify *M. tb* is essential in anti-*M. tb* drug screening and useful in TB diagnosis. CFU analyses, while representing the gold standard for quantifying viable, cultured bacilli, suffer from the tendency of *M. tb* to clump, its long replicating time and the labor intensity. A number of *M. tb* biomarkers have been proposed [21], some of which may be candidates for quantification employing modern analytical chemistry instrumentation with better precision and sensitivity than conventional methods. In the case of TBSA analysis, as little as 40.5 picograms (10^{-12} g) of pure compound was detected in a single injection using GC-MS/MS.

The mycobacterial cell wall is a complex structure that accounts for 60% of the cellular dry weight and consists primarily of a combination of lipids and carbohydrates. Tuberculostearic acid is a lipid tail of phosphatidyl-*myo*-inositol mannosides (PIMs) formed through the linkage of a phosphatidyl glycerol while PIMs are lipopolysaccharides that directly associate with the *M. tb* primary plasma membrane [6, 72, 73]. Among the most abundant long chain fatty acids containing 14-26 carbons, TBSA is detected in most mycobacterial species but not in mammalian hosts [7, 54, 74]. For this reason detection of TBSA in clinical samples has been explored as a diagnostic biomarker of TB [59-62, 75, 76]. While these represent semi-quantitative measurements of TBSA in human clinical samples, reports performing a validated and selective quantification of TBSA from lung tissue, for use in animal models, were non-existing. According to a recent report hexacosanoic acid (labeled as "C_{26}") can be a secondary biomarker (in addition to TBSA) for *M. tb* in sputum samples [60]. This study also monitored C_{26} as the methyl ester (labeled as "C_{26}ME") in our *in vitro* samples and the response to INH and

RMP was similar to that seen with TBSA (**Figure 10**). However concentrations of C_{26} were approximately 100-fold lower than those of TBSA and provided no additional advantage over monitoring of TBSA.

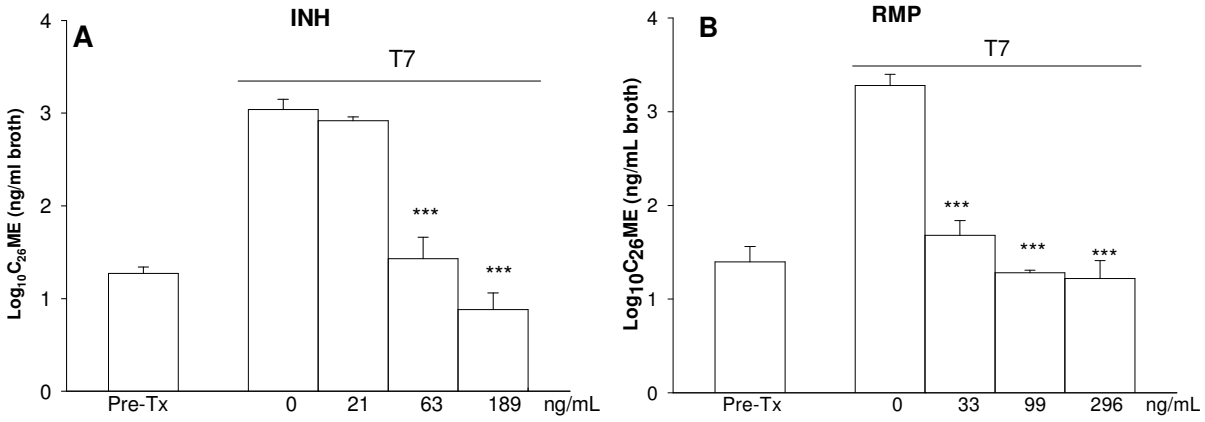

Figure 10. C_{26}ME response to INH (A) and RMP (B). (* 0.01 < p < 0.05; ** 0.005 < p < 0.01; *** p < 0.005)

This study validated TBSA as a quantitative biomarker for *M. tb* in axenic medium, in macrophages and in the lungs of infected mice. That TBSA persists after *M. tb* is no longer able to replicate was clearly evident when monitoring growth in axenic medium. This is consistent with the fact that TBSA is a chemically stable, intrinsic cell wall component. Likewise, once bio-synthesized, TBSA persists, but does not further accumulate in the presence of effective concentrations of bactericidal or bacteriostatic drugs. In both macrophage and GKO mouse experiments there was a higher correlation of TBSA with CFU in *M. tb* that was growing and not exposed to drugs vs. the correlation of these parameters when considering both treated and untreated cultures/mice. This is consistent with the observation that CFU stops/declines more

abruptly than TBSA after drug exposure likely due to the persistence of the marker in dead cells. The stability of TBSA in non-viable *M. tb* limits its utility in drug studies to those that measure inhibition of growth and requires sufficient treatment duration such that significant differences can be observed between treated and untreated cells or mice. Therefore, TBSA can serve as a bacteriostatic, but not as a bactericidal biomarker.

For most drugs the concentration/dosages were highly correlated with TBSA or CFU in both models (**TABLE I**; **TABLE II**) with the exception of 1) EMB by CFU in the macrophage model and by both readouts in the mouse model and 2) PA 824 in the mouse using the TBSA readout where there was no further reduction at dosages above 50 mg/kg/day. The more pronounced dose-responses observed in TB-infected macrophages compared to mice is possibly due to a more direct correlation between the amount of drug applied and the resulting exposure in the former. Although this study failed to demonstrate any heightened sensitivity of TBSA synthesis vs. CFU overall with respect to the response to individual drugs, the results with ethambutol in both macrophages and mice suggested that some degree of decreased TBSA might be tolerated without compromising viability. Ethambutol, a classical bacteriostatic drug, has previously been shown to reduce both the amount of TBSA and octadecenoic acid (18:1) in *Mycobacterium vaccae* growing *in vitro*. Ethambutol inhibits the activity of arabinosyl transferase which in turn is responsible for glycosylation in the biosynthesis of the cell wall-associated arabinogalactan and lipoarabinomannan [77], the result of which is disorganization of the cell wall outer layer, loss of cellular integrity and changes in free lipid composition [7].

When using TBSA as the biomarker for *M. tb* viability in drug screening assays, our goal is to distinguish at least a one $\log_{10}$ difference between treated and untreated samples. The limit

of detection of the GC-MS/MS instrument used in this study is ~10^3 cells/mL broth and 10^4 cells/mL macrophage lysate or per GKO mouse, rivaling the sensitivity of a reporter enzyme-based fluorescence method that can be used in live mice [78]. At this level of sensitivity, inhibition of growth in the lungs of mice by drugs could easily be detected in immune-deficient GKO mice, a model enabling high lung titers of *M. tb* to be achieved prior to significant morbidity and mortality. Based on these results, TBSA-monitored evaluation of drug activity in immune-competent mice should also be feasible using currently available mass spectrometer upgrades that increase sensitivity.

In summary GC-MS/MS based quantification of TBSA is useful for rapidly quantifying the degree of drug-mediated growth inhibition of *M. tb in vitro*, in macrophage culture and in mice and can be used with any strain without genetic manipulation. The processing cost is low and time allowed is as short as less than 24 hrs. The exceptional heat stability of TBSA enables cultures to be autoclaved prior to analysis, simplifying downstream processing and biosafety concerns.

These advantages of TBSA as an *M. tb* biomarker facilitate its utilization in the *in vivo* active principle screening procedures at the earlier stages of purification of single constituents from complex mixtures. Due to the short infection and treatment cycle of GKO mice, relatively large sample numbers of extracts or fractions prioritized *in vitro* can be tested in a single dosage for an efficacy study. At the end of the treatment, the determination of TBSA concentration in the lung tissues using GC-MS/MS provides instant results in comparison with the conventional CFU enumeration. This keeps the total duration of an *in vivo* efficacy study within 25 days.

3. Quantification of TB-specific RNAs with real-time PCR

3.1 Introduction

Determination of CFU remains the routine and gold standard method for enumeration of bacteria in host tissue, while most metabolic surrogates, such as redox dye reduction, fluorescent protein expression, and intracellular ATP measurement, lack sensitivity or specificity for use in samples containing low numbers of *M. tb* and a large amount of host tissue. While the GC-MS/MS quantification of tuberculostearic acid for such a purpose was described in the previous chapter [79], the extraordinary stability of the analyte precludes its use in distinguishing bacteriostatic from bactericidal activity.

Previously, the detection of *M. tb*-specific insertion sequences with high copy numbers, such as IS6110, were reported to be good candidate analytes for clinical diagnosis of *M. tb* infection using DNA-based real-time PCR [80-84]. However, some DNA sequences may not be useful for the assessment of bacterial viability and monitoring growth response to drug therapies due to DNA persistence in the host samples following bacterial death. In contrast, amplification of RNA fragments of *M. tb* in infected host samples provides a determination of viable cell counts since RNA is not easily amplified from dead *M. tb* [85]. The *M. tb* surface protein, antigen 85B (*fbp-B*) [86-88], encoding a mycolyl transferase [89], ranks among the top 25 most abundantly expressed genes of *M. tb* [90]. However, real-time PCR quantification of antigen 85B to monitor the efficacy of drug treatment using the sputum samples of TB patients was shown to have relatively low sensitivity [85, 91]. Alternatively, the mRNA of isocitrate lyase (ICL), an enzyme of the glyoxylate shunt (an alternative pathway to the tricarboxylic acid cycle,

shown to be related to the mycobacterial persistence in macrophages), was proven to be a more reliable biomarker than *fbpB* for *M. tb* viability due to its strong correlation with CFU isolated from patient sputum before and during therapy [92]. Although the mycobacterial genome codes for two *icl* isoforms, *icl1* and *icl2*, there are two domains in the *icl2* sequence that overlap with the sequence of *icl1*, rendering *icl1* twice as abundant in copy numbers as *icl2* [93]. Based on this consideration, *icl1* was selected as another gene target for our *in vivo M. tb* quantification studies, and was anticipated to rival the expression level of *fbpB* with better sensitivity in the mouse samples containing low bacterial titers. In addition, 16S rRNA, the highly expressed housekeeping gene, has served as a target for the assessment of *M. tb* viability. The quantification of 16S rRNA was adopted for its sensitivity and susceptibility to anti-*M. tb* agents in clinical samples, and its correlation to CFU was comparable with *fbpB* and *icl1* [94-98].

Despite recent progress in this methodology, there are no reports of the use of real-time PCR for *M. tb* mRNA quantification in animal tissues, in particular for the purposes of determining bacterial load during growth and drug treatment. In this study, three target RNAs were evaluated for the correlation between the absolute RNA level of target genes using real-time PCR and the CFU counts, and for the determination of the dose responses in mice treated with various anti-*M. tb* agents.

3.2 Materials and methods

3.2.1 *In vitro* correlation of RNA level with CFU

M. tb Erdman (ATCC 35801) was inoculated into 300 mL of Middlebrook 7H9 culture media (Becton Dickinson and Co.) in a 1 L flask and incubated with shaking at 120 rpm for 16 days. A small aliquot was used for CFU determination on Middlebrook 7H11 agar media (Becton

Dickinson and Co.). Eight 10-fold serial dilutions were prepared in triplicate by transferring 5 mL of bacterial culture media into 45 mL of PBS solution followed by thorough mixing. Five milliliters from the final dilution was discarded to keep 45 mL of bacterial culture media in each tube. Following centrifugation at 1485 × g at 25 °C for 10 min, the supernatant liquid was gently decanted. One milliliter of PBS solution was added to the pellets and the tubes were vortexed. After centrifugation as above, the pellets were used for total RNA extraction. An equal volume (5 µL) of total RNA was used for reverse transcription (RT) and PCR.

3.2.2 *In vitro M. tb* growth in axenic medium

M. tb Erdman (approximately 6.4 × 10^2 CFU/mL, in logarithmic growth phase) was inoculated into 400 mL of Middlebrook 7H9 culture media and incubated at 37 °C with shaking at 120 rpm for 18 days. At two-day intervals, 1 mL aliquots of culture were removed in triplicate, a small portion of each was inoculated onto Middlebrook 7H11 agar media for CFU determination, and the samples were then centrifuged at 1485 × g for 10 min at 25 °C. After decanting the supernatant, 50 µL of RNAlater solution (Sigma) was added to each pellet to maintain RNA integrity, followed by a brief vortex and storage at 4 °C. RNA extraction was carried out simultaneously for all samples after the last day of sampling. Equal volumes (14.2 µL) of total RNA were used for RT and PCR.

3.2.3 Correlation of RNA level with CFU in the presence of mouse lung tissue

M. tb Erdman was incubated in Middlebrook 7H9 culture media until reaching plateau phase (4 × 10^7 CFU/mL). Eight 10-fold serial dilutions were prepared in triplicate by transferring 5 mL of bacterial culture into 45 mL PBS. Following centrifugation as described above, the

supernatant was discarded. RNAlater solution was added to the pellets and these were stored at 4 °C. Lung tissue from four uninfected BALB/c mice (female, 19~20 g, Jackson Laboratory) was each homogenized in 3 mL of HBSS. Aliquots (0.5 mL) of the pooled lung homogenate were spiked into each of the bacterial pellets. Each sample was then centrifuged as above, the supernatant was discarded, and the pellets were used for RNA extraction. Five-hundred nanograms of RNA from each sample was used for RT PCR. The lung tissue from five uninfected BALB/c mice was also collected without bacterial spiking to serve as controls.

3.2.4 Acute and chronic growth of *M. tb* in infected BALB/c mice

Female BALB/c mice were infected in an aerosol infection chamber (Glas Col, Terre Haute, IN) with a suspension containing 2×10^6 CFU/mL of *M. tb* Erdman. In the acute infection model, growth was monitored in untreated mice at T3, T10 and T31 post-infection. From T10, a group of 5 mice were treated by oral gavage daily on five consecutive days a week for 3 weeks with 15 mg/kg/day RMP suspended in 200 µL of 0.5% CMC. Mice were euthanized at T31, three days following the final dose. In the chronic infection model, growth was monitored in untreated mice at T45, T73 and T94 post-infection. Starting from T45, 5 mice per group were treated with 15 mg/kg/day RMP for five consecutive days per week for seven weeks. Mice in the chronic model were euthanized at T94, three days following the final dose. Following euthanasia, both lobes of the lungs were homogenized (Pro Scientific pro250 homogenizer, rotor speed: 18,000 rpm) in 3 mL of HBSS. An aliquot was removed for CFU determination on Middlebrook 7H11 agar. Another 0.5 mL of the homogenates was also centrifuged, the pellets were suspended with RNAlater solution, and stored at 4 °C for RNA extraction and RT PCR (500 ng RNA each).

3.2.5 Growth inhibition of *M. tb* in gamma-interferon gene knock-out (GKO) and BALB/c mice treated with anti-*M. tb* drugs

Ninety-two GKO mice (11 weeks old, female, Jackson Laboratory) were infected with *M. tb* Erdman as described above. Growth was monitored by CFU in untreated mice at 3, 10, 17 and 24 days post-infection. Ten days after infection, groups of 5 mice were treated daily for 14 days by oral gavage with one of three two-fold dosages of rifampin (RMP), isoniazid (INH), moxifloxacin (MOX), PA 824 (PA) and ethambutol (EMB), each suspended in 0.5% CMC. All drugs were administered in 200 µL of CMC solution, except for MOX (Bayer) which was delivered in 100 µL, 200 µL and 400 µL of a 1.6 mg/mL stock solution in 0.8% saline (**TABLE III**). Three days following the final dosage, mice were euthanized and both lungs were homogenized in 3 mL of HBSS. After removal of an aliquot for determination of CFU, 0.5 mL of the lung homogenates were centrifuged, supernatants were discarded, and the pellets were preserved in RNAlater solution and used later for RNA extraction. A total of 500 ng RNA from each individual sample was used for RT-PCR.

One hundred and eight BALB/c mice were infected, grouped and treated following a similar protocol as the GKO mice except growth was monitored on T3, T10 and T31 post-infection, and treatment was carried out five days a week for three weeks following the same regimen (**TABLE III**).

TABLE III. DRUG DOSAGES (mg/kg/DAY) USED TO TREAT INFECTED GKO AND BALB/C MICE [a]

	RMP			INH			MOX			PA			EMB		
	L	M	H	L	M	H	L	M	H	L	M	H	L	M	H
GKO	3.75	7.5	15	6.25	12.5	25	8	16	32	25	50	100	100	200	400
BALB/c	5	10	20	6.25	12.5	25	8	16	32	25	50	100	100	200	400

[a] L: Low dose; M: Medium dose; H: High dose.

Another thirty-five BALB/c mice were infected as above for assessment of ecumicin, a new cyclic peptide isolated from an actinomycete strain by Wei Gao at ITR. Ten days after infection, groups of seven mice were treated subcutaneously once daily for 18 days with 32 mg/kg/day (high) or 20 mg/kg/day (low) of ecumicin suspended in micelle solution (formulated by Wei Gao at ITR), micelle solution alone as vehicle, 15 mg/kg/day RMP, or with 0.5% CMC. Mice were euthanized and lung samples were processed as above. CFU enumeration and PCR determination of *icl1* mRNA expression in each mouse were conducted as described above.

3.2.6 Total RNA extraction

One milliliter of Trizol (Life Technologies, Grand Island, NY) was added to each pellet. Sediments were suspended by vortex with 0.2 mL of 0.1 mm glass beads (Biospec, Bartlesville, OK), and the contents were transferred to a screw cap tube. Processing in a Mini-Beadbeater-8 (Biospec) consisted of 3 rounds of pulverization for 30 sec followed by gentle inversion and cooling for 1 min on ice. The samples were then centrifuged at 16,100 × g for 1 min. The Trizol solution in the upper liquid phase was transferred to another new screw cap tube, where 300 µL of chloroform (99+%, Molecular biology grade, Sigma-Aldrich, St. Louis, MO) was added. The tubes were inverted rapidly for 2 min, and centrifuged at 16,100 × g for 10 min. The aqueous layer (upper phase, ~540 µL) was carefully transferred to a new tube containing 540 µL of isopropanol (> 99.5%, Sigma-Aldrich). At this point, *M. tb* in the samples were demonstrated to be non-viable and the tubes can be taken out of the Biosafety Level III lab for the downstream procedures. The tubes were inverted slowly for 2 min and centrifuged at 4 °C for 10 min at 16,100 × g. The isopropanol-water layer was decanted, and the RNA sediment was rinsed with 1 mL of 75% EtOH (Sigma-Aldrich). The tubes were inverted several times and then centrifuged at

4 °C at 16,100 × g for 5 min to re-precipitate RNA. EtOH was decanted from the tubes, and the residual EtOH was discarded by pipette after brief centrifugation. The dried RNA was re-suspended with 90 µL of RNase-free water (Ambion, Austin, TX). The RNA solution was mixed with 10 µL of 10 × DNaseI buffer and 4 µL of DNaseI (Thermo Scientific), and incubated at 37 °C for 30 min. Approximately 416 µL of pure EtOH was then added to the DNase-treated solution to achieve a final concentration of 75% EtOH. After centrifugation for 10 min, the supernatant was removed, the pellets rinsed with 1 mL of 75% EtOH, and re-dissolved in 40 µL of RNase-free water. All RNA extraction procedures were conducted on ice. Two microliters of RNA solution was used for OD260/280, 260/230 and total RNA concentration measurement with the Nanodrop 1000 spectrophotometer (Thermo Scientific, Waltham, MA), using three measurements for each RNA sample. All RNA solutions were stored at -80 °C.

3.2.7 Reverse transcription and real-time PCR

The following reagents (Applied Biosystems, Foster City, CA) were mixed in sterile microtubes on ice to a final volume of 20.5 µL: 14.2 µL of RNA (typically 500 ng) in RNase-free water, 2 µL of RT random primer mix, 2 µL of RT reaction buffer (10 ×), 0.8 µL of dNTP (100 mM), 1 µL of RTase, and 0.5 µL of RNase inhibitor. Reverse transcription was initiated in the thermo cycler (Eppendorf Mastercycler Gradient, Hamburg, Germany) following the temperature cycle setting: 25 °C for 10 min, 37 °C for 120 min, 85 °C for 5 min, and 4 °C before storage of the synthesized cDNA templates at -20 °C.

Taqman probes and primer pairs (**TABLE IV**) for the amplification of *fbpB* [91], *icl1* [92] and 16S rRNA [99] were synthesized by Applied Biosystems in Custom *Taqman* Gene Expression Assay kits. The following reagents were added into each well of a 96-well optical reaction plate

(Applied Biosystems) to create a final volume of 20 µL reaction mixture: 1 µL of *Taqman* gene expression assay (20 ×), 10 µL of *Taqman* gene expression master mix (2 ×, Applied Biosystems), 4 µL of cDNA, and 5 µL of RNase-free water. The plate was tightly sealed and real-time PCR was carried out in an ABI 7900HT Fast Real-Time PCR System following the temperature cycle setting: 1) 95 °C for 10 min, 2) 95 °C for 15 sec, 3) 60 °C for 1 min, with steps 2) and 3) repeated for 40 cycles. The total run takes approximately 1.5 hrs.

TABLE IV. SEQUENCES OF PRIMER PAIRS AND *TAQMAN* PROBES USED FOR QUANTIFICATION OF SPECIFIC RNA PRODUCTS

Target	PCR primer sequence (5' to 3') [b]	*Taqman* probe sequence (5' to 3') [c]	Length of amplicons in bp (5' to 3')
fbpB [a] (X62398.1, 978bp)	F: CGA CCC TAC GCA GCA GAT C R: TTC CCG CAA TAA ACC CAT AGC	TGG TCG CAA ACA ACA C	66 (693 to 758)
icl1 (CP002992.1, 1,287bp)	F: CAC ATC CGC ACT TTG ACG TC R: ATC ACC ACC GTG GGA ACA TC	CTC GGC TCG CGG CCG ATG T	65 (613 to 677)
16S rRNA (X52917.1, 1,464bp)	F: ATG ACG GCC TTC GGG TTG TAA R: CGG CTG CTG GCA CGT AGT TG	CCA CGC CGA CGA AGG TCC GGG TTC TCG CGT GG	109 (370 to 478)

[a] Genbank accession number and length of genes in basepairs;

[b] F, forward; R, reverse.

[c] Probes were labeled on the 5' end with 6-carboxyfluorescein (FAM) and on the 3' end with dihydrocyclopyrroloindole tripeptide minor groove binder (MGB).

3.2.8 Standard curve establishment

Purified double stranded DNA solutions of the amplified *fbpB*, *icl1* or 16S rRNA fragments were obtained individually from the PCR products with QIAquick PCR purification kit (Qiagen). The concentration (C) of each of the three pure DNA solutions was measured with a Nanodrop spectrophotometer in three repeated measurements, and the average value was used for calculations. Sixteen 10-fold serial dilutions of each of the three DNA solutions were prepared independently with RNase-free water. Each diluted solution was used as the cDNA template for real-time PCR amplified with the corresponding primer pairs and probe. Linear correlations between Ct values and $\log_{10}$C of the DNA template in ng/µL were established for each of the three gene targets, and the R^2 values were > 0.99 in all three regressions (**TABLE V**).

TABLE V. LINEAR CORRELATION BETWEEN Ct AND LOG_{10}C OF DNA TEMPLATE IN ng/µL [a]

Gene targets	Equations	R^2
fbpB	y = -3.50x+6.94	0.990
icl1	y = -2.62x+8.41	0.991
16S rRNA	y = -3.24x+15.50	0.994

[a] y = Ct, x = $\log_{10}$C (DNA template in ng/µL)

3.2.9 Statistical analysis

The Ct values were generated in real-time PCR with a manual threshold setting at 0.15 in all circumstances. To calculate the RNA copy numbers ($\log_{10}$RNA) of each gene target in the samples, the equation below was used:

$$Log_{10}RNA = \mathrm{Log}_{10}[4 \times C \times N_A \times (V/v)/10^9/M] \qquad \text{Equation 1}$$

where *C* is the cDNA concentration calculated by Ct values in corresponding regression equations; N_A is the Avogadro constant; *V* is the total volume (μL) of the extracted RNA; *v* is the volume (μL) of RNA used for reverse transcription; *M* is the approximate molecular weight (g/mol) of double strand DNA, which can be calculated using the equation:

$$M = bp \times 607.4 + 157.9 \text{ (by Life technologies)} \qquad \text{Equation 2}$$

where *bp* is length of DNA fragments in base pairs.

The number '4' in **Equation 1** indicates 4 μL of cDNA used for PCR. The term is divided by '10^9' to convert the unit from nanogram (ng) to gram (g). The molar counts of RNA and cDNA fragments were assumed identical after reverse transcription.

Correlation curves were established and correlation coefficients were generated by SigmaPlot 2001. Student's t-tests were processed by comparing the group data against the untreated counterparts with one-tailed distribution and two-sample homoscedastic analysis. Line curves were generated with SigmaPlot 2001 software.

3.3 Results

3.3.1 Correlation of RNA copies with CFU *in vitro*

The $\log_{10}$RNA copy numbers of *fbpB*, *icl1*, and 16S rRNA in the 10-fold serially diluted bacterial pellets showed linear relationship with the actual $\log_{10}$CFU counts within the range of 3.5 and 7.5 (**Figure 11**). The data points tend to plateau off on both ends in a slightly sigmoidal shape for all three species of RNA. The overall $\log_{10}$RNA level of 16S rRNA was greater than that

of *fbpB* and *icl1*, suggesting that 16S rRNA was in highest abundance of all three, and *fbpB* also has greater abundance than *icl1*.

At the lowest CFU density of approximately 32 CFU/mL (log_{10}CFU = 1.5), all three RNAs were still detectable.

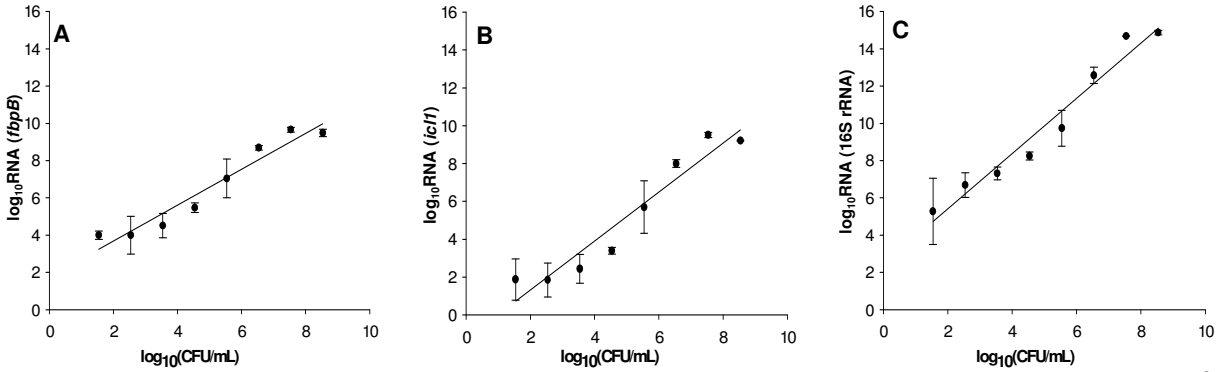

Figure 11. Correlation between log_{10}CFU/mL culture and log_{10}RNA/mL culture of *fbpB* ('A', R^2 = 0.938), *icl1* ('B', R^2 = 0.925), and 16S rRNA ('C', R^2 = 0.961) from real-time PCR analysis in serially diluted bacterial culture media

3.3.2 Correlation of CFU and RNA levels during *in vitro* growth

Starting from the day of inoculation, *M. tb* growth continued gradually in liquid media for 12 days with a 5 log_{10} increase in CFU (gray line in **Figure 12**) before reaching plateau.

The RNA copy numbers of all three genes increased gradually during the 18-day incubation. While the RNA level of *fbpB* remained higher than *icl1* in general, 16S rRNA maintained a significantly higher level throughout the incubation (black lines in **Figure 12**). Linear correlation between CFU and log_{10}RNA of all three genes (R^2 = 0.754 for *fbpB*, 0.723 for

icl1, and 0.816 for 16S rRNA) was obtained in *in vitro* conditions, and 16S rRNA has slightly better correlation than the RNA levels from the other two genes.

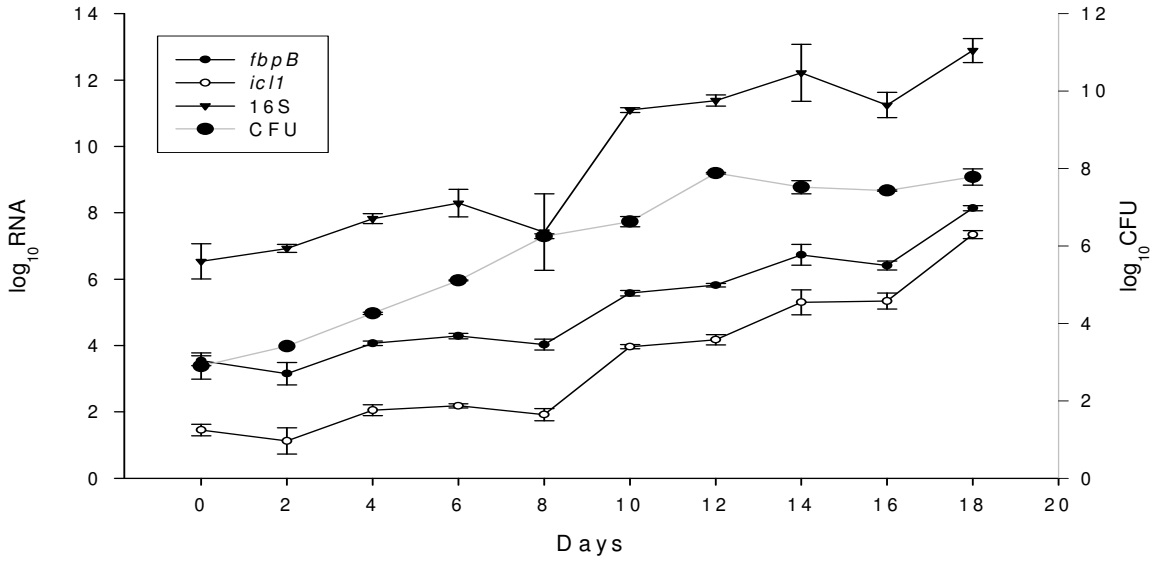

Figure 12. Growth curve in log_{10}CFU/mL culture (gray line), and in log_{10}RNA of *fbpB* (closed dots), *icl1* (open dots), and 16S rRNA (triangles) (black lines)

3.3.3 Correlation of RNA copies with CFU in lung tissue-spiked bacterial culture

Linear correlations were established between CFU counts and RNA copy numbers from the amplification of these three TB-specific genes in the presence of added uninfected lung tissue (**Figure 13**). Although the overall response generates quasi-sigmoidal curves, better linearity was observed between log_{10}CFU values of 2.6 to 6.6. These three correlation curves were all in similar ranges as those established from serially diluted bacterial cultures without spiked lung tissues (**Figure 11**) and again, 16S rRNA exhibited a higher expression level than

either *fbpB* or *icl1*. All three pairs of primers and the probe were specifically targeting *M. tb* RNAs and there was no mismatching of amplicons from the lung tissue genome.

A significant PCR signal was detected for all three RNAs at 4 CFU/mL, the lowest density tested in this quasi-*in vivo* model. None of the three gene targets yielded detectable PCR signal with any of the five control uninfected lung homogenate samples (Ct > 40).

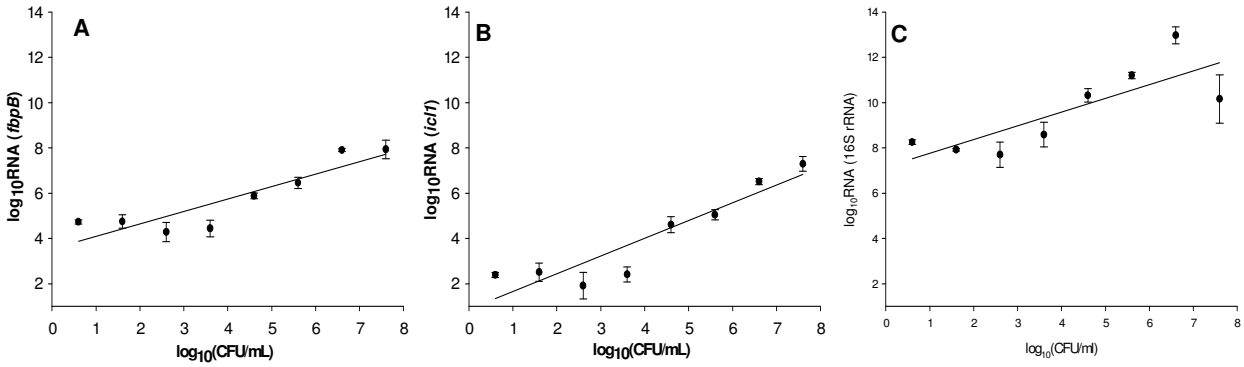

Figure 13. Linear correlation between log_{10}CFU/mL culture and log_{10}RNA of *fbpB* ('A', R^2 = 0.802), *icl1* ('B', R^2 = 0.855), and 16S rRNA ('C', R^2 = 0.641) in serially diluted bacterial cultures spiked with uninfected BALB/c mouse lung tissue

3.3.4 Acute and chronic mouse models of *M. tb* infection

Beginning at day 10 post-infection, *M. tb* CFU increased by 3.3 log_{10} in CFU (from 3.3 to 6.6 log_{10}CFU) in untreated BALB/c mice and by 1.6 log_{10} in mice treated by oral gavage with 15 mg/kg/day RMP from T10 post-infection for three weeks. In a separate chronic infection model in BALB/c mice, growth of *M. tb* reached 6.3 log_{10}CFU after 45 days post-infection, whereupon either RMP or CMC alone (untreated mice) was administered daily by oral gavage for another 7 weeks. The *M. tb* count remained constant from T45 to T94 post-infection in untreated mice,

while it dropped to 3.0 $\log_{10}$CFU on T73 and was maintained at this level until T94 under RMP treatment.

Copy numbers of 16s rRNA, although the highest of the three targets throughout the acute and chronic stages of infection, increased by just over 1 $\log_{10}$ between T10 and T31 in untreated mice while the response to rifampin (a reduction of 0.6 $\log_{10}$) was not significantly lower at the latter time point (**Figure 14**), but achieved a differential of 1 $\log_{10}$ following treatment during chronic infection. In contrast to the other two markers, there was no detectable change between T3 and T10 for *fbpB* and only an increase of 1.7 $\log_{10}$ between the latter time point and T31. The difference in *fbpB* copy number between untreated and rifampin treatment at T31 was 0.8 $\log_{10}$ and at the end of chronic infection (T94) this increased to 1.2 $\log_{10}$. Copy numbers of *icl1* demonstrated the greatest increase (3.9 $\log_{10}$) in untreated mice between T10 and T31 and the largest differential in response to rifampin treatment during acute (1.9 $\log_{10}$) and chronic (2.6 $\log_{10}$) infection.

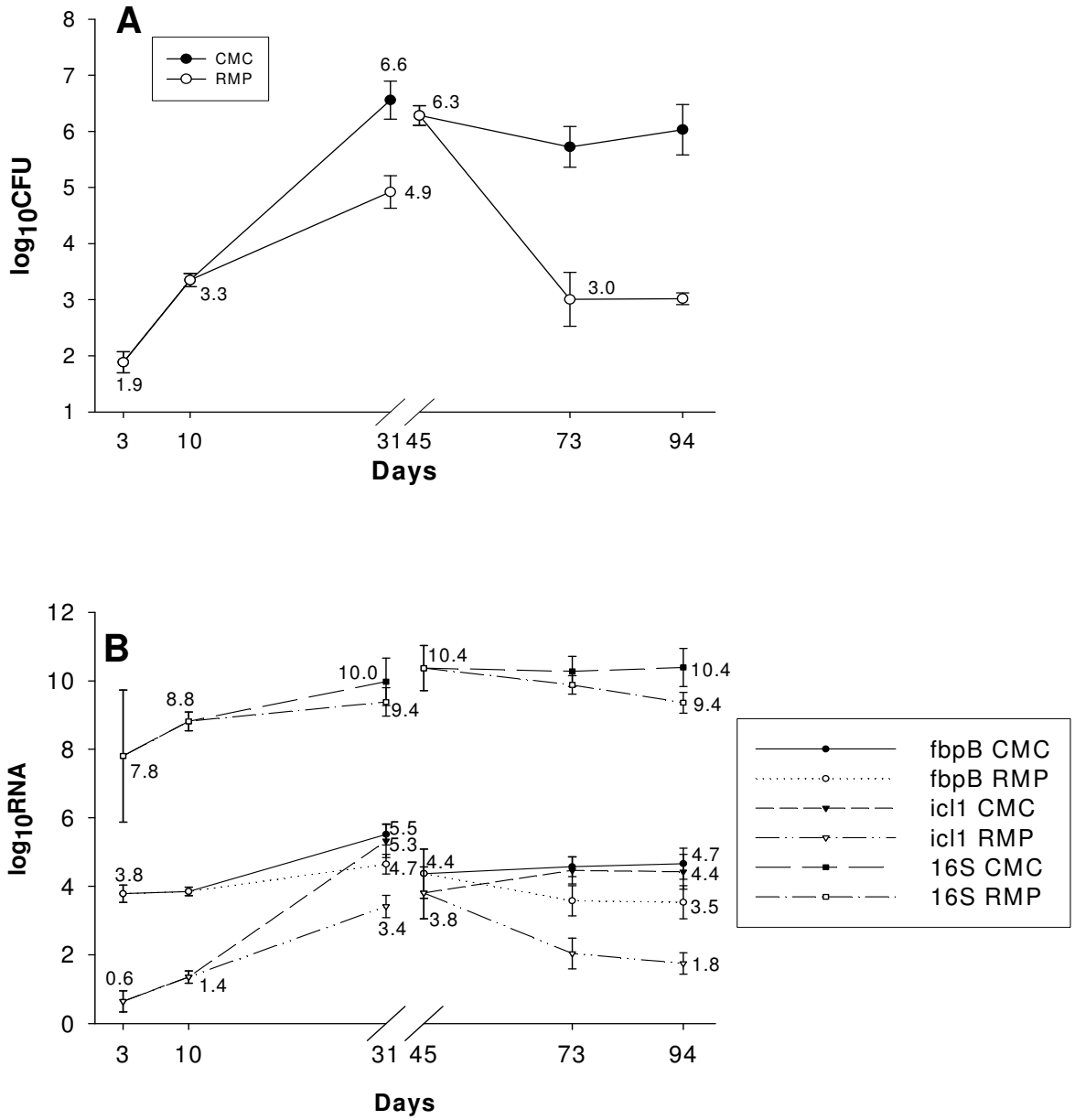

Figure 14. **Growth of *M. tb* in BALB/c mice**. CFU (**A**) and $\log_{10}$RNA of *fbpB*, *icl1*, and 16S rRNA in acute and chronic infection models of BALB/c mice gavaged with CMC or RMP (**B**). Each data point represents the mean of replicate mouse samples.

Correlation coefficients of group-averaged CFU vs. RNA levels of each of these genes (**TABLE VI**) demonstrated good linear relationship between the two quantitative indices in both

treated and untreated control mice. *icl1* and 16S rRNA shared the highest R^2 values in the acute model. Since the differences in *fbpB* and 16S rRNA levels between treated and untreated mice were not as significant as *icl1*, *icl1* appeared superior to the other two RNAs as the bacterial quantitative indicator for *in vivo* samples in both acute and chronic infection models.

TABLE VI. LINEAR CORRELATIONS BETWEEN LOG_{10}RNA AND LOG_{10}CFU IN BALB/C MOUSE ACUTE AND CHRONIC INFECTION MODELS

Groups	R^2 values	
	mRNA targets	log_{10}RNA-log_{10}CFU
Acute	*fbpB*	0.92
	icl1	0.97
	16S rRNA	0.97
Chronic	*fbpB*	0.92
	icl1	0.90
	16S rRNA	0.82
Overall	*fbpB*	0.74
	icl1	0.93
	16S rRNA	0.66

3.3.5 Inhibition of *M. tb* growth in GKO and BALB/c mice treated with anti-*M. tb* drugs

In a GKO model, substantial bacterial growth was revealed in the lungs of untreated mice by both the net increase in CFU (from 2.9 log_{10} in CFU on T3 to 8.0 log_{10} on T24), and in the RNA levels of *fbpB*, *icl1* or 16S rRNA (from T10 to T24). However, the real-time PCR quantification of targets, including the more abundantly expressed 16S rRNA, approached the limit of detection at T3. After 14 days of treatment, with the exception of the lowest dosage of RMA, all three dosages of the five established and experimental anti-*M. tb* drugs effected a

dose-dependent decrease in CFU as well as RNA levels of these genes in the lung homogenates, compared with untreated mice (CMC T24) (**Figure 15**). In general, 16S rRNA > *fbpB* > *icl1*, with respect to copy number.

As expected, in the BALB/c mouse model, bacterial growth was more restricted (increase in CFU from 2.0 $\log_{10}$CFU on T3 to 6.6 $\log_{10}$CFU on T31) than that observed in GKO mice and this was also reflected in the levels of *fbpB*, *icl1* or 16S rRNA in PCR (from T3 to T31). All three dosages (except the lowest dosage of RMP and MOX) of the five drugs effected a significant dose-dependent decrease in CFU as well as RNA levels of the target genes, compared with untreated mice (CMC T31) (**Figure 16**). Levels of 16S rRNA were much greater than those of the other two RNAs, while those of *fbpB* were greater than those of *icl1*, although the variation of *icl1* showed more apparent dose response effects than that of *fbpB* and 16S rRNA.

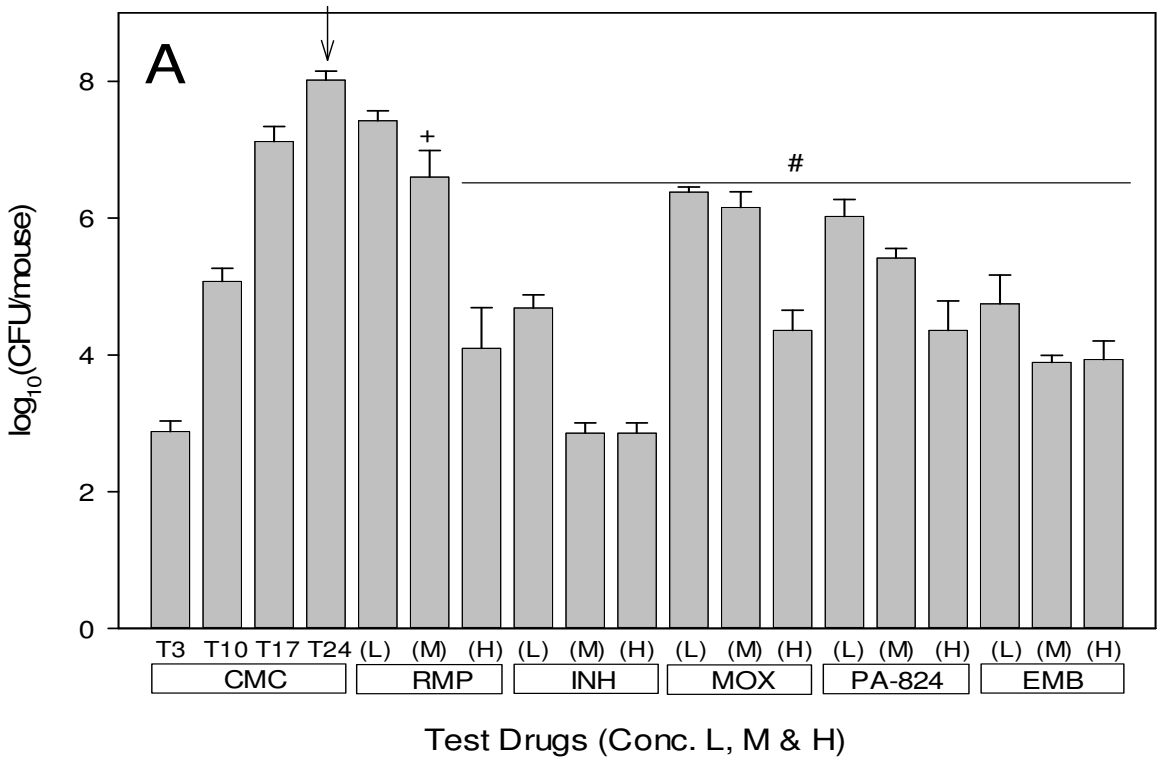
A
log10(CFU/mouse)
0
2
4
6
8
T3 T10 T17 T24 (L) (M) (H) (L) (M) (H) (L) (M) (H) (L) (M) (H) (L) (M) (H)
CMC
RMP
INH
MOX
PA-824
EMB
Test Drugs (Conc. L, M & H)

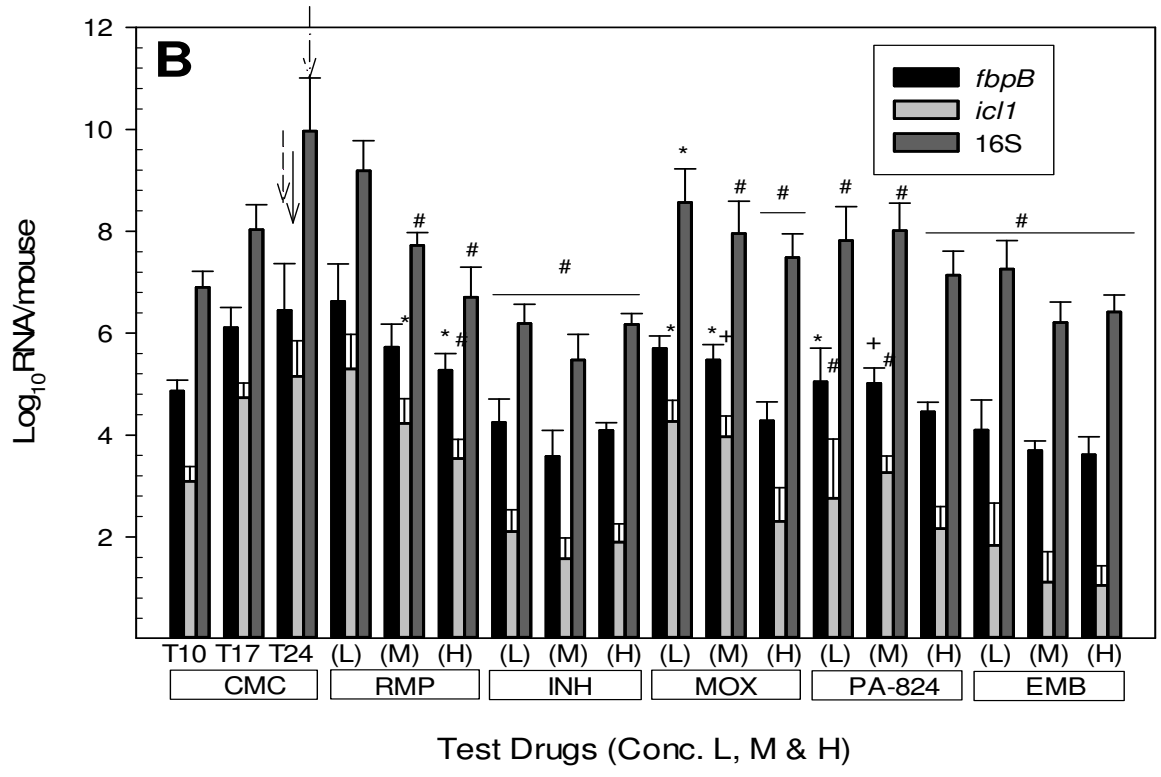
B
fbpB
icl1
16S
Log10RNA/mouse
2
4
6
8
10
12
T10 T17 T24 (L) (M) (H) (L) (M) (H) (L) (M) (H) (L) (M) (H) (L) (M) (H) (L) (M) (H)
CMC
RMP
INH
MOX
PA-824
EMB
Test Drugs (Conc. L, M & H)

Figure 15. Growth inhibition of *M. tb* in infected GKO mice as determined by CFU and transcription levels of the three RNAs. (**A**) CFU enumeration of *M. tb* in infected GKO mouse lung homogenates; (**B**) Log_{10}RNA/mouse of *fbpB*, *icl1* and 16S rRNA in cDNA of *M. tb*-infected GKO mouse lung homogenates. Each data point represents the mean of five replicate mouse samples. L: low dosage; M: medium dosage; H: high dosage. * 0.01 < p < 0.05; + 0.005 < p < 0.01; # p < 0.005 compared with CMC T24, labeled with "↓" for CFU in (**A**), " ↓ " for *fbpB*, "↓" for *icl1*, and " ↓ " for 16S rRNA in (**B**).

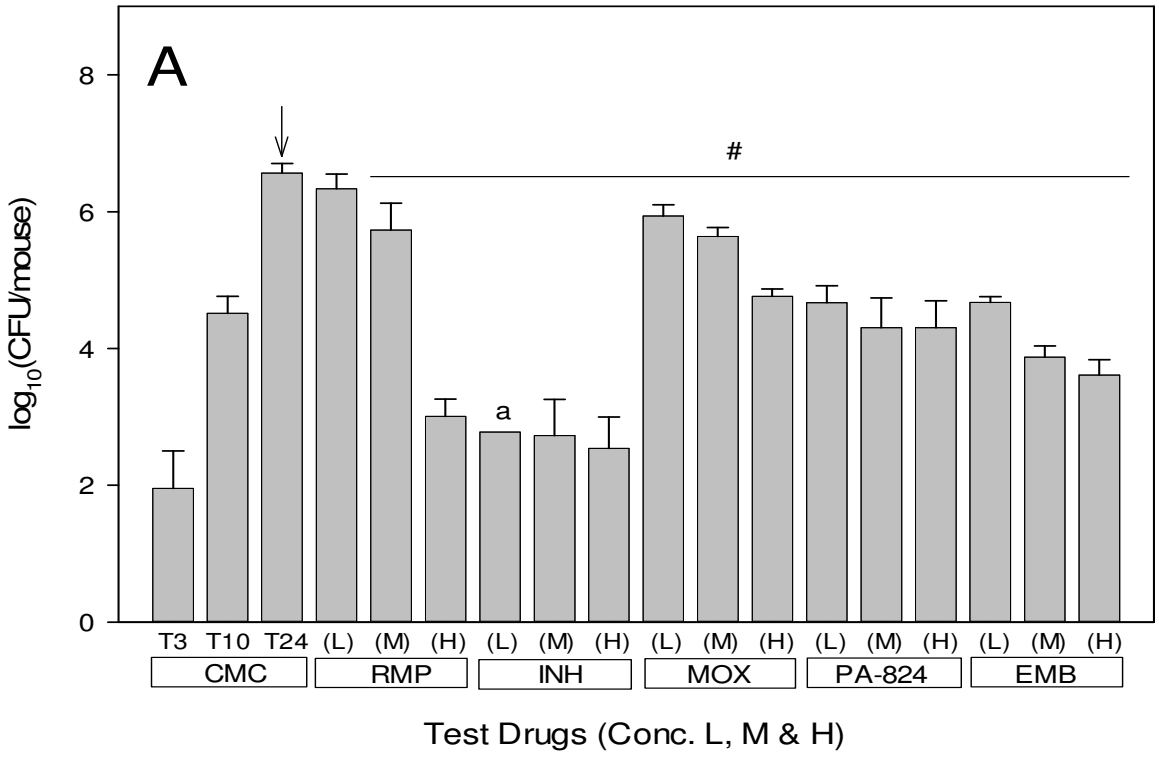

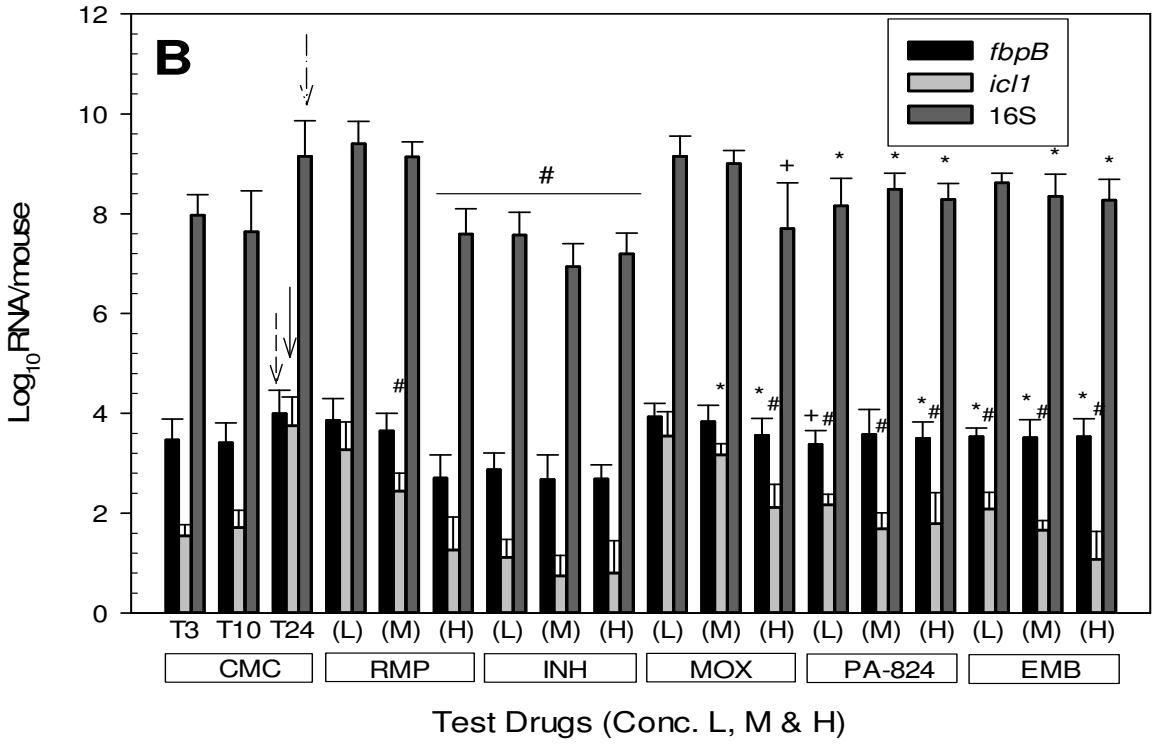

Figure 16. Growth inhibition of *M. tb* in infected BALB/c mice as determined by CFU and transcription levels of the three RNAs. (**A**) CFU enumeration of *M. tb* in infected BALB/c mouse lung homogenates; [a] The six CFU values from the low dosage of INH group were extrapolated due to too high dilution levels that did not cover appropriate countable colonies; (**B**) Log_{10}RNA/mouse of *fbpB*, *icl1* and 16S rRNA in cDNA of *M. tb*-infected BALB/c mouse lung homogenates. Each data point represents the mean of six replicate mouse samples. L: low dosage; M: medium dosage; H: high dosage. * $0.01 < p < 0.05$; + $0.005 < p < 0.01$; # $p < 0.005$ compared with CMC T31, labeled with "↓" for CFU in (**A**), " ⇓ " for *fbpB*, "↓" for *icl1*, and " ⇓ " for 16S rRNA in (**B**).

Linear correlation coefficients (R^2) between log_{10}RNA and log_{10}CFU, log_{10}RNA and dosage, and CFU and dosage in the GKO mouse lung homogenate samples were generated (**TABLE VII**). In the untreated (CMC) group (R^2 = 0.82 in *icl1* and 0.71 in 16S rRNA), the linearity was better than that in the "overall" correlation where all samples were included (R^2 = 0.64 in

icl1 and 0.71 in 16S rRNA). Better correlations were found in the RMP and MOX groups, compared to the other three drugs, consistent with the CFU-dosage correlation in these two groups.

TABLE VII. LINEAR CORRELATIONS IN LOG_{10}RNA-LOG_{10}CFU, LOG_{10}RNA-DOSAGE, AND LOG_{10}CFU-DOSAGE IN GKO MICE

Groups	R^2 values			
	mRNA targets	log_{10}RNA-log_{10}CFU	log_{10}RNA-dosage	CFU-dosage
[a] Overall	*fbpB*	0.66	-	-
	icl1	0.64		
	16S rRNA	0.67		
CMC	*fbpB*	0.64		
	icl1	0.82		
	16S rRNA	0.71		
RMP	*fbpB*	0.51	0.51	
	icl1	0.51	0.64	0.92
	16S rRNA	0.63	0.77	
INH	*fbpB*	0.13	0.00	
	icl1	0.24	0.01	0.59
	16S rRNA	0.17	0.01	
MOX	*fbpB*	0.69	0.81	
	icl1	0.65	0.76	0.91
	16S rRNA	0.21	0.38	
PA 824	*fbpB*	0.31	0.27	
	icl1	0.05	0.12	0.87
	16S rRNA	0.19	0.23	
EMB	*fbpB*	0.17	0.27	
	icl1	0.08	0.20	0.35
	16S rRNA	0.45	0.25	

[a] All samples included

Comparing the three target RNAs in parallel in GKO mice, 16S rRNA had slightly better overall R^2 and better correlations in the RMP group; while *fbpB* had a slightly better R^2 for MOX;

icl1 gave a better RNA and CFU relationship in CMC correlation. There was no significant superiority among any of these three gene targets in correlation to CFU.

Gene expression levels of *icl1* in BALB/c mice (**TABLE VIII**) had much better CFU correlation in almost all groups, compared with those of *fbpB* or 16S rRNA. Levels of *icl1* also demonstrated good correlation with dosages of RMP, MOX, and EMB, consistent with the CFU-dosage correlation in these groups.

TABLE VIII. LINEAR CORRELATIONS IN LOG_{10}RNA-LOG_{10}CFU, LOG_{10}RNA-DOSAGE, AND LOG_{10}CFU-DOSAGE IN BALB/C MICE

Groups	R^2 values			
	mRNA targets	log_{10}RNA-log_{10}CFU	log_{10}RNA-dosage	CFU-dosage
Overall	*fbpB*	0.43	-	-
	icl1	0.70		
	16S rRNA	0.49		
CMC	*fbpB*	0.22		
	icl1	0.63		
	16S rRNA	0.24		
RMP	*fbpB*	0.73	0.61	0.94
	icl1	0.75	0.73	
	16S rRNA	0.81	0.77	
INH	*fbpB*	0.03	0.03	0.07
	icl1	0.03	0.05	
	16S rRNA	0.00	0.05	
MOX	*fbpB*	0.26	0.22	0.93
	icl1	0.83	0.72	
	16S rRNA	0.61	0.55	
PA 824	*fbpB*	0.20	0.01	0.12
	icl1	0.55	0.08	
	16S rRNA	0.07	0.01	
EMB	*fbpB*	0.00	0.00	0.71
	icl1	0.44	0.57	
	16S rRNA	0.10	0.13	

Comparing both models of GKO and BALB/c mice, the following observations are worth further attention: 1) Both *fbpB* and 16S rRNA had much better dose response in the GKO model than in the BALB/c model; 2) The abundance of *fbpB* and *icl1* was greater in GKO mice than in BALB/c mice, while that of 16S rRNA remained almost the same between the two models; 3) In the BALB/c model, *icl1* almost reached the expression level of *fbpB* in the high bacterial titer groups such as T31 CMC and in low dosage of RMP and MOX groups, whereas in the GKO model, the *fbpB* level was much greater than the *icl1* levels in all groups; 4) In BALB/c mice, *fbpB* had very poor dose response, but *icl1* showed a fairly consistent linear relationship with dosages; *icl1* levels had much better correlation with CFU in BALB/c mice.

In a separate *in vivo* study on the anti-*M. tb* efficacy of ecumicin, CFU from BALB/c mice treated with ecumicin, rifampin or vehicle demonstrated good correlation with the expression level of the *icl1* RNA. There was a robust linear correlation between these two values in the groups of mice under different drug treatment (R^2 = 0.993) (**Figure 17**; **Figure 18**). Ecumicin reduced the growth of *M. tb* by 1 $\log_{10}$CFU compared with CMC treated mice, while the difference between the two dosages of ecumicin treatment was not significant. As a control drug, rifampin reduced the growth by more than 3 $\log_{10}$CFU. CMC treated mice showed slightly lower CFU than the micelle vehicle treated counterparts. The level of *icl1* RNA expression was lower than the CFU values in that group due to the inhibitory effect of RMP on RNA polymerase expression.

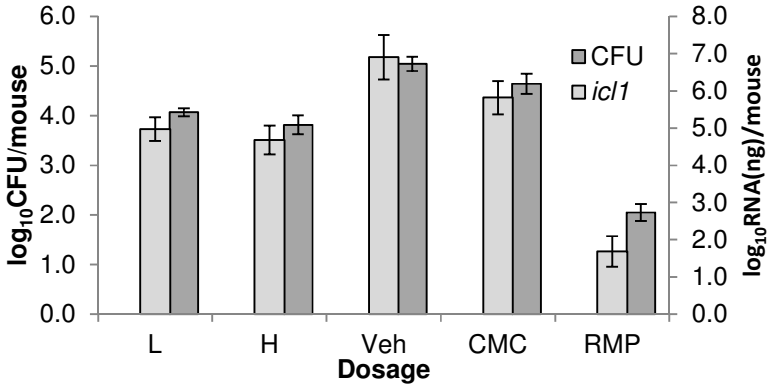

Figure 17. Log_{10}CFU enumeration and log_{10}RNA expression of *icl1* in BALB/c mice. L, Low dosage of ecumicin (20 mg/kg/day); H, High dosage of ecumicin (32 mg/kg/day); Veh=micelle vehicle; CMC=0.5% CMC; RMP=15 mg/kg/day rifampin.

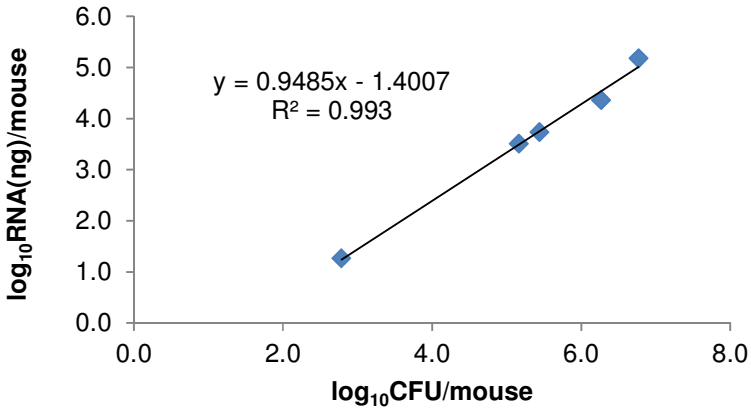

Figure 18. Linear correlation between CFU and *icl1* RNA expression in BALB/c mice

3.4 Discussion

Since its first publication in 1992 [100], real-time PCR, or quantitative PCR, has been exploited for use in numerous molecular biology applications [101]. Quantitative analysis of *Helicobacter pylori* infection in mice was achieved by normalizing bacterial genes in host DNA samples with real-time PCR [102]. In a kinetic infection model of Rift Valley Fever, plaque forming units (PFU) were correlated with viral RNA copy numbers in mouse tissues using

quantitative RT-PCR [103]. Real-time PCR has been applied to the quantitative monitoring of the distribution of fungal infection in mice [104]. Human breast cancer cells genetically tagged with a bacterial vector were quantified by *Taqman* real-time PCR after inoculation into nude mice to trace the metastatic burden in different organs [105]. In all these circumstances, real-time PCR was used for quantification of cellular gene expression levels to detect, target, quantify and even kinetically monitor bacterial or cellular counts in vast matrices, such as murine host tissues.

M. tb quantification with real-time PCR has been applied to TB diagnosis since the early 1990s, mostly through the amplification of DNA sequences of high copy numbers, such as IS6110 [80-84, 106, 107], instead of targeting the more labile and transient messenger RNA fragments that disintegrate rapidly after cell death of the bacteria, and therefore more accurately reflect bacterial growth or bactericidal effects of antimicrobial agents.

In this study, the copy numbers of *fbpB*, *icl1* and 16S rRNA were quantitatively determined by real-time PCR assisted with specific *Taqman* probes in *in vitro* samples from serially diluted *M. tb*, either spiked with uninfected lung tissue or without spiking, in sample aliquots collected throughout different growth phases in liquid culture media, and in lung homogenates of TB-infected mice treated with anti-*M. tb* drugs in both GKO and BALB/c models. RNA copy numbers were calculated from threshold cycles (Ct) and the correlation was established between Ct and concentration of purified cDNA templates, presuming that the RNA extraction rate and reverse transcription rate are both ideally 100%. The RNA levels of each target gene were then correlated with the corresponding *M. tb* CFU counts in each individual sample.

Although the data points in the correlative regression between RNA copies and CFU in serially diluted *M. tb* culture *in vitro* form a slightly sigmoidal shape, either spiked with uninfected mouse lung tissues or without spiking, the overall linearity range reinforces the positive correlation between RNA levels and the CFU counts, which validates the use of real-time PCR to measure the actual bacterial counts in a given TB-infected cellular or animal sample. The differences in bacterial cellular mass used for these two serial dilution experiments *in vitro* may affect the efficiency in RNA extraction, thus possibly explaining the plateau shapes on both ends of the correlation curves.

The limited variation in RNA copy numbers throughout the different growth phases of *M. tb* growth in axenic media suggests that these $\log_{10}$RNA values can be utilized to reflect CFUs in growth monitoring.

It has been demonstrated that *fbpB* and 16S rRNA levels remain higher than *icl1*, but the dose response of these two RNAs to anti-*M. tb* drugs is less pronounced in BALB/c mice; in GKO mice on the other hand, all three RNAs reflected good correlation with CFU and showed consistent relationships with drug dosages (**Figure 16**).

As a component of the 30S small subunit of prokaryotic ribosomes, 16S rRNA is highly conserved between different species of bacteria and commonly used as a signature sequence for bacterial identification [108] including the mycobacteria [109]. The abundance of *M. tb* 16S rRNA was reported to be approximately 100-fold (2 $\log_{10}$) greater than *fbpB* in the sputum samples of infected patients [96]. This coincides with our observation that 16S rRNA has been constantly maintained at a much higher abundance than the other two RNAs.

16S rRNA sequences have been employed for the purpose of quantifying *M. tb* [97, 98], although rRNA is considered to be less responsive than mRNA to drug exposure with respect to correlation with bacterial counts [92]. It was also inferred that there is a period following exposure to drugs during which *M. tb* is no longer cultivable *in vitro*, but rRNA can still be detected with PCR, making rRNA inappropriate for distinguishing viable and dead organisms [94, 95]. These observations are consistent with our own findings in *M. tb* growth and drug susceptibility studies in BALB/c mice where there was an absence of a dose response with respect to 16S rRNR levels. In GKO mice, due to faster growth of *M. tb* in the absence of gamma-interferon, housekeeping genes, such as 16S rRNA, reflected cell viability more quickly, in response to effective drugs.

Antigen 85 complex (*fbp*), which has also been considered to be a housekeeping gene, codes for a secretion product from *M. tb* that stimulates cellular and humoral immunity [86, 88]. The superiority of using the mRNA of antigen 85B to using DNA targets for *M. tb* quantification was clearly illustrated [85, 91, 110], in response to antimicrobial therapies. Antigen 85A, with 73% homology to 85B [88], was shown to cause significant gamma-interferon induction in patients and spleen cells from mice [111]. In BALB/c mice, the immune system quickly responds to such surface antigens of *M. tb* cell wall upon infection and, in consequence, suppresses expression of the *fbpB* gene, which may explain our finding that the *fbpB* levels were greatly reduced in all test groups of BALB/c mice relative to those in the GKO mice.

That the drug dose response of *fbpB* is delayed relative to that of CFU in BALB/c mice, while remaining in parallel in the GKO mice, a tendency similar to that of 16S rRNA, likely reflects the constitutive expression of these abundant functional genes. RNA expression from

these genes maintained survival of the bacteria in hosts, even in a damaged or uncultivable state while exposed to drugs. Meanwhile, these genes still retained some uncontrolled expression within a period of time from drug exposure due to slow degradation [94, 95]. The similarity of the kinetics of *fbpB* and 16S rRNA expression during *in vitro* growth, despite quantitative differences (**Figure 12**), was consistent with a report on the ratio between mRNA and rRNA during the growth of *M. tb in vitro* [112].

Referred to as a required enzyme in maintaining *M. tb* persistence *in vivo*, isocitrate lyase (*icl*) plays an essential role in fatty acid catabolism and virulence where carbon sources are metabolized through the glyoxylate shunt [19, 93]. Interestingly, the level of *icl1* went through regulated stages during bacterial growth and drug inhibition. Firstly, *icl* was apparently up-regulated in *M. tb* from mouse lungs relative to an *in vitro* environment [92, 113]. In the BALB/c acute model, the initial *icl1* expression remained at a fairly low level compared to *fbpB*, but eventually increased steeply attaining a similar level to that of *fbpB* (**Figure 14**). In addition, *icl1* RNA levels approximated those of *fbpB* in the CMC group, low dose RMP and low dose MOX groups in the BALB/c drug treatment study (**Figure 16**). This is consistent with the observation of a strong induction of *icl1* RNA expression *in vivo* while that of *fbpB* remained suppressed.

Secondly, although it has much lower expression levels than *fbpB* and 16S rRNA in *in vitro* culture media and the two mouse models, *icl1* levels demonstrated the most consistent and robust correlation with CFU counts, whether under different doses of drug treatment or in the immune-competent BALB/c model. This was especially evident in the later stages of infection in both BALB/c acute and chronic models, in which an abrupt decline in *icl1* RNA levels occurred in parallel with CFU upon RMP exposure, whereas there was a more modest decline in

the transcriptional levels of the other two RNAs. Similar to *fbpB*, the immune-competent characteristics of BALB/c mice still constrained the overall expression level of *icl1* in contrast to that of GKO mice.

With respect to the effects of the five anti-*M. tb* agents in *in vivo* studies on gene expression, RMP, a known inhibitor of RNA polymerase [114], could directly impact RNA levels. However, there were no outstanding differences between the RNA-dose correlation and CFU-dose correlation in all five drug groups, indicating that the RNA levels responded to different concentration of drug exposure in the same tendency, as did the CFU values. No other obvious drug effects were observed contributing to significant changes in transcription levels of these target RNAs.

In order to identify species-specificity of the three target RNAs, pellets of the centrifuged bacterial culture medium from eight other strains in the *Mycobacterium* genus, other than *M. tb* Erdman, were harvested and real-time PCR was carried out using the cDNA templates from an equal amount (500 ng) of RNA extracted from those pellets. Among the other *Mycobacteria* species, *M. kansasii*, *M. bovis* BCG, and *M. tb* H_{37}Rv also maintained high copy numbers of all three target RNAs that were used to amplify the *M. tb* Erdman; *M. avium* only showed homologous 16S rRNA to that of *M. tb* Erdman (**TABLE IX**). In the phylogenetic tree generated based on 16S rRNA homology [109], all these four above-mentioned *Mycobacterium* species were clustered with a fairly close relationship in the slow grower category. None of the three target RNAs produced any positive hits in the non-infected mouse lung tissues (data not shown). Therefore, the gene amplification method using the primers and probes of these three

selected targets will not bind non-specifically to the host genome sequences, nor to the genome of other species such as *M. smegmatis* within the genus *Mycobacterium*.

TABLE IX. SPECIFICITY OF *fbpB*, *icl1*, AND 16S rRNA IN *MYCOBACTERIAL* SPECIES [a]

	av	sm	ch	tb	ab	ka	bo	ma
fbpB				+		+	+	
icl1				+		+	+	
16S	+			+		+	+	

[a] '+', Ct value determined (< 40) in real-time PCR. av: *M. avium*; sm: *M. smegmatis*; ch: *M. chelonae*; tb: *M. tb* H_{37}Rv; ab: *M. abscessus*; ka: *M. kansasii*; bo: *M. bovis* BCG; ma: *M. marinum*.

In the efficacy study of ecumicin, real-time PCR method was able to quantitatively predict its inhibitory effect on *M. tb* growth *in vivo* within only five days after the tissue samples were obtained, while the CFU enumeration method took as long as three weeks before visible colonies started to form on the agar culture media. The linear correlation between CFU and *icl1* RNA expression confirmed that real-time PCR precisely and much more efficiently predicted the inhibition of *M. tb* growth in advance of CFU.

In conclusion, after preliminary validation studies *in vitro*, using a real-time PCR method, three RNAs, *fbpB*, *icl1*, and 16S rRNA were used to quantitatively reflect *M. tb* burden in lung tissue of infected GKO and BALB/c mice following treatment with five drugs at three dosages. Although highly abundant in copy numbers, *fbpB* and 16S rRNA lagged behind the CFU fluctuation in response to drug exposure in BALB/c mice, thus the dose-response gradients were compromised. *icl1* RNA remained more consistent with CFU in all circumstances, thus representing a superior quantitative marker for monitoring *M. tb* growth inhibition of anti-*M. tb* agents in a mouse model.

4. Phenotypic screening (Methodology)

The 96-well microplate format for antimicrobial screening offers the advantages of small sample consumption, low cost, and compatibility with high throughput automation facilities for sample handling [32]. While most microbial growth can be reflected by the optical density of the culture broth, the quantitative detection of the growth of replicating and non-replicating (NR) *M. tb* has been greatly facilitated by MABA [33] and LORA [115], respectively. These two methods have been adopted for routine anti-*M. tb* and other antimicrobial tests with crude extracts from natural sources, as well as the downstream fractions or purified compounds obtained from chemical purification procedures. The methodologies used in this study included:

- A primary determination of the percentage of inhibition of a test sample on *M. tb* growth relative to untreated bacterial controls to identify samples showing > 90% inhibition;
- The determination of MIC with replicating *M. tb* under normoxic (normal oxygen level) and NR *M. tb* under hypoxic conditions to further prioritize active samples that preferably show < 1 µg/mL MIC values under both conditions;
- The protein MIC shift assay to eliminate samples that could be bound and deactivated by serum proteins;
- The MIC determination with mono-drug resistant *M. tb* strains to deprioritize samples that might be hitting targets exploited by existing anti-*M. tb* drugs;
- The MICs against bacteria other than mycobacteria so as to profile active samples with respect to broad or narrow spectra of activity;

- Enumerating an MBC value to disclose the actual killing efficiency of the test samples on *M. tb*;
- The measurement of cytotoxicity for mammalian cells to provide evidence, in conjunction with MIC and MBC, of selective toxicity.

These phenotypic screening procedures were used throughout the bioassay-guided fractionation (BGF) (see "Section **4.6**"), and utilize empirical cut-off criteria of inhibitory concentrations in the bioactivity tests (**Figure 19**), including > 90% inhibition rate in primary screening, < 1 μg/mL MIC against *M. tb* with either MABA and LORA, > 10 μg/mL MIC against non-*Mycobacterium* strains, > 50 μg/mL IC_{50} reflecting mammalian cytotoxicity, > 50 selectivity index (SI), < 1 μg/mL MBC tested against *M. tb*, and < 1 μg/mL MIC in protein MIC shift assay. In this scheme, only prioritized extracts, bioactive fractions, and purified lead compounds were submitted for *in vivo* potency studies represented by the GC-MS/MS and real-time PCR methods established above, which bypass the routine bioavailability studies of active compounds before *in vivo* studies. The prioritized extracts and fractions were also applied directly to bioautography or qPAR methods to be introduced in the upcoming chapters so that the chemical and biological characteristics of each individual constituent, ideally compound, can be obtained while avoiding the tedious fractionation steps.

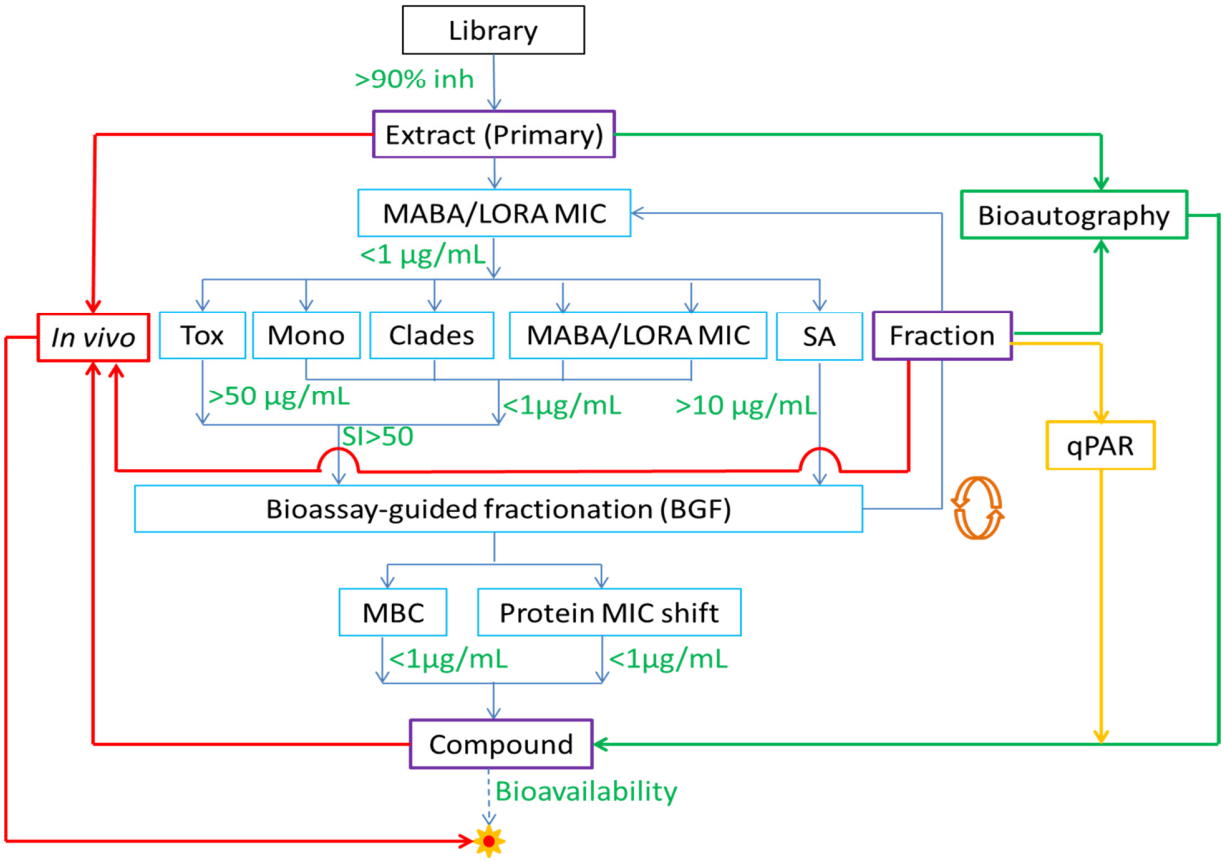

Figure 19. Phenotypic screening flow chart. Primary=primary screening on *M. tb* growth inhibition; Mono=MIC against mono-drug resistant strain; Clades=MIC against clinically isolated clades; SA=spectrum of activity; SI=selectivity index; BGF=bioassay-guided fractionation; MBC=minimum bactericidal concentration.

4.1 Percentage inhibition

4.1.1 Assay plate configuration

In a 96-well clear-bottom assay plate, 100 µL of 7H12 media was added to all wells in rows A and H, and columns 1 and 12; whereas 98 µL was added to all the other testing wells in row B to row G from column 2 through 11 (60 wells), and 2 µL of testing compound was added to the testing wells (**Figure 20**).

A 100 µL inoculum of approximately 1×10^6 CFU/mL *M. tb* in 7H12 media was added to all wells in columns 2 through 12. The plates were incubated for 7 days at 37 °C with 5% CO_2 and 95% humidity. On day 7, 12.5 µL of 20% Tween-80 and 20 µL of Alamar blue (Life Technologies) (or 0.6 mM resazurin dye solution) [23, 33] were added to all wells in columns 1-12 in rows B-G. The plate was incubated for another 24 hrs. Fluorescence was measured at 530 nm excitation and 590 nm emission. Any wells that exhibited inhibition of 90% or greater were considered to be "hits". Percentage inhibition (*%Inhibition*) was calculated as follows:

$$\%\ Inhibition = (Mean_{Bacteria} - Test)/(Mean_{Bacteria} - Mean_{Media}) \times 100\% \qquad \text{Equation 3}$$

	1	2	3	4	5	6	7	8	9	10	11	12
A												
B	Media											Bacteria
C	Media											Bacteria
D	Media											Bacteria
E	Media											Bacteria
F	Media											Bacteria
G	Media											Bacteria
H												

Figure 20. Assay plate configuration for percentage inhibition testing. Shaded grids indicate inoculated wells, in which column 12 was not loaded with test samples.

The working concentration of test samples is empirically 5 µg/mL or 10 µg/mL. Due to the complexity of the sample composition, the 90% inhibition cut-off line for the downstream fractionation is flexible depending on the numbers of hits and the overall efficiency of inhibition within each batch of test samples.

4.1.2 Z' factor calculation

The mean and standard deviation (SD) of "Bacteria" and "Media" columns are calculated for each 96-well plate as positive and negative controls, respectively. Z' factor can be calculated as in the following equation:

$$Z' = 1 - 3 \times \frac{SD_{Bacteria} + SD_{Media}}{|Mean_{Bacteria} - Mean_{Media}|}$$ Equation 4

Z' factor could be a number near 1 or negative. The closer it is to 1, the better the quality of the experiment. A Z' factor larger than 0.5 is acceptable, while Z' factor smaller than 0.5 indicates the experiment may not be reliable.

4.2 Minimum inhibitory concentrations (MICs)

4.2.1 Normoxic condition – microplate Alama Blue assay (MABA)

7H12 culture media was added to the wells of a clear-bottom 96-well assay plate according to the volume configuration in the protocol (**Figure 21**). Testing samples (2 µL) were added to wells in three replicates on each of column 1 through 3 (row A and row H were left blank). A 2-fold serial dilution was carried out by pump-mixing 50 µL of the solution at least 4 times and performing serial 100 µL transfers from column 3 through column 10. The last 100 µL of solution was discarded. A 100 µL aliquot of *M. tb* H_{37}Rv inoculum was added to wells in column 2 through column 11, and the plate was incubated for 7 days at 37 °C with 5% CO_2 and 95% humidity. On day 7, 12.5 µL of 20% Tween-80 and 20 µL of Alamar blue (or 0.6 mM resazurin dye solution) were added to columns 1-12, rows B-G. The plate was incubated for

another 24 hrs and fluorescence was measured. MABA MICs were defined as the minimum concentrations effecting > 90% reduction in fluorescence relative to untreated control cultures in column 11. Bacteria-free, sample-containing controls were used to factor out any background fluorescence by the samples at high concentration in column 1. A standard drug plate was always prepared together in each batch of MIC testing (**TABLE X**). Other than the negative control drug, metronidazole (MET), all of the other five drugs show fairly strong anti-*M. tb* activities in MABA. The MICs of the standard drugs are described in Chapters 7 and 8.

MABA was the routinely used susceptibility test for anti-*M. tb* drug screening throughout the bioassay-guided fractionation procedures. It is a robust, sensitive and relatively low-cost method that gives consistent and comparable results between repeated tests. This method was adaptable to most of the other MIC tests involving different *M. tb* strains and other species from the *Mycobacterium* genus.

	1	**2**	**3**	**4**	**5**	**6**	**7**	**8**	**9**	**10**	**11**	**12**
	Drug	High Conc	Dil 1	Dil 2	Dil 3	Dil 4	Dil 5	Dil 6	Dil 7	Dil 8	Bact Ctrl	Med Ctrl
A												
B	198	98	198	100								200
C												
D												
E												
F												
G												
H												

Figure 21. Volume (µL) of 7H12 media used for MABA plate configuration. Shaded grids indicate inoculated wells. High Conc=highest concentration; Dil=dilution fold; Bact Ctrl=bacteria control; Med Ctrl=media control.

TABLE X. STOCK CONCENTRATION OF STANDARD DRUGS FOR MABA AND LORA [a]

	Stock Concentration (mM)	
	MABA	LORA
RMP	0.4	1.6
INH	0.8	102.4
MET	51.2	51.2
CAP	1.6	32
SM	1.6	3.2

[a] RMP=rifampin; INH=isoniazid; MET=metronidazole; CAP=capreomycin; SM=streptomycin.

4.2.2 Hypoxic condition – low oxygen recovery assay (LORA)

White-bottom 96-well assay plates were used for LORA with the same plate configuration as MABA. The LORA utilizes an *M. tb* strain bearing a pFCA-*luxAB* luciferase gene [115]. A brief sonication (~15 sec) of the bacterial inoculum is required before inoculation into the assay plate. The LORA plates were incubated in an anoxic chamber for 10 days at 37 °C, then exposed to normoxic condition for 28 hrs of oxygen recovery before reading the bioluminescence. Before plate reading, 1% *n*-decyl aldehyde prepared in ethanol was freshly diluted 10-fold with PBS and used as the chemiluminescence reagent. Luminescence was measured immediately after adding 100 µL of the diluted *n*-decyl-aldehyde solution into each well with an auto-injector (Perkin Elmer Wallac 1420 Victor2 Microplate Reader). A standard drug plate was used in parallel with the sample plates in each individual batch (**TABLE X**). Alternatively, in a more recent version of the LORA, MICs were determined with the luciferase-bearing *luxABCDE* strain of *M. tuberculosis* instead of the *luxAB* strain, without any need to add *n*-decyl-aldehyde.

LORA is a specific assay for testing the MIC of samples under low oxygen conditions. INH, a bactericidal drug only to rapidly dividing mycobacteria, is not active against NR *M. tb*,

therefore it shows high MIC in LORA, which serves as an indicator of the quality of the low oxygen condition during each run. Metronidazole also shows weak activity against NR *M. tb*, whereas the other four drugs remain active. The LORA MIC of a test sample is usually higher than its MABA MIC.

4.2.3 Protein MIC shift assay

Bovine serum albumin (BSA, Fisher Scientific) or fetal bovine serum (FBS, Atlanta biologicals, Lawrenceville, GA) were added to culture media in running MABA or LORA to achieve the final concentrations of 4% w/v and 10% v/v, respectively, to assess their effects on the bioactivities of the test samples. Test samples that are easily bound to serum proteins usually show a reduced activity compared with the normal culture conditions which contain only 0.5% w/v BSA. Samples with highly increased MICs in the presence of increased BSA or with FBS, may require excessively high *in vivo* exposures.

4.2.4 Mono-drug resistant strains and clinical isolates

MABA was also used for testing the MICs against strains that are monodrug-resistant and strains representing global clades (clinical isolates). Clinical isolate code X001354 corresponds to an Indo-Oceanic lineage, X004439 and X004244 to East Asian lineages, X005282 and X005319 to Euro-American lineages, X001354 to East African-Indian lineage [116, 117]. Monodrug-resistant strains include *Mycobacterium tuberculosis* resistant to streptomycin (rSM, ATCC 35820), rifampin (rRMP, ATCC 35838), kanamycin (rKM, ATCC 35827), isoniazid (rINH, ATCC 35822), cycloserine (rCS, ATCC 35826), moxifloxacin and capreomycin (rMOX and rCAP, the latter two generated in the Institute for Tuberculosis Research at the University of Illinois at

Chicago). An active constituent is expected to be active against all of these strains if it hits a unique target.

4.2.5 Spectrum of activity (SA)

MICs against *Escherichia coli* (ATCC 25922), *Staphylococcus aureus* (ATCC 29213), *Acinetobacter baumannii* (ATCC BAA-747), *Enterococcus faecalis* (ATCC 29212), and *Pseudomonas aeruginosa* (ATCC 27853) were determined using photometry at OD_{570} after 16 hrs of incubation in 2.2% Mueller Hinton II broth (Becton Dickinson, Sparks, MD), for *Streptococcus pneumonia* (ATCC 49619) at OD_{490} after 20 hrs in 2.2% Mueller Hinton II broth with addition of 2% horse blood, and for *Candida albicans* (ATCC 10231) at OD_{570} after 48 hrs in 1% Cellgro RPMI 1640 media (Mediatech Inc., Manassas, VA) with addition of 1.8% D-(+)-dextrose (ICN Biomedicals, Aurora, OH) and 3.5% MOPS (Acros, NJ). MICs were defined as the lowest concentration resulting in > 90% reduction in absorption relative to untreated control cultures. MICs against *Mycobacterium smegmatis* (ATCC 700084) were determined by the MABA method [118] in a manner similar to that used for *M. tb* except that the cultures were incubated for 72 hrs prior to addition of 0.6 mM resazurin and Tween 80, then fluorescence was recorded after an additional 4 hrs of incubation.

In some cases, antimicrobial agents share similar structural cores or related targets, and therefore exhibit universal antimicrobial activities. Considering the relatively long treatment duration for TB, it is more desirable for an active agent to specifically inhibit only the growth of *M. tb* and not normal flora. The spectrum of activities discloses the specificity of the antimicrobial agents according to the gram reaction, taxonomy, and pathogenicity of the

bacteria. Prioritized extracts or fractions are those that show specific activities against *M. tb*, but low activity against bacteria other than *Mycobacterium* species.

4.3 Minimum bactericidal concentration (MBC)

MBCs were determined using the plate formats and incubation conditions described above for the MABA or LORA, with each sample tested in triplicate rows. On day 0 (for untreated bacterial controls) and again on day 7 for MABA or day 10 for LORA, the contents of the triplicate wells were combined in microtubes which were then centrifuged at 10,000 rpm (Eppendorf centrifuge 5415D, 24-place fixed-angle rotor) for 1 min. The supernatants were discarded and pellets were re-suspended in 500 µL of fresh culture media. Two to three 10-fold serial dilutions of the bacterial suspension were made in PBS buffer solution and then 50 µL was plated on Middlebrook 7H11 agar media in 6-well plates. CFUs were determined after 3-4 weeks incubation at 37˚C. The MBC_{90} was defined as the lowest concentration of the test compound resulting in a one $\log_{10}$ reduction in CFU relative to that determined at T0. Rifampin was used as positive control.

MIC monitors the lowest concentration of a test sample at which the bacterial growth is inhibited, but the viability of the bacteria under this drug concentration is not accurately reflected. The value of minimum bactericidal concentration (MBC)/MIC ratio is often used to determine whether an agent is strongly or weakly bactericidal or completely bacteriostatic.

4.4 Cytotoxicity test

Cytotoxicity IC_{50} determinations with Vero cells (CCL-81, American Type Culture Collection, Rockville, MD) were carried out according to previously published methods [118,

119]. In detail, samples were prepared in DMSO at a stock concentration of 5 mg/mL, while rifampin stock concentration was prepared at 2 mg/mL. Five 3-fold serial dilutions were prepared with D-MEM culture media in a 96-well plate and then inoculated with an equal volume of Vero cell suspension (2×10^4 cells in each well), and incubated at 37 °C for 72 hrs. Plates were washed twice with 100 µL/well HBSS and 100 µL/well D-MEM culture media was added, followed by 20 µL of the mixture (20:1) of MTS tetrazolium reagent and phenazine methosulfate (PMS) (Promega CellTiter 96 Aqueous One Solution Cell Proliferation Assay). Following incubation in a CO_2 incubator for another 2.5 hrs, absorption was measured at 490 nm. Compounds were considered to be cytotoxic, moderately cytotoxic and non-cytotoxic if they yielded IC_{50}s of < 0.5 µg/mL, 0.5 µg/mL-128 µg/mL and > 128 µg/mL, respectively. The IC_{50} for rifampin is approximately 80 µg/mL.

As the final selection determining a successful drug lead as a safe candidate for human consumption, the mammalian cytotoxicity index unveils whether an antimicrobial agent is specifically active on bacteria while not detrimental to human cells, or alternatively the potential activity actually comes from its universal cytotoxicity.

4.5 Selectivity Index (SI)

Given the IC_{50} and the MIC, the selectivity index (*SI*) for a sample can be calculated as:

$$SI = IC_{50}/MIC \qquad \text{Equation 5}$$

The selectivity index provides an essential insight into the combination of antimicrobial activity and toxicity of a test sample. A higher SI predicts a larger therapeutic window, which in turn predicts a more flexible dose range in the subsequent animal studies.

For the purpose of prioritization for further study, the threshold level of activity of extracts, fractions or compounds was empirically defined as 1 μg/mL in MABA including mono-drug resistant *M. tb* strains and clinical isolates representing the various clades. Similarly, the IC_{50} value for Vero cells of a test sample must be > 50 μg/mL. Therefore, a sample showing an SI > 50 μg/mL was regarded as a priority hit. Other target thresholds included MICs > 10 μg/mL against bacterial strains other than mycobacteria, MBCs < 1 μg/mL, and MICs < 1 μg/mL in the presence of serum proteins. These empirical values provide predefined criteria that aid in the selection and prioritization process.

4.6 Bioassay-guided fractionation (BGF)

Starting with prioritized extracts, the fractionation steps were conducted in parallel with bioassays, i.e. bioassay-guided fractionation (BGF). In brief, an empirical scheme of BGF includes a basic C_{18} cartridge fractionation to crudely separate the principles in different chemical classes, fractionation through a Sephadex LH-20 column to separate molecules of different size and polarity, high-speed counter current chromatography (HSCCC) by liquid-liquid partition, and preparative HPLC to obtain finer fractions and eventually pure compounds from all fractions. Thin layer chromatography (TLC) was applied for monitoring the purity of the fractions. High-resolution mass spectroscopy (HR-MS) such as ion-trap time-of-flight mass spectrometer (IT-TOF-MS) was utilized for acquiring the accurate mass (molecular weight) of a pure compound. Elemental composition (molecular formula) can be determined with better

than 5 ppm accuracy using the Shimadzu molecular formula predictor software. Structural elucidation by NMR was followed after a recollection and enrichment of the pure constituents, including data collection of the 1D proton spectrum, HSQC, COSY, HMBC, TOCSY, and ROESY/NOESY, if necessary, with 400MHz or 600MHz nuclear magnetic resonance (NMR) instruments (**Figure 22**). Details of BGF protocols will be discussed in the two examples introduced in Chapters 7 and 8.

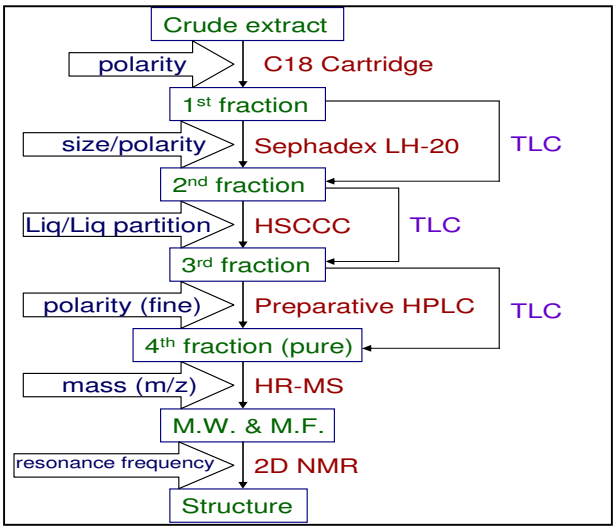

Figure 22. Fractionation scheme

In summary, these phenotypic screening methodologies serve as a series of useful tools for screening, selecting, and prioritizing samples for their robust anti-*M. tb* properties and for selecting samples to be assessed *in vivo*. These well-defined protocols are conducted in high throughput settings, and possess high efficiency and reproducibility.

5. Bioautography

5.1 Introduction

In classical bioassay-guided fractionation, the ambiguity of impurities contained in active fractions can present obstacles in the prioritization procedures on the path to lead compounds. The difficulty in detection, isolation, and characterization of bioactive minor constituents that are often buried under major but less active constituents, has also impeded identification of activities in crude fractions. This situation often results in loss of activity during the isolation procedures, or the dismissal of fractions due to the false interpretation of synergy. Thus, early characterization of active principles in crude fractions during a bioassay guided fractionation procedure is highly recommended, preferably, prior to isolation and purification of the active principles.

The microplate Alamar blue assay (MABA) [23, 33] is characterized by high efficiency and low cost in high throughput screening for anti-*M. tb* constituents, but its capability to interface with the chemical and structural identification of test samples is intrinsically limited. Thin layer chromatography (TLC), however, has the capability of separating constituents in a complex test sample, visualized through photometric or fluorescent properties of the compounds before or after applying colorizing dye reagents. Instead of manipulating one sample at a time as in each injection for HPLC analysis, TLC simultaneously deploys a series of samples for chemical separation in one run.

This TLC-based bioassay methodology adds a new dimension to anti-*M. tb* compound screening, enabling the simultaneous collection of both biological and chemical information of

the anti-*M. tb* active principles. This provides a direct link between bioactivity and chemical properties of the active constituents. In fact, in addition to its use in detecting antimicrobial, antifungal, and antiprotozoal activities, TLC hyphenated with bioautography has also been used in anti-phage, antiviral, and cytotoxicity testing [120]. However, it is a novel technology for *M. tb*, therefore, extensive development has to be done to overcome the challenges presented by such a slow growing pathogenic bacterium.

The original concept of developing a bioautography method for microbiological detection of antimicrobial activities of chemical agents was based upon inhibitory assays in which the test sample diffuses from a disc placed on the surface of an agar plate or a well cut into the agar. In either case, an active substance forms an inhibition zone in the bacterial lawn. The diameter of the inhibition zone is measurable with calipers and thus quantitatively indicative of the antibacterial potency in cases where zone sizes have previously been correlated with MIC determinations [121-123]. Different techniques were introduced to distribute the bacterial inoculum in the agar culture, such as using a roller to spread out the inoculum on the agar surface [124], or mixing liquid culture media with molten agar media held just above the solidification temperature of 40 °C [123].

TLC-linked bioautography for antibacterial activity testing can be categorized into three main versions, i.e., contact-, direct-, and immersion-bioautography [122, 125, 126] (**Figure 23**):

1) The contact method requires the isolated samples on the TLC plate to diffuse onto the inoculated agar through face-to-face attachment of the TLC plate and the agar surface. The efficiency of sample transfer from plate to water-based agar is mostly dependent on the polarity and other physicochemical properties of the constituents. After sample transfer, the

agar plate is incubated without the TLC plate in order to detect growth inhibition of the transferred constituents on the agar.

2) In the case of direct bioautography, an inoculum in liquid culture media is either sprayed onto the TLC plate with a sprayer [127], or the TLC plate is briefly dipped into inoculated bacterial liquid or agar culture media for a few seconds. Both methods produce a thin film of bacteria covering the surface of the developed TLC plate. The culture media-covered TLC plate is then incubated to reveal the growth inhibition on its surface.

3) In the immersion method, a modification of direct bioautography, warm inoculated agar media is poured over the TLC plate or added on its surface with a pipette to form a solidified layer above the plate followed by incubation. The thickness of the agar layer on top of the TLC plate is the factor that differentiates this method from direct bioautography. This method may not be applicable for growth detection of obligately aerobic bacterial species, such as *Staphylococcus aureus* 209P [128].

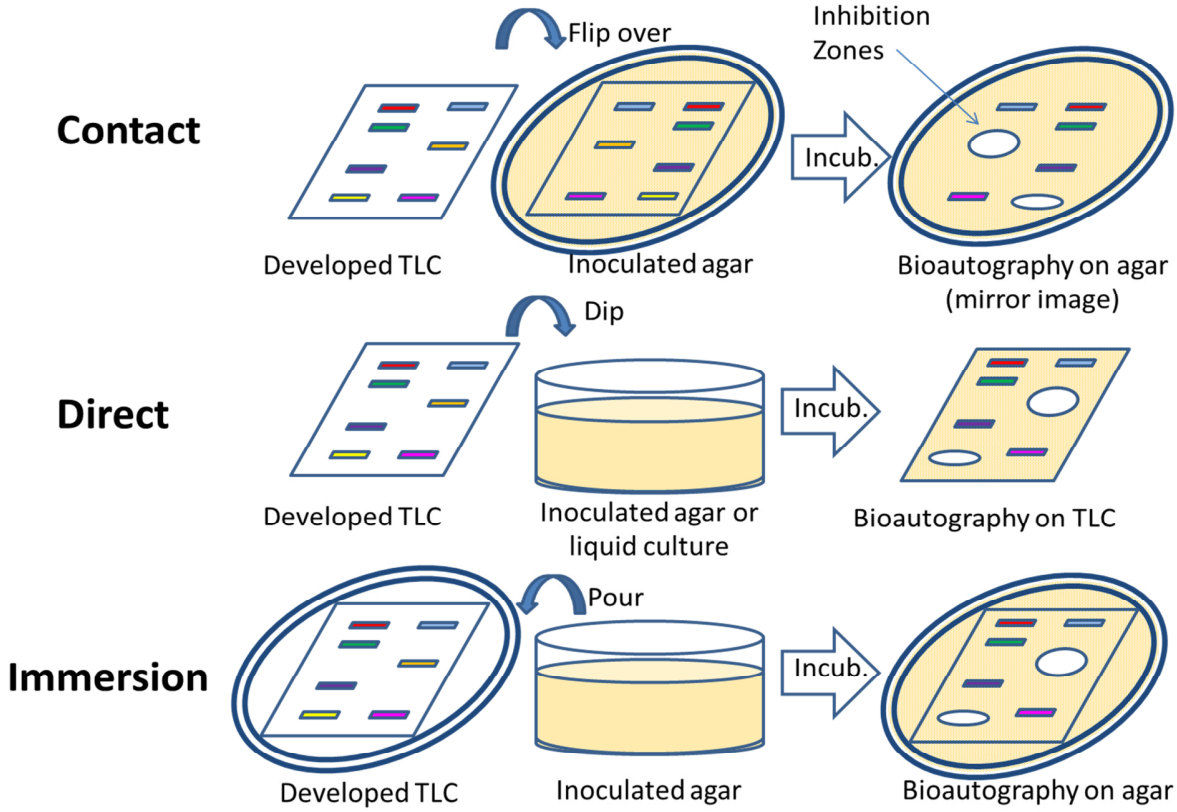

Figure 23. Bioautography methods. After incubation, individual antimicrobial constituents form inhibition zones on the bacterial lawn, as shown by the white circles.

The use of reagents to detect the cellular reductase activity of the microorganism is commonly applied to visualize bacterial growth. The inoculated TLC plate is dipped in an aqueous solution of tetrazolium salts, potential substrates for the reductive enzymatic reaction of bacterial dehydrogenase, such as methyl thiazolyl tetrazolium (MTT), *p*-iodonitrotetrazolium violet (INT), or tetranitro blue tetrazolium (TNBT), then recorded by colorimetry scanner [129]. MTT can also be sprayed onto the surface of the plate to colorize the bacterial zone [121, 124], or the reagent can be readily mixed in the agar. However, this method is not suitable for *M. tb*.

To overcome the difficulty of detecting *M. tb* (and its inhibition zones) due to its slow growth, a non-virulent, luciferase expressing *M. tb* recombinant was constructed, which does not require the addition of dye reagents or further processing. The *luxABCDE* cassette, coding for both the production of luciferase as well as the aldehyde substrate, has been integrated into the *M. tb* genome (**Figure 24**) and has been used to quantify growth *in vitro* and *in vivo* [130, 131]. This modified *M. tb* strain is inherently bioluminescent and if the vector is introduced into an avirulent strain would be able to be used in a biosafety level-2. Thus the detection of anti-TB principles in mixtures could be greatly enhanced by means of the TLC-bioautography method.

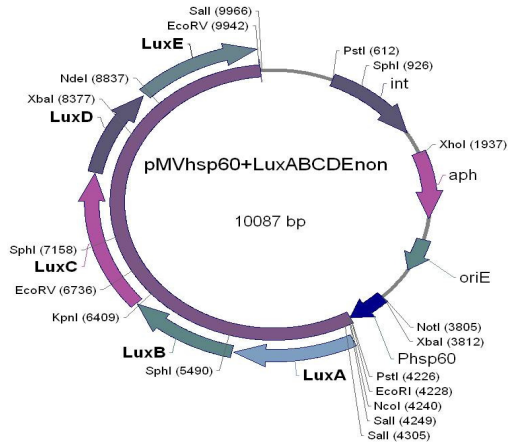

Figure 24. The *luxABCDE* vector

5.2 Material and methods

5.2.1 Construction of the bioluminescent *M. tb* strain

The pMV306hsp60 + *LuxABCDE* vector, created and provided by Dr. Siouxsie Wiles, was incorporated into the avirulent *M. tb* $mc^2$7000 strain. The MABA MICs of 12 drugs against both the recombinant strain and H_{37}Rv was evaluated with a smaller than 2-fold difference between the strains for all 12 drugs, confirming that the bioluminescent strain can serve as a useful surrogate for H_{37}Rv testing of most compounds at the screening stage. Before expressing it in *M. tb*, this vector was used in a transformed *E. coli* strain to assess the production of luminescence.

5.2.2 Working stock preparation

The $mc^2$7000 *luxABCDE* strain was inoculated and incubated for approximately 3 days in 200 mL of Middlebrook 7H9 culture media supplemented with 10% (v/v) oleic acid, albumin, dextrose, and catalase (OADC, Fisher Scientific) and 100 µg/mL pantothenic acid (Sigma-Aldrich). Growth was monitored until the culture reached 0.2-0.3 at A_{570} and > 10,000 RLU per 200 µL.

5.2.3 Contact bioautography

Duplicate TLC plates were prepared using a CAMAG TLC auto-sampler and a CAMAG AMD automatic multi-solvent developing device with a solvent mixture of $CHCl_3$:MeOH = 95:5 as a standard condition. One TLC plate served as a chemical reference and was processed with 0.4% vanillin spray (prepared with 2% sulfuric acid in EtOH).

Inoculated 7H9 broth was diluted with 7H11 agar media (see "Section **5.2.4**"), mixed well, poured into square petri dishes (12cm × 12cm), and allowed to solidify for 30 min. The TLC plate was placed on the surface of 7H11 bacterial agar and held for 15 min at 4 °C. The TLC

plate was then carefully detached from the 7H11 bacterial agar and incubated at 37 °C for 24 hrs. Luminescence image of the agar was recorded by the IVIS instrument (Advanced Molecular Vision, Lincolnshire, UK).

5.2.4 Direct bioautography: dipping the TLC plate into liquid or agar culture broth

In this method, 200 mL of $mc^2$7000 *luxABCDE* culture (OD_{570} = 0.2-0.3) was poured into a sterile CAMAG glass trough and the developed TLC plate was dipped into the culture for 5-10 sec. Then, the TLC plate was placed into a covered petri dish, sealed and incubated at 37 °C for 24 hrs. The plate image in luminescence was recorded by a Xenogen IVIS Spectrum instrument.

In order to apply the direct bioautography method to agar culture media, 200 mL of 7H11 media was autoclaved and cooled to ca. 50 °C and maintained in a thermostatic water bath. A 1:5 fold dilution was made with the $mc^2$7000 *luxABCDE* (OD_{570} = 0.2-0.3) in 7H9 broth and the 7H11 agar media, and poured into the glass trough after gentle mixing. The TLC plate was dipped into the 7H11 bacterial agar suspension for 5-10 sec, and then incubated.

5.2.5 TLC-bioautography with ECUM8412 and E14046 extracts/fractions

The extracts ECUM14046 GE and 14046 GE3 (see “Chapter 7”) were loaded on normal phase TLC plates and developed with a solvent mixture of EtOAc-Toluene-MeOH-HCOOH (95%) = 60:40:5:1. The extracts and fractions ECUM8412 GE, ECUM8412 VC5, and ECUM8412 S1 (see “Chapter 8”) were loaded and developed with a solvent mixture of $CHCl_3$-MeOH = 95:5. The “contact method” was carried out to detect activity according to the protocols described above. The extraction and recollection of the isolated constituents on the TLC plate were accomplished

with a CAMAG TLC-MS interface (CAMAG Scientific Inc.) linked to a solvent pump. The molecular weights of the isolates were confirmed with a Shimadzu IT-TOF-MS.

5.3 Results and discussion

5.3.1 Rifampin inhibition zone

Inhibition of *M. tb* mc^{2}7000-*luxABCDE* by rifampin was determined by luminescence recorded after 24 hrs incubation. The inoculum density varied, from the minimum in panel A through the maximum in panel D (**Figure 25**). An increasing intensity of luminescence was detected from the bacterial lawn in the rifampin-free area, and inhibition zones were clearly distinguished where rifampin was applied. Panel D showed the best resolution of the drug spots, indicating that the level with the highest bacterial inoculum is optimal to visualize inhibition of *M. tb*.

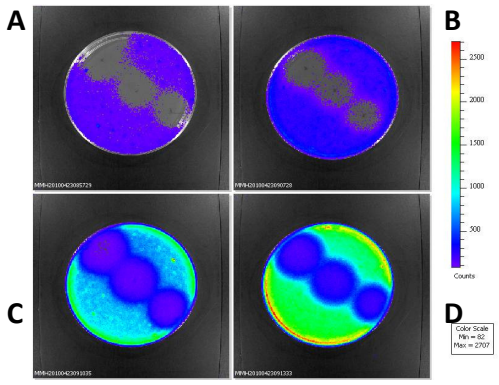

Figure 25. Inhibition zones formed by applying rifampin to the bacterial lawn of *M. tb* mc^{2}7000-*luxABCDE* strain as determined by luminescence. Panel (**A**) through panel (**D**) received an increasing quantity of bacterial inoculum.

5.3.2 Bioautography method

The size of bacterial inhibition zones on TLC plates are influenced by the bacterial growth/metabolism rate, the potency and the physicochemical properties of the drug molecules, most importantly the hydrophobicity, the interaction between drug molecules with liquid or agar culture media. In the “contact method”, the formation of inhibition zones mainly depends on the translocation rate of the compounds from TLC plates to the agar surface. Hydrophilic compounds can easily diffuse into the agar. Hereby, the active compounds become diluted, which makes it difficult to localize or refer to their concentrations. In the “direct bioautography” method, after dipping the TLC plate into the inoculated culture media, gravity affects the efficiency of culture media coverage on its surface. Considerable sample diffusion from the TLC plate may also occur during the dipping procedure. Therefore, a short but efficient dipping time was essential. The “immersion method” provides a more substantial thickness of agar coverage on top of the TLC plate, compared with the direct bioautography method; however, the amount of agar covering the TLC plate may influence the growth rate of inoculated bacteria and the formation of an inhibition zone around the active principles on the TLC plate.

Other environmental factors may affect the formation of inhibition zones. For example, the translocation of the constituents from TLC plates to the agar tends to be slower at lower temperature (4 °C). This prevents the migration of compound molecules through the agar base [132]. In the immersion method, where the warm agar is poured on the developed TLC plate, growth of oxygen-sensitive bacteria will depend on the availability of oxygen at the interface of

TLC and agar layer. To offset the depletion of oxygen in respiration, 0.1% potassium nitrate has been incorporated into the agar [128], to improve bacterial growth.

5.3.3 Bioautography of cyclic peptides

Both ECUM14046 GE and 14046 GE3 (see "Chapter 7") showed visible bands on the developed TLC plate (**Figure 26A**) and significant inhibition (blue spots) of bacterial growth (against the green background) on the bioautography plate (**Figure 26B**). One of the two distinguishable bands of 14046 GE3 (black arrows in **Figure 26A**) was in alignment with the weak band of 14046 GE. Based on the TLC results (see "Section **7.2.2**"), these bands can be assigned to the two anti-*M. tb* cyclic peptides, the hytramycins, which were isolated from these extracts. This assignment was reinforced by the determination of the molecular weights of these isolates on the TLC plate. As the hytramycins in fraction 14046 GE3 were enriched, the bioautography of 14046 GE3 revealed a stronger inhibition zone than the 14046 GE extract.

In the case of the ECUM8412 GE extract and fractions (see "Chapter 8"), a decreasing number of TLC bands was detected in the three consecutive samples, from extract 8412 GE to fractions 8412 VC5, and 8412 S1 (**Figure 26C**). The TLC profile matches the inhibition zones (dark blue spots) determined with bioluminescence (**Figure 26D**). Two bands appeared on a TLC plate with sample 8412 S1 (right lane) -- the upper one as the bioactive xylamycin and the lower one was later identified by the mass spectrometer as an inactive isoflavone dimer. Therefore, the 8412 S1 fraction formed only a single inhibition spot in the bioautography (right lane). In a previous isolation attempt, the isolate (an isoflavone) from the lower band on the TLC was mistaken as the active constituent. With bioautography, the active principle could be assigned to the correct structure.

The mother fraction, 8412 VC5, showed additional bands to those in 8412 S1. Inhibition zones on the bioautography were detected in the area that xylamycin was resolved (middle lane). However, more bioactive compounds were detected, indicating a greater complexity of anti-*M. tb* constituents in this fraction rather than only xylamycin.

Extract 8412 GE (left lane) had a variety of constituents visualized on TLC. The bioautography method revealed a more extensive inhibition zone (purple area) from the starting point to the xylamycin spot. The broader inhibition areas on the bioautography of both 8412 GE extract and 8412 VC5 fraction indicate that the strong antibacterial constituents, the xylamycins, co-exist with other less active ones. These results indicate that some of the bioactive constituents in the mother fraction may be lost during the classical purification procedures and not be detected if the focus is restricted to the chromatographically dominant constituents. The polarity of hytramycins and xylamycin falls in the hydrophobic range, thus the contact method was suitable to transfer the samples from TLC plates to an agar surface efficiently, as well as to retard diffusion of the constituents in the water-based agar.

These two pieces of evidence further consolidated the initial perspective of screening anti-*M. tb* crude extracts with TLC-bioluminescence before running an activity-oriented bioassay-guided isolation, so as to keep track of the actual active constituents rather than the chemically major constituents in the fraction.

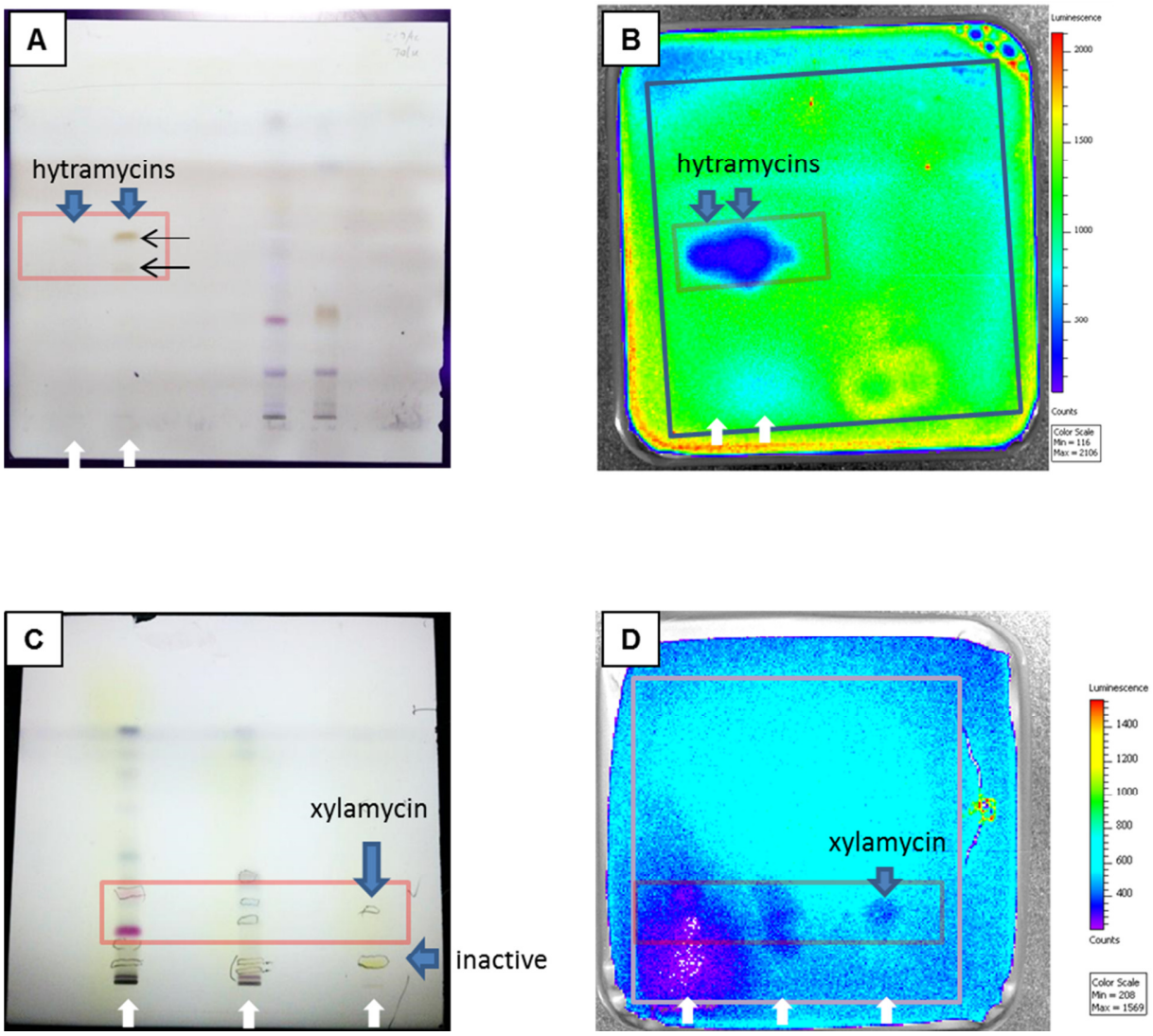

Figure 26. Bioautography of hytramycins and xylamycin. ECUM14046 GE and 14046 GE3 (white arrows) were developed on TLC plates, colorized by vanillin spray (**A**) and anti-TB activity visualized by bioluminescence with the contact method (**B**); Similarly ECUM8412 GE, ECUM8412 VC5, and ECUM8412 S1 (white arrows) were colorized (**C**) and visualized by bioluminescence (**D**).

Previously, TLC methodology has been introduced as a hyphenated adjunct in a variety of bioassays, including antimicrobial activity, enzymatic inhibition, antioxidant testing, and free radical scavenging activity [127]. High-performance TLC has been aligned with GC-MS [129] and

LC-MS [133-135], which allows acquisition of some structural data for specific TLC spots. The chemical structural mapping of the TLC chromatogram can be superimposed with the anti-*M. tb* activity map generated via bioautography and thus the anti-*M. tb* activity can be correlated with the chemical structure of the active constituents, namely, TLC-MS-Bioautography [125]. This multi-dimensional approach optimizes sample resolution, precision, and reliability of bioactivity. Structural information, such as molecular weight of individual constituents in the active principles at the early fractionation level is a major asset for a targeted isolation procedure and therefore a key to a rational search for anti-*M. tb* active principles in complex mixtures.

6. Quantitative purity-activity relationship (qPAR)

6.1 Introduction

The conventional natural product drug discovery process relies on classical bioassay-guided fractionation to isolate individual bioactive constituents. However, the risk of loss or partial loss of bioactivity during the fractionation often diminishes the efficiency of discovering potent compounds. One common attribute to this phenomenon is the neglect of the role of minor constituents, or impurities, in the bioactivity of the overall fraction, co-existing with other abundant constituents, especially when the minor constituents have strong intrinsic bioactivities or interact with major constituents through a synergistic or similar effect. Determination of the relationship of the bioactivity of a fraction with its chemical composition is indispensable at a very early stage of bioassay-guided fractionation to keep track of the most correlated constituents.

A biochemometric approach has been proposed [136] to pinpoint multiple bioactive compounds in ethnobotanicals with the help of a two dimensional strategy using countercurrent chromatography and GC-MS methods. By recognizing the structural characteristics of each constituent referenced by the GC-MS library, biologically significant marker compounds could be identified, inactive constituents could be excluded, and potential loss of active principles could be avoided.

Similar to the theory in the biochemometric approach, a purity-activity relationship (PAR) study permits quantitative evaluation of the effects of multiple minor constituents on the bioactivity of residually complex natural products. In one quantitative PAR (qPAR) study, the

amount of residual complexities (RCs) was measured by quantitative ^{1}H-NMR (qHNMR) evaluation of the purity of each constituent together with the determination of anti-*M. tb* activity of the fractions, both of which were correlated by linear regression analysis, to generate a mathematical qPAR model [137, 138]. Since a lower MIC value reflects greater bioactivity of a fraction, an inverse correlation between the purity of the constituents and the MIC values can be established if the qPAR of a bioactive constituent is monitored; whereas in other scenarios synergistic effects or impurities from RC may alter the trends of the correlation. This method was previously established and verified by Dr. Feng Qiu at ITR.

6.2 Example 1: Dereplication of phytols in *Taxillus chinensis*

6.2.1 Background

Tradition Chinese Medicines (TCMs) give precious guidance on the modern drug discovery knowledge for the treatment of infectious diseases in terms of the sources, processing, and routes of administration of potential drugs in their crude forms. As one of the initial goals was to look for ethno medicines with anti-TB activity, this study included a search on the literature for ethnobotanicals used for tuberculosis treatment in Chinese minority populations. One herbal medicine, a preparation from *Taxillus chinensis* (DC.) Danser (Loranthaceae), was selected for the bioassay-guided fractionation procedure, with the aim of isolating a single potentially bioactive constituent as an anti-*M. tb* drug lead. This section is based on a patent documenting the Chinese “Bai” minority’s recipe for the treatment of tuberculosis in Yunnan province of southwestern China, which used *Taxillus chinensis* as part of a mixture of an herbal medicine. Literature also suggests that parasitic *Loranthus*, another

genus in the same plant family of Loranthaceae, showed inhibitory effects on fatty acid synthase (FAS) in rats [139-141], an enzyme that plays an essential role in the biosynthesis of mycolic acids which eventually construct the impermeable *M. tb* cell wall [142].

In the course of a bioassay-guided fractionation of this traditional Chinese herb, biochromatograms were created based on the anti-*M. tb* MICs of the HSCCC sub-fractions from an initial column chromatography fraction, and compared with the concentrations of a diterpenoid in each sub-fraction, (*E*)-phytol, which was identified as the major bioactive constituent in the *Taxillus* fractions [143, 144]. Correlation of the MICs and the phytol concentrations was established to confirm the *in vitro* anti-*M. tb* activity of this *Taxillus*-derived active principle.

6.2.2 Materials and methods

Twigs (500 g) of *Taxillus chinensis* (D.C.) Danser were purchased from Yin Wall City in the Chinatown of Chicago, IL (voucher specimen to be deposited). After a brief rinse with water, the twigs were soaked in 5 L of ethanol/H_2O (1:1, V/V) overnight. The materials were vacuum-filtered through filter paper (2.7 μm). The filtrate was dried *in vacuo* and then lyophilized to obtain approximately 15 g of extract.

First degree column fractionation: The extract was mixed with an equal weight of polygoprep 100-50 C_{18} (40~63 μm, 100 Å, Macherey Nagel) and loaded onto a C_{18} column [diameter (Φ) 59 mm × 215 mm]. Vacuum column chromatography was used for the fractionation using a 250 mL solvent combination of MeOH/H_2O following the gradient: 100% H_2O, 25% MeOH, 50% MeOH, 75% MeOH, 100% MeOH, and neat CH_2Cl_2 twice, combined, to yield fractions (Fr) 1 through 6. The anti-*M. tb* activity of the fractions was tested with MABA.

Second degree column fractionation: Fraction Fr6 representing the CH_2Cl_2 wash (approx. 693.8 mg) was mixed with 80 g of C_{18} powder, loaded on another column (Φ 30 mm × 230 mm), and fractionated with 80 mL of the elution of MeOH/CH_2Cl_2 gradient: 100%, 90%, 80%, 70%, 60%, 50% MeOH, and neat CH_2Cl_2, yielding sub-fractions Fr6-1 through Fr6-7. MABA was used for testing the anti-*M. tb* activity of these sub-fractions.

GC-MS parameter settings: GC column oven temperature started at 60 °C held for 2 min, rose to 300 °C in a 10 °C/min rate, and held for another 2 min, to make the total run time 28 min. Injection volume was 5 µL. A 1:1 split mode was used. Mass spectrometer was set in MS1 scan mode covering *m/z* 50 to 800. Peak integration was carried out using Agilent MassHunter Quantitative software.

Countercurrent chromatography (CCC) was used in reverse phase (Pharma-Tech Research Corp: CCC-1000) for further fractionation of the sub-fraction Fr6-3. A combination of *n*-hexane:MeCN:MTBE (10:10:1), was chosen as the solvent system running head to tail. The rotation rate was set at 800 rpm. The system was first filled with 130 mL (120 mL in coil and 10 mL in tubing) of the upper phase. A total of 66 mL of the upper phase was extruded after the lower phase was flowing through at a rate of 1.5 mL/min. The sample (3 mL) was injected in 1.5 mL of upper phase and 1.5 mL of lower phase through the injection loop. The volume of mobile phase in the system was 56 mL (66 mL – 10 mL), and stationary phase was 64 mL (120 mL – 56 mL). Therefore, the total volume (V_t) to be collected was calculated according to the volume of mobile phase (V_m) and stationary phase (V_s) in the equation shown below:

$$Vt = Vm + Vs \times K \qquad \text{Equation 6}$$

where the partition coefficient (*K* = 2.5) was used for the estimation of the total volume required for each run.

Thus, the total volume of elute for collection was calculated to be 216 mL. A total of 36 subfractions (6 mL each) were collected for each fraction. The first 16 fractions (96 mL) were combined as the "Front", then each of the next 20 fractions was collected, and finally 66 mL of the stationary phase was extruded. Two aliquots of each of the 20 fractions collected, the CCC "Front", and the stationary phase extrusion were collected, dried and re-dissolved either in MeOH in equal concentration for GC-MS analysis, or in DMSO for MABA MIC determination. (*E*)/(*Z*)-Phytol standard compound (Sigma-Aldrich) was used for GC-MS analysis and MABA test.

Establishment of a biochromatogram, mathematical modeling and statistical processing was accomplished with the Regression function of the Data Analysis module in Microsoft Excel 2010.

6.2.3 Results and discussion

The crude extract of *Taxillus chinensis* and the first degree fractions all showed MICs larger than 100 μg/mL; however, Fr6 showed a 65% inhibition at 100 μg/mL. Most second degree fractions also showed MICs larger than 100 μg/mL, except Fr6-3 which had an MIC of 73 μg/mL.

The GC-MS chromatograms demonstrated the presence of (*E*)-phytol (**Figure 27**) (eluting at 24.5 min) in fractions, Fr6-3 and Fr6-4 (**Figure 28**), based on comparison of the elution time of the two phytol isomers in the commercial standard (**Figure 29**). The concentration of (*E*)-phytol in Fr6-3 was much greater than in Fr6-4. Other peaks in those two fractions mainly represented fatty acids or their esters. (*E*)-phytol was also detected in the "Front" of CCC, but

not in the stationary phase extrusion (**Figure 29**). In the GC-MS chromatograms of countercurrent chromatography fractions, (*E*)-phytol was also detected in the CCC fractions 14 through 16 (**Figure 30**). Peak integration of the GC-MS chromatogram allowed a relative quantification of the concentrations of (*E*)/(*Z*)-phytols in these 20 fractions.

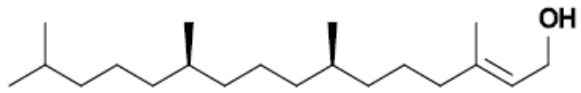

Figure 27. Structure of (*E*)-phytol

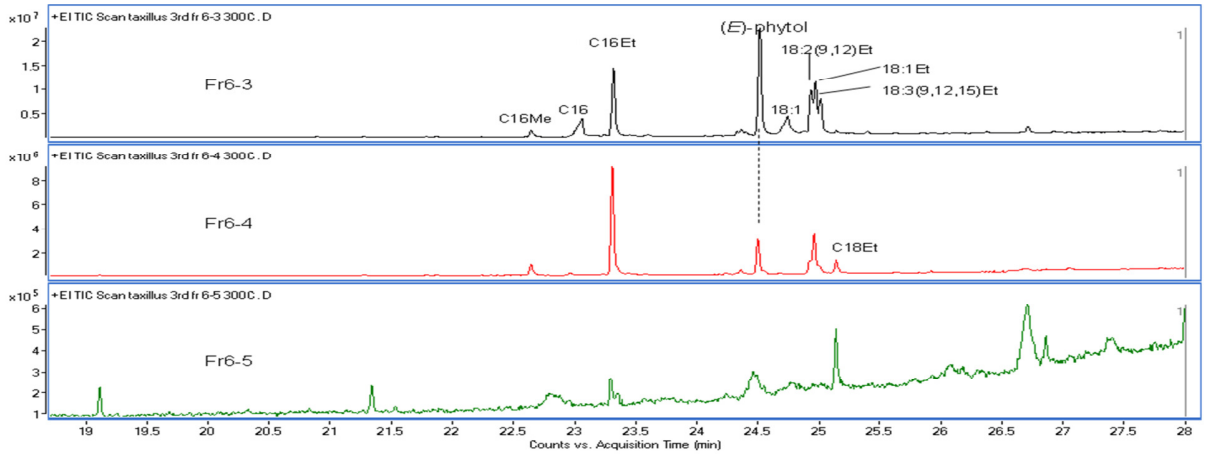

Figure 28. GC-MS chromatogram of Fr6-3, Fr6-4, and Fr6-5. Major peaks in Fr6-3, as identified by the NIST library, include (sorted by elution time): palmitic acid methyl ester (C_{16}Me), palmitic acid (C_{16}), palmitic acid ethyl ester (C_{16}Et), (*E*)-phytol, oleic acid (18:1), linoelaidic acid ethyl ester [18:2(9,12)Et], oleic acid ethyl ester (18:1Et), and α-linolenic acid ethyl ester [18:3(9,12,15)Et]. In Fr6-4, stearic acid ethyl ester (C_{18}Et) was identified.

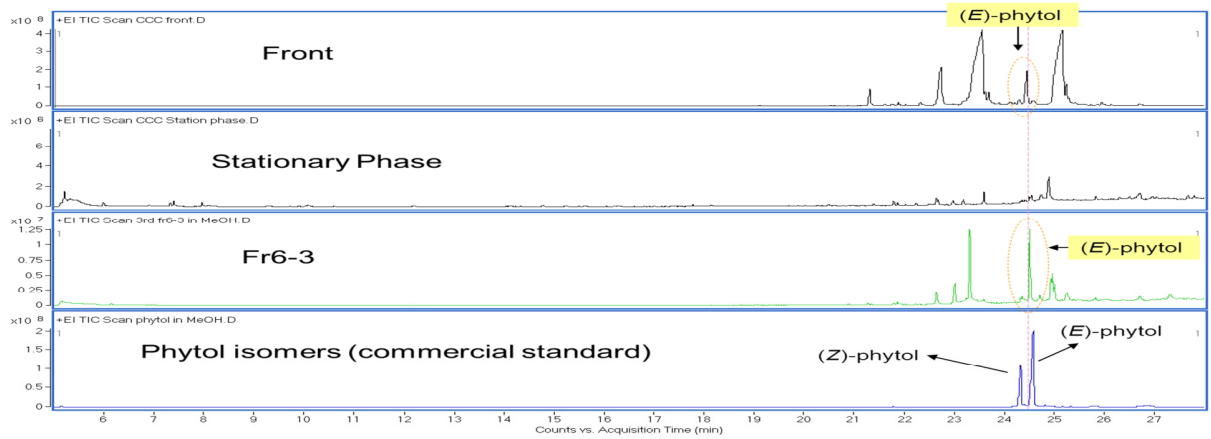

Figure 29. GC-MS chromatogram of the CCC "Front", Stationary phase extrusion, fraction Fr6-3, and commercial standard of phytol isomers

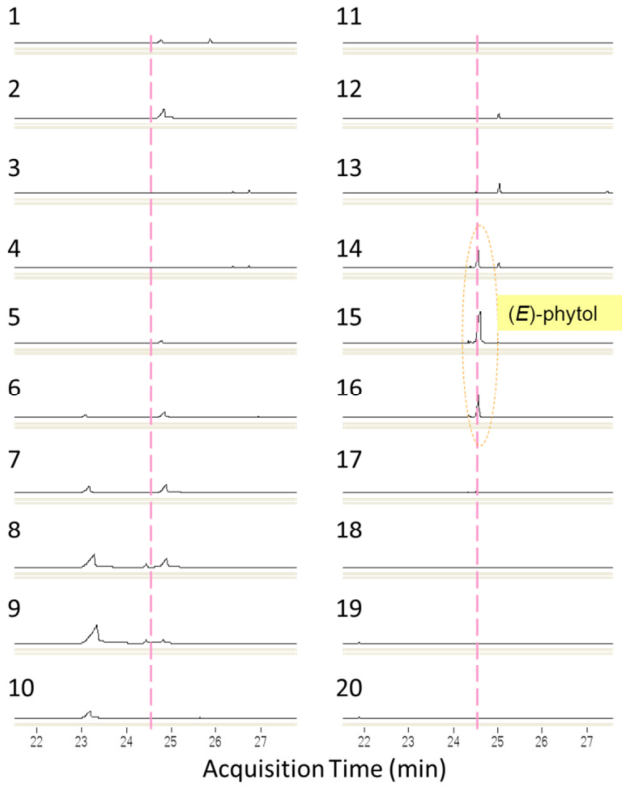

Figure 30. GC-MS chromatogram of 20 CCC sub-fractions, showing (*E*)-phytol, eluted in fractions CCC-14 through CCC-16 at around 24.5 min

Weight (mg) distribution of the 20 CCC fractions, the "Front", and extruded stationary phase are plotted in a figure (**Figure 31A**). The MICs of the 20 CCC fractions are presented in a biochromatogram together with the relative concentration (peak area %) of phytol (**Figure 31B**). Fractions CCC-13 through CCC-16 were anti-TB active, showing lower MICs than the other fractions; CCC-16 had the lowest MIC value of 21 µg/mL. This variation of MICs coincided with the percentage concentration of (*E*)-phytol in these fractions, exhibiting high abundance in fractions CCC-14 through CCC-16. The MIC of extruded stationary phase was > 100 µg/mL, whereas the MIC of the standard of phytol isomers, containing both (*E*)- and (*Z*)-phytols, was 49 µg/mL.

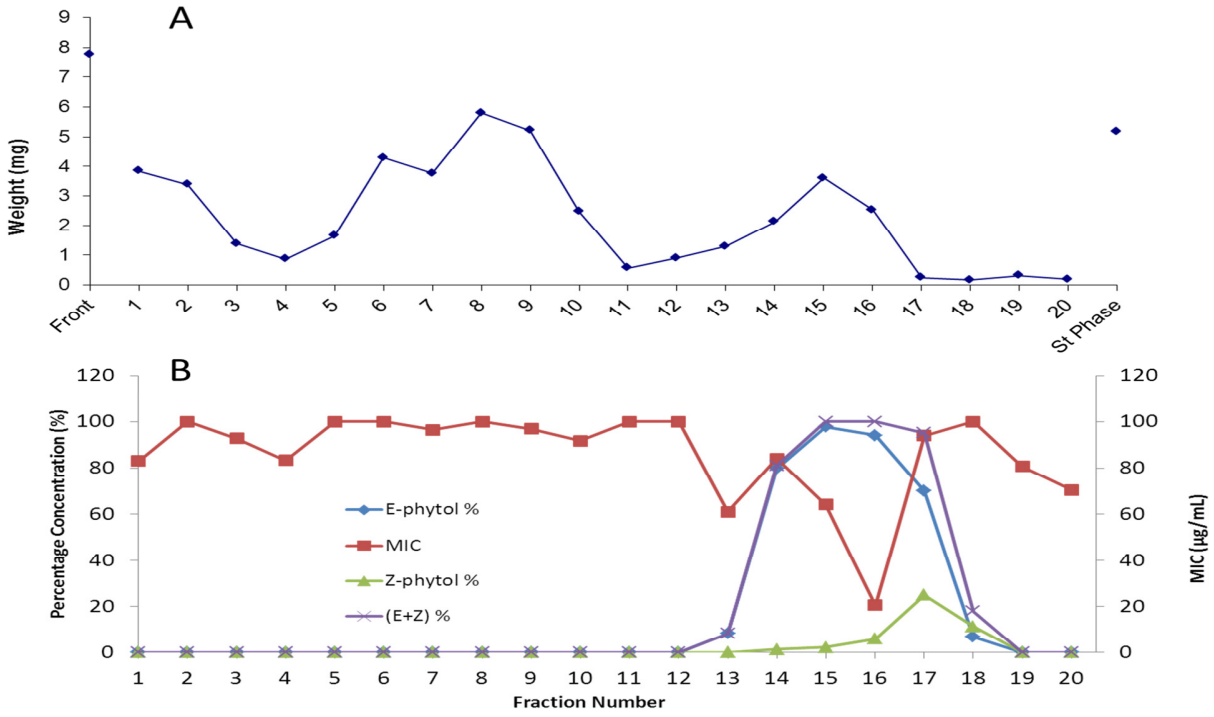

Figure 31. (A) Weight distribution of CCC fractions. Fractions 14 through 16 contain higher concentration of phytols. **(B) Quantitative PAR presentation of the CCC fractions in MICs of each fraction and the percentage concentration (w/w) of phytol**

Other than the major constituents in the fractions, it is not usually easy to determine the bioactivities of each individual minor constituent by means of isolation and purification due to the small amount present. To quantitatively evaluate the effects of (*Z*)-phytol and other RCs, i.e., the components that contribute to the residual complexities of the active fractions, on the MIC variation of (*E*)-phytol as a major active, a mathematical model is established, based on the assumption that the relationship between the concentration of the constituents and the MIC of the fraction is linear, and that the effects of each constituent in a fraction are additive, without synergistic interactions [137]. By fitting the percentage concentration of (*Z*)-phytol and other RC, with the MICs of each of the 20 fractions into a multiple variable linear regression model, the MIC values can be expressed as a linear function of the percentage concentration of (*Z*)-phytol (*Z*) and the degree of residual complexity (*RC*) as below:

$$MIC = 48.6 + 1.48Z\% + 0.43RC\% \ (\mathrm{R}^2 = 0.45) \qquad \text{Equation 7}$$

This function can be interpreted mathematically in terms of how the MIC of (*E*)-phytol can be affected by the amount of (*Z*)-phytol and other RCs added: A) The equation extrapolated in the situation when both Z% and RC% equal zero, i.e., 100% (*E*)-phytol, gives the MIC of the fraction as 48.6 μg/mL. Similarly, if an equation is established in which (*E*)-phytol and RC are independent variables, the MIC of (*Z*)-phytol can also be extrapolated to be 196.2 μg/mL, and the MIC of RC to be 91.1 μg/mL; B) A higher concentration of either (*Z*)-phytol or RC results in a higher MIC of the fraction, defined by the positive coefficients in both terms; C) (*Z*)-phytol,

bearing a larger coefficient than the RC, has a more significant effect on lowering, or antagonizing, the activity of the fractions containing (*E*)-phytol.

By means of this relationship, the MICs of the three constituents in the pure form can be determined without testing in the lab. It is clear that (*Z*)-phytol has less anti-*M. tb* activity compared to (*E*)-phytol, and the RC alone also showed very weak activity. Although the mathematical model does present a theoretical prediction of the MIC of the pure phytols, and explains how these constituents generate the fluctuation of MICs of the fractions, the values extrapolated from the formula can only provide an estimation, especially in this method where the peak areas integrated from the GC-MS chromatograms only represent the percentage concentration of volatile constituents in each fraction, and not to consider those substances that are not detectible in gas chromatography. The R^2 value in the regression equation is also relatively low due to the inclusion of unbiased outliers, such as the data points representing the fractions without phytols.

The anti-*M. tb* effect of (*E*)-phytol has been reiterated repeatedly in literature, but the MICs reported were not consistent values. Using the radiorespirometrical BACTEC method, previously determined MICs of (*E*)-phytol against *M. tb* H_{37}Rv strain have varied substantially from 2 μg/mL [144] to 32 μg/mL [145]. Moreover, the MIC was found to be 100 μg/mL using the same method when a mixture of *cis*- and *trans*-isomers (1:1) was used [143]. In the CCC biochromatogram of the *T. chinensis* fractions, it was shown that the MIC of fraction CCC-16 (MIC=20.6 μg/mL), in which (*E*)-phytol accounted for approximately 94% of the total amount, was lower than that of the standard phytol isomers (MIC=49.1 μg/mL), where the ratio of the amount of (*E*)-phytol to (*Z*)-phytol was about 7:3 as indicated by the integration of the two

peaks in the GC-MS chromatogram. These findings prove that the (*E*)-phytol diastereomer has anti-*M. tb* activity, whereas (*Z*)-phytol, its stereoisomer, impairs the effect of (*E*)-phytol and negatively interferes with its anti-*M. tb* activity. Nevertheless, the biochromatogram reinforces that (*Z*)-phytol, most abundant in the fraction CCC-17 (about 25%), resulted in a much higher MIC (93.9 μg/mL) compared with the adjacent fraction, CCC-16.

From the results of this qPAR model, the anti-*M. tb* activities of these two stereoisomers, (*E*)/(*Z*)-phytols, were clearly distinguished by mathematical extrapolation without testing the MICs of the purified compounds individually. It confirms (*E*)-phytol as the major anti-*M. tb* active constituent in *Taxillus chinensis*, whereas (*Z*)-phytol is not active and antagonistic against the activity of co-existing (*E*)-phytol. This method greatly expedites the identification of bioactive constituents in complex fractions without isolation of each constituent in a pure form.

6.3 Example 2: qPAR of hytramycins in ECUM14046 GE fractions

In this example, the extracted ion chromatograms specifically focusing on the molecular weights of the two hytramycins were applied for quantifying the relative concentration of these two constituents in fractions 14046 GE2 through 14046 GE5. The biochromatograms depicting anti-*M. tb* MIC values of each fraction and the percentage peak abundance of the hytramycins were generated. Linear regression was established between the abundance of either hytramycins and MABA or LORA MIC values. The two hytramycins were confirmed to be major bioactive constituents in the four fractions, whereas the impurities were inactive. Details of the application of this method will be introduced in “Chapter 7”.

7. Discovery of hytramycins, new anti-*M. tb* hexapeptides [1]

7.1 Introduction

The Actinomycetaceae, inhabiting extremely diversified environments where they produce a variety of secondary metabolites [50, 52], have been the source of almost two-thirds of the pharmacophores of clinically used antibiotics, including amphotericin, chloramphenicol, erythromycins, gentamicin, lincomycin, rifamycins, streptomycin, and tetracyclines. Advances in technology have led to a resurgence in the discovery of novel antibiotics from bacterial sources after the decline that followed intensive explorations in the 1950s and 1960s.

Anti-*M. tb* drug discovery from natural sources stagnated and until recently no new drugs have emerged for several decades, not because the resources of the actinomycete treasury had been exhausted but because pharmaceutical research has been focused elsewhere. A large number of nature-derived anti-tubercular antibiotics have been discovered in recent years [45, 46, 48], most of which were found active against *M. tb* in screening panels of other bacteria. This study focuses the screening directly on *M. tb*, therefore, the potential number of new anti-*M. tb* antibiotics to be discovered from actinomycetes still remains enormous.

[1] Contents presented in this chapter has been partially published in: Geping Cai, José G. Napolitano, James B. McAlpine, Yuehong Wang, Birgit U. Jaki, Joo-Won Suh, Seung Hwan Yang, In-Ae Lee, Scott G. Franzblau, Guido F. Pauli, and Sanghyun Cho. Hytramycins V and I, Anti-*Mycobacterium tuberculosis* Hexapeptides from a *Streptomyces hygroscopicus* Strain. *Journal of Natural Products*, 2013, 76(11), 2009-2018 (Appendix G).

7.2 Experimental section

7.2.1 General Experimental Procedures

Optical rotation was measured on a Perkin-Elmer 241 polarimeter (Source: Na, Integration sec = 1, Energy: 85 D.C. microamperes). UV spectra were measured on a SpectraMax Plus384 Spectrophotometer (Molecular Devices, LLC) scanning 200-800 nm, at 2 nm intervals. IR spectra were recorded with a Thermo Nicolet 6700 FT-IR spectrometer (Model: 912A0750) with an ATR unit, by loading the dried samples in MeCN solution. 1D and 2D-NMR spectra including ^{1}H NMR, COSY, HSQC, HMBC, and semi-selective HMBC spectra focusing on 160-180 ppm ^{13}C region were obtained on a Bruker Avance DRX 600 MHz NMR spectrometer with a 5 mm CPTXI Z-gradient probe, whereas a Bruker Avance 400 MHz NMR spectrometer with a 5 mm ATM probe was used to acquire the DEPT-135, NOESY and ^{13}C spectra. HR-ESI-MS data were obtained on a Shimadzu LC-IT-TOF mass spectrometer by flow injection. ^{1}H iterative Full Spin Analysis (HiFSA) was performed with the PERCH software package v.2010.1 (PERCH Solutions Ltd., Kuopio, Finland) (**Appendices C** and **D**) [146].

Both hytramycin V (**1**) and I (**2**) were fragmented using the LC/MS^{2} instrument (AB 4000 Q-TRAP LC/MS/MS system) in the product ion mode. The elution of both compounds in LC was achieved with a gradient of MeCN with 0.1% formic acid (A) and aqueous 0.1% formic acid (B) starting with 75% A from 0-2 min and reaching 75%-95% A over 2-30 min, using an Xterra MS C_{18} column (2.5 µm, 2.1 × 50 mm) and a flow rate of 0.2 mL/min. The mass spectrometer was set up to select *m/z* 634.4 for **1** and *m/z* 648.4 for **2** as precursor ions, followed by the *m/z* range from 50 to 634 and *m/z* from 50 to 648 as the scanning window of the fragments with a scan time of 0.3 sec.

7.2.2 Screening and Prioritization

The Extract Collection of Useful Microorganisms (ECUM), an institute at Myongji University in Korea, maintains a culture collection of over 15,000 actinomycete isolates from Korea, China, Nepal, the Philippines, Vietnam, Antarctica, and the Arctic. The isolates were initially fermented in 20 mL of cultures in 3 different culture media – Glutamine Synthetase System (G.S.S.), Bennett's, and DYC (**Appendix F**). Following fermentation, mycelia and culture media were separated. The mycelium was extracted with methanol, and the culture supernatant was separated by liquid-liquid partition with ethyl acetate and water. Nine extracts were, therefore, generated from each microbial isolate.

Thirty-five thousand actinomycete extracts from ECUM were screened for anti-*M. tb* activity with replicating *M. tb* $H_{37}Rv$ under normoxic conditions using the microplate Alamar blue assay (MABA) [33]. Extracts effecting > 90% inhibition of growth-associated fluorescence were screened against non-replicating cultures of *M. tb luxABCDE* strain (with inherent luminescence) using the low oxygen recovery assay (LORA) [115]. Thirty-seven extracts were prioritized according to both anti-*M. tb* activities. C_{18} cartridge (Varian Bond Elut, 6 mL) fractionation of these 37 extracts was followed by elution of 6 mL of each 17%, 65%, 85%, 95% MeOH in H_2O, and finally CH_2Cl_2, designated as GE1 to GE5. MABA and LORA MIC testing, as well as determination of IC_{50} values against Vero cells were repeated with the five C_{18} cartridge fractions from all extracts. The fraction eluted with 85% MeOH from the EtOAc extract of strain 14046 cultured in G.S.S. medium, designated as "14046 GE3", showed MABA and LORA MIC 0.5 and 1.1 µg/mL, respectively, and the IC_{50} for Vero cells was 71.9 µg/mL. Fractions eluted with 17% and 65% MeOH showed MICs larger than 9 µg/mL tested by either MABA or LORA, while

the fraction eluted with CH_2Cl_2 showed MICs between 2 to 3 µg/mL. The fraction eluted with 95% MeOH had similar MICs and chromatographic profile to that of GE3, but was produced in smaller yield. Fraction GE3 was selected for further purification (**Figure 32**). The scale-up fractionation of 14046 GE (924 mg) was carried out on a C_{18} (polygoprep 100-50 C_{18}, 40~63 µm, 100 Å, Macherey Nagel) column (Φ 30 mm × 230 mm), using the scale-up (80 mL) of the same eluting solvents.

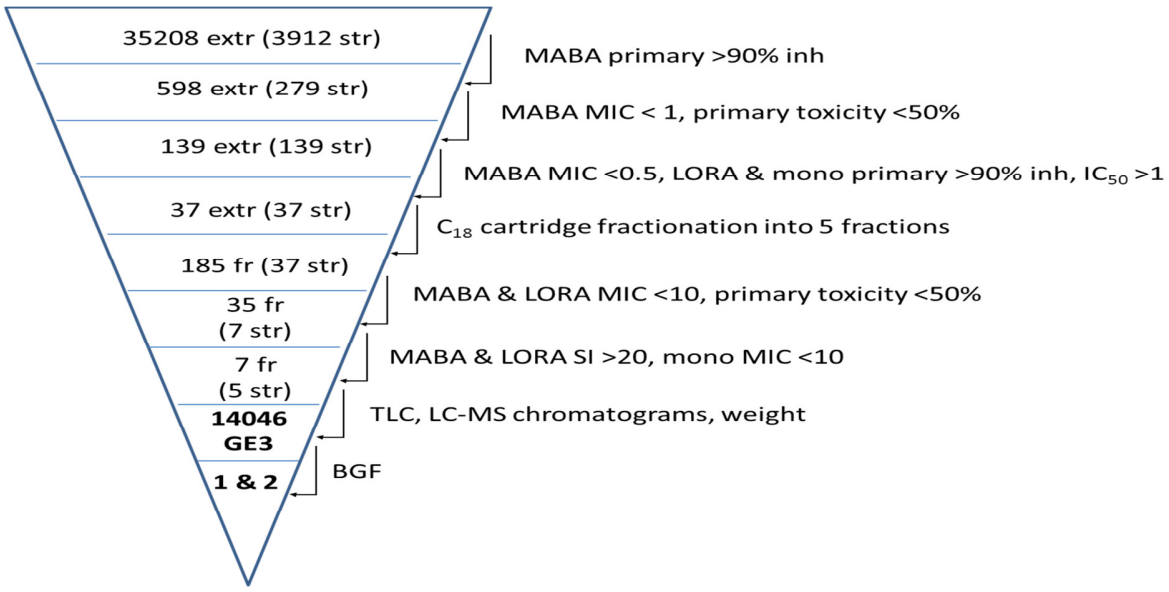

Figure 32. Screening of 14046 GE3 from 35,000 actinomycete extracts. (extr=extract; str=strain; fr=fraction; inh=inhibition; mono=mono-drug resistant *M. tb* strain; SI=selectivity index; BGF=bioassay-guided fractionation)

Thin layer chromatography (TLC; Macherey-Nagel Alugram Sil G/UV_{254}), developed with a solvent system of EtOAc-Toluene-MeOH-HCOOH (95%) = 60:40:5:1 and colorized with vanillin sulfuric acid spray, showed major well-defined bands from 14046 GE3. Preparative HPLC was

carried out on an LC system equipped with 717plus Auto Sampler, Waters 2996 photodiode array (PDA) detector, Waters 600 controller, Waters Delta 600 pumps, and a YMC-pack ODS-AQ C_{18} column (250 × 10 mm I.D., 5 µm, 12 nm). The solvent system consisted of MeCN (A) and 0.1% aqueous formic acid (B) with a gradient of 60-95% (A) over 0-30 min. The flow rate was 1.8 mL/min, and the photodiode array (PDA) detector was set up at the wavelength of 220 nm. The compounds of interest eluted at 24.7 min and 29.0 min, respectively (**Figure 33**).

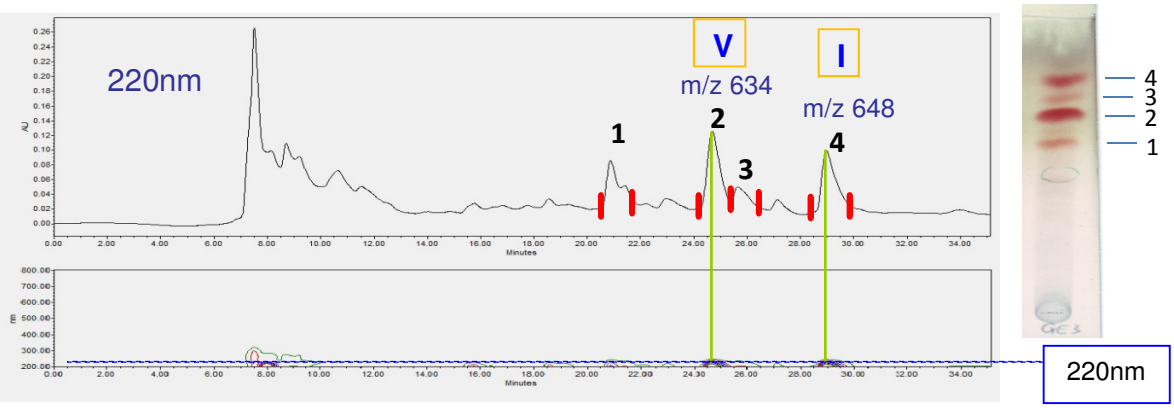

Figure 33. Preparative HPLC and thin layer chromatogram of the constituents contained in fraction 14646GE3

7.2.3 Marfey's experiments

The absolute configuration of the amino acid residues was determined by Marfey's experiment using lab synthesized 1-fluoro-2,4-dinitrophenyl-5-L-alanine amide (Marfey's reagent, L-FDAA) with L-alanine amide (Aldrich) and 1,5-difluoro-2,4-dinitrobenzene (Aldrich) according to established methods [147, 148]. In brief, approximately 5 mg of each of **1** and **2**

were hydrolyzed in 1 mL of 6 N HCl in air-tight containers with an automated microwave synthesizer (CEM Discover Explorer 48, NP-1002) maintained at 180 °C for 10 min. The hydrolysates were air-dried and each dissolved in 50 µL of H_2O. Two hundred microliters of 1% L-FDAA in acetone and 40 µL of 5% aqueous $NaHCO_3$ were added to each solution, and the mixtures were heated at 37 °C on a shaker for 1 hr, followed by the addition of 20 µL of 2 N HCl. The derivatized hydrolysates were then air-dried and re-dissolved in 1 mL of MeCN. LC-MS analyses (Shimadzu LC-MS 2020) were performed on a reverse-phase column (YMC-pack ODS-AQ C_{18}, 250 × 4.6 mm I.D., 5 µm, 12 nm) with a flow rate of 0.5 mL/min. MeCN (A) and 0.1% aqueous formic acid (B) were used as mobile phase following a linear gradient of 40 to 70% (A) in 50 min. The injection volume was 2 µL and UV detection (Shimadzu SPD-M20A Diode Array Detector) was set at 340 nm. Retention time in selective ion monitoring (SIM) chromatograms of derivatized hydrolysates was compared against L-FDAA derivatized amino acid standards. The retention time of the two derivatized piperazic acid stereoisomers, L-FDAA-(D,L)-Pips, was determined in reference to previous reports [149, 150]. At this point, the HPLC retention time of D-Ile is still undistinguishable from that of D-*allo*-Ile (**TABLE XI**).

The elution of L-FDAA derivatized D,L-*N*-methylalanine (TCI, Tokyo, Japan) was performed with the mobile phase consisting of MeCN with 0.1% formic acid (A) and 0.1% aqueous formic acid (B) using a gradient of 40% A to 65% B within 30 min, and with LC-QTRAP detection. L-FDAA-L-*N*-methylalanine eluted at 12.16 min and the D-diastereomer at 12.58 min [151].

TABLE XI. RETENTION TIME OF THE FDAA DERIVATIVES AND SOURCES OF THE UNDERIVATIZED AMINO ACIDS

FDAA derivatives	Retention time (min)	Amino acid source
L-FDAA-L-leucine	21.46	Alfa Aesar, Ward Hill, MA
L-FDAA-D-leucine	26.88	Aldrich
L-FDAA-L-valine	16.57	Sigma-Aldrich
L-FDAA-D-valine	20.74	Aldrich
L-FDAA-L-isoleucine	20.07	Acros Organics, NJ
L-FDAA-D-isoleucine	25.46	Acros Organics
L-FDAA-L-*allo*-isoleucine	20.13	MP Biometricals Ltd
L-FDAA-D-*allo*-isoleucine	25.48	Alfa Aesar
L-FDAA-*R*-Pip	10.45	} Synchem OHG, Felsberg, Germany
L-FDAA-*S*-Pip	11.44	

To determine the configuration of the isoleucine β-carbon in **2**, a chiral column (Crownpak CR+, Daicel Chemical Industries Ltd., 150 × 4.0 mm I.D.) was used with the isocratic elution of 0.5% aqueous formic acid to separate the amino acids with different chiral centers. SIM of the ion with *m/z* 132 was set up in the mass spectrometer. The HCl hydrolysate of **2** showed a D-*allo*-Ile peak at 3.82 min and an L-Leu peak at 4.79 min, while D-Ile eluted at 4.07 min.

Identification of the positions of the three Pip moieties in **1** and **2** was accomplished by performing the advanced Marfey's experiment. D-FDAA was synthesized with D-alanine amide hydrochloride (Novabiochem, Hohenbrunn, Germany) and 1,5-difluoro-2,4-dinitrobenzene (Aldrich). Equal amounts of D-FDAA and L-FDAA (100 μL each, 1% in acetone) were used for Marfey's derivatization of the hydrolysate of **1** and **2**. The retention times of both derivatized L-FDAA and D,L-FDAA of **1** and **2** were determined with the LC-QTRAP system by gradient elution with 40-70% MeCN containing 0.1% formic acid in 0.1% aqueous formic acid within 50 min and

selective ion monitoring (SIM) on channels of *m/z* (+) 495, 468 and 496, which corresponds to the molecular weights of derivatized amino acid dimers, FDAA-Pip^3-Pip^2, FDAA-Pip^2-*N*MeAla (or FDAA-*N*Me-Ala-Pip^1) and FDAA-Pip^1-Leu, respectively [152]. The flow rate was 0.4 mL/min.

7.2.4 Antibacterial activity assays

See "Chapter 4. Phenotypic screening"

7.2.5 qPAR of hytramycins by LC-MS

The LC-PDA-MS instrument (Shimadzu LC-2020) was equipped with a YMC-pack ODS-AQ C_{18} column (250 × 4.6 mm I.D., 5 µm, 12 nm), an ESI & APCI (DUIS) interface, and a column oven maintained at 40 °C. The mobile phase consisted of MeCN (A) and water (B) following a linear gradient of 30%, 95%, 95%, and 30% of (A) at 0 min, 25 min, 30 min, and 31 min. The flow rate was set up at 0.4 mL/min. Segments 1 to 4 were set up as *m/z* 295-700, *m/z* 695-1000, *m/z* 995-1500, and *m/z* 1495-2000, respectively, in positive mode, and segments 5 to 8 were set up in the same mass range in negative mode in the mass spectrometer. Samples were prepared at 500 µg/mL. The injection volume was set at 5 µL. A MeOH blank was injected between each two consecutive samples to wash out sample carry-over in the column.

Total ion chromatograms (TIC) were recorded in each of the four individual segments by the mass spectrometer. Peaks eluting at 24.7 min (hytramycin V) and at 27.2 min (hytramycin I) in segment 1 were integrated. The percentage ratio of the peak areas corresponding to hytramycins V and I was based on the total accumulative peak areas in all four segments and was plotted together with the anti-*M. tb* MICs of each fraction. Statistical analyses were performed with Microsoft Excel 2010.

7.3 Results and discussion

As part of an ongoing collaboration between the University of Illinois at Chicago and Myongji University, 35,000 actinomycete extracts were screened for anti-*M. tb* activity from the Extract Collection of Useful Microorganisms (ECUM). After primary screening against *M. tb*, prioritized extracts, including one from strain ECUM14046, were processed in bioassay-guided fractionation. Using C_{18} cartridge fractionation with a MeOH-H_2O gradient elution, and purification via reverse phase preparative HPLC, two new cyclic hexapeptides, designated hytramycin V (**1**) and I (**2**) according to their structural difference in the valine and isoleucine residues, were isolated in appreciable yield (ca. 30 mg each from a 20 L fermentation) from strain ECUM14046 (**Figure 34**). The structures of each of these antibiotics contain three moieties of piperazic acid (Pip). The producing organism is classified as a strain of *Streptomyces hygroscopicus* as its 16S rRNA shows 99% homology to the type strain of this species, thus designated as the hytramycins (*hygroscopicus* + ITR + mycin).

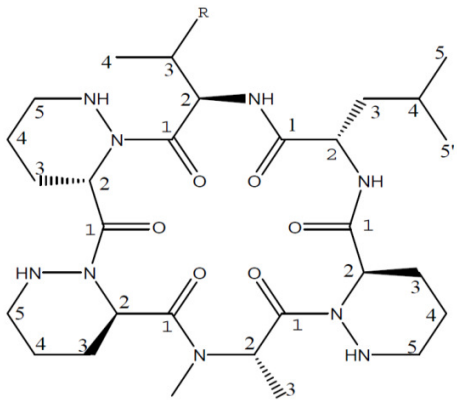

Figure 34. Structures of 1 and 2

7.3.1 Physicochemical Properties and Masses of the Isolates

The protonated and sodiated molecular ions as determined by LC-ESI-IT-TOF mass spectroscopy for **1** had *m/z* 634.4043 and *m/z* 656.3769, theoretical for $C_{30}H_{52}N_9O_6$ and $C_{30}H_{51}NaN_9O_6$, respectively, and those for **2** had *m/z* 648.4176 and *m/z* 670.3928, theoretical for $C_{31}H_{54}N_9O_6$ and $C_{31}H_{53}NaN_9O_6$, respectively (**Appendix A**, **Figure A-1**). These combined with NMR data established the molecular formulas as $C_{30}H_{51}N_9O_6$ and $C_{31}H_{53}N_9O_6$, respectively. The LC-MS/MS fragmentation of both **1** and **2** confirmed the connectivity of amino acid residues in these two molecules (**Appendix A**, **Figure A-2**). The UV spectra of each of the two compounds showed no peak absorption from 200-800 nm, but OD_{200} was 0.58 and 0.63 for **1** and **2**, respectively, and OD values decreased to zero in wavelength regions higher than 268 nm. The OD results suggest lack of major UV-visible chromophores in these molecules. The IR spectra of the two compounds exhibited a strong and sharp absorption band at 1630-1635 cm^{-1} (C=O, stretching), a broad weak absorption band at 3265-3268 cm^{-1} (N-H, stretching), medium absorption bands at 2850-2960 cm^{-1} (aliphatic C-H, stretching), overall suggesting the peptidic nature of the molecules (**Appendix A**, **Figure A-3**).

Hytramycin V (**1**): colorless, amorphous powder; $[\alpha]^{22}_D$ +9.24 (*c* 1.266, MeCN); UV (MeCN) no peak absorption from 200 nm to 800 nm; IR (neat liquid) ν_{max} 920, 1249, 1407, 1507, 1633, 2870, 2956, 3268 cm^{-1}; ^1H and ^{13}C NMR, COSY, HMBC, and NOESY (in MeOH-d_4 and DMSO-d_6) data (see "Section **7.3.2**"); HR-ESI-MS *m/z* 634.4043 $[M + H]^+$ (calcd for $C_{30}H_{52}N_9O_6$, 634.4035).

Hytramycin I (**2**): colorless, amorphous powder; $[\alpha]^{22}_D$ +12.21 (*c* 1.294, MeCN); UV (MeCN) no peak absorption from 200 nm to 800 nm; IR (neat liquid) ν_{max} 919, 1248, 1406, 1441,

1507, 1632, 2872, 2934, 3265 cm^{-1}; ^{1}H and ^{13}C NMR data (see "Section **7.3.2**"); HR-ESI-MS *m/z* 648.4176 $[M + H]^+$ (calcd for $C_{31}H_{54}N_9O_6$, 648.4192).

7.3.2 Structural Elucidation

Presumably, six amide carbonyl carbons were identified in the ^{13}C NMR spectrum of **1** in DMSO-d_6 (δ 175.68, 175.68, 174.19, 172.22, 172.92, and 172.47 ppm), among the total 30 carbons detected. Analysis of the DEPT-135 spectrum (in MeOH-d_4) indicated the presence of 14 methyl/methine carbons, 10 methylene carbons, and these 6 quaternary carbons (carbonyls) (**Figure 35**). In the ^{1}H NMR spectrum of **1** in MeOH-d_4, most exchangeable protons were invisible, except one that integrated slightly less than one proton (δ 7.50), which was later assigned as the NH of valine and only slowly exchanged compared to other nitrogen protons (**Figure 36**). In DMSO-d_6, all NH proton resonances were clearly observed (**Figure 37**).

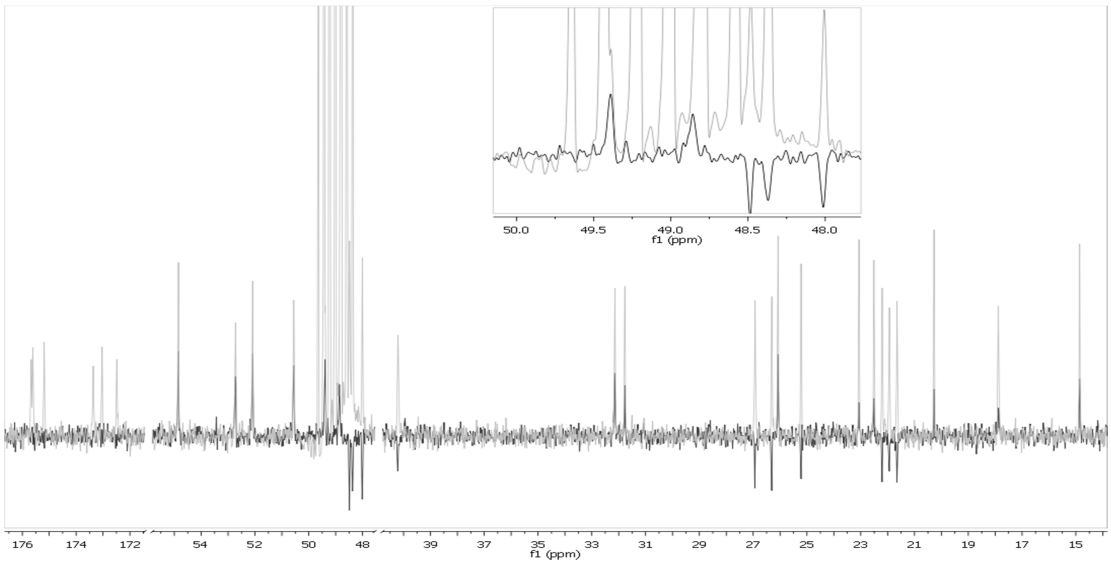

Figure 35. ^{13}C (gray) and DEPT-135 (black) spectra of 1 overlapped (100 MHz, MeOH-d_4)

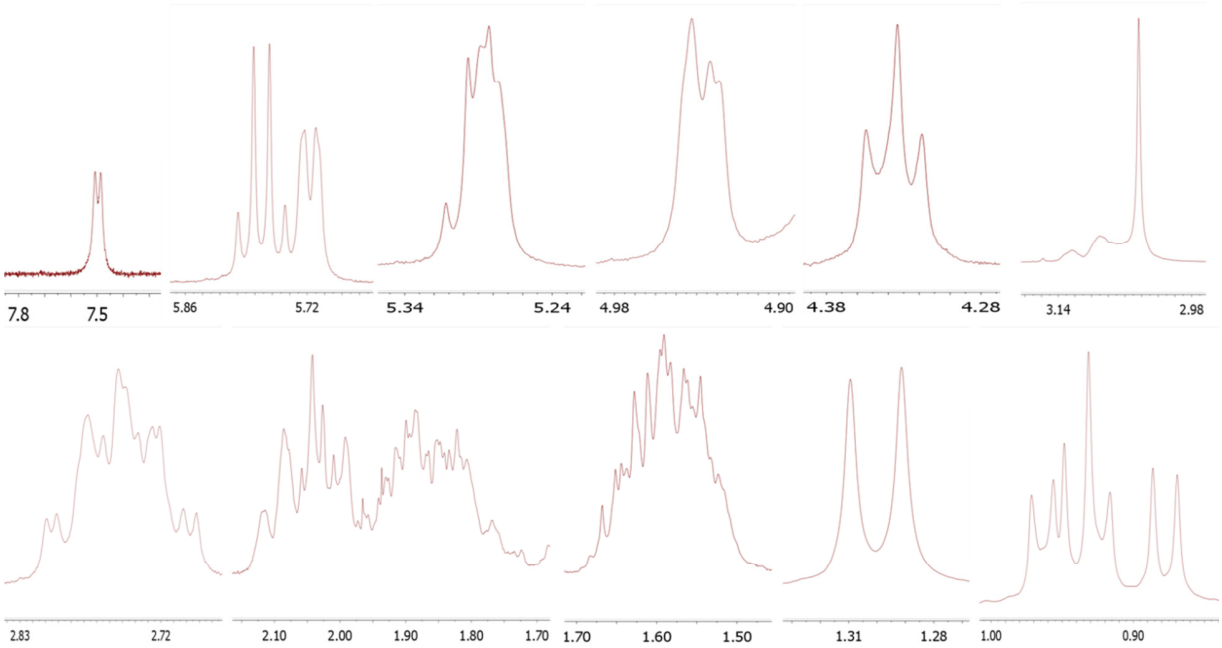

Figure 36. ^{1}H NMR expansion spectra of 1 in MeOH-d_4 (400 MHz, Exponential -0.3 Hz, Gaussian 0.5 Hz)

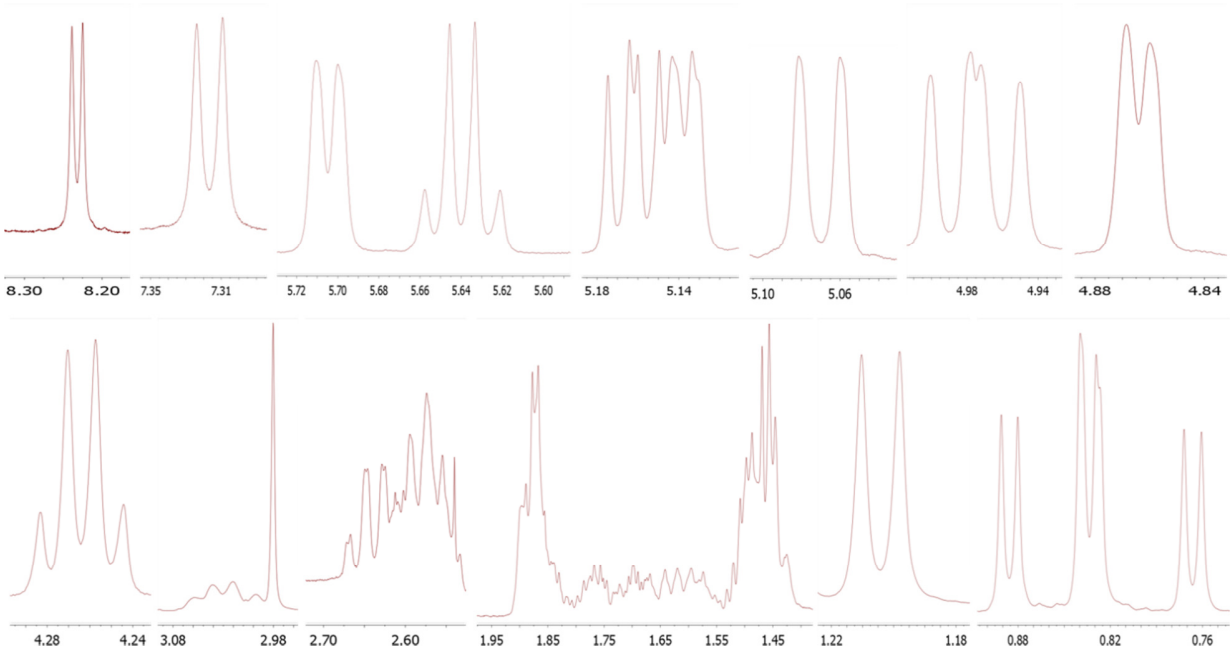

Figure 37. ^{1}H NMR expansion spectra of 1 in DMSO-d_6 (600 MHz, Exponential -0.3 Hz, Gaussian 0.5 Hz)

Six protons resonated in the 4-6 ppm region and were identified as α protons of the amino acid moieties. One proton (δ_H 5.639 in DMSO-d_6) resonated as a quartet (J = 7.3 Hz), suggesting it was vicinal to a CH_3 group, which resonated as a doublet (δ 1.209). In the HMBC spectrum, a singlet (δ 2.980) integrating for three protons correlated with the same carbon to which the proton resonating as a quartet is connected. Both COSY and HMBC spectra confirmed this group of signals to belong to an *N*-methylated alanine (**Figure 38**).

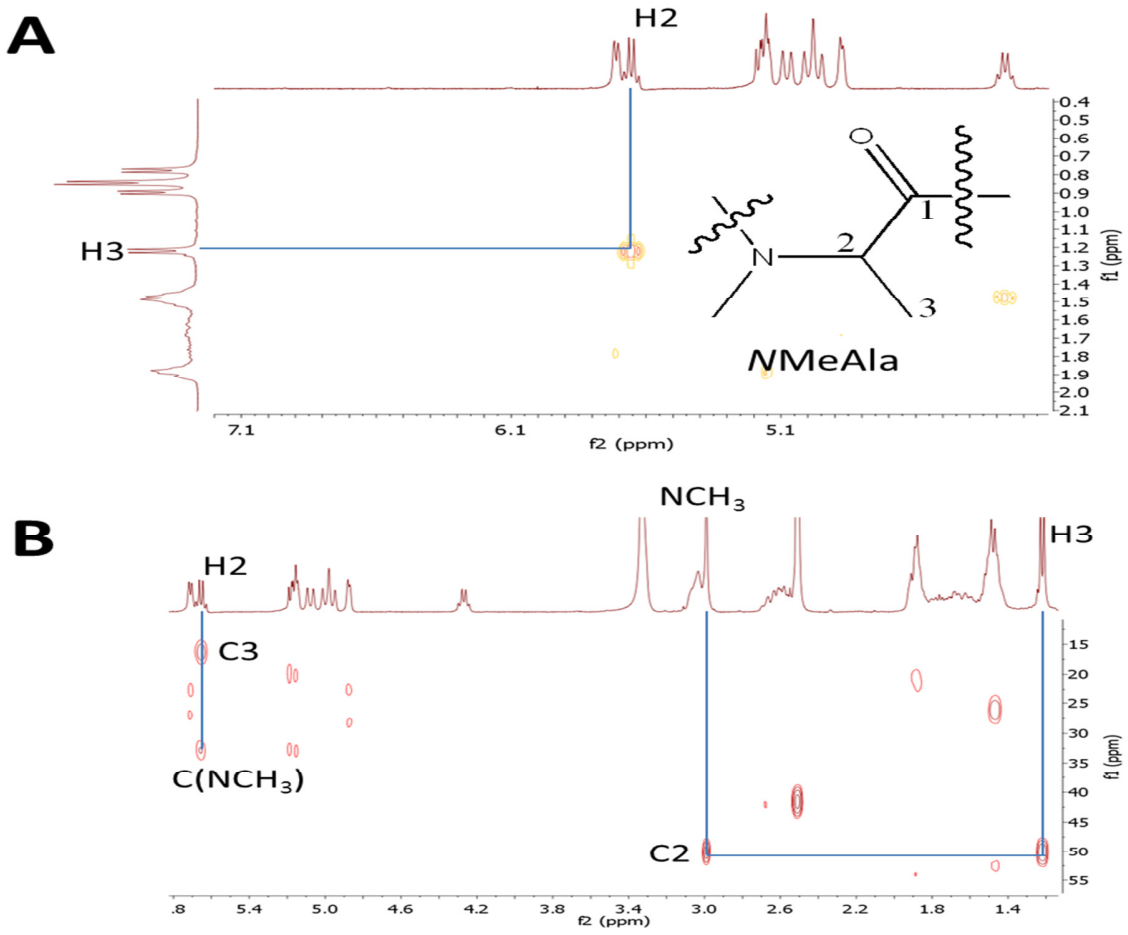

Figure 38. COSY (A) and HMBC (B) spectra highlighting the *N*-methylalanine (*N*MeAla) residue in 1 (400 MHz, DMSO-d_6)

In the COSY spectrum, a proton resonating at δ 5.162 and two methyls (δ 0.832 and 0.766) correlated with the same methine proton (δ 1.872). The COSY and HMBC confirmed that these signals arose from a valine moiety (**Figure 39**).

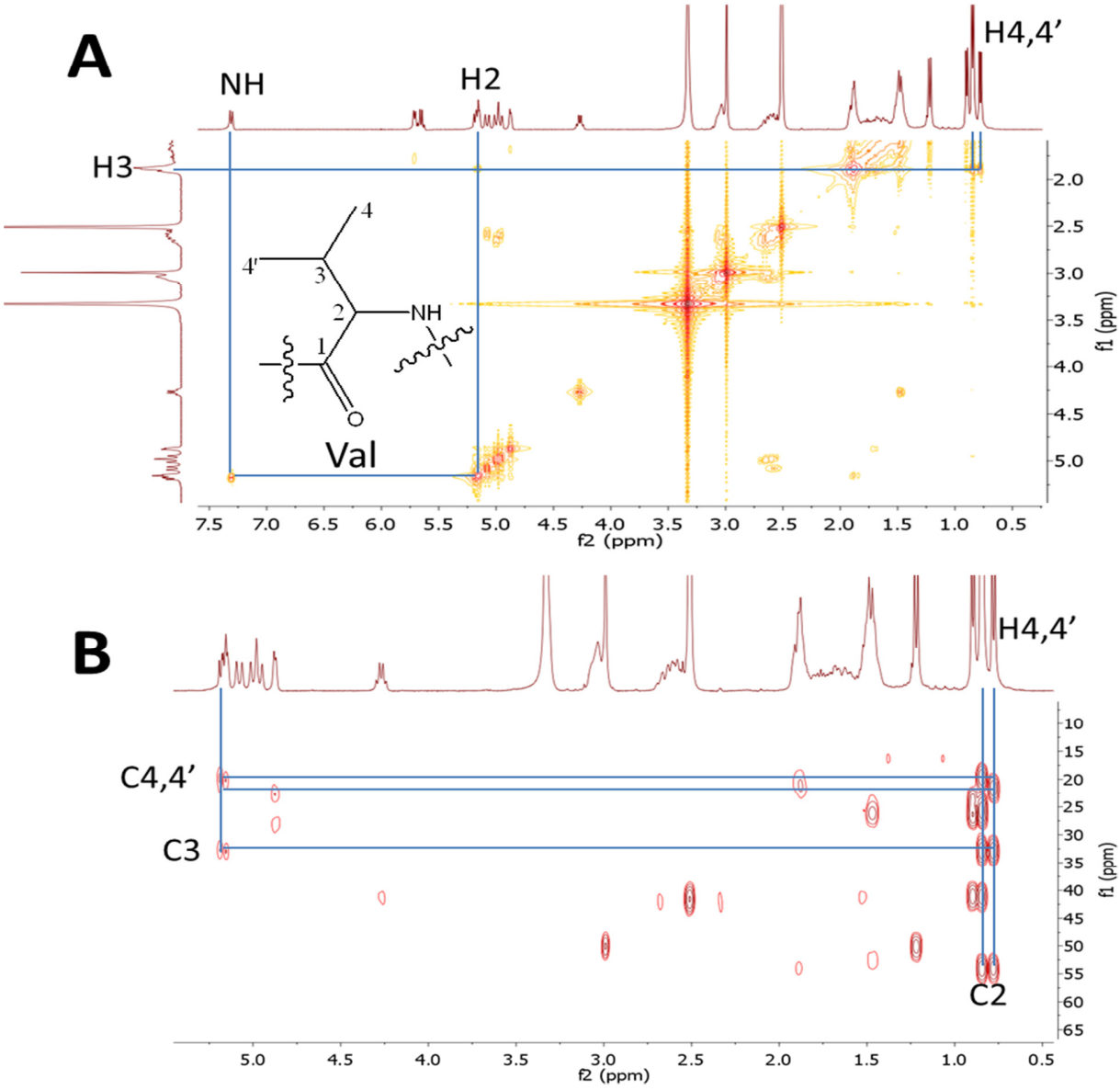

Figure 39. COSY (A) and HMBC (B) spectra highlighting the valine (Val) residue in 1 (400 MHz, DMSO-d_6)

By the interpretation of the COSY and HMBC spectra, the proton resonating at δ 4.264 was assigned to a leucine, with the two methyls (δ 0.834 and 0.885) correlating with the same methine proton (δ 1.530), which was neighboring to a methylene (δ 1.456 and 1.485) next to the α proton (**Figure 40**).

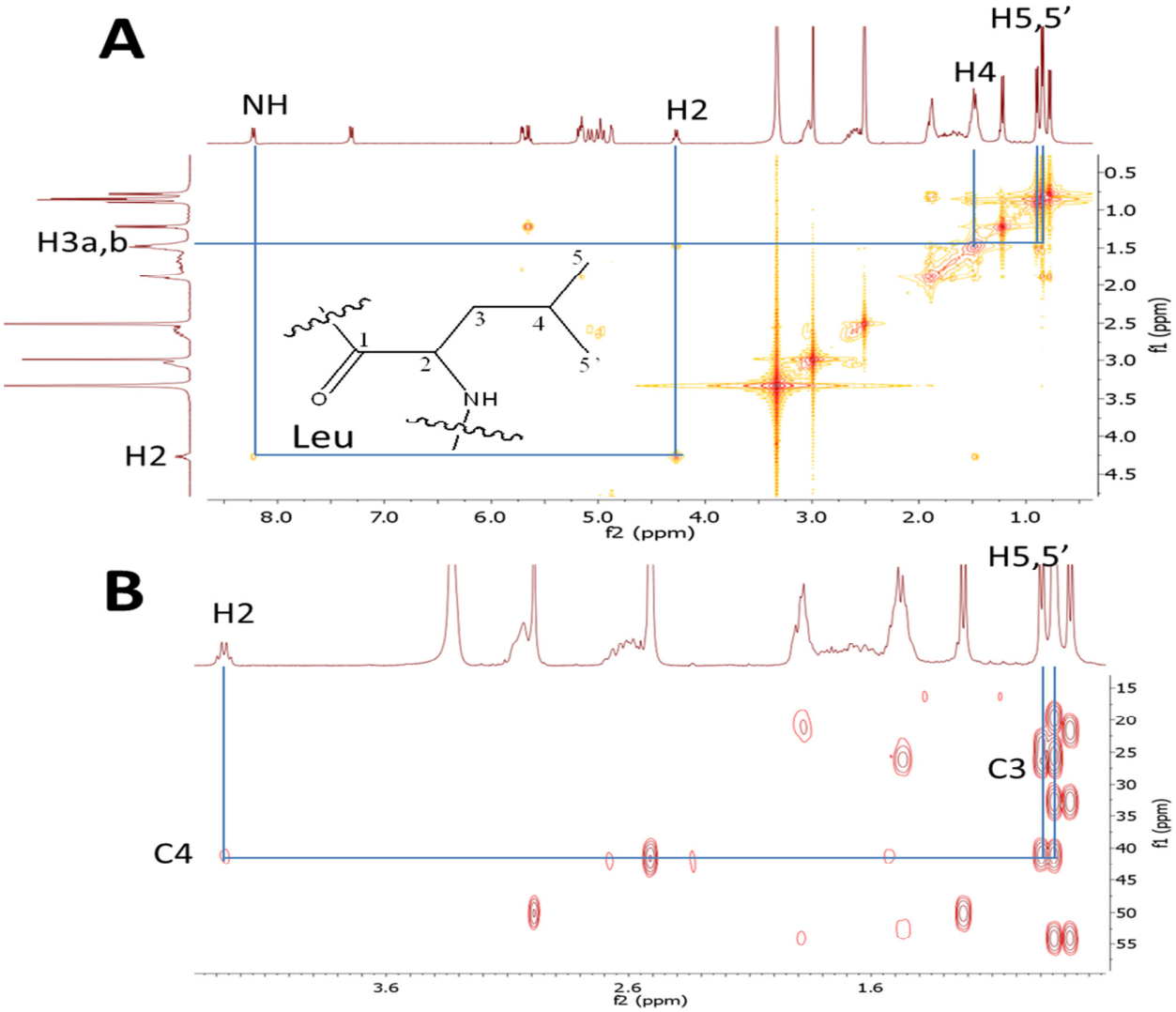

Figure 40. COSY (A) and HMBC (B) spectra highlighting the leucine (Leu) residue in 1 (400 MHz, DMSO-d_6)

Another three α proton signals (δ 5.704, Pip^3; 5.137, Pip^2; and 4.863, Pip^1 respectively) were assigned to three piperazic acid (Pip) moieties based on the three characteristic doublet protons of NH's (δ 5.070, 4.989 and 4.960) showing up in the ^{1}H dimension of COSY and HMBC spectra in DMSO-d_6. This showed that the three NH's in the Pip moieties are actively exchangeable in protic solvents as they were not visible in MeOH-d_4 solution. The two δ protons adjacent to the NH's of the three Pip units resonated in the 2.5-2.8 and 3.0-3.2 ppm regions of the ^{1}H NMR spectrum. The NH of leucine appeared at δ 8.232, and the NH of valine appeared at δ 7.316 (**Figure 41**).

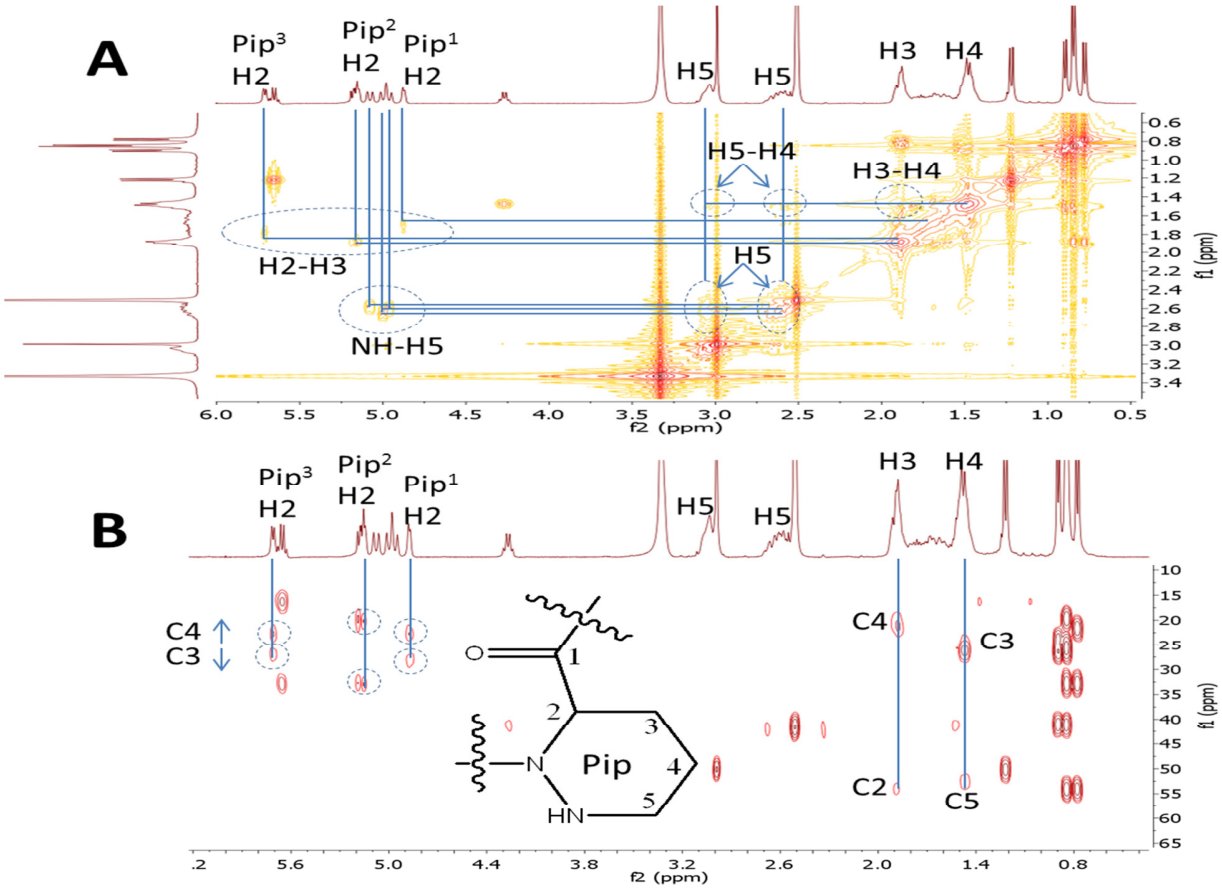

Figure 41. COSY (A) and HMBC (B) spectra highlighting the three piperazic acid (Pip) residues in 1 (400 MHz, DMSO-d_6)

The connectivity between these six amino acid moieties was determined through a semi-selective HMBC experiment [153], in which a high resolution carbon region only focuses on the carbonyls between 160 and 180 ppm (**Figure 42**). Each α proton correlates to two carbonyls, one within the amino acid residue and the other one in connection with its neighbor. Thus, the order of the six moieties was shown to be the cyclic *N*Me-Ala-Pip-Leu-Val-Pip-Pip. In the semi-selective HMBC spectrum, the NH's of the Pip moieties all correlated with the neighboring carbonyls, and the two NH's of valine and leucine correlated with two carbonyls, one within the amino acid moiety and one from the adjacent amino acid. These correlations helped to confirm the linkage of the six amino acid moieties into a ring system. It was also noticed that the difference in carbon chemical shift between carbonyls in leucine and Pip^2 is < 1 ppm. The NOESY spectrum (**Appendix A**, **Figure A-8**) provided additional evidence for the structural elucidation of Pip in that the β protons have spatial correlation with the δ protons in a chair conformation of the six-membered ring. There is also a weak but distinct spatial NOE relationship between all adjacent α protons, suggesting that the rigid ring system shortens the time-averaged distances between these α protons.

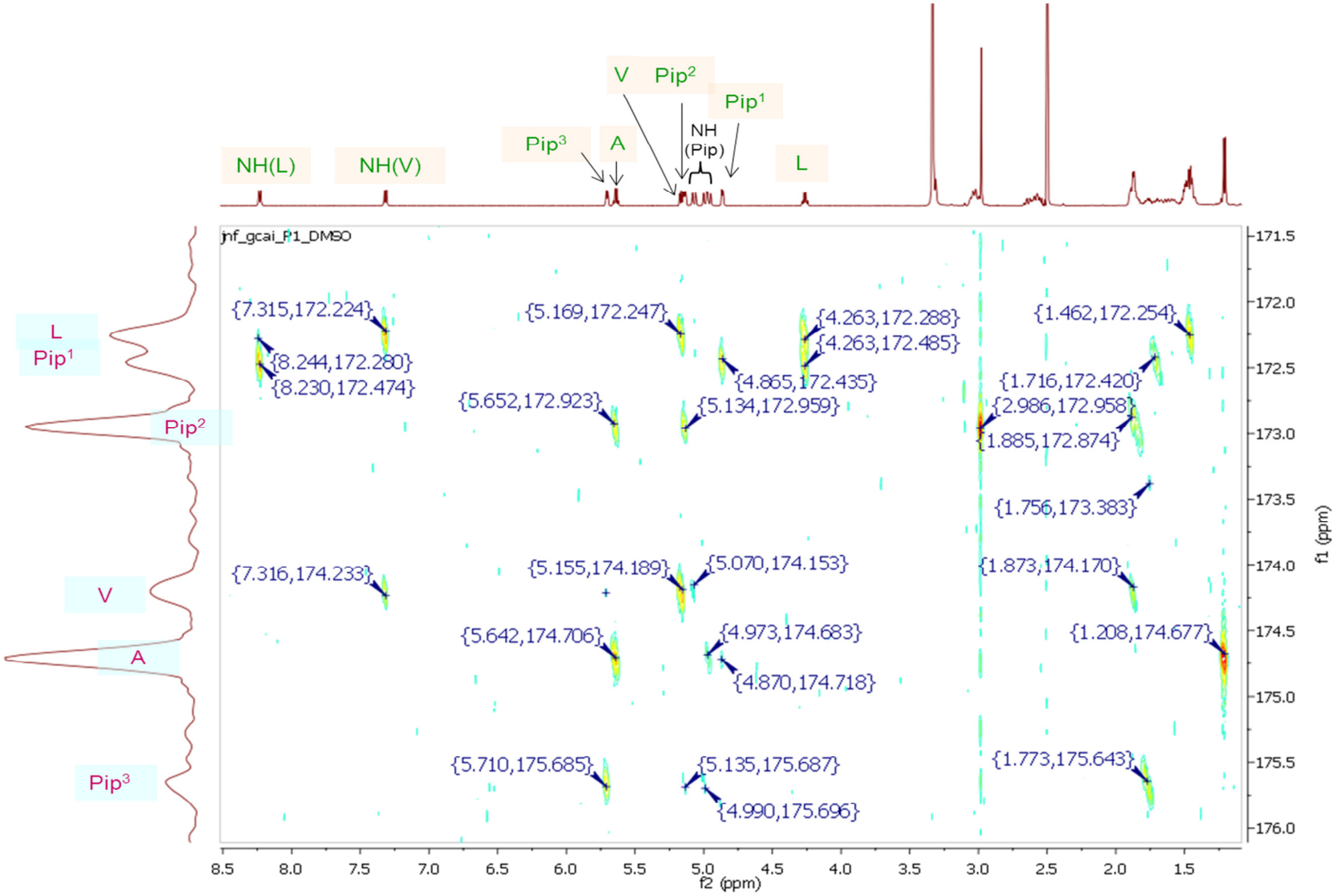

Figure 42. Semi-selective HMBC spectrum of 1 (600 MHz, DMSO-d_6)

Overlapping the ^{1}H NMR spectra of **1** and **2** acquired in MeOH-d_4, it was straightforward to recognize the two additional signals at δ 1.194 and 1.402 of **2** (**Figure 43**). These two additional protons share the same carbon in an HSQC (**Figure 44**). By 2D-NMR they were assigned as belonging to the methylene in an isoleucine, which replaces the valine of **1**. The α proton of the isoleucine in **2** was also shifted downfield (δ 5.401 in MeOH-d_4) compared with that of the valine (δ 5.291 in MeOH-d_4) in **1**, standing as an evidence of the substituent chemical shifts (SCS) of the α proton effected by the introduction of substituents into the reference molecule, in this case the CH_2 unit to the valine residue. The entire NMR data of **1** and **2** (**TABLE XII**; **TABLE XIII**), and key correlations observed in the 2D-NMR experiments of **1** are illustrated (**Figure 45**).

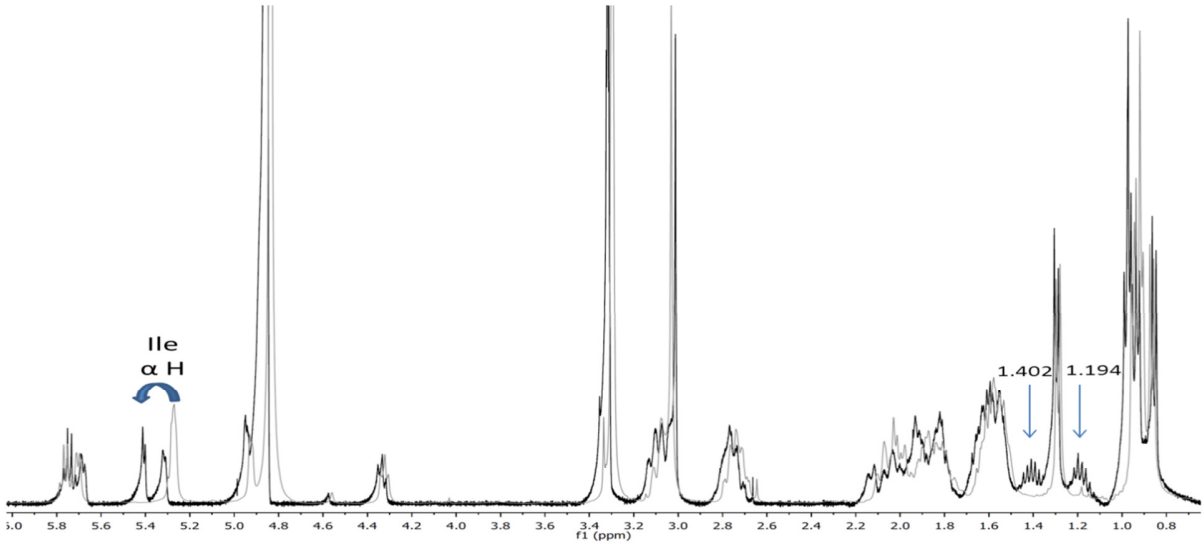

Figure 43. ^{1}H NMR spectra of 1 (gray) and 2 (black) overlapped (400 MHz, MeOH-d_4). In **2**, two methylene protons (δ 1.194 and 1.402, marked by arrows) appeared, and the α proton of isoleucine (δ 5.401) is shifted downfield and appears separated from the α proton of one Pip (δ 5.309).

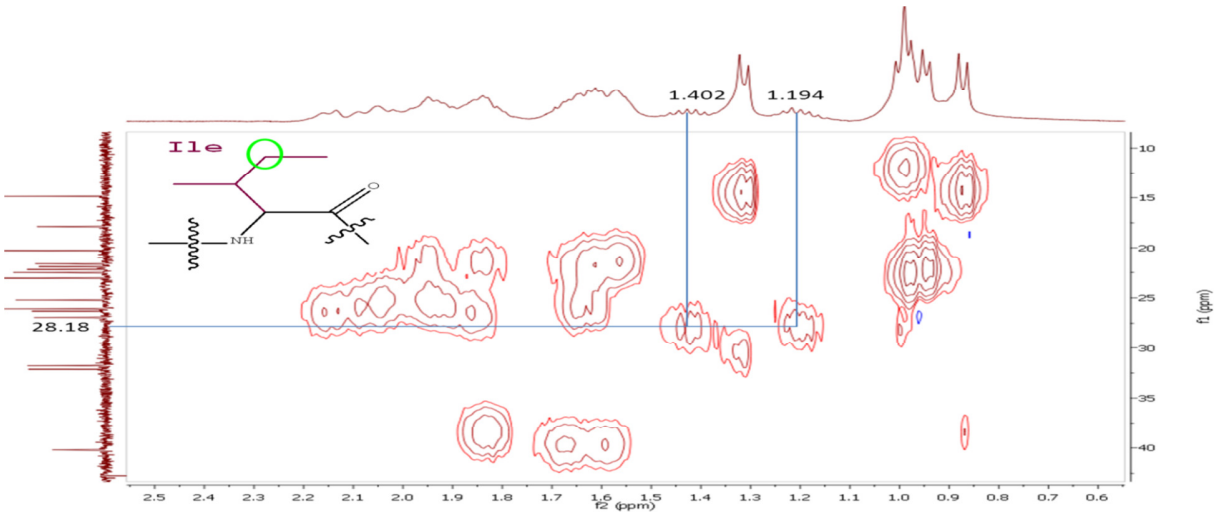

Figure 44. HSQC spectrum of 2, highlighting the additional methylene from the isoleucine residue which distinguishes 2 from 1, containing values (400 MHz, MeOH-d_4, vertical axis showing the ^{13}C spectrum of 1)

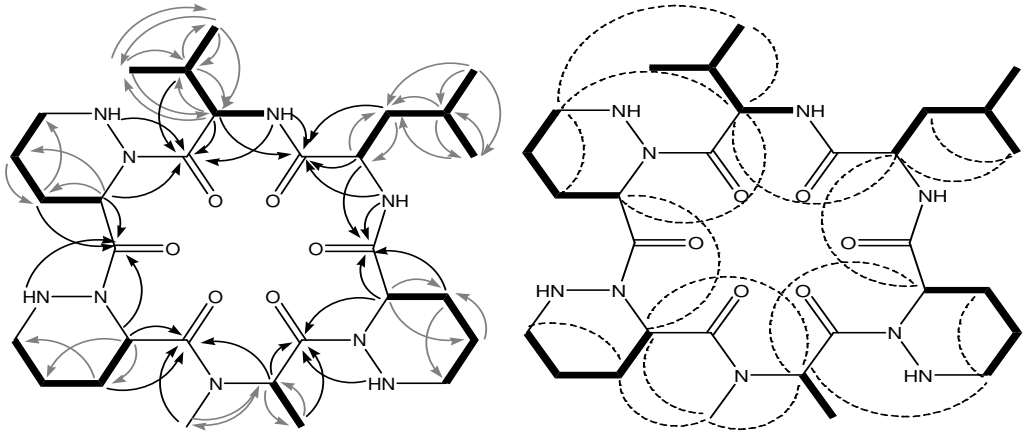

Figure 45. Key correlations in the 2D-NMR spectra of 1. Bold bonds: COSY/TOCSY ^{1}H spin systems (MeOH-d_4); Gray arrows: HMBC H → C; Dotted lines: NOESY (MeOH-d_4); Black arrows: Semi-selective HMBC focusing on the carbonyl region (DMSO-d_6).

Due to spectral overlap, especially of the piperazic methylene resonances, the corresponding coupling constants and chemical shifts could hardly be determined accurately in the observed ^{1}H NMR spectra. ^{1}H iterative full spin analysis (HiFSA) using the PERCH toolset has

recently been shown to provide an unequivocal interpretation of the ^{1}H NMR spectra of pure compounds, even with very complex spectra [146, 154, 155]. In order to resolve the spectral overlap, HiFSA analyses were performed for the ^{1}H NMR spectra of **1** (**Appendix C**) and **2** (**Appendix D**) to yield an unambiguous assignment of all their δ_H and *J* values. A comparison of the HiFSA optimized *vs.* the experimental ^{1}H NMR spectrum of **1** is shown (**Figure 46**). The sum of the individual spectra of the six amino acids fully matches the experimental data of the hexapeptide, **1**. The ^{1}H NMR spin parameters generated by HiFSA are consistent with the proposed structures and unambiguously confirm the identity of the amino acid moieties.

The HiFSA analysis produces a complete and reproducible ^{1}H NMR profile that can be used as a fingerprint for the identification of compounds with similar structures. The calculated chemical shifts and coupling constants provide a reference for the correct assignments of all the protons on the spectrum, and distinguish the traces of the impurities from the peaks of the analyzed compound. HiFSA also integrates the stereo configurations of chiral atoms into the spectral prediction, which consolidates the elucidation of the entire structure. The advantages of HiFSA analysis include the clarification of spectral overlapping, the deconvolution of spectral distortion in higher order coupled spin networks and distinguishing impurity peaks, the field-independent parameters that can be used on ^{1}H NMR simulation acquired from different field strengths, and the detailed analysis of spin systems with small scalar coupling constants [155]. The quantitative analysis of botanical markers in *Gingko* extracts with the aid from quantitative NMR measurements was realized by the unequivocal assignment of these markers in ^{1}H NMR spectra with HiFSA [146]. HiFSA was also applied to the evaluation of enzymatic reaction in intact cells by the deconvolution of the isotopomers in a glucose-lactate transformation [154].

TABLE XII. 1D & 2D ^{1}H AND ^{13}C NMR DATA OF 1 [a]

	Methanol-d_4		DMSO-d_6		Key 2D-NMR Correlations		
position	δ_C, mult.	δ_H, mult. (*J*)	δ_C, mult.	δ_H, mult. (*J*)	COSY	HMBC (H→C)	NOE [c]
D-Val 1	175.19, C	–	174.19, C	–	–	–	–
2	54.84, CH	5.291, d (5.8)	54.09, CH	5.162, dd (6.2, 8.7)	Val-3, Val-NH [b]	Val-1, Val-3, Val-4', Leu-1	Val-4, Leu-2, Pip^3-2, Pip^3-5
3	32.10, CH	2.034, dqq (5.8, 6.8, 6.8)	32.84, CH	1.872, dqq (6.2, 6.8, 6.8)	Val-2, Val-4, Val-4'	Val-1, Val-2, Val-4	–
4	20.35, CH_3	0.940, d (6.8)	21.65, CH_3	0.832, d (6.8)	Val-3	Val-2, Val-3, Val-4'	Val-2, Pip^3-5
4'	18.03, CH_3	0.877, d (6.8)	19.66, CH_3	0.766, d (6.8)	Val-3	Val-2, Val-3, Val-4	–
NH	–	–	–	7.316, d (8.7)	Val-2 [b]	Val-1, Leu-1 [b]	–
L-Leu 1	173.35, C	–	172.22, C	–	–	–	–
2	52.60, CH	4.338, dd (6.3, 8.4)	52.52, CH	4.264, ddd (6.8, 8.2, 8.3)	Leu-3, Leu-NH [b]	Leu-1, Leu-4, Pip^1-1	Val-2, Pip^1-2, Leu-5'
3	26.21, CH_2	1.646, ddd (6.3, 7.4, -12.7)	26.40, CH_2	1.485, ddd (6.8, 7.1, -12.8)	Leu-2	Leu-2	Leu-5'
		1.556, ddd (5.7, 8.4, -12.7)		1.456, ddd (4.7, 8.2, -12.8)	Leu-2, Leu-4	Leu-1, Leu-2	–
4	40.19, CH	1.610, ddqq (5.7, 6.3, 6.4, 7.4)	41.09, CH	1.530, ddqq (4.7, 7.1, 6.6, 6.6)	Leu-3, Leu-5, Leu-5'	Leu-2, Leu-5'	–
5	23.04, CH_3	0.925, d (6.3)	23.76, CH_3	0.834, d (6.6)	Leu-4	Leu-3, Leu-4, Leu-5'	–
5'	22.46, CH_3	0.965, d (6.4)	25.67, CH_3	0.885, d (6.6)	Leu-4	Leu-3, Leu-4	Leu-2, Leu-3
NH	–	–	–	8.232, d (8.3)	Leu-2 [b]	Leu-1, Pip^1-1 [b]	–
D-Pip^1 1	172.48, C	–	172.47, C	–	–	–	–
2	51.91, CH	4.937, dd (2.0, 5.4)	51.03, CH	4.863, dd (1.9, 5.8)	Pip^1-3	Pip^1-1, Pip^1-3, Pip^1-4, Ala-1	Leu-2, Pip^2-2
3	26.90, CH_2	2.097, ddddd (1.2, 2.0, 2.1, 4.0, -13.4)	27.97, CH_2	1.886, ddddd (1.1, 1.9, 2.1, 4.1, -13.4)	Pip^1-2, Pip^1-4	Pip^1-5	Pip^1-5
		1.869, dddd (0.7, 5.4, 12.2, -13.4)		1.694, dddd (0.8, 5.8, 12.7, -13.4)	Pip^1-2, Pip^1-4	Pip^1-1, Pip^1-5	–
4	22.09, CH_2	1.621, ddddd (4.0, 4.9, -11.3, 12.2, 13.6)	22.95, CH_2	1.607, ddddd (4.1, 4.8, -11.5, 12.7, 13.9)	Pip^1-3, Pip^1-5	Pip^1-3	–
		1.581, ddddd (0.7, 1.2, 2.7, 3.5, -11.3)		1.498, ddddd (0.8, 1.1, 2.9, 3.5, -11.5)	Pip^1-3, Pip^1-5	Pip^1-3	–
5	48.48, CH_2	3.076, dddd (2.1, 3.5, 4.9, -13.8)	48.83, CH_2	3.009, dddd (2.1, 3.5, 4.8, -13.8)	Pip^1-4, Pip^1-NH [b]	–	–
		2.729, ddd (2.7, 13.6, -13.8)		2.566, dddd (2.9, 12.7, -13.8, 13.9)	Pip^1-4, Pip^1-NH [b]	–	Pip^1-3, Ala-2
NH	–	–	–	4.960, d (12.7)	Pip^1-5 [b]	Ala-1, Pip^1-4 [b]	–

TABLE XII. (CONTINUED)

	Methanol-d_4		DMSO-d_6		Key 2D-NMR Correlations		
position	δ_C, mult.	δ_H, mult. (*J*)	δ_C, mult.	δ_H, mult. (*J*)	COSY	HMBC (H→C)	NOE[c]
NMe-L-Ala 1	175.61, C	–	174.68, C	–	–	–	–
2	50.49, CH	5.775, q (7.2)	50.07, CH	5.639, q (7.3)	Ala-3	Ala-1, Ala-3, Ala-*N*Me, Pip^2-1	Pip^1-2, Pip^2-2, Pip^1-5, Ala-*N*Me
3	14.86, CH_3	1.303, d (7.2)	16.55, CH_3	1.209, d (7.3)	Ala-2	Ala-1, Ala-2	–
*N*Me	31.80, CH_3	3.048, s	32.96, CH_3	2.980, s	–	Ala-2, Pip^2-1	Ala-2, Pip^2-2, Pip^2-3
D-Pip^2 1	173.03, C	–	172.92, C	–	–	–	–
2	48.73, CH	5.281, dd (2.5, 6.0)	49.03, CH	5.137, dd (1.7, 6.5)	Pip^2-3	Pip^2-1, Pip^2-3, Pip^2-4, Pip^3-1	Ala-2, Pip^3-2, Ala-*N*Me
3	24.83, CH_2	2.004, ddddd (1.3, 2.0, 2.5, 4.1, -13.0)	32.96, CH_2	1.877, ddddd (1.2, 1.7, 2.1, 4.1, -13.1)	Pip^2-2, Pip^2-4	Pip^2-5	Ala-*N*Me, Pip^2-5
		1.931, dddd (6.0, 7.1, 10.7, -13.0)		1.839, dddd (6.5, 7.0, 10.6, -13.1)	Pip^2-2, Pip^2-4	Pip^2-1, Pip^2-5	–
4	21.77, CH_2	1.833, ddddd (2.0, 3.4, 4.2, 7.1, -13.6)	20.19, CH_2	1.494, ddddd (2.1, 3.7, 4.0, 7.0 -13.8)	Pip^2-3, Pip^2-5	–	–
		1.534, ddddd (2.1, 4.1, 10.7, 11.9, -13.6)		1.462, ddddd (2.6, 4.1, 10.6, 11.9, -13.8)	Pip^2-3, Pip^2-5	–	–
5	48.65, CH_2	3.107, dddd (1.3, 2.1, 4.2, -13.4)	48.64, CH_2	3.039, ddddd (1.2, 2.6, 4.0, 12.9, -13.5,)	Pip^2-4, Pip^2-NH[b]	–	–
		2.775, ddd (3.4, 11.9, -13.4)		2.643, ddd (3.7, 11.9, -13.5)	Pip^2-4, Pip^2-NH[b]	–	Pip^2-3
NH	–	–	–	4.989, d (12.9)	Pip^2-5[b]	Pip^2-4, Pip^3-1[b]	–
L-Pip^3 1	175.69, C	–	175.68, C	–	–	–	–
2	49.27, CH	5.721, dd (2.2, 6.7)	48.58, CH	5.704, dd (1.9, 6.6)	Pip^3-3	Pip^3-1, Pip^3-3, Pip^3-4, Val-1	Val-2, Pip^2-2
3	26.34, CH_2	2.059, ddddd (1.7, 2.2, 3.1, 4.0, -13.4)	27.02, CH_2	1.875, ddddd (1.6, 1.9, 3.0, 4.0, -13.2)	Pip^3-2, Pip^3-4	Pip^3-4	Pip^3-5
		1.881, dddd (5.4, 6.7, -13.4, 14.2)		1.766, dddd (5.4, 6.6, -13.2, 14.8)	Pip^3-2, Pip^3-4	Pip^3-1, Pip^3-4	–
4	22.39, CH_2	1.784, ddddd (3.0, 4.0, -11.8, 13.3, 14.2)	22.77, CH_2	1.506, ddddd (3.3, 4.0, -11.7, 13.4, 14.8)	Pip^3-3, Pip^3-5	Pip^3-3	–
		1.551, ddddd (1.1, 3.1, 3.7, 5.4, -11.8)		1.444, ddddd (1.2, 3.0, 3.7, 5.4, -11.7)	Pip^3-3, Pip^3-5	Pip^3-3	–
5	48.18, CH_2	3.060, dddd (1.1, 1.7, 3.0, -14.0)	48.71, CH_2	3.037, dddd (1.2, 1.6, 3.3, -14.1)	Pip^3-4, Pip^3-NH[b]	–	Val-2
		2.749, ddd (3.7, 13.3, -14.0)		2.582, dddd (3.7, 12.9, 13.4, -14.1)	Pip^3-4, Pip^3-NH[b]	–	Val-4, Pip^3-3
NH	–	–	–	5.070, d (12.9)	Pip^3-5[b]	Pip^3-4, Val-1[b]	–

[a] NMR data with detailed analysis generated by HiFSA matching experimental NMR data collected at 600 MHz and 298 K.

[b] Correlations observed only in DMSO-d_6.

[c] Correlations observed in MeOH-d_4.

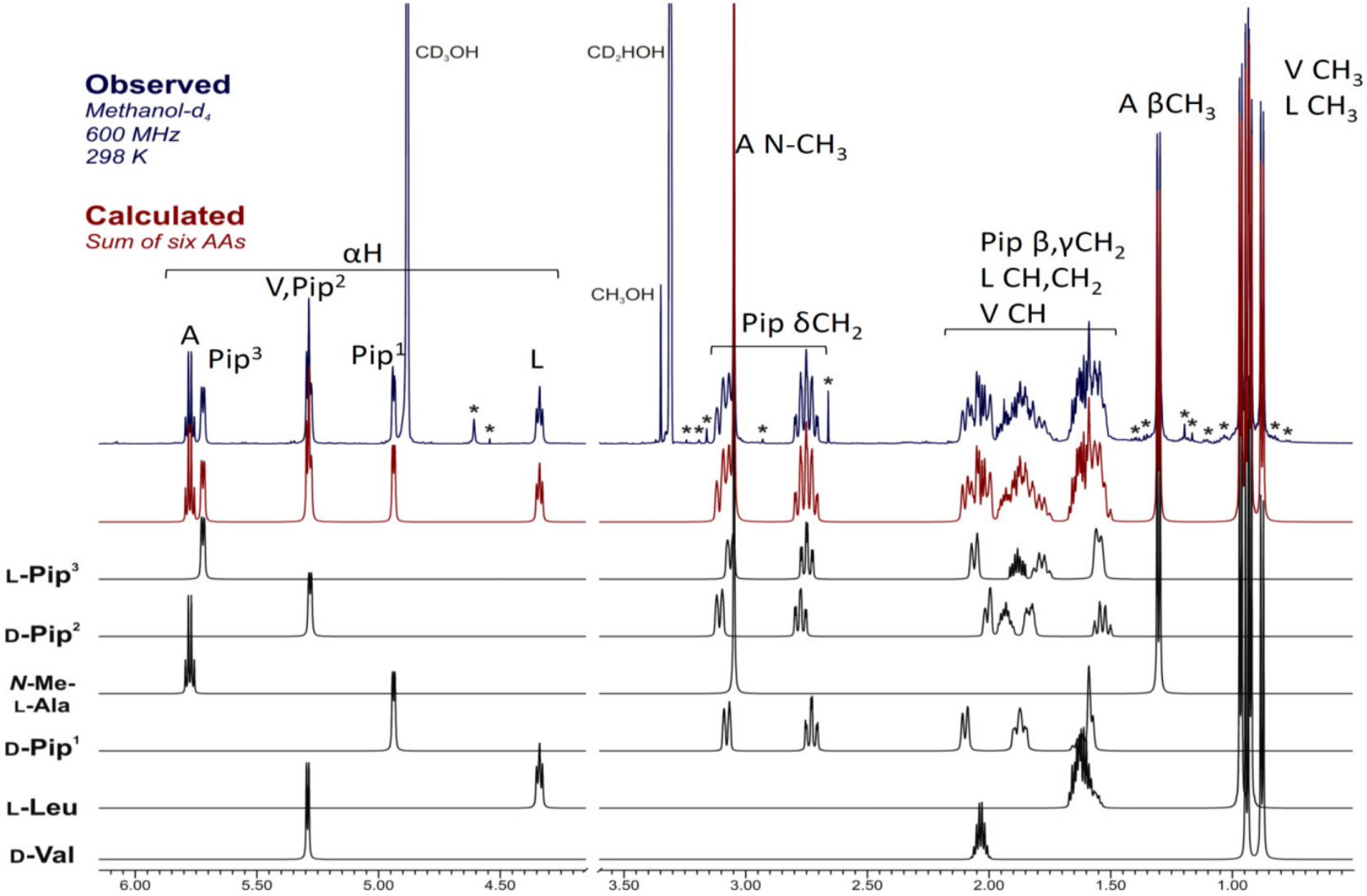

Figure 46. Comparison of experimental and calculated ^{1}H NMR spectra of 1. HiFSA fingerprints of the individual amino acids were included (*denotes unidentified impurities; A=*N*MeAla; V=Val; L=Leu; Pip=piperazic acid).

TABLE XIII. ^{1}H AND ^{13}C NMR DATA OF 2 [a]

position	δ_C, mult.	δ_H, mult. (*J*)
D-Ile 1	174.73, C	-
2	53.11, CH	5.401, d (4.5)
3	38.69, CH	1.997, dddq (4.5, 6.1, 6.9, 8.3)
4	28.18, CH_2	1.402, ddq (6.1, 7.4, -14.0) 1.194, ddq (7.4, 8.3, -14.0)
5	11.78, CH_3	0.967, dd (7.4, 7.4)
6	14.60, CH_3	0.849, d (6.9)
L-Leu 1	172.58, C	-
2	52.78, CH	4.329, dd (6.6, 8.5)
3	39.76, CH_2	1.625, ddd (5.5, 6.6, -12.1) 1.531, ddd (4.2, 8.5, -12.1)
4	25.67, CH	1.601, ddqq (4.2, 5.5, 6.5, 6.5)
5	22.50, CH_3	0.923, d (6.5)
5'	22.85, CH_3	0.961, d (6.5)
D-Pip^{1} 1	172.06, C	-
2	52.41, CH	4.938, dd (2.6, 5.8)
3	26.73, CH_2	2.124, ddddd (0.9, 2.6, 2.8, 4.8, -11.5) 1.824, dddd (1.7, 5.8, -11.5, 12.0)
4	21.54, CH_2	1.652, ddddd (4.8, 6.1, 12.0, 13.7, -14.2) 1.573, ddddd (0.9, 1.7, 3.0, 4.3, -14.2)
5	48.50, CH_2	3.055, dddd (2.8, 4.3, 6.1, -14.3) 2.733, ddd (3.0, 13.7, -14.3)
NMe-L-Ala 1	175.71, C	-
2	50.88, CH	5.737, q (7.1)
3	14.84, CH_3	1.290, d (7.1)
*N*Me	31.79, CH_3	3.006, s
D-Pip^{2} 1	172.26, C	-
2	48.76, CH	5.309, dd (1.8, 5.8)
3	25.61, CH_2	1.940, ddddd (1.4, 1.8, 2.1, 3.9, -13.1) 1.889, dddd (5.8, 6.6, 10.1, -13.1)
4	21.91, CH_2	1.818, ddddd (2.1, 3.3, 4.7, 6.6, -11.2) 1.533, ddddd (2.5, 3.9, 10.1, 10.4, -11.2)
5	48.32, CH_2	2.776, ddd (3.3, 10.4, -11.7) 3.112, dddd (1.4, 2.5, 4.7, -11.7)
L-Pip^{3} 1	175.25, C	-
2	49.64, CH	5.675, dd (2.5, 7.0)
3	25.99, CH_2	1.907, dddd (4.3, 7.0, -13.7, 14.8) 2.046, ddddd (1.3, 2.5, 2.6, 5.8, -13.7)
4	22.00, CH_2	1.795, ddddd (2.7, 5.8, 13.0, -14.1, 14.8) 1.554, ddddd (1.7, 2.6, 3.6, 4.3, -14.1)
5	48.37, CH_2	3.046, dddd (1.3, 2.7, 1.7, -15.4) 2.757, ddd (3.6, 13.0, -15.4)

[a] NMR data with detailed analysis generated by HiFSA matching experimental NMR data observed in methanol-d_4 collected at 600 MHz and 298 K

7.3.3 Stereochemical Determination

The absolute configuration of the amino acid residues was determined by Marfey's method (see "Section **7.2.3**"). The derivatized hydrolysate of **1** showed peaks with retention times in alignment with the derivatized L-leucine and D-valine standards, whereas those from **2** were in alignment with L-leucine and D-*allo*-isoleucine standards. Both derivatized **1** and **2** showed a peak in alignment with the derivatized L-*N*-methylalanine standard. Chiral column chromatography was required to distinguish between D-Ile and D-*allo*-Ile.

According to LC peak areas, the ratio of *R*- and *S*-Pips was 2:1 in both **1** and **2**. An advanced Marfey's experiment was applied to the determination of the positions of *R*- and *S*-forms of Pip in **1** and **2**. Comparing the *m/z* 496 channel of the LC-QTRAP chromatograms between the L-FDAA and D,L-FDAA products of **1**, the peak eluting at 40.09 min only originated from the D,L-FDAA products, whereas the peak eluting at 27.60 min was due to both the L- and D,L-FDAA products. As L-FDAA-*R*-Pip eluted earlier than L-FDAA-*S*-Pip, it can be concluded that the peak at 27.60 min is L-FDAA-*R*-Pip^{1}-Leu, while the peak at 40.09 min is D-FDAA-*R*-Pip^{1}-Leu. Therefore, Pip^{1} has an *R*-form in **1**. Chromatograms from the *m/z* 468 channel showed two major peaks at 20.32 min and 23.55 min from the D,L-FDAA products, while only one peak at 20.32 min from L-FDAA products was observed. The peak abundance at 20.32 min equaled to that of the peak at 27.60 min in the *m/z* 496 channel, suggesting this dimer has similar molar abundance in the L-FDAA derivatized products as the dimer Pip^{1}-Leu. This excludes the possibility of the detected dimer being the *N*Me-Ala-Pip^{1} dimer product (*m/z* 468 as well) that shares the same Pip^{1} moiety, but rather is consistent with a Pip^{2}-*N*MeAla dimer product. This provides evidence for Pip^{2} being in the *R*-form as well. There were no significant peaks in the

m/z 495 channel for either L-FDAA or D,L-FDAA products of the Pip^3-Pip^2 dimer, but as there are two *R*-configured Pips, and one *S*-Pip, Pip^3 can be proven to be *S*-configured. The configuration of the three Pip units in **2** was determined using the same methodology.

Overall, the absolute configurations of D-valine, L-leucine, and L-*N*-methylalanine were confirmed in **1**, and D-*allo*-isoleucine, L-leucine and L-*N*-methylalanine in **2**. Both **1** and **2** were shown to contain two *R*- and one *S*-Pip. Throughout the cyclohexapeptide ring structure in the molecules, the *R*- and *S*-configured amino acid moieties are connected in an alternating order (**Figure 47**). The IUPAC nomenclatures for **1** and **2** are described as (1*S*,8*R*,11*S*,18*R*,21*S*,24*R*)-10,11-dimethyl-21-(2-methylpropyl)-24-(propan-2-yl)-3,4,10,13,14,20,23,26,27-nonaazatetracyclo[24.4.0.$0^{3,8}$.$0^{13,18}$]triacontane-2,9,12,19,22,25-hexaone, and (1*S*,8*R*,11*S*,18*R*,21*S*,24*R*)-10,11-dimethyl-21-(2-methylpropyl)-24-[(*S*)-1-methylpropyl]-3,4,10,13,14,20,23,26,27-nonaazatetracyclo[24.4.0.$0^{3,8}$.$0^{13,18}$]triacontane-2,9,12,19, 22,25-hexaone.

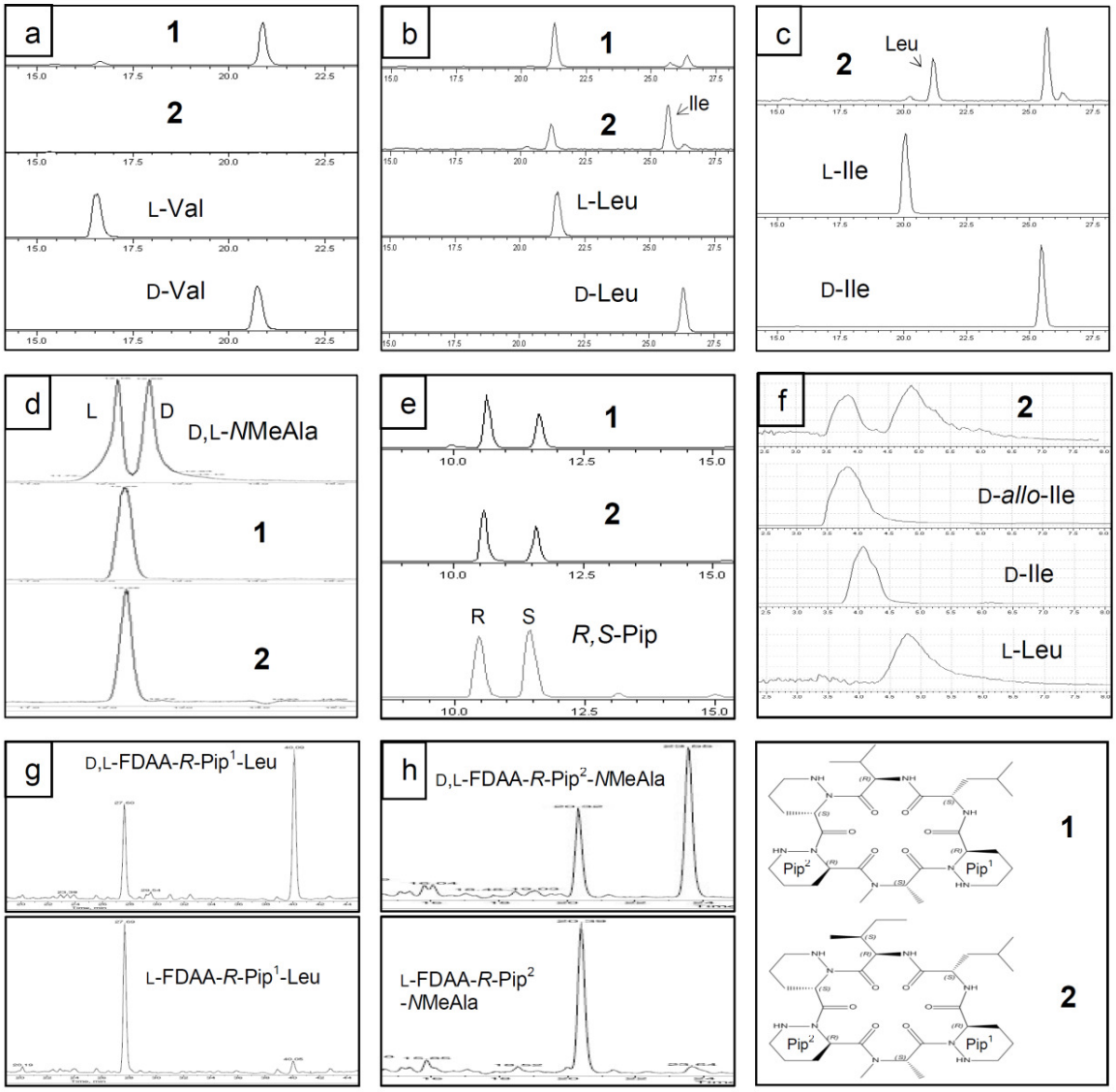

Figure 47. LC-MS chromatograms of derivatized 1 and 2 in Marfey's experiment. Selective ion monitoring (SIM) channels were set up as *m/z* 370 in (**a**), *m/z* 384 in (**b**) and (**c**), *m/z* 356 in (**d**), *m/z* 383 in (**e**), *m/z* 132 in (**f**), *m/z* 496 in (**g**) and *m/z* 468 in (**h**). (**a**) L-FDAA-D-valine in **1** eluted at 20.74 min, while L-FDAA-L-valine eluted at 16.57 min; (**b**) L-FDAA-L-leucine in both **1** and **2** eluted at 21.48 min, while L-FDAA-D-leucine eluted at 26.88 min; (**c**) L-FDAA-D-isoleucine (or D-*allo*-isoleucine) in **2** eluted at 25.46 min, while L-FDAA- L-isoleucine eluted at 20.07 min; (**d**) L-FDAA- L-*N*-methylalanine in both **1** and **2** eluted at 12.16 min, while L-FDAA-D-*N*-methylalanine eluted at 12.58 min; (**e**) L-FDAA-*R*-Pip eluted at 10.45 min, while L-FDAA-*S*-Pip eluted at 11.44 min, the ratio of peak areas between the *R*-form and *S*-form derivatives was approximately 2 in both **1** and **2**; (**f**) Chiral column separated D-*allo*-isoleucine (3.82 min) in HCl hydrolysate of **2** from D-isoleucine (4.07 min); (**g**) L-FDAA-*R*-Pip^1-Leu eluted at 27.60 min, while D-FDAA-*R*-Pip^1-Leu eluted at 40.09 min; (**h**) L-FDAA-*R*-Pip^2-*N*MeAla eluted at 20.32 min, while D-FDAA-*R*-Pip^2-*N*MeAla eluted at 23.55 min.

7.3.4 Antimicrobial Activity

The MICs of **1** and **2** against *M. tb* under normoxic conditions were 11 and 6 μg/mL, respectively, determined with MABA. The MICs under hypoxic conditions were 2 and 1.5 μg/mL, respectively, as measured by LORA. These activities, especially under hypoxic conditions, are in the same range as those of the commonly used TB drugs, capreomycin (CAP, 3 μg/mL), and streptomycin (SM, 1 μg/mL) (**TABLE XIV**). Importantly, the initially observed MICs of the crude fraction, 14046 GE3, were lower (0.5 and 1 μg/mL in MABA and LORA, respectively) than those of the isolates, and the isolates were subportions of this fraction (16% each). This can be caused by the synergistic effects from other ingredients in the fraction that were not included in the isolates or by the minor active constituents still remaining in the isolates.

TABLE XIV. *IN VITRO* ANTI-*M. tb* ACTIVITIES AND CYTOTOXICITY OF 1 AND 2 (μg/mL), IN COMPARISON TO FIVE ANTI-*M. tb* DRUGS

Compound	MABA MIC	MBC [a]	hypoxic MIC [b]	hypoxic MBC [c]	IC_{50}
1	11.3	> 50	2.4	19.5	24.2
2	6.0	44.2	1.5	10.5	7.7
RMP	< 0.02	0.1	< 0.1	0.5	143
INH	0.03		> 140		
MET	> 87.6		> 87.6		
CAP	0.7		3.0		
SM	0.3		0.6		

[a] Tested in normoxic condition.

[b] Determined via luminescence.

[c] Determined via CFU.

In order to assess this further, the MIC values of **1**, **2**, and the fraction 14046 GE3, were converted into volume equivalents of *M. tb* culture which would be inhibited in growth by 90% based on the total weight of each of the samples (ca. 30 mg of **1**, 30 mg of **2**, and 182 mg of 14046 GE3; calculation: Weight ([mg] / MIC [µg/mL] = Volume [L]). Compounds **1** and **2** together accounted for 2.1% and 20.4% of the bioactivity by MABA and LORA, respectively, relative to the mother fraction, 14046 GE3. Accordingly, while the bioassay-guided procedure led to the identification of a major portion of the LORA active principle(s), it can be concluded that further MABA active constituents remain to be discovered and probably represent minor constituents with higher potency.

The minimum bactericidal concentrations (MBC) under normoxic conditions resulting in a one $\log_{10}$ reduction in colony forming units (normoxic MBC_{90}) of **1** and **2** were > 50 and 44 µg/mL, respectively, suggesting that **1** and **2** are actually acting as bacteriostatic rather than bactericidal agents. The MBC_{90} values for **1** and **2** obtained following exposure under hypoxic conditions (hypoxic MBC_{90}), were 20 and 11 µg/mL, respectively, and both were higher than the corresponding luminescence-derived LORA MICs cited above and lower than the normoxic MBCs. The former may be consistent with the bacteriostatic nature of these compounds, while the latter, considered together with MICs tested with LORA that are five times lower than the corresponding MICs tested with MABA, suggests a molecular target that is more efficiently exploited in the non-replicating phenotype. Overall, the data also suggest that **2** has slightly higher potency than **1**.

The IC_{50}s of **1** and **2** against Vero cells were 24 and 8 µg/mL, resulting in rather poor selectivity indices (SI = IC_{50}/MIC). There was relatively little variability in the MICs of **1** and **2**

among representatives of the major global clades (clinical isolated strains) of *M. tb* (**Table XV**) and against isogenic, monodrug-resistant strains (**TABLE XVI**). Again, **2** consistently appears more active than **1**. Overall, the data suggest a molecular target that is conserved throughout the species, but is not exploited by existing TB drugs as they maintain activity against drug-resistant strains.

TABLE XV. MICs OF 1 AND 2 AGAINST STRAINS REPRESENTING MAJOR GLOBAL CLADES OF *M. tb*

Compound	MIC (μg/mL) vs. strain[a]					
	X001354	X003899	X004244	X004439	X005282	X005319
1	9.7	22.9	16.9	9.3	9.6	19.2
2	4.7	4.8	4.7	4.4	4.7	4.8
RMP	0.02	0.1	0.1	0.02	0.03	0.1
INH	0.1	0.1	> 1.1	0.1	0.1	0.9
MET	> 87.6	> 87.6	> 87.6	> 87.6	> 87.6	> 87.6
CAP	0.3	0.7	0.5	0.3	0.3	0.7
SM	0.4	0.2	0.3	0.3	0.6	1.0

[a] X001354 corresponds to an Indo-Oceanic lineage, X004439 and X004244 to East Asian lineages, X005282 and X005319 to Euro-American lineages, X001354 to East African-Indian lineage.

TABLE XVI. MICs OF 1 AND 2 AGAINST MONODRUG-RESISTANT STRAINS OF *M. tb*

Compound	MIC (μg/mL) vs. *M. tb* resistant to:						
	SM	RMP	MOX	KM	INH	CS	CAP
1	11.6	9.6	9.0	12.4	12.1	20.6	12.1
2	4.7	4.7	4.0	4.9	4.7	7.4	4.8
RMP	< 0.01	> 3.3	0.1	< 0.01	0.01	< 0.01	0.04
INH	0.03	0.1	0.1	0.1	> 1.1	0.03	0.1
MET	> 87.6	> 87.6	> 87.6	> 87.6	> 87.6	> 87.6	> 87.6
CAP	0.6	1.0	1.2	8.3	0.5	1.2	> 11
SM	> 9.3	0.1	0.5	1.1	0.1	0.4	1.1

In addition to activity against *M. tb*, **1** and **2** mostly also demonstrated MICs of < 10 µg/mL against Gram-positive bacteria (**TABLE XVII**), but not against the Gram-negative representatives, the yeast *Candida albicans*, nor against *Mycobacterium smegmatis*. Studies have proven that 12 out of 19 virulence genes in *M. tb* share closely related homologs in *M. smegmatis*, and *M. smegmatis* was considered as a surrogate organism of *M. tb* for studying the pathogenic properties of mycobacteria [156]. However, in this anti-*M. tb* drug discovery process, it is clearly demonstrated that anti-*M. tb* compounds may not show activity against *M. smegmatis in vitro*. Therefore, it is not an ideal choice to use *M. smegmatis* as a surrogate for *M. tb* in anti-*M. tb* drug screening procedures, such as in BGF.

MICs of **1** and **2** under normoxic conditions increased by approximately two-fold when the culture media contained 4% bovine serum albumin (BSA) or 10% fetal bovine serum (FBS), while MICs under hypoxia increased by almost ten-fold (**TABLE XVIII**). This suggests that the two hytramycins are likely to undergo moderate serum protein binding.

TABLE XVII. *IN VITRO* ANTIBACTERIAL SPECTRUM OF ACTIVITY OF 1 AND 2 [a]

	MIC in µg/mL (% inhibition)																			
	M. smegmatis		*A. baumannii*		*E. coli*		*S. aureus*		*C. albicans*		*E. faecalis*		*P. aeruginosa*		*S. pneumonia*					
1	> 10 (3)[b]		> 10 (37)[b]		> 10 (17)[b]		> 10 (86)[b]		> 10 (17)[b]		8.0		> 10 (7)[b]		8.4					
2	> 10 (0)[b]		> 10 (77)[b]		> 10 (2)[b]		4.5		> 10 (0)[b]		3.5		> 10 (10)[b]		2.4					
RMP	< 0.3	DO	0.1	AMP	8.9	AMP	1.2	AB	0.4	AMP	> 10 (66)[b]	AMK	1.8	RMP	< 0.01					
INH	13	DE	0.1	GE	1.2	GE	0.6	KE	< 0.004	RMP	0.2	GE	0.5	VAN	0.1					
CLF	1.1	MI	0.2							CIP	4.9	RMP	18	OFL	1.1					
SM	0.1	KM	0.7							VAN	2.3	CIP	0.2	ERY	0.1					
		GE	0.2							OFL	2.3	OFL	1.2							
										ERY	1.9									

[a] CLF=clofazimine; DO=doxycycline; DE=demeclocycline; MI=minocycline; KM=kanamycin; GE=gentamicin; AMP=ampicillin; AB=amphotericin B; KE=ketoconazole; CIP=ciprofloxacin; VAN=vancomycin; OFL=ofloxacin; ERY=erythromycin; AMK=amikacin.

[b] Percent growth inhibition at highest test concentration (10 mg/mL) given in parentheses.

TABLE XVIII. EFFECT OF SUPPLEMENTAL SERUM AND ALBUMIN ON NORMOXIC AND HYPOXIC ACTIVITY OF 1 AND 2

Compound	MIC (µg/mL)			
	Normoxic w/4% BSA	Normoxic w/10% FBS	Hypoxic w/4% BSA	Hypoxic w/10% FBS
1	24.1	29.2	19.1	20.9
2	11.9	9.4	10.8	9.9
RMP	0.02	< 0.02	0.2	0.1
INH	0.1	0.04	> 140	> 140
MET	> 87.6	> 87.6	13.5	5.3
CAP	0.3	0.6	0.8	1.2
SM	0.8	0.6	0.4	0.6

7.3.5 qPAR of hytramycins in ECUM14046 GE

The total ion chromatogram (TIC) of the four bioactive fractions of 14046 (GE2, GE3, GE4, and GE5) showed the peaks of both hytramycins V (**1**) and I (**2**) at 24.7 min and 27.2 min respectively (**Figure 48**), as identified by the extracted ion chromatograms that exclusively selected the molecular ions with the *m/z* of 634 and 648 in these fractions (data not shown).

As mentioned above, fractions eluted with 85% and 95% MeOH (GE3 and GE4) showed much lower MABA and LORA MICs (higher activity, expressed as 1/MIC) than the other two fractions (GE2 and GE5). Accordingly, the abundance of both hytramycins V (**1**) and I (**2**) peaks was at higher levels in the fractions GE3 and GE4. The concentration curve representing the unisolated impurities inversely correlated with the curves of bioactivities, 1/MIC (**Figure 49**).

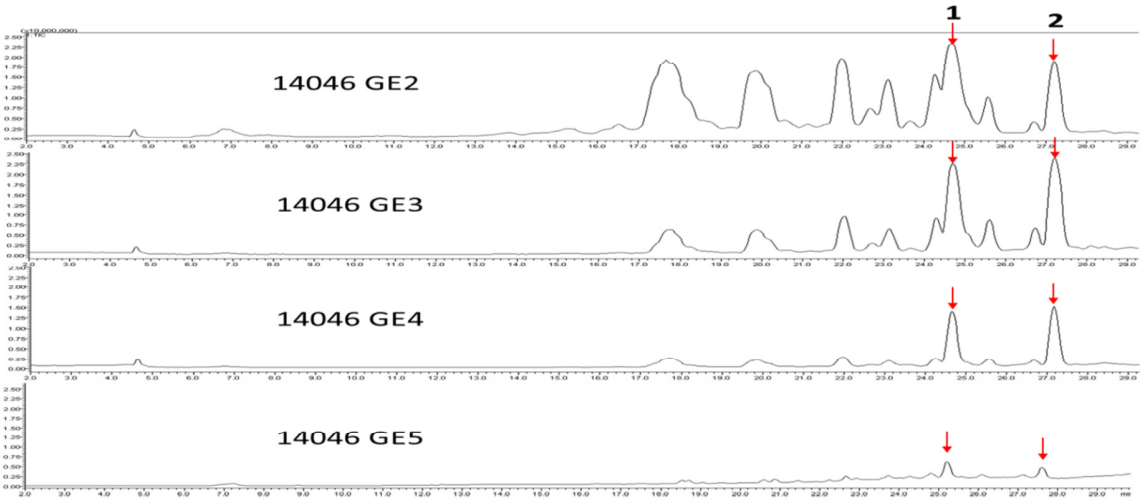

Figure 48. Total ion chromatogram (TIC) of 14046 GE fractions. Peaks eluted at 24.7 min and 27.2 min represent hytramycins V (**1**) and I (**2**) respectively, as indicated by the red arrows. Total run time was 30 min.

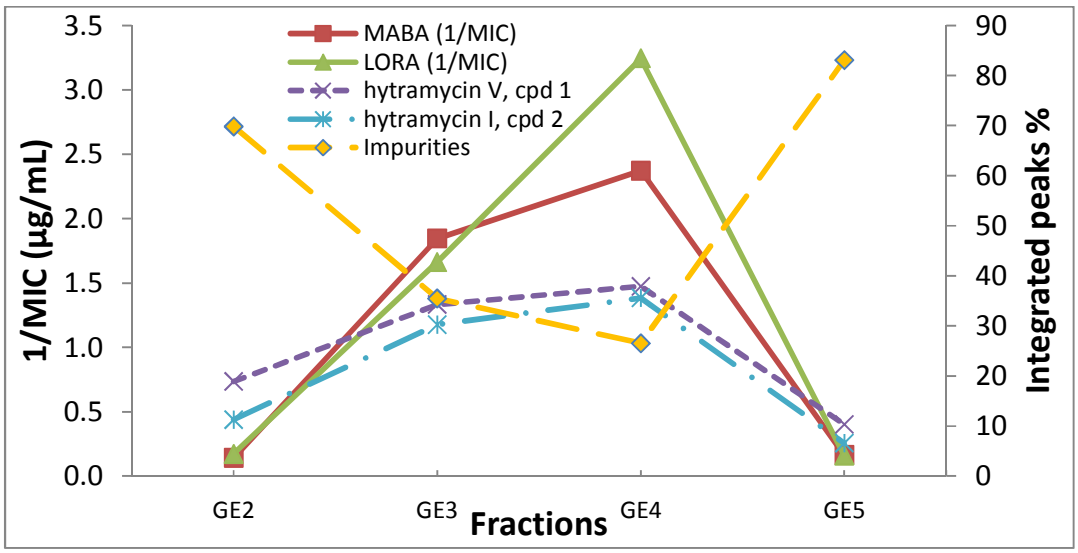

Figure 49. Biochromatogram of 1/MIC of 1 and 2, and their abundance in the column fractions of 14046 GE

Similar to the qPAR study of diastereomeric phytols using a mathematical model (see "Section **6.2**"), the 1/MIC and MIC values of MABA and LORA were correlated with the

percentage concentration of hytramycins V (**1**) and I (**2**) in the hytramycin-containing fractions as follows:

$$1/\mathrm{MIC}_{MABA} = 0.09\,V\% - 1.03\ (\mathrm{R}^2 = 0.92) \quad \text{Equation 8}$$

$$1/\mathrm{MIC}_{MABA} = 0.08\,I\% - 0.55\ (\mathrm{R}^2 = 0.98) \quad \text{Equation 9}$$

$$1/\mathrm{MIC}_{LORA} = 0.10\,V\% - 1.31\ (\mathrm{R}^2 = 0.83) \quad \text{Equation 10}$$

$$1/\mathrm{MIC}_{LORA} = 0.10\,I\% - 0.75\ (\mathrm{R}^2 = 0.90) \quad \text{Equation 11}$$

$$\mathrm{MIC}_{MABA} = 9.93 - 0.25\,V\%\ (\mathrm{R}^2 = 0.85) \quad \text{Equation 12}$$

$$\mathrm{MIC}_{MABA} = 9.40 - 0.24\,I\%\ (\mathrm{R}^2 = 0.95) \quad \text{Equation 13}$$

$$\mathrm{MIC}_{LORA} = 8.56 - 0.24\,V\%\ (\mathrm{R}^2 = 0.92) \quad \text{Equation 14}$$

$$\mathrm{MIC}_{LORA} = 7.97 - 0.23\,I\%\ (\mathrm{R}^2 = 0.98) \quad \text{Equation 15}$$

This mathematical model proved that the percentage concentrations of hytramycins V (**1**) and I (**2**) correlated with the 1/MIC (in **Equations 8-11**) or MIC (in **Equations 12-15**) values of MABA or LORA, showing high correlation coefficients. This confirmed that both constituents were indeed anti-*M. tb* active principles in these fractions. This mathematical model was also able to extrapolate the MIC values of neat hytramycins V (**1**) and I (**2**) at 100% purity (V% or I% = 100) to be 0.1 μg/mL for both MABA and LORA, a convincing estimation of the theoretical MIC values of individual pure constituents from the fractions where other constituents are present.

In **Equations 12-15**, the intercepts of these linear equations, where the independent variables, i.e., hytramycin percentage concentrations, equal to zero (V% or I% = 0), reflected

that the bioactivity (MIC) of the impurities was much lower (MICs >> 7 μg/mL) than that of the hytramycins. This finding excludes the possibility of the presence of another highly potent lead compound in the other peaks visible in the chromatograms of the four fractions shown above.

To conclude, the qPAR study of hytramycins consolidates the activities of these two major constituents in the column chromatography fractions by establishing a pronounced relationship between the percentage concentration and the anti-*M. tb* MIC values of the fractions. By applying a percentage concentration vs. bioactivity comparison, this method only requires prior knowledge of the chromatographic properties and molecular weight of target principles, but considerably facilitates the bioassay-guided fractionation procedures in identifying active constituents during dereplication, scaling-up purification, and keeping track of target fractions.

7.3.6 Summary

First discovered in 1959, natural products containing a piperazic acid moiety have been isolated and proven to exhibit extraordinary biological activities [157]. The anti-cancer agents, himastatin [158-160] and chloptosin [161], in the form of dimers, as well as a recently reported hexadepsipeptide, piperazimycin [162], share great structural similarity with **1** and **2**, together with a series of hexapeptide antibiotics, the NW-G compounds (NW-Gs), isolated from *Streptomyces alboflavus* 313 strain [152, 163-166]. Himastatin, chloptosin, and NW-Gs all have a cyclic structure with six amino acids and contain a hydroxyhexahydropyrroloindole carboxylic acid motif, which in **1** and **2** is replaced by a leucine. All NW-Gs, piperazimycin, as well as the hytramycins **1** and **2** have three piperazic acid moieties in the cyclic structure, two adjacent and the third flanked by other amino acids. NW-G01, G05, and piperazimycin even coincide with

hytramycins in the positions of two *R*-forms and one *S*-form of piperazic acid. The results obtained in the present study are consistent with the strong antibacterial activity of the cyclic piperazic acid-containing NW-Gs [152, 163-166] against Gram-positive bacteria, including methicillin-resistant *Staphylococcus aureus*, and lack of activity against Gram-negative species, and extends this profile to include activity against *M. tb*. In fact, NW-G01 was obtained from Dr. Hatakeyama at Nagasaki University and its anti-*M. tb* MIC was determined to be 18.6 µg/mL in the MABA, virtually identical to that of the hytramycins. The structure of the cyclodepsipeptide, lydiamycin A, isolated from the actinomycete *Streptomyces lydicus*, also includes two piperazic acid residues, and this cyclodepsipeptide inhibited growth of both *M. tb* H_{37}Rv and a resistant *M. tb* strain [167]. Another piperazic acid bearing depsipeptide, depsidomycin, has been isolated from the growth medium of *Streptomyces lavendofoliae*, and the compound inhibited *Mycobacterium vaccae* with an MIC of 3.12 µg/mL [168]. However, the multiple piperazic acid moieties found in **1** and **2** represent uncommon building blocks of peptidic molecules. As their particular spatial arrangement may potentially contribute to the unusual ring structures of these molecules, future studies might address the structural relationship between piperazic acid-containing cyclic peptides and the growth inhibition of mycobacteria and other Gram-positive bacteria.

The final notable point relates to the screening rationale of this project, which has explored actinobacterial secondary metabolites as potential agents against *M. tb*, another bacterium also in the Actinomycetales order. There is evidence that bacterial metabolites that are used as antibiotics induce unexpected changes in expression patterns which can underlie a variety of intrinsic drug resistance systems of bacteria. Accordingly, drug resistance

mechanisms in *M. tb* can eventually be related to microbial competition which eventually drives evolutionary processes [169]. Therefore, laboratory screening for new actinomycete metabolites as antimicrobials can be viewed as being similar to the selection of a competitive strain under the adverse surviving conditions in a natural environment. As such, the study of actinobacterial metabolites represents a rational approach to anti-*M. tb* drug discovery for the discovery of potentially new active pharmacophores.

8. Discovery of xylamycins

8.1 Introduction

Actinomycetes are widely regarded to be a rich source of useful antibiotics [170]. Other than the isolation of hytramycins from ECUM extract 14046 GE, a 65,000 extract library from these microorganisms has been evaluated in ITR through collaboration with ECUM. After primary bioactivity screening, ECUM8412 E, the ethyl acetate extract of an actinomycete strain 8412 was prioritized and used in this study for downstream purification through column chromatography, countercurrent chromatography and preparative HPLC.

The fractionation strategy of ECUM8412 E featured countercurrent chromatography (CCC) as the preferred chromatographic method. In fact, CCC has become an invaluable tool for fractionation of natural extracts [171, 172]. CCC has many favorable separation advantages over other techniques, including high recovery rates of analytes introduced into the column, and the characteristic distribution and retention of analytes in solvent combinations. In the present case, CCC was employed both as a low-resolution high-sample-recovery enrichment technique and a high resolution chromatographic method with a narrow polarity window. The routine use of elution-extrusion countercurrent chromatography (EECCC) ensures that the partition coefficient (K) can be calculated for each fraction. These values act as a guide for further purification and ensure the reproducibility of the whole process.

Solvent system selection is the key to success in CCC. The Generally Useful Estimation of Solvent Systems (G.U.E.S.S.) method [173, 174] was introduced avoiding tedious shake-flask experiments to determine chemical distribution of analytes in mixtures, in which TLC was used

as a simplistic tool that drives the process and serves as a link between CCC behavior and monitoring of constituents in the fractions. The G.U.E.S.S. method has been developed as a chemistry driven method of selecting biphasic solvent systems in both the ChMWat (chloroform:methanol:water) and HEMWat (hexane:ethyl acetate:methanol:water) solvent system families.

At the end of the separation/purification process, a cyclic heptapeptide, **B14**, exhibiting potent inhibition against *M. tb in vitro*, was isolated. Its planar structure was determined by 1D/2D NMR. The structure coincides with one in a series of compounds with similar structures, described as ilamycins, or rufomycins, in a patent by Eli Lilly and Company in 1999, and **B14** was designated as "xylamycin". However, the anti-TB activities of the individual compounds or further development of these compounds for the anti-*M. tb* properties have not been described.

8.2 Materials and methods

8.2.1 Culture and Extraction of ECUM8412 E

Actinomycete strain ECUM8412 was mass cultured (20 L) in G.S.S. media (**Appendix F**). Following fermentation, the mycelia and culture media were separated. The aqueous filtrate was then exhaustively extracted with ethyl acetate. The ethyl acetate portion was back extracted with water and then dried to yield 3.134 g of crude extract.

8.2.2 Column Chromatography

Vacuum liquid chromatography (VLC) of the ethyl acetate extract was performed on an RP-18 stationary phase. A 20% step gradient of MeOH/H_2O was employed after starting with 20%

aqueous MeOH. The column was finally washed with $CHCl_3$. Each of the six fractions was tested for anti-*M. tb* activity with MABA and LORA assays. The MICs were compared with their Vero cell cytotoxicity IC_{50}s, and fractions with high selectivity indices (SI, see "Section **4.5**") were prioritized for HSCCC separation.

8.2.3 High Speed Counter Current Chromatography (HSCCC)

The HSCCC fractionation using all solvent systems (except HEMWat -4) was performed on a CCC-1000 J-type three-coiled planetary motion HSCCC (Pharma-Tech Research Corp., Baltimore, MD, USA), which has a rotation radius (*R*) of 7.5 cm, using 3 × 108 mL PTFE Teflon coils with an inner diameter of 1.6 mm, an outer diameter of 2.7 mm, and β values from 0.47 to 0.73 (β = *r*/*R* where *r* is the distance from the edge of the coil to the holder shaft) for all coils. The sample loop volume was 10 mL. The rotational speed was set at 1000 rpm with a high speed countercurrent chromatograph electronic controller PTR (Pharma-Tech Research Corp., Baltimore, MD, USA). The HSCCC system was equipped with a Lab-Alliance Series III digital single-piston solvent pump, a Shimadzu SPD-10A VP UV-Vis detector with preparative flow cell, a Cole-Parmer modular paperless recorder model 80807-00, and a LKB Bromma 2111 Multirac fraction collector.

The separation that utilized HEMWat -4 as solvent system was conducted in a TBE-300A (Shanghai Tauto Biotech Co., Shanghai, China) with three multilayer coil separation columns connected in series (1.6 mm tubing I.D.) and 240 mL of total column volume with a 20 mL sample loop. The revolution radius or the distance between the holder axis and the central axis of the centrifuge (R) was 5 cm, and the β values of the multilayer coil varied from 0.5 at the internal terminal to 0.8 at the external terminal. The rotational speed of the apparatus could be

regulated with a speed controller in the range 0-1000 rpm, but in this study was fixed at 800 rpm. A Neslab RTE7 constant temperature-circulating bath (Thermo Electron Corporation) was used to control the temperature at 25 °C. The HSCCC system was equipped with a ChromTech Series I digital single-piston solvent pump, a JMST Systems VUV-14D fixed wavelength UV-Vis detector with preparative flowcell (detection done at 254 nm), and a Advantec CHF122SC fraction collector. Data were recorded on a PEAK-ABC Chromatography Data Handling System and then transferred to an Excel worksheet for further treatment.

All the HSCCC separations were performed in reversed-phase mode with the aqueous phase mobile. The samples were dissolved in equal volumes of lower and upper phase, and injected after equilibrating the HSCCC at the established rotational speed. All HSCCC collected fractions were analyzed by TLC in silica gel (Alugram Silica G/UV254 20 × 20 cm plates with a thickness of 0.20 mm, Macherey-Nagel, Germany). The solvent system used for TLC development was $CHCl_3$:MeOH (9:1, v/v) unless otherwise specified. Compound detection was performed with UV light (254 and 366 nm) and a non-specific spraying coloring reagent (98% ethanol, 2% H_2SO_4, 0.4% vanillin).

8.2.4 LC-PDA-MS analysis of HEMWat-0 fractions

Qualitative analysis was performed on a Shimadzu LC-MS-2020 (Shimadzu Scientific Instruments, Inc. Columbia, Maryland U.S.A.) comprised of LC-20AD LC pumps, SIL-20AC auto sampler, DGU-20A_5 degasser, CBM-20A communications bus module, SPD-M20A Diode Array Detector (190-800nm) and CTO-20AC column oven (40 °C). Separation was performed on a YMC-pack ODS-AQ C_{18} column (250 × 4.6 mm I.D., 5 µm, 12 nm) with the flow rate 0.4 mL/min of mobile phase. The solvent system consisted of MeCN with 0.1% formic acid (A) and 0.1%

aqueous formic acid (B) and followed the gradients with 50, 95, 95, and 50% (A) at 0, 15, 30, and 30.1 min, respectively. The sample concentration was adjusted to 50 µg/mL and the injection volume was 5 µL. UV detection was performed at 282 nm. The compounds of interest eluted between 20 and 25 min.

The mass spectrometer set up to scan *m/z* values between 995 and 1500 in positive mode detected the peaks of the compounds of interest. Total ion chromatograms (TIC) describes the retention time of the compound of which the molecular weight is determined.

8.2.5 Preparative HPLC of the HEMWat-0 B14 fraction

Preparative HPLC purification of the **B14** fraction which showed one predominant constituent was performed with Waters 717plus Auto Sampler, Waters 2996 photodiode array (PDA) detector, Waters 600 controller and Waters Delta 600 pumps. A YMC-pack ODS-AQ C_{18} column (250 × 10 mm I.D., 5 µm, 12 nm) was used. The solvent system consisted of MeCN (A) and water (B) and followed the gradient of 90 to 95% (A) from 0 to 19 min, and back to 90% (A) from 19 min to 20 min. The flow rate was 1.8 mL/min, and the PDA was set up at 282 nm. The compound of interest eluted at 10.75 min as the major single peak on the chromatogram (**Figure 50**).

8.2.6 Antibacterial activity assays

See “Chapter 4. Phenotypic screening”.

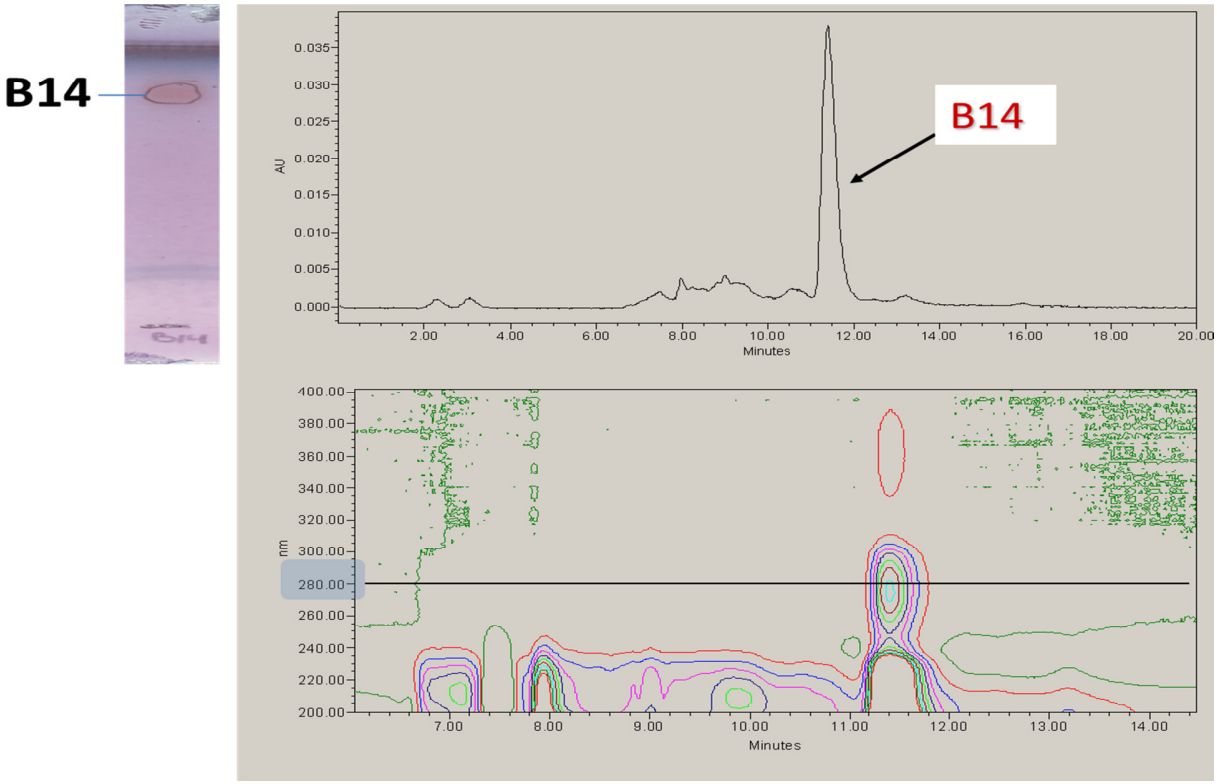

Figure 50. Chromatogram of ECUM8412 B14 fraction showing the elution of compound B14 with preparative HPLC and TLC of B14 fraction on silica gel F_{254} developed with $CHCl_3$:MeOH (9:1)

8.3 Results and discussion

After primary screening of 65,000 ECUM actinomycete extracts for anti-*M. tb* activity, prioritized extracts were processed by a rapid VLC-bioassay-guided fractionation scheme. Following the initial C_{18} cartridge fractionation with MeOH/H_2O gradient elution, three rounds of HSCCC fractionation, and subsequent purification via reverse phase preparative HPLC, one cyclic heptapeptide, xylamycin, structurally similar to the ilamycins (also named “rufomycins”), were isolated from strain ECUM8412 (**Figure 51**). The structure of this heptapeptide contains unusual amino acid residues, such as a nitrotyrosine (NTyr), an *N*-prenyltryptophan (pTrp), a

cyclized dehydrogenated *N*-methyl-leucine (c*N*MeLeu) and a 2-amino-4-hexenoic acid (Hex). The producing organism was tentatively identified as a strain of either *Streptomyces atratus* or *S. sanglieri*. The MABA MIC of **B14** was determined to be 0.05 µg/mL, while the MIC under hypoxic condition measured by LORA was > 10 µg/mL. Under the normoxic condition, **B14** maintained good activities against mono-drug resistant *M. tb* strains, the clinical isolates, as well as *M. smegmatis*, with low cytotoxicity to mammalian cells.

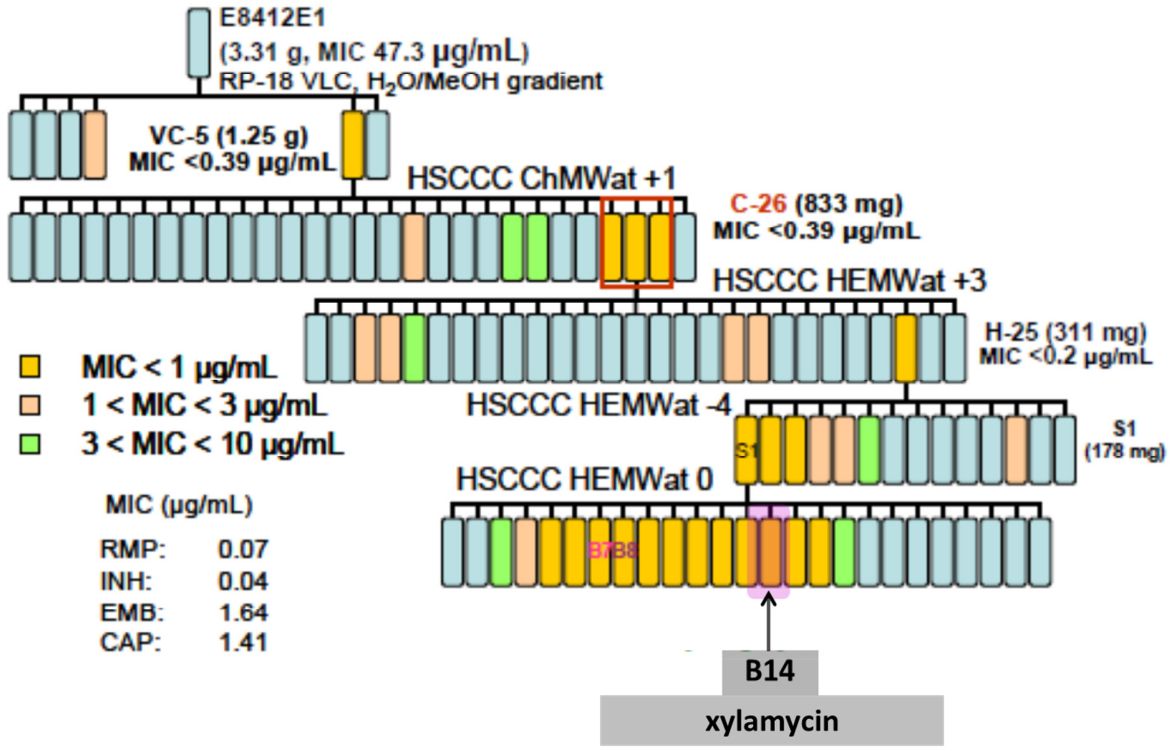

Figure 51. Bioassay-guided fraction scheme of ECUM8412 E extract (performed by Dr. M. Florencia Rodriguez-Brasco)

8.3.1 Physicochemical properties of B14

Ilamycin analogue (**B14**): Light yellow, amorphous powder; IR (neat liquid) ν_{max} 1083, 1210, 1257, 1319, 1420, 1538, 1630, 2957, 3324, cm^{-1} (**Appendix B, Figure B-1**); ^{1}H and ^{13}C NMR, COSY, HSQC, and HMBC data were included in **Appendix B** (**Figure B-3, Figure B-5, and Figure B-6**).

The protonated and sodiated molecular ions from **B14** had *m/z* 1060.5263 (calculated for $C_{54}H_{75}N_9O_{11}{}^{35}Cl$ as 1060.5269) and *m/z* 1082.5221 ($C_{54}H_{74}NaN_9O_{11}{}^{35}Cl$), respectively, as determined by HR-ESI-IT-TOF mass spectroscopy (**Appendix B, Figure B-2**). These combined with NMR data established the molecular formula of **B14** as $C_{54}H_{74}N_9O_{11}Cl$. The UV absorption spectrum of **B14** (**Appendix B, Figure B-1**) showed a strong shoulder peak at 220 nm, and weak peaks at 274 nm and 358 nm. The IR spectrum of **B14** exhibited a strong and sharp absorption band at 1630 cm^{-1} (C=O, stretching), a broad weak absorption band at 3324 cm^{-1} (N-H, stretching), medium absorption bands at 2850-2960 cm^{-1} (aliphatic C-H, stretching), overall consistent with a peptidic nature of the molecule; a medium absorption at 1538 cm^{-1} indicating the nitro-aromatic ring of the molecule (N=O, stretching).

8.3.2 Screening, prioritization and fractionation of ECUM8412 E extract

From the 65,000 crude extracts of actinomycetes source, a total of 349 extracts (0.55%) exhibited > 90% inhibition of *M. tb* growth, based on the primary screening using MABA. Ninety of the high inhibition hits were profiled in terms of IC_{50} against Vero cells, non-replicating *M. tb* with LORA, mono-drug resistant *M. tb* with MABA, and the spectrum of activity against bacteria other than the mycobacteria. Twenty-two samples with promising activities were then re-tested to confirm activities. Based on the cumulative data, 18 of these hits were re-fermented

at a 20 L scale at ECUM with subsequent fractionation and bioassay at UIC. The ethyl acetate extract of actinomycete strain ECUM8412 was chosen based on its performance in these bioassays.

The initial VLC fractionation of 3.31 g of crude extract of ECUM8412 led to a 1.25 g bioactivity-enriched fraction, VC5, with an MIC of 0.3 μg/mL. This represents a greater than 50-fold bioactivity per mass enrichment from the crude extract.

8.3.2.1 Step 1: HSCCC separation with ChMWat +1 (10:4:6)

The choice of solvent system for the subsequent CCC step was based on evidence provided by TLC of fraction VC5 in chloroform/methanol/water (ChMWat) 80:20:1 [173, 174]. The flow rate was 3 mL/min, and the stationary phase retention volume ratio (Sf) was 0.84. The HSCCC was run in elution mode until reaching a K value of 3.24 before switching to extrusion mode [175]. In total, 164 fractions (9 mL each) were collected and then recombined into 28 fractions, according to the TLC results.

The CCC step with the ChMWat +1 (10:4:6) solvent system provided a bioactivity-enriched fraction representing 67% of the VLC fraction's mass. The position of the active fractions outside the region of optimal separation, the so-called "sweet spot," for the CCC experiment indicates that the active constituents would not be expected to be highly resolved in this separation. Indeed, the TLC of the fractions, which were combined into a fraction VC5C26 ($13 \leq K \leq \infty$), showed a rather wide polarity range for the compounds present. This fraction had a total mass of 833 mg and an MIC of < 0.4 μg/mL.

8.3.2.2 Step 2: HSCCC with HEMWat +3 (4:6:4:6)

Instead of adjusting the polarity of the ChMWat solvent system, an orthogonal solvent system [hexane/ethyl acetate/methanol/water (HEMWat)] was used for the next separation step. The HEMWat solvent system chosen was 4:6:4:6, which is the portal solvent system for the HEMWat family [176]. This means that the partition coefficient (K) of an analyte in this solvent system can be extrapolated to predict the K value of the analyte in any other HEMWat family. The mobile phase flow rate was 1.5 mL/min and Sf was 0.74. The HSCCC was run in elution mode until K = 2.50, followed by switching to extrusion mode and the flow rate was changed to 3 mL/min. A total of 200 fractions (6 mL each) were collected and were recombined into 27 fractions based on TLC. The active fraction VC5C26H25 ($18 \leq K \leq 37$) had a mass of 311 mg and an MIC of < 0.2 μg/mL. This represents a significant increase in the specific activity of the sample, but the position of the active fraction was again outside the sweet spot and the active compound would not be expected to be highly resolved from other compounds of similar chemical properties.

8.3.2.3 Step 3: HSCCC with HEMWat -4 (7:3:6:4)

According to the previously published graphic [174, 176], a compound with K = 27 in HEMWat 4:6:4:6 (HEMWat +3) should have a K value of approximately 1 in HEMWat 7:3:6:4 (HEMWat -4). Therefore, the solvent system was switched to HEMWat -4 in this round of HSCCC separation (Step 3). The mobile phase flow rate was 2 mL/min, and Sf was 0.77. The HSCCC was run in elution mode until K = 1.26, followed by switching to extrusion mode. The 113 fractions collected were recombined into 14 fractions based on the TLC of individual fractions. The MIC value observed for active fraction VC5C26H25S1 (178 mg) was < 0.2 μg/mL, which is in the

range of the anti-*M. tb* gold standard drug, rifampin (0.1-0.2 µg/mL). Fractions S2 and S3 also had significant anti-tuberculosis activity, but, because of their diminutive masses, were not carried on to the next step. In this case, the active fractions ended up in the low K-value end. Even so, the chromatographic step resulted in an enrichment of bioactivity by retaining 57% the mass of the active fraction from the previous active fraction.

8.3.2.4 Step 4: HSCCC with HEMWat-0 (5:5:5:5)

At this point a different approach was taken to determine the optimal solvent system. A traditional shake-flask experiment was performed to determine how the bioactivity would partition between the upper and lower phases of a biphasic solvent system. When shaken with equal volumes of HEMWat 5:5:5:5 (HEMWat-0), the active fraction from the previous step showed a distribution of activity with an MIC of 0.2 µg/mL in the upper phase and an MIC of 0.4 µg/mL in the lower phase (K_{MIC} = 0.65). This step of fractionation indicated that the compounds responsible for the bioactivity of the sample would likely be eluted in the sweet spot $0.25 \leq K \leq 8$ (**Figure 51**; **TABLE XIX**). The result also suggests that HEMWat-0 is a preferable solvent system for HSCCC separation of the active principles in this fraction from the beginning.

In this HSCCC run, the mobile phase flow rate was 2 mL/min and Sf was 0.60. The HSCCC was run in elution mode until K = 6.25, followed by switching to extrusion mode. A total 476 fractions collected and recombined into 25 fractions based on TLC results. The anti-*M. tb* activity of fractions 5 to 16 representing $0.80 \leq K \leq 4.07$ generally fell in the range of that of rifampin. According to the TLC results, these active fractions contained a variety of distinct compounds (**Figure 53**). Several of the fractions were sufficiently pure for structural elucidation of the major constituent.

TABLE XIX. ANTI-*M. tb* ACTIVITY OF SUB-FRACTIONS OF FRACTION S1

Fraction names	MIC (µg/mL)	Mass (mg)
ECUM8412 E-1-VC-5-C26-H25	< 0.2	
ECUM8412 E-1-VC-5-C26-H25-S1-B1	23.5	37.0
B2	38.4	17.3
B3	6.2	10.2
B4	1.6	6.1
B5	0.7	3.3
B6	0.7	2.9
B7	2.9	6.1
B8	< 0.2	8.9
B9	0.6	6.5
B10	< 0.2	11.4
B11	0.2	4.5
B12	< 0.2	5.4
B13	< 0.2	2.7
B14	**< 0.2**	**7.8**
B15	0.6	2.7
B16	< 0.2	3.2
B17	3.5	2.6

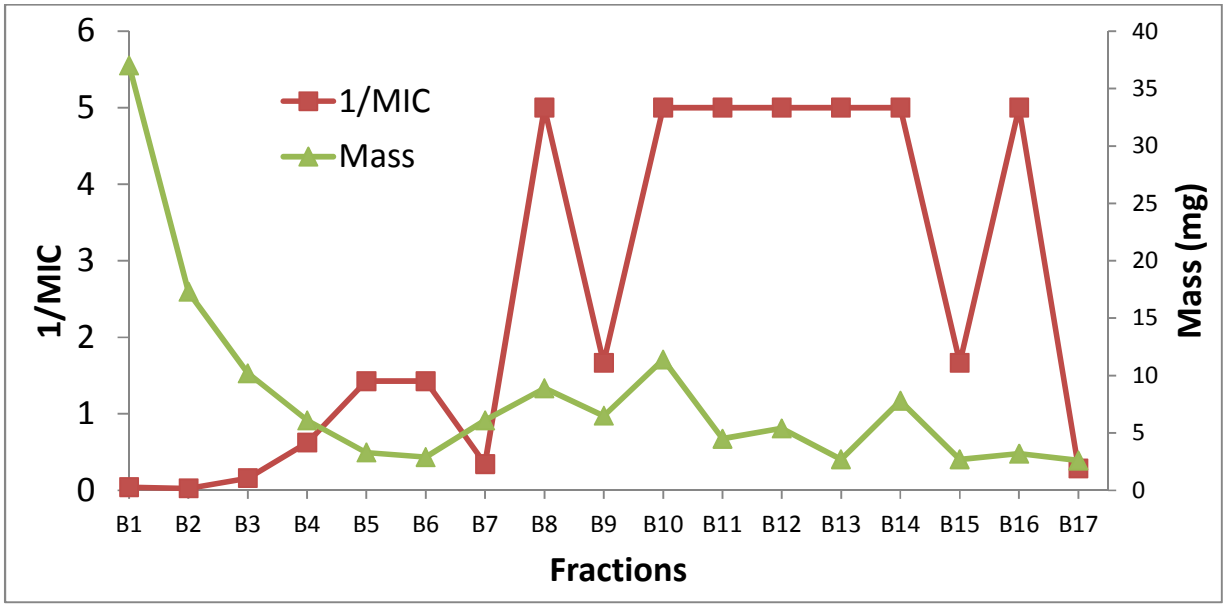

Figure 52. Biochromatogram (mass vs. 1/MIC) of fractions B1 through B17

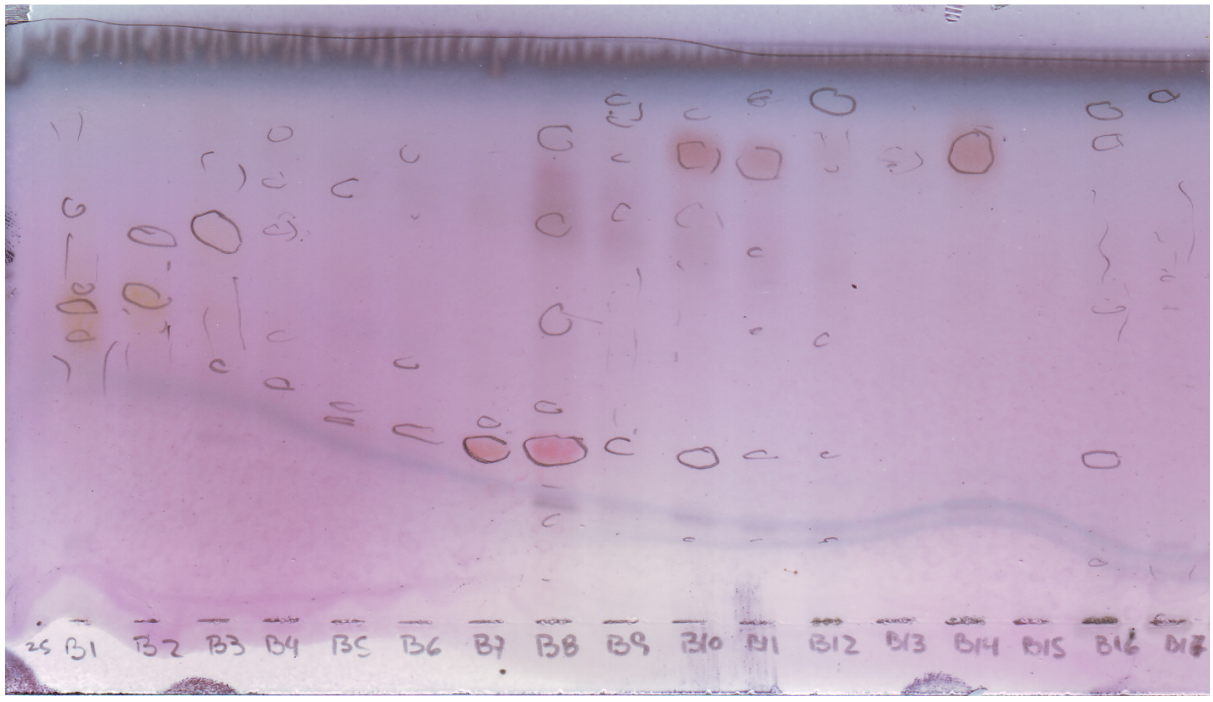

Figure 53. TLC of fractions B1 through B17 on silica gel F_{254} developed with $CHCl_3$:MeOH (9:1) (by Dr. M. Florencia Rodriguez-Brasco)

As the resolving power of HSCCC is focused on a relatively small number of compounds within a limited polarity range, the sweet spot defined by the choice of the biphasic solvent system was not easily determined for the hundreds of HSCCC fractions. After four rounds of HSCCC separation using different solvent systems, the bioactive fractions in extract ECUM8412 eventually fell in the sweet spot of distribution within an appropriate K value range. Although HSCCC has the weakness of exhibiting rather narrow windows where small numbers of compounds in specific polarity ranges can be resolved, each of the four sequential rounds of HSCCC separation contributed to the purification of the active constituents from the extract. This conclusion highlights the importance of selecting the appropriate solvent systemts for different target compounds. Due to the CCC advantage of essential lack of sample loss, the yield of bioactive fractions was still sufficient for structural elucidation and the performance of subsequent bioassays.

Fractions B9 through B16 were analyzed using the LC-PDA-MS system to determine sample purity and obtain molecular mass information of the principal constituents. One or more peaks with molecular masses between *m/z* 1017 and 1124 were detected in positive ionization mode for each fraction. Fraction **B14** with a mass of 7.8 mg was chosen for a final preparative HPLC purification step due to its relatively singular composition. As a result, 2.2 mg of **B14**, xylamycin, could be recovered from this fraction by multiple HPLC injections. The recovery rate of **B14** from the initial crude extract of 20 L re-fermented ECUM8412 was 0.01% (w/w), or 111 ppm.

8.3.3 Structural elucidation

The 4-5 ppm region of the ^{1}H NMR spectrum of **B14** and the correlation of these resolved protons to the carbonyl carbons between 160 and 180 ppm from the HMBC spectrum gave evidences of the peptidic nature of **B14**. Seven carbonyl carbons were identified in the ^{13}C NMR spectrum of **B14** in MeOH-d_4 (δ 174.2, 173.4, 173.1, 172.1, 171.5, 169.8, and 168.1 ppm), among the 54 carbons detected in total (**Figure 54, TABLE XX**). Data from ^{1}H NMR (**Figure 55**, **Figure 56**) and 2D NMR spectra (**Figure 57**) confirmed the structure of **B14** as a cyclic peptide with seven amino acid residues.

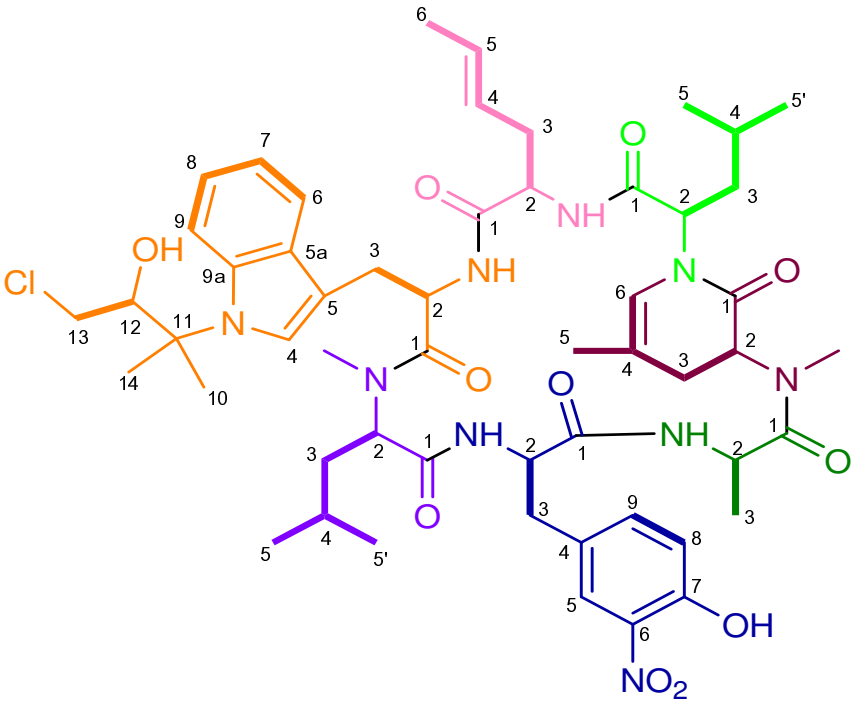

Figure 54. Structure of B14 showing color coded amino acid residues

TABLE XX. ^{1}H AND ^{13}C NMR DATA OF B14 IN METHANOL-d_4 [a]. AMINO ACID RESIDUES ARE CODED IN DIFFERENT COLORS.

position	δ_C, mult.	δ_H, mult. (*J*)	COSY	HMBC (H→C)
pTrp 1	174.23, C	-		
2	51.46, CH	4.825, dd (10.1, 6.2)	pTrp-3	pTrp-3, -5, Hex-1
3	28.77, CH_2	3.188, dd (16.0, 10.1)	pTrp-2, -4	pTrp-1, -2, -4, -5, -5a
		3.169, dd (16.0, 6.2)	pTrp-2, -4	pTrp-1, -2, -4, -5, -5a
4	126.02, CH	7.094, s	pTrp-3	pTrp-2, -3, -5, -5a, -9, -9a, -11,
5	109.01, C	-		
5a	130.76, C	-		
6	119.89, CH	7.558, ddd (7.9, 1.2, 0.7)	pTrp-7, -8	pTrp-5, -5a, -8, -9a
7	120.46, CH	7.064, ddd (7.9, 6.9, 0.7)	pTrp-6, -8	pTrp-5a, -9
8	122.55, CH	7.138, ddd (8.5, 6.9, 1.2)	pTrp-6, -7, -9	pTrp-6, -9a
9	114.66, CH	7.655, ddd (8.5, 0.7, 0.7)	pTrp-8	pTrp-5a, -7
9a	136.39, C	-		
10	26.31, CH_3	1.760, s		pTrp-11, -12, -14
11	63.02, C	-		
12	76.38, CH	4.482, dd (9.7, 2.2)	pTrp-13	pTrp-10, -11, -13, -14
13	46.84, CH_2	3.293, dd (9.6, 2.2)	pTrp-12	pTrp-12
		2.923, dd (9.7, 9.6)		
14	23.01, CH_3	1.650, s		pTrp-10, -11, -12
NMeLeu 1	169.90, C	-		
2	59.22, CH	4.327, dd (10.7, 4.0)	*N*MeLeu-3	*N*MeLeu-1, -3, -4, -6, pTrp-1
3	37.69, CH_2	-0.408, ddd (13.1, 8.6, 4.0)	*N*MeLeu-2, -4	*N*MeLeu-1, -2, -4, -5, -5'
		1.544, ddd (13.1, 10.7, 5.0)	*N*MeLeu-2, -4	*N*MeLeu-1, -2, -4, -5, -5'
4	25.33, CH	0.950, ddqq (8.6, 6.7, 6.6, 5.0)	*N*MeLeu-3, -5, -5’	*N*MeLeu-5, -5’
5	23.25, CH_3	0.441, d (6.7)	*N*MeLeu-4	*N*MeLeu-3, -4, -5’
5’	21.22, CH_3	0.079, d (6.6)	*N*MeLeu-4	*N*MeLeu-3, -4, -5
6	29.24, CH_3	2.361, s		pTrp-1
NTyr 1	171.60, C	-		
2	56.76, CH	4.617, dd (10.8, 5.8)	NTyr-3	NTyr-1, -3, -4, *N*MeLeu-1
3	37.69, CH_2	3.106, dd (13.3, 5.8)	NTyr-2	NTyr-1, -2, -4, -5, -9
		2.916, dd (13.3, 10.8)	NTyr-2	NTyr-1, -2, -4, -5, -9
4	130.71, C	-		
5	126.45, CH	7.787, d (2.2)	NTyr-9	NTyr-3, -4, -6, -7, -9
6	135.35, C	-		

TABLE XX. (Continued)

position	δ_C, mult.	δ_H, mult. (*J*)	COSY	HMBC (H→C)
7	154.34, C	-		
8	120.46, CH	7.069, d (8.5)	NTyr-9	NTyr-6, -7
9	138.64, CH	7.391, dd (8.5, 2.2)	NTyr-5, -8	NTyr-3, -5, -6, -7
Ala 1	173.13, C	-		
2	47.26, CH	4.855, q (6.7)	Ala-3	Ala-1, -3, NTyr-1
3	17.61, CH_3	1.269, d (6.7)	Ala-2	Ala-1, -2
cNMeLeu 1	168.05, C	-		
2	59.86, CH	4.178, dd (11.4, 7.5)	c*N*MeLeu-3	c*N*MeLeu-1, -3, -4, -7, Ala-1
3	33.37, CH_2	2.851, dddq (18.4, 11.4, 1.4, 0.4)	c*N*MeLeu-2, -5	c*N*MeLeu-1, -2, -4, -5, -6
		2.399, dddq (18.4, 7.5, 2.1, 0.4)	c*N*MeLeu-2, -5	c*N*MeLeu-1, -2, -4, -6
4	116.52, C	-		
5	19.84, CH_3	1.766, dt (0.4, 0.4)	c*N*MeLeu-6	c*N*MeLeu-3, -4, -6
6	118.02, CH	5.772, tq (2.1, 1.4)	c*N*MeLeu-5	c*N*MeLeu-1, -3, -4, -5, Leu-2
7	38.67, CH_3	3.300, s		c*N*MeLeu-2, Ala-1
Leu 1	172.04, C	-		
2	55.00, CH	5.252, dd (12.0, 4.3)	Leu-3	Leu-1, -3, -4, c*N*MeLeu-1, -6
3	36.61, CH_2	1.938, ddd (14.2, 10.6, 4.3)	Leu-2, -4	Leu-2, -4, -5, -5’
		1.760, ddd (14.2, 12.0, 0.8)	Leu-2, -4	Leu-2, -4, -5’
4	25.50, CH	1.514, ddqq (10.6, 6.7, 6.6, 0.8)	Leu-3, -5, -5’	Leu-5, -5’
5	23.69, CH_3	0.974, d (6.7)	Leu-4	Leu-3, -4, -5’
5’	21.22, CH_3	0.903, d (6.6)	Leu-4	Leu-3, -4, -5
Hex 1	173.40, C	-		
2	53.47, CH	4.614, dd (9.7, 5.0)	Hex-3	Hex-1, -3, -4, Leu-1
3	35.49, CH_2	2.624, dddd (14.3, 9.7, 7.4, 0.6)	Hex-2, -3, -4	Hex-2, -4, -5
		2.591, dddd (14.3, 6.4, 5.0, 0.9)	Hex-2, -3 -4	Hex-2, -4, -5
4	127.11, CH	5.438, dddq (15.2, 7.4, 6.4, 1.5)	Hex-3, -5	Hex-3, -5, -6
5	129.76, CH	5.589, dddq (15.2, 6.4, 0.9, 0.6)	Hex-4, -6	Hex-3, -4, -6
6	18.33, CH_3	1.677, dd (6.4, 1.5)	Hex-4, -5	Hex-4, -5

[a] NMR data generated by HiFSA matching experimental NMR data observed at 900 MHz and 298 K in MeOH-d_4.

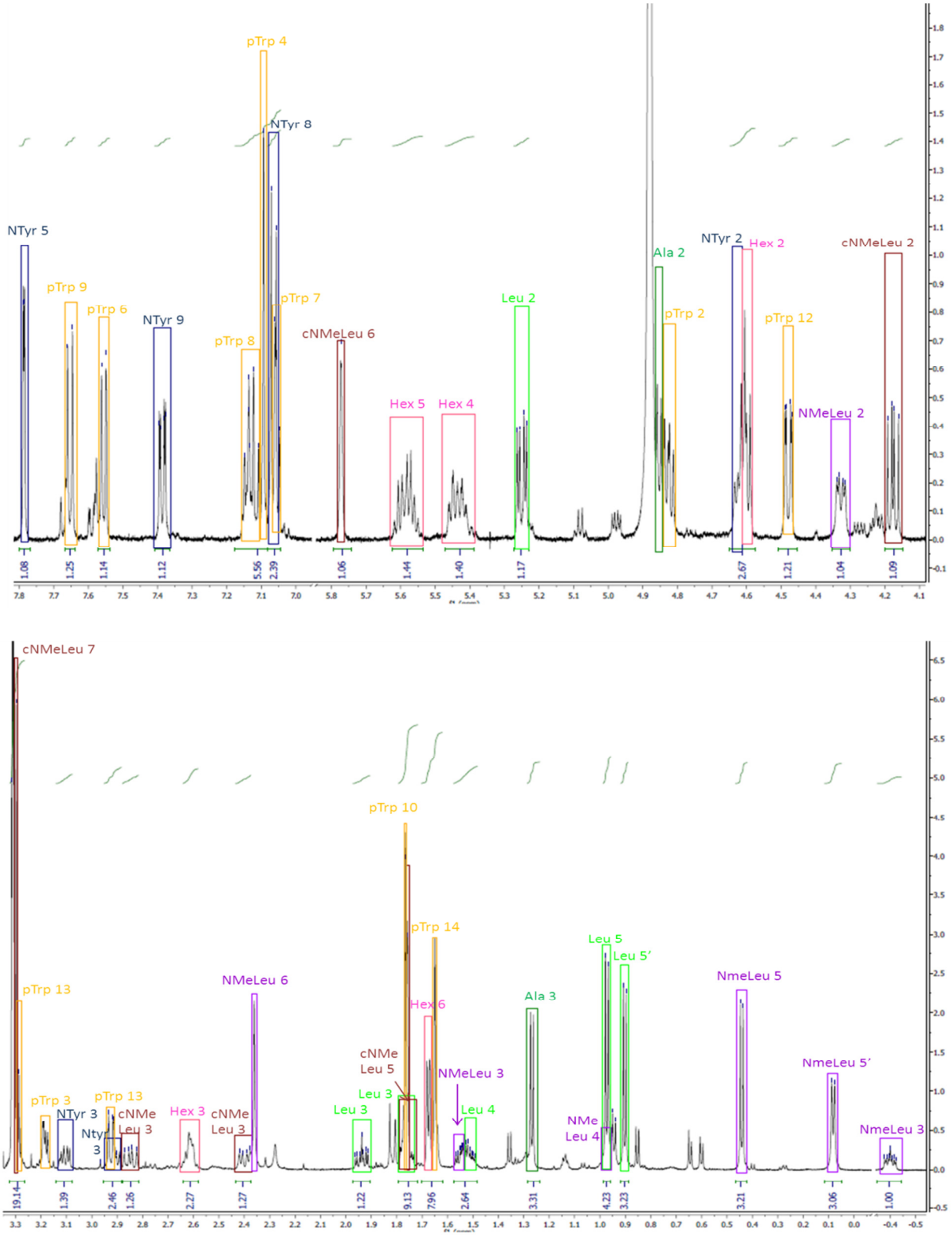

Figure 55. ^{1}H NMR spectra of B14 in MeOH-d_4 (600 MHz)

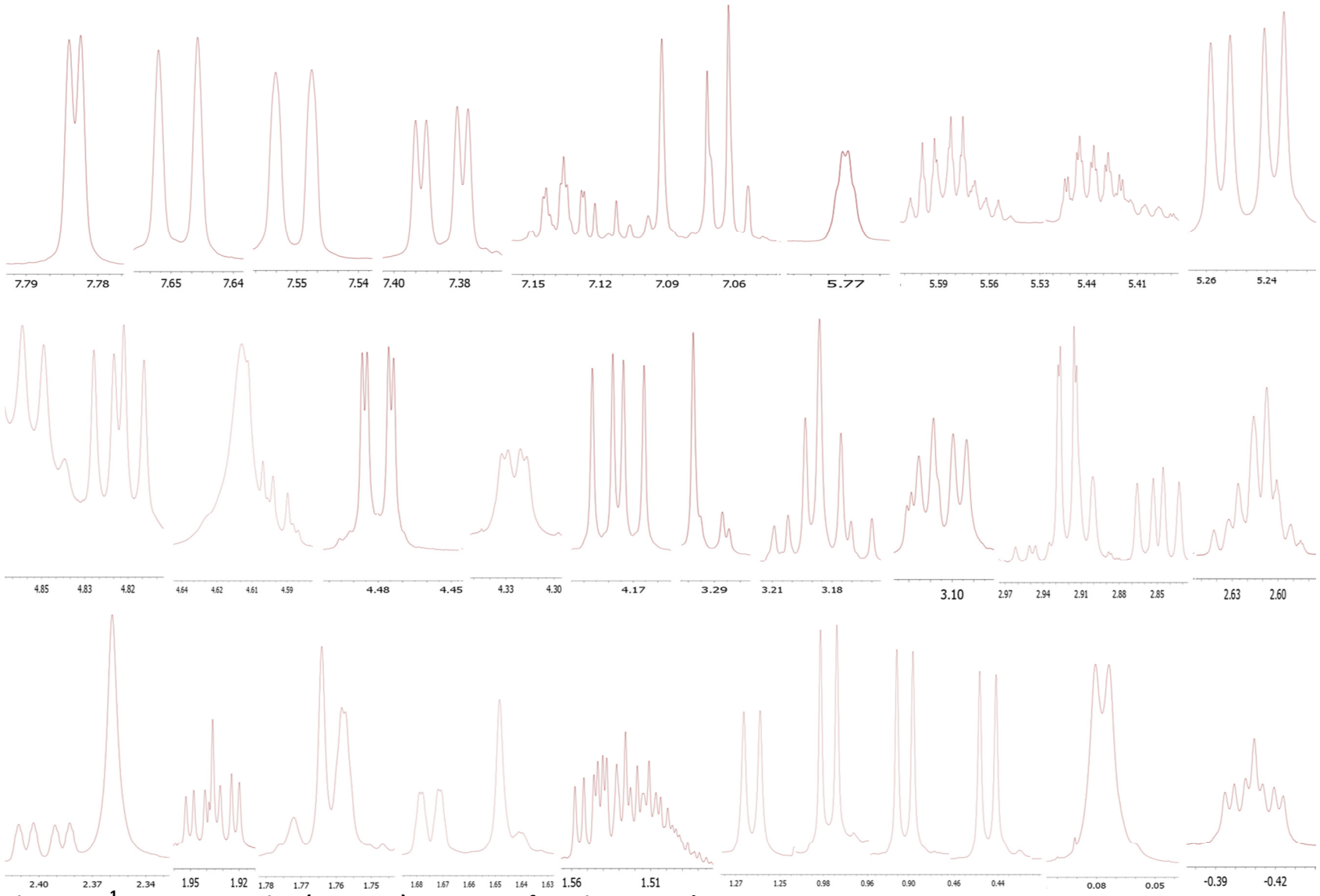

Figure 56. ^{1}H NMR expansion (900 MHz) spectrum of B14 in MeOH-d_4

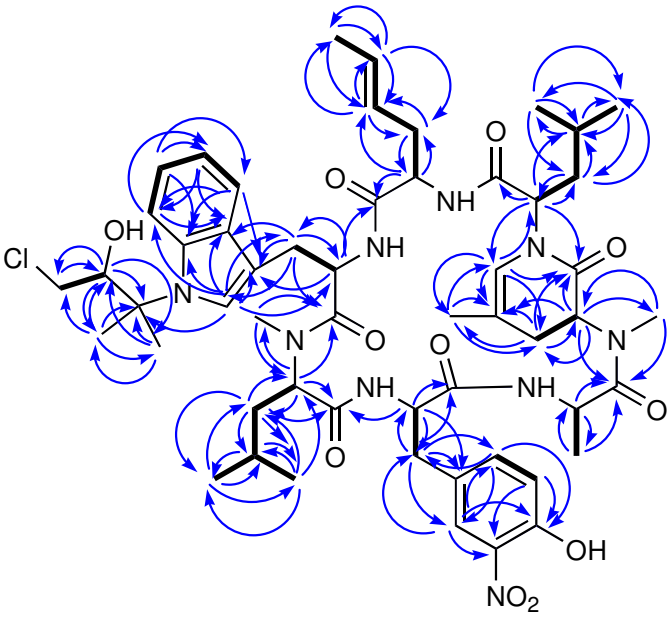

Figure 57. Key correlations in the 2D-NMR spectra of B14. Bolded bonds: COSY ^{1}H spin systems; Blue arrows: HMBC H → C.

Eight protons resonated in the 4.1-5.3 ppm region and were identified as α protons of the amino acid moieties, except for one proton (δ 4.479, dd) which was identified as the hydroxyl proton of the modified prenyl group on the tryptophan residue.

The proton resonating at δ 4.852 appeared as a quartet (*J* = 6.67 Hz), suggesting it is vicinal to a CH_3 group, which resonated as a doublet (δ 1.268). COSY and HMBC spectra confirmed this group of signals to belong to an alanine (Ala), (**Figure 58**).

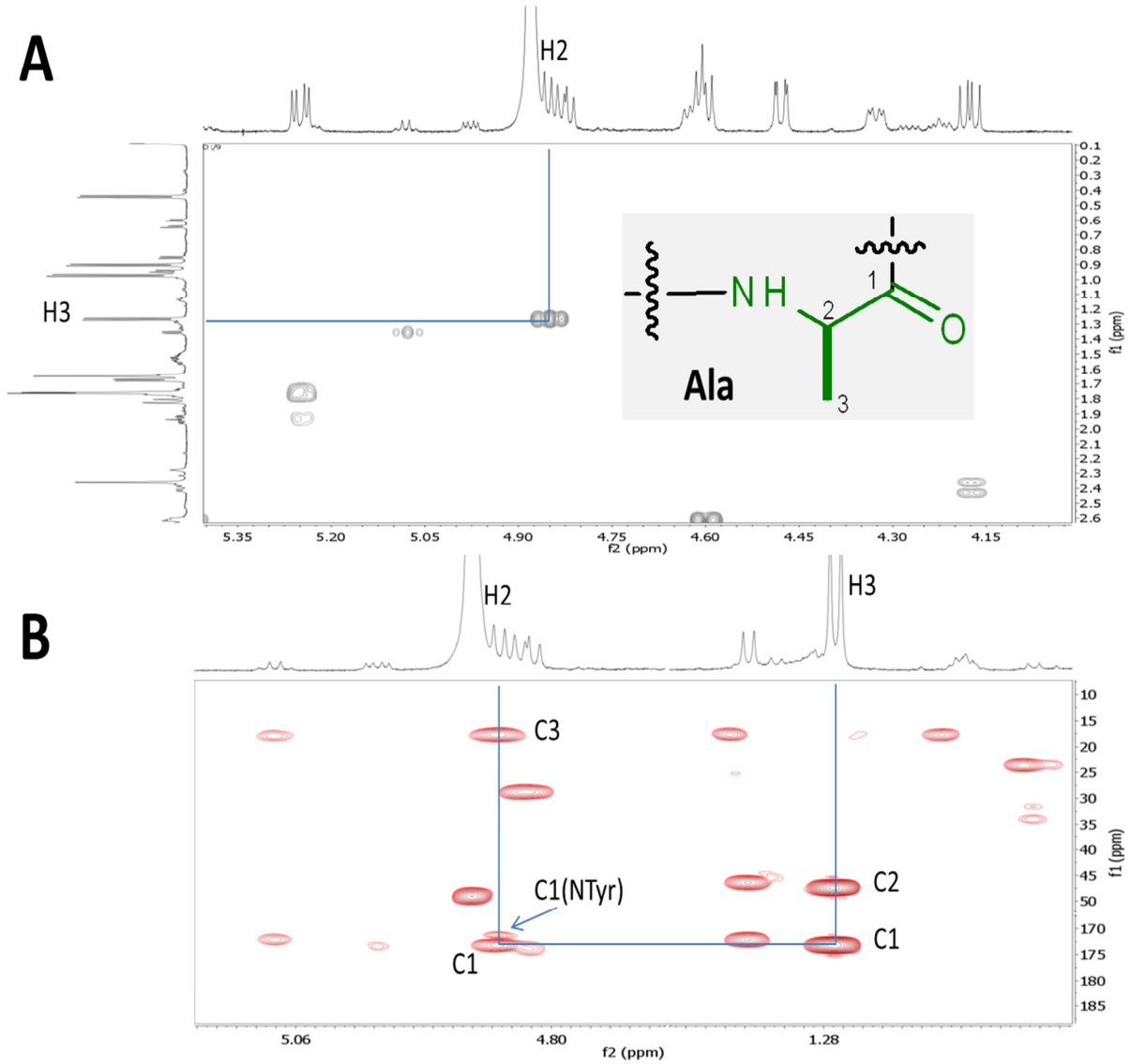

Figure 58. COSY (A) and HMBC (B) spectra highlighting the alanine (Ala) residue in B14 (600 MHz, MeOH-d_4)

By the interpretation of the COSY and HMBC spectra, the proton resonating at δ 5.249 (dd, *J* = 12.28, 4.29 Hz) was assigned to a leucine (Leu) α proton, with the two methyls (δ 0.973 and 0.903) correlating with the same methine proton (δ 1.510), which is neighboring a methylene (δ 1.938 and 1.770) next to the α proton (**Figure 59**).

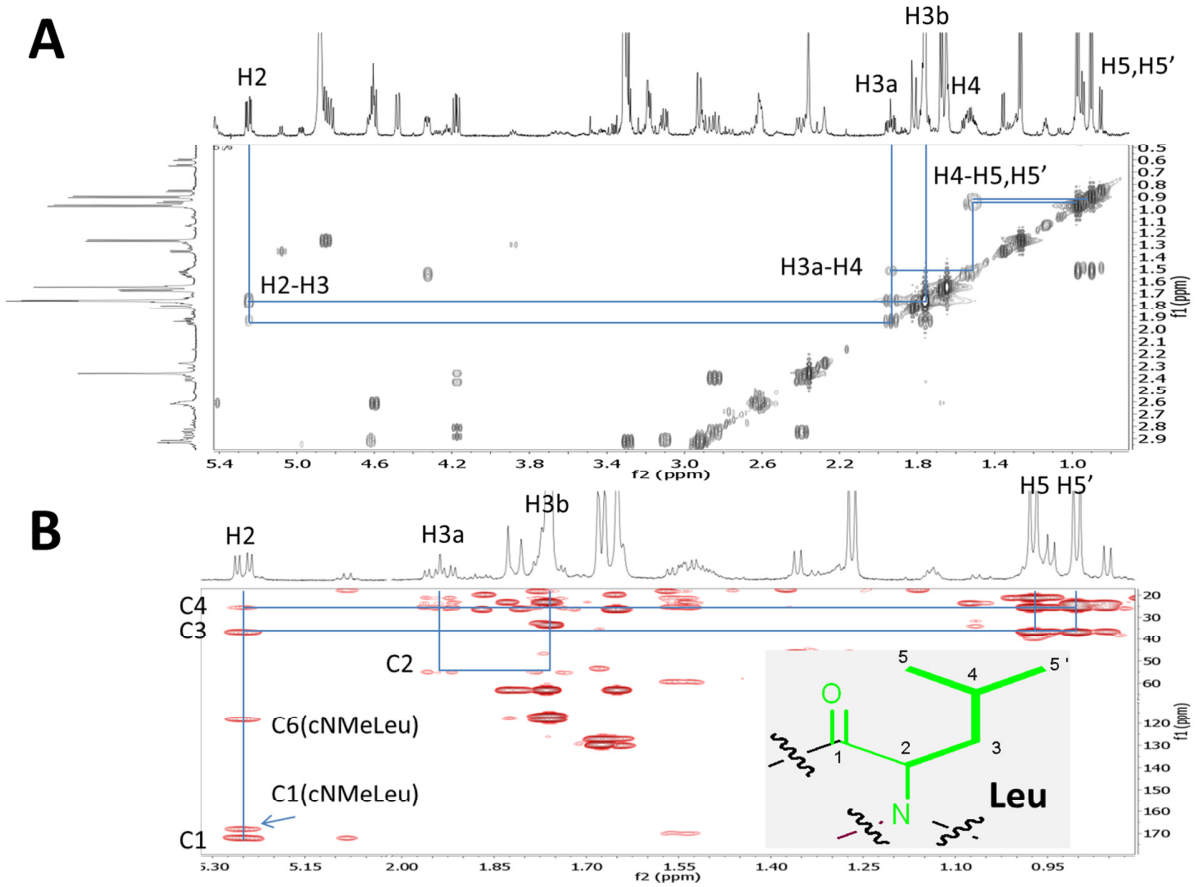

Figure 59. COSY (A) and HMBC (B) spectra highlighting the leucine (Leu) residue in B14 (600 MHz, MeOH-d_4)

In the same manner, an *N*-methyl leucine (*N*MeLeu) was identified containing an *N*-methyl (δ 2.361, s), an α proton (δ 4.327), one methylene with an extremely shielded proton exhibiting an unusual negative chemical shift (δ -0.400 and 1.530), a methine (δ 0.970), and two methyls (δ 0.442 and 0.082). Comparing the spectra of Leu and the *N*MeLeu, it can be noticed that the all proton chemical shifts of *N*MeLeu are distinguishably moved upfield, including an

extremely shielded methylene proton resonating at δ -0.4, suggesting that *N*MeLeu is overall situated in a strongly shielded environment in the molecule (**Figure 60**).

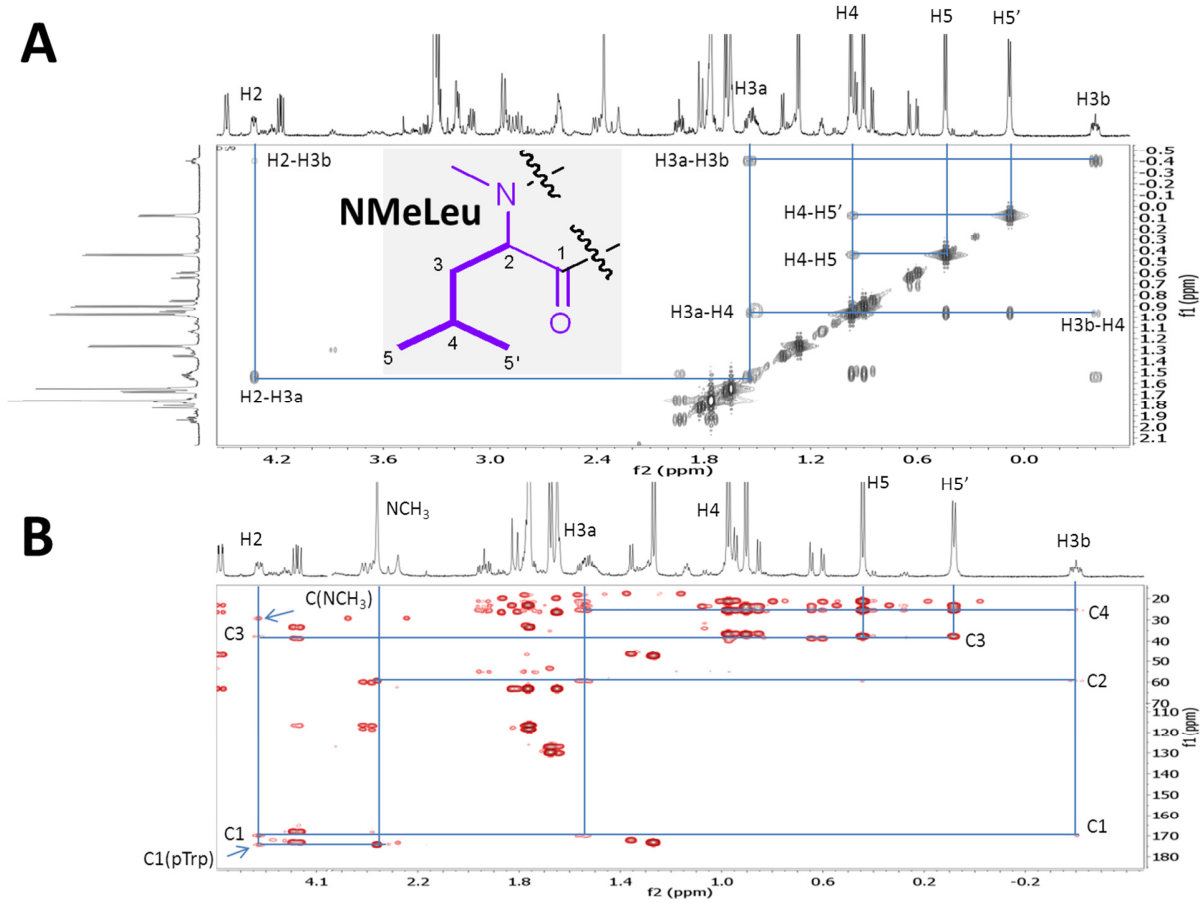

Figure 60. COSY (A) and HMBC (B) spectra highlighting the *N*-methyl leucine (*N*MeLeu) residue in B14 (600 MHz, MeOH-d_4)

Another *N*-Methyl leucine was biosynthetically modified by dehydrogenation on the methine and a methyl, followed by a cyclization that connected the terminal methyl with the nitrogen in the amide bond from a neighboring amino acid, turning the original *N*-methyl leucine into a cyclized *N*-methyl leucine (c*N*MeLeu). The c*N*MeLeu contained an *N*-methyl (δ 3.298, s), an α proton (δ 4.176), a methylene (δ 2.848 and 2.398), a methyl (δ 1.764), and the

proton resonating as a multiplet (δ 5.772, tq) with a characteristic splitting pattern of small coupling constants, i.e., long distance couplings. This multiplet also has characteristic correlation with the carbonyl of the neighboring residue in the HMBC spectrum. From the biosynthetic perspective, the *N*-methyl leucine likely experienced oxidization at one CH_3 to a terminal aldehyde, which subsequently condensed with the nitrogen of the adjacent amino acid through dehydration of the resulting aminol to form the cyclized *N*-methyl leucine derivative (**Figure 61**).

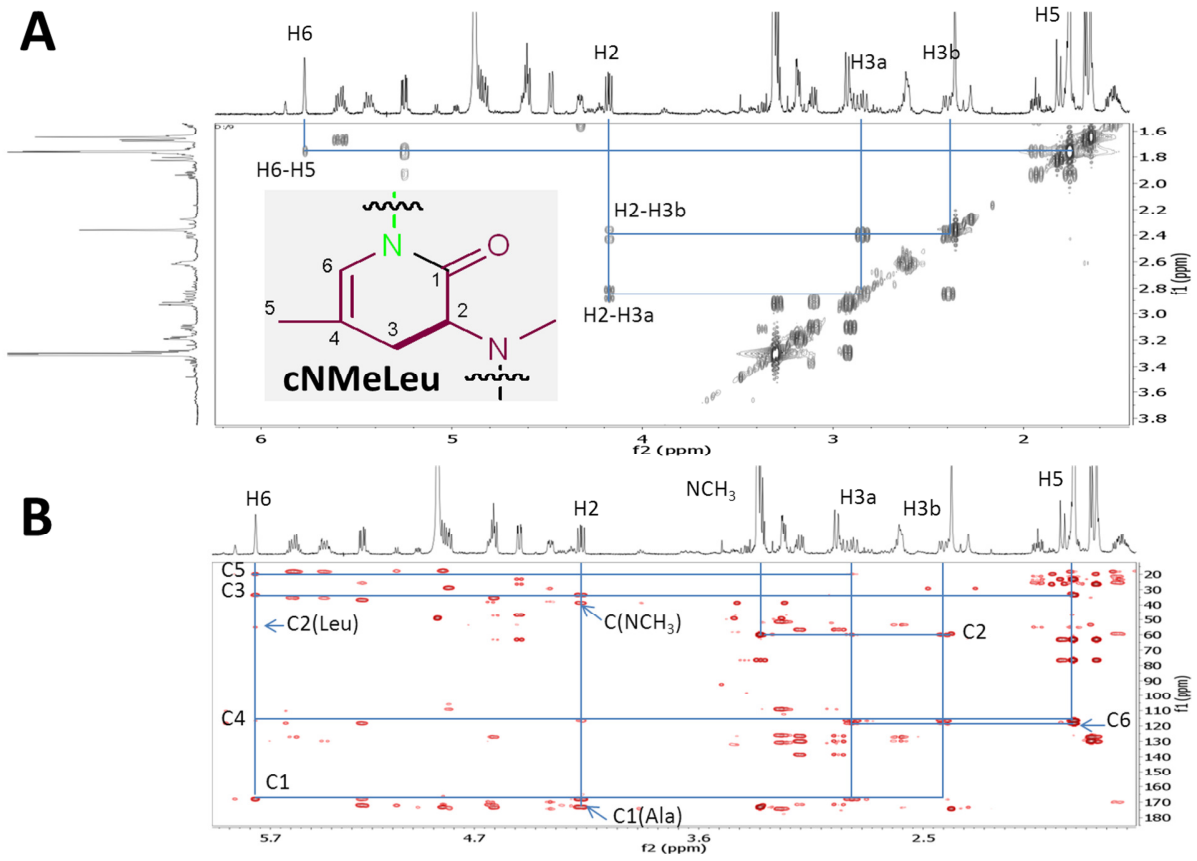

Figure 61. COSY (A) and HMBC (B) spectra highlighting the cyclized *N*-methyl leucine (c*N*MeLeu) residue in B14 (600 MHz, MeOH-d_4)

The COSY and HMBC spectra easily distinguished the protons of an amino hexenoic acid residue (Hex) as belonging to the same spin system, including an α proton (δ 4.595), a methylene (δ 2.610, 2.610), two alkene methines with complex coupling patterns (δ 5.436, dtq; 5.582, dqt) and a terminal methyl (δ 1.676) (**Figure 62**).

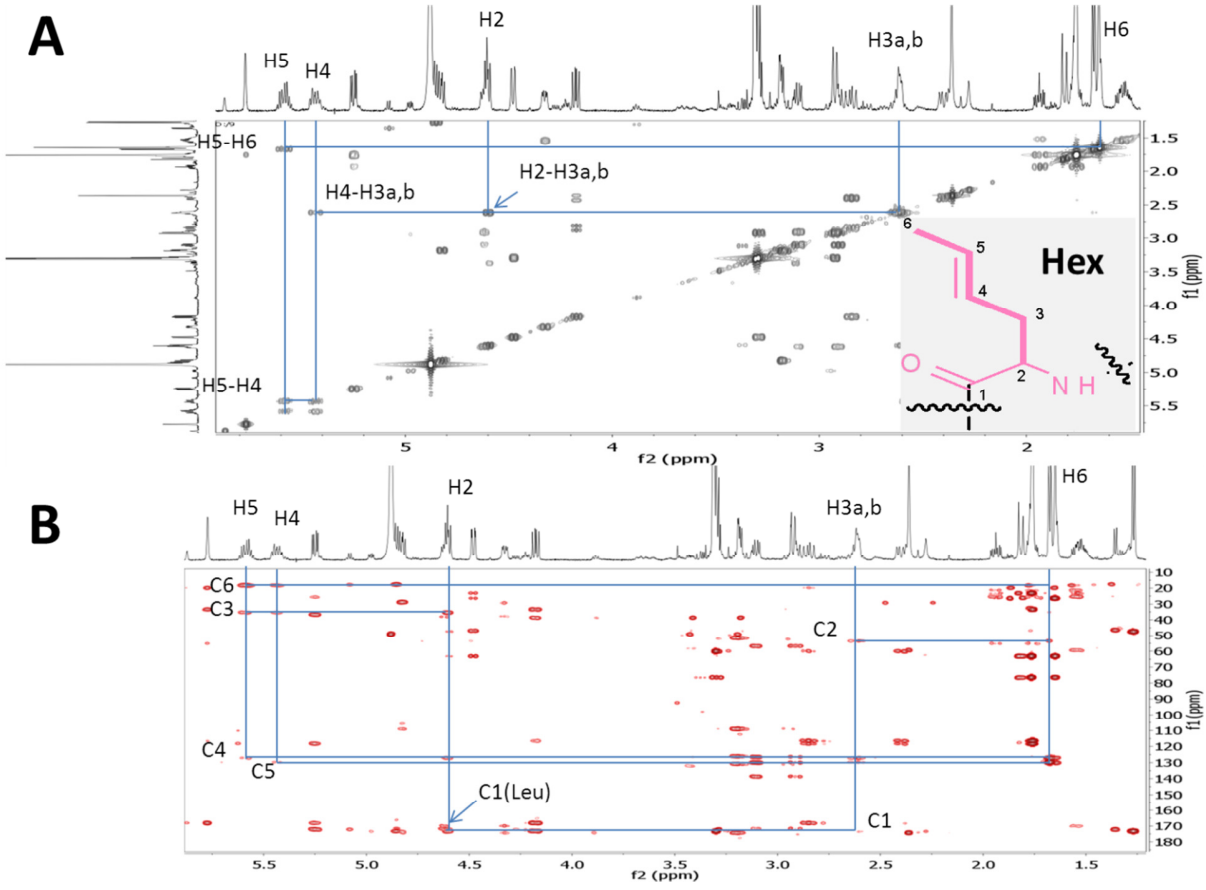

Figure 62. COSY (A) and HMBC (B) spectra highlighting the amino hexenoic acid (Hex) residue in B14 (600 MHz, MeOH-d_4)

Eight protons of **B14** resonated in the 7-8 ppm region and were identified as aromatic protons. The protons resonating at δ_H 7.786, 7.386, 7.065 form an ABX spin system according to the splitting patterns and coupling constants, and were identified as the three aromatic protons of the nitrotyrosine (NTyr) with the help of COSY and HMBC spectra. The NTyr moiety also contained a methine-methylene spin system, identified as the α (δ 4.611) and the benzyl protons (δ 3.108 and 2.910) (**Figure 63**).

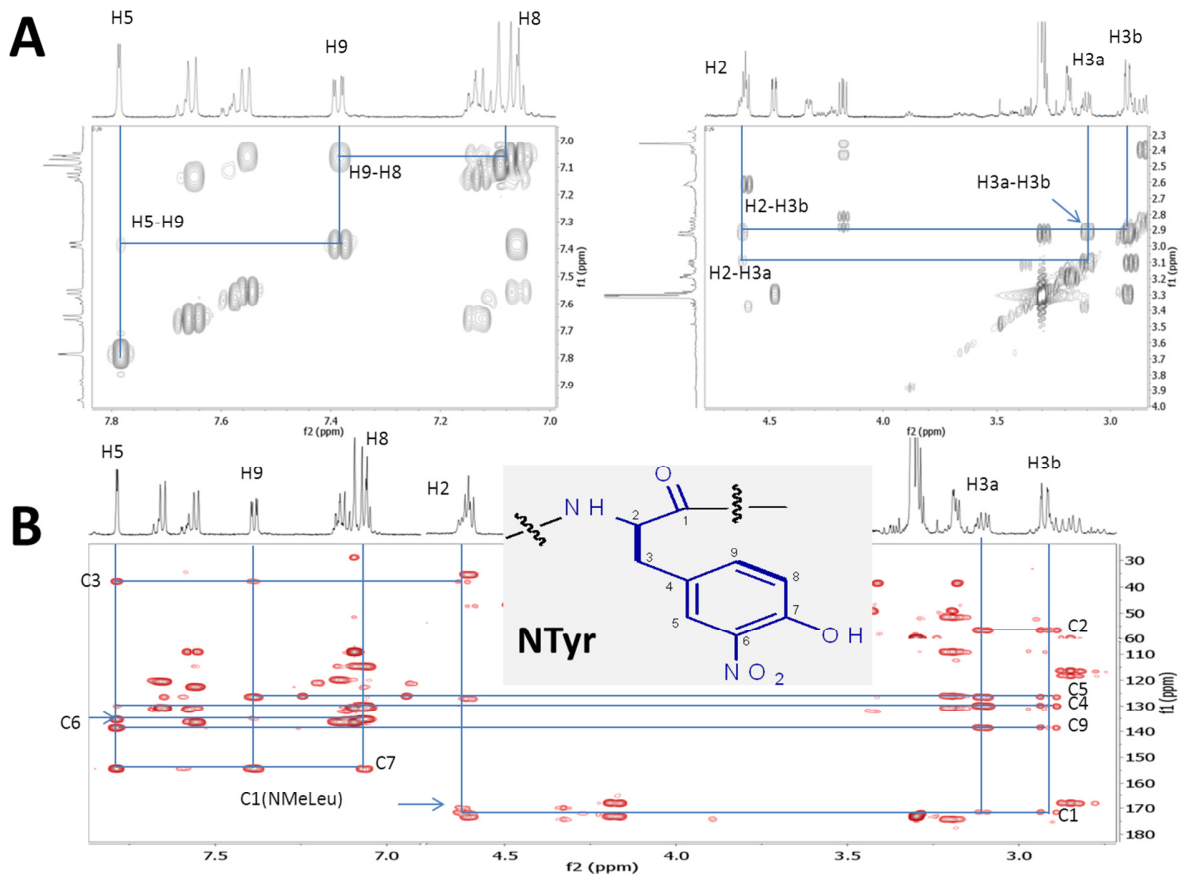

Figure 63. COSY (A) and HMBC (B) spectra highlighting the nitrotyrosine (NTyr) residue in B14 (600 MHz, MeOH-d_4)

Similarly, the other resonating aromatic protons at δ 7.653, 7.555, 7.136, and 7.055 were assigned as the four adjacent protons on an indole ring based on the values of the coupling constants, and the proton showing a singlet peak (δ 7.094) was assigned as the proton next to indole nitrogen. Thus the five aromatic protons of a tryptophan moiety were identified.

The prenylated tryptophan (pTrp) contained two moieties, the tryptophan, including the α proton (δ 4.825) and the methylene (δ 3.187 and 3.181), and the modified isoprene unit, including a hydroxyl methine (δ 4.479) and a chloromethylene moiety (δ 3.282 and 2.925). Two methyls were detected as being attached to the modified part of the tryptophan (δ 1.770, s; 1.650, s) referring to a correlation between the methyl proton and one of the tryptophan carbons (**Figure 64**).

Residual impurities in chloroform as the solvent for the extraction of drugs and metabolites have caused formation of artifacts [177]. The carbons in an epoxide group are very reactive electrophiles partly due to the relieved ring strain when the ring opens upon nucleophilic attack, and the reaction can occur under either acidic, basic, or neutral conditions, including when HCl is present [178]. As it is possible that the addition of a hydroxychloro group in the molecule may have been introduced via an epoxide by the residual HCl in the chloroform used as a solvent during HSCCC separation, it cannot be ruled out that this partial structure represents an isolation artifact.

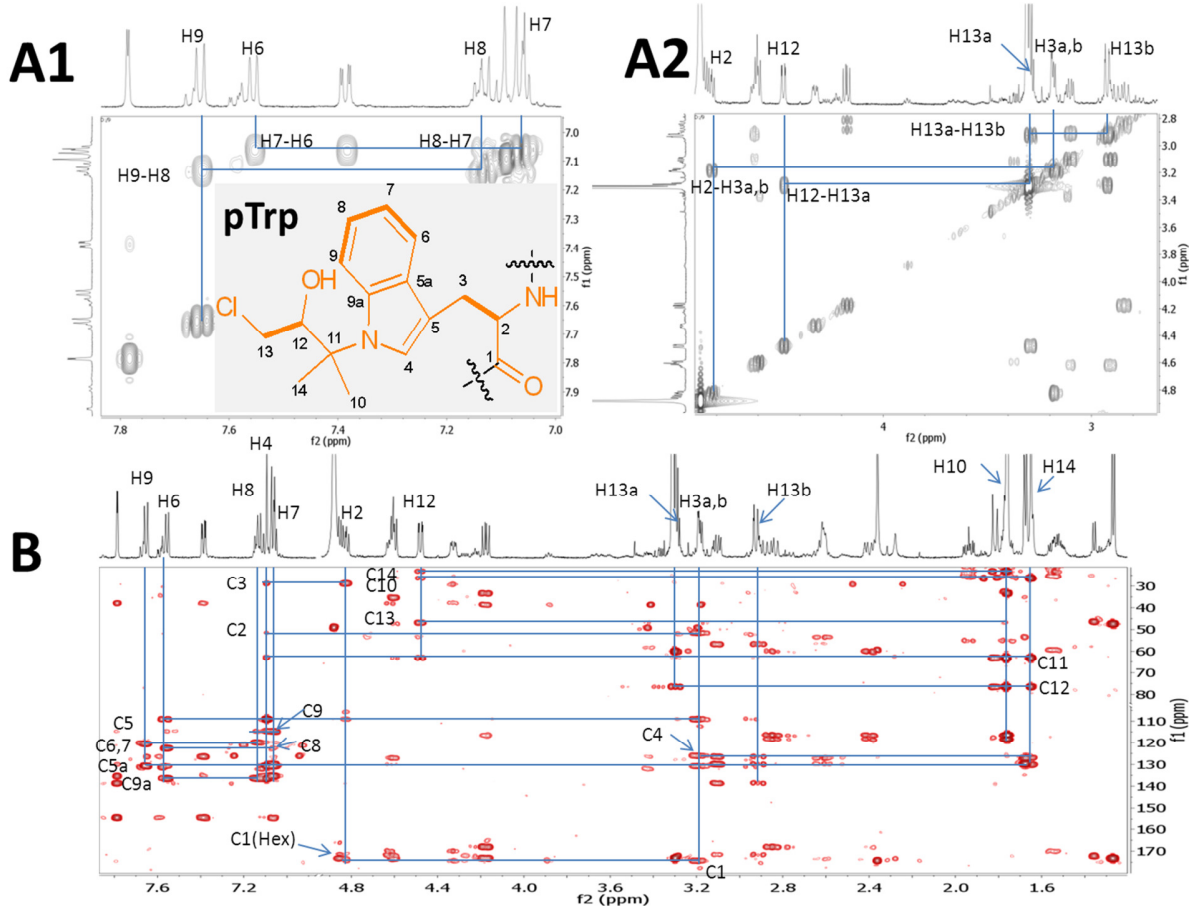

Figure 64. COSY (A1, A2) and HMBC (B) spectra highlighting the prenylated tryptophan (pTrp) residue in B14 (600 MHz, MeOH-d_4)

The connectivity between the seven amino acid residues was confirmed by the observation of HMBC correlations of α protons to both the carbonyl within the residue and to the neighboring carbonyl. Thus, the linkage of the seven moieties was shown to be the cyclic (pTrp-*N*MeLeu-NTyr-Ala-c*N*MeLeu-Leu-Hex).

The ^{1}H NMR spectra and the structure of **B14** are color-coded indicating each individual amino acid residue to facilitate recognition. As peptides have characteristic spin systems,

representing each amino acid unit isolated by the peptide bonds, the chemical shifts and splitting patterns of the proton signals arising from an individual amino acid remain relatively consistent, and only the chemical shifts are slightly affected by the different chemical environment in the molecule, e.g., the different orientation or location of moieties in a 3D molecular structure, in which the coupling constants usually remain unchanged. Color-shading fingerprints aid in the efficient identification of each amino acid based on the ^{1}H NMR spectrum and facilitate dereplication of known compounds and the rapid elucidation of new structures. In the structural elucidation of putatively unknown analogs, identical amino acids can be easily recognized in overlapped proton NMR spectra by comparing the color coded protons corresponding to the specific amino acids with those from an already elucidated peptide structure.

Similar to the spectra of the hytramycins, ^{1}H iterative full spin analysis (HiFSA) was performed to provide unequivocal interpretation of the ^{1}H NMR spectra of pure **B14** with unambiguous assignment of all the chemical shifts and coupling constants. The HiFSA optimized sum of individual spectrum of the amino acids fully matches the experimental spectrum, which confirms the identities of the amino acid moieties in this molecule (**Figure 65; Appendix E**).

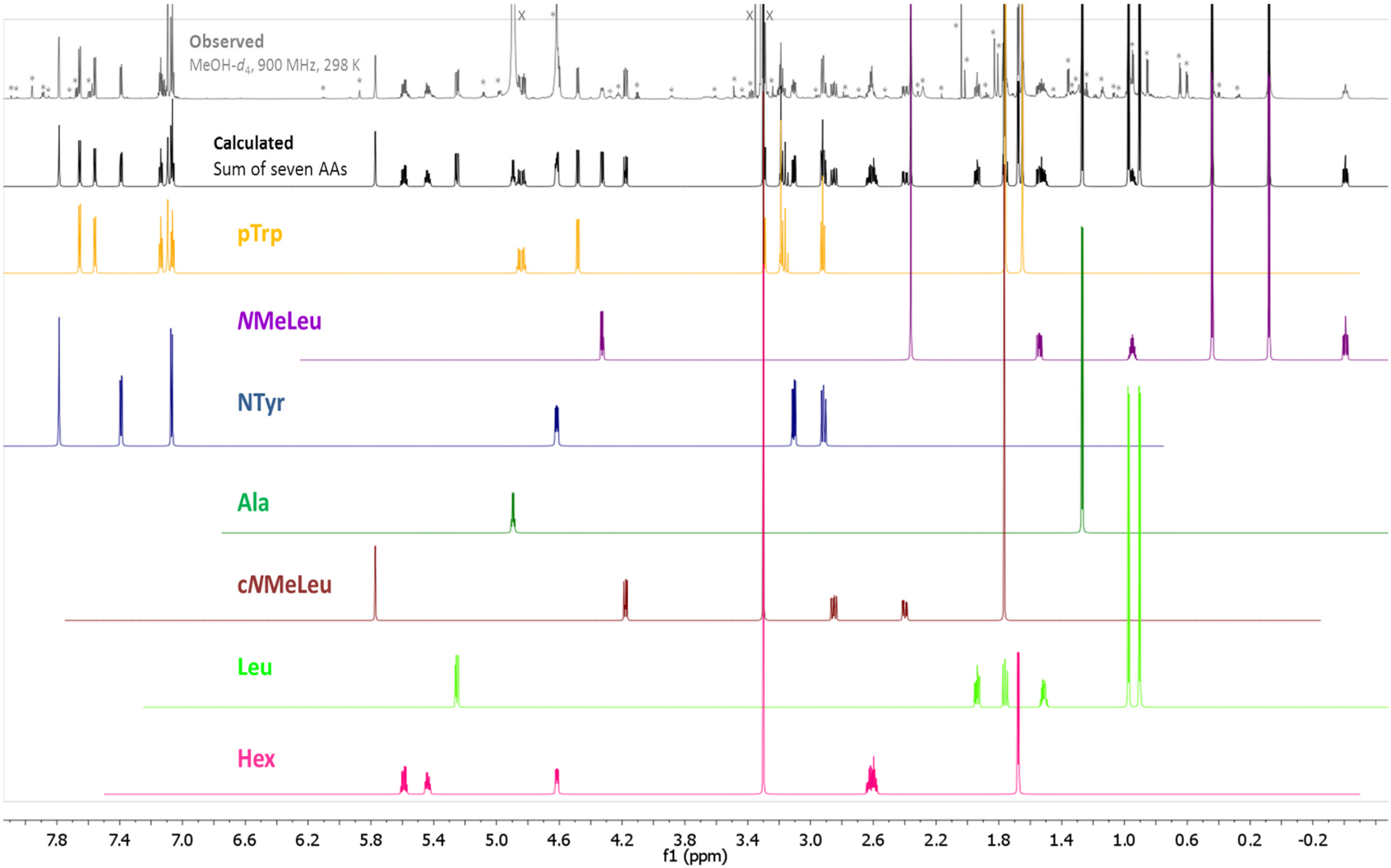

Figure 65. Comparison of experimental and calculated ^{1}H NMR spectra of B14. HiFSA fingerprints of the individual amino acids were included (* denotes unidentified impurities; X denotes solvent peaks; pTrp=prenylated tryptophan; *N*MeLeu=*N*-methyl leucine; NTyr=nitrotyrosine; Ala=alanine; c*N*MeLeu=cyclized *N*-methyl leucine; Leu=leucine; Hex=aminohexenoic acid.

8.3.4 Antimicrobial Activity

The anti-*M. tb* MIC of **B14** (**TABLE XXI**) under normoxic conditions was 0.05 μg/mL, determined with MABA, which is in the same range as the first-line TB drugs rifampin (RMP) and isoniazid (INH). The exact MABA MIC values of **B14** and its mother fractions were so low that they could not be accurately determined until **B14** was diluted to 0.1 mg/mL as the stock concentration for MABA. The MIC under hypoxic conditions was larger than 10 μg/mL measured by LORA. These values indicate that the anti-*M. tb* activity of **B14** is also oxygen dependent as is INH, which suggests that the activity of **B14** is possibly restricted to replicating *M. tb*.

TABLE XXI. *IN VITRO* ANTI-*M. tb* ACTIVITIES AND IC_{50} (μg/mL) OF B14, IN COMPARISON TO ANTI-*M. tb* DRUGS

MIC (μg/mL)	hypoxic MIC [a]	MABA	IC_{50} (Vero)
B14	> 10 (82%)	0.05	> 50
RMP	< 0.05	0.02	128
INH	> 140	0.03	
MET	> 87.6	> 87.6	
CAP	6.2	1.3	
SM	1.0	0.4	

[a] Determined via luminescence.

The *in vitro* macrophage MIC (**TABLE XXII**) of **B14** was < 0.04 μg/mL, rivaling the activity range of RMP upon macrophage cell penetration. The IC_{50} of **B14** against Vero cells as an indicator of cytotoxicity of test compounds was > 50 μg/mL, resulting in a high selectivity index ($SI = IC_{50}/MIC$).

TABLE XXII. *IN VITRO* MACROPHAGE ACTIVITY OF B14

	Test conc.			EC_{90}	EC_{99}	MIC
	H	M	L			
B14	2	0.4	0.08	0.067	0.067	< 0.04
CAP	2	0.4	0.08	0.39	0.64	0.3
SM	2	0.4	0.08	0.24	0.25	0.2
RMP	1	0.2	0.04	0.04	0.05	0.04

H, M and L refer to high, medium and low testing concentrations

B14 maintains potent *in vitro* activity against isogenic, monodrug-resistant strains (**TABLE XXIII**) and toward representatives of the major global cladesof *M. tb* (**TABLE XXIV**) although two of the lower showed higher MICs (> 0.2 μg/mL).

TABLE XXIII. MICs OF B14 AGAINST MONODRUG-RESISTANT STRAINS OF *M. tb*

	MIC (μg/mL) vs. *M. tb* resistant to:						
	CAP	CS	INH	KM	RMP	SM	MOX
B14	0.2	0.05	0.1	0.09	0.2	0.2	0.1
RMP	0.1	< 0.01	0.03	0.02	> 3.3	0.02	0.05
INH	0.1	0.1	> 1.1	0.1	0.1	0.04	0.03
MET	> 87.6	> 87.6	> 87.6	> 87.6	> 87.6	> 87.6	> 87.6
CAP	> 10.7	1.3	1.3	> 10.7	1.2	1.1	0.6
SM	1.1	0.4	0.6	1.4	0.5	> 9.3	0.3

TABLE XXIV. MICs OF B14 AGAINST STRAINS REPRESENTING MAJOR GLOBAL CLADES OF *M. tb*

	MIC (μg/mL) vs. strain (%inhibition)					
	X001354	X003899	X004244	X004439	X005282	X005319
B14	0.04	> 0.2 (64)	> 0.2 (53)	0.1	0.04	0.1

RMP	0.02	0.05	0.05	0.03	0.04	0.05
INH	0.1	0.03	0.1	0.1	0.1	0.1
MET	> 87.6	> 87.6	> 87.6	> 87.6	> 87.6	> 87.6
CAP	0.6	1.3	1.2	1.1	1.3	1.2
SM	0.4	0.2	0.3	0.3	0.8	0.6

In addition to activity against *M. tb*, **B14** also selectively demonstrated its activity on *M. smegmatis* with MICs of 0.1 μg/mL (**TABLE XXV**), a much stronger inhibition compared with the hytramycins V and I (both > 10 μg/mL), but not against the other Gram-positive, Gram-negative representatives, nor the yeast *Candida albicans*. Although **B14** shows a slightly higher MIC against *M. smegmatis* than against *M. tb*, the difference is not significant. This result confirms that **B14** is more likely an antimycobacterial agent showing genus specificity than the hytramycins, which are selectively active on other Gram-positive bacteria as well, but not on *M. smegmatis*. The anti-TB standard drugs, such as RMP and SM, also show inhibition on the growth of *M. smegmatis*, whereas INH shows rather weak activity (> 10 μg/mL). This finding may suggest that the selective activity of potential drug leads against *M. smegmatis* cannot serve as a prioritization criterion during the drug discovery and screening procedures.

The MIC of **B14** under normoxic condition remained at the same level when the culture media contained 4% BSA or 10% FBS, suggesting that **B14** is not strongly bound to or degraded by serum proteins when delivered into mammalian blood vessels (**TABLE XXVI**). Therefore, it is likely that **B14** is a very potent and specific bactericidal agent against most of fast-replicating mycobacteria *in vitro*, exhibiting a unique mechanism of action.

TABLE XXV. *IN VITRO* ANTIBACTERIAL SPECTRUM OF ACTIVITY OF B14 [a]

	MIC in µg/mL (% inhibition)															
	M. smegmatis		*A. baumannii*		*E. coli*	*S. aureus*	*C. albicans*		*E. faecalis*		*P. auruginosa*		*S. pneumoniae*	
B14	0.121		> 10 (4)[b]		> 10 (9)[b]	> 10 (0)[b]	> 10 (0)[b]		> 10 (27)[b]		> 10 (9)[b]		> 10 (0)[b]	
RMP	< 0.3	DO	0.1	AMP	7.9	0.6	AB	0.8	AMP	> 10 (50)[b]	AMK	1.8	RMP	0.05
INH	13.3	DE	0.2	GE	1.1	0.1	KE	0.03	RMP	0.1	GE	0.5	VAN	0.1
CLF	3.0	MI	0.2						CIP	0.6	RMP	9.9	OFL	1.0
SM	0.1	KM	0.7						VAN	2.3	CIP	0.2	ERY	0.03
		GE	0.3						OFL	1.2	OFL	1.1		
									ERY	0.9				

[a] CLF=clofazimine; DO=doxycycline; DE=demeclocycline; MI=minocycline; KM=kanamycin; GE=gentamicin; AMP=ampicillin; AB=amphotericin B; KE=ketoconazole; CIP=ciprofloxacin; VAN=vancomycin; OFL=ofloxacin; ERY=erythromycin; AMK=amikacin.

[b] Percent growth inhibition at highest test concentration (10 mg/mL) given in parentheses.

TABLE XXVI. EFFECT OF SUPPLEMENTAL SERUM AND ALBUMIN ON ANTI-*M. tb* ACTIVITY OF B14 UNDER NORMOXIC CONDITIONS

Compound	MIC (µg/mL)	
	Normoxic w/4% BSA	Normoxic w/10% FBS
B14	0.08	0.07
RMP	0.02	< 0.02
INH	0.1	0.04
MET	> 87.6	> 87.6
CAP	0.3	0.6
SM	0.8	0.6

8.3.5 Summary

As early as in 1960s, the discovery of the ilamycins was already reported by a Japanese research group [179-181]. The secondary structure of ilamycin B1 was elucidated by NMR and

X-ray analysis in the following years. It was demonstrated that ilamycin B1 consists of only L-amino acids that form the cyclic peptide with an odd number of residues in an antiparallel β-type conformation, in which the amide bonds are in the *cis* configuration between alanine and methylated leucine, tryptophan and the other methylated leucine, stabilized by two transannular intramolecular hydrogen bonds [182, 183]. The structure of **B14** falls into the ilamycin family, but shows slight differences from ilamycin B1 in the modification of the tryptophan residue and the dehydrogenation and cyclization of one *N*-methyl leucine between one terminal methyl group and the nitrogen of the neighboring amino acid residue. Apart from these two variable moieties in the molecules, the structures of all other ilamycins share a common backbone (**Figure 66**).

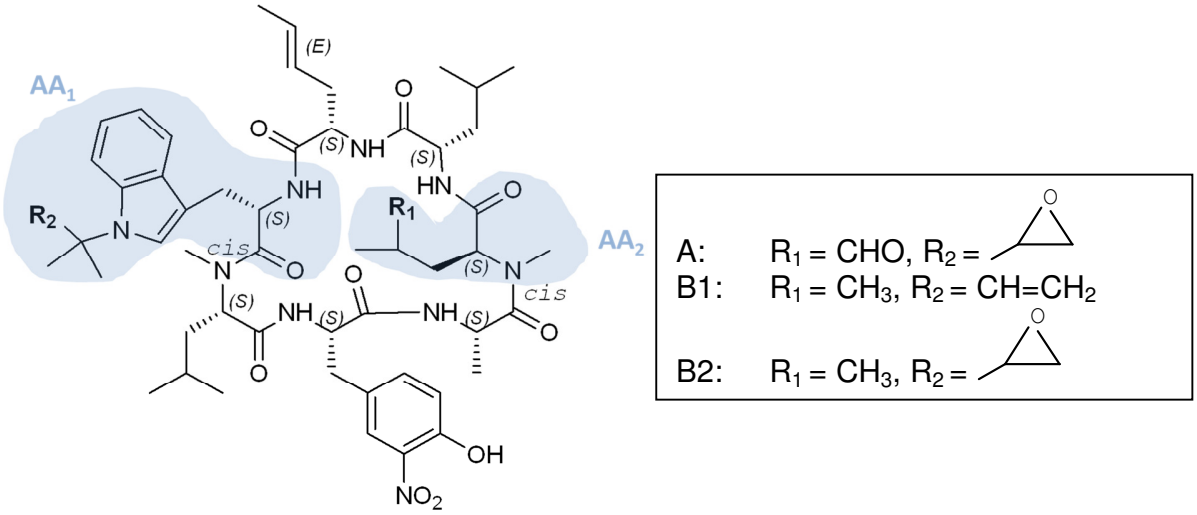

Figure 66. Structure of ilamycins A, B1, and B2, highlighting the two variable amino acid residues, AA_1 and AA_2

The structures of the ilamycins contain two variable amino acid residues. One is an *N*-prenylated tryptophan residue (AA_1), in which the two carbons on the tail of the isoprene contain either a double bond or an epoxide. In **B14**, however, the isoprene moiety is

hydroxychlorinated, which presumably resulted from an addition of HCl from the solvent, more likely from the residual acid in the presence of chloroform, onto the epoxide ring. In this sense, **B14** is likely to be an artifact compound generated during the purification procedures. Using the SIM mode of the LC-MS, whether or not any constituents with the same molecular weight as **B14** are detected from the fractions prior to the introduction of chloroform during fractionation is expected to solve this conundrum.

The other changeable part (AA_2) in the ilamycin structures resides in the *N*-methylated leucine oxidized on the terminal methyl group, which contributes to forming a variety of structural characteristics, including an aldehyde group or cyclization with the amide nitrogen of the neighboring amino acid residue to form a six-membered ring, followed by dehydration of the resulting aminol. This results in a double bond between the γ and δ carbons of the cyclized leucine as is in **B14**.

Cyclic peptides derived from microorganisms have been demonstrated to be a group of potentially bioactive agents, exemplified by the clinically used antibacterial drug, daptomycin, and the immunosuppressant drug, cyclosporine. Moreover, the wide range of bioactivities exerted by the cyclic peptides also include anti-HIV [184], antifungal, and anti-cancer effects [94]. While the environment plays a huge impact on the specificity and timing in the biosynthesis of these functional metabolites, microorganisms also tend to adapt to the otherwise harsh and unfavorable niche where they survive, and circular peptides have better resistance to boiling, extremes of pH, and proteolytic enzymes due to their semi-rigid nature than linear peptides [185]. Moreover, because the hydrolysis of peptides requires the amide

bond to be twisted during the enzymatic reaction, linear peptides are much easier to be hydrolyzed than the rigid cyclic peptides.

The BGF of extract 8412 E followed four steps of HSCCC separation with different solvent systems referring to the G.U.E.S.S. theories. However, none of the first three steps was able to determine the “sweet spot” range of bioactive fractions because the G.U.E.S.S. theories are mainly based on the chemical properties of the constituents on thin layer chromatography plates instead of the biological activities. This method overlooks the underlying minor active principles that are not necessarily visible on the developed TLC plate, and therefore may skew the bioautogram and its relationship with the chemical distribution. The TLC-bioautography method that was discussed in the earlier chapter will be an appropriate solution to fill that gap since the inhibition zones of bioautography directly reflects the location of the bioactive constituents on the TLC plate, thus it allows us to determine the K values by bioactivity instead of chemistry before the HSCCC separation. The combination of bioautography and G.U.E.S.S. methods (designated as “Bioauto-G.U.E.S.S.”) will provide a much more accurate prediction of the appropriate solvent systems to be used in the HSCCC separation of bioactive constituents.

The present study purified xylamycin and determined its planar structure by NMR. With regard to its bioactivity against replicating *M. tb*, this compound shows strong inhibition of bacterial growth *in vitro* at a level that rivals the MIC of rifampin (< 0.1 μg/mL). Macrophage penetration data also verifies its potency and trans-membrane bioavailability. As early as the year 1999, Eli Lilly and company had already filed a patent entitled “RUFOMYCIN DERIVATIVES USEFUL AS ANTIBIOTICS”, reporting the discovery of 173 ilamycin (or rufomycin) derivatives as well as the anti-*M. tb* activities of some selected compounds. The planar structure **B14** matches

that of “compound 10” described in the patent [186]. The reported chemical properties and NMR data of the “compound 10” were also consistent with those obtained from **B14**. The MIC of “compound 10” against *M. tb* H_{37}Ra was reported as between 0.1 and 1.3 μg/mL (possibly mislabeled as “μL/mL” in the patent), 3- to 30-fold higher than the MIC of 0.05 μg/mL against *M. tb* H_{37}Rv determined in our laboratory. No *in vivo* activities were reported in the patent. At this point, the feasibility of developing **B14** as a clinical anti-TB agent still remains to be verified.

9. Overall summary (Figure 67)

9.1 Aim 1: *In vivo* quantification of *M. tb* with GC-MS/MS and real-time PCR methods

Although there are currently available *M. tb* quantification methods for the purpose of *in vivo* anti-*M. tb* drug screening, most of these methods remain less sensitive, inaccurate, and not efficient. The *M. tb* quantification method most commonly adopted in lab settings still depends on counting the colony forming units (CFU), a labor-intensive process requiring 2-3 weeks incubation, and is intrinsically inaccurate due to the propensity of the mycobacterial hydrophobic cell wall to form clumps. However, the CFU method remains as the gold standard for enumeration of *M. tb* growth. Tuberculostearic acid (TBSA), a cell wall associated biomarker found in *Mycobacterium tuberculosis*, has been investigated for clinical diagnosis of tuberculosis, but few reports exist of attempts to quantify it. The *M. tb* quantification method uses GC-MS/MS through the determination of TBSA during growth of *M. tb* in axenic medium, macrophage cultures, and in the lungs of gamma interferon knockout (GKO) mice with and without exposure to anti-*M. tb* agents. The method is robust, cheap and efficient to reflect a correlation of TBSA with CFU and, thus, the efficacy of these agents on *M. tb* growth. However, it is important to note the limitation that TBSA is a persisting, non-degradable, and thermally stable biomarker which is only applicable to monitoring the bacteriostatic activities of the agents rather than any bactericidal effects.

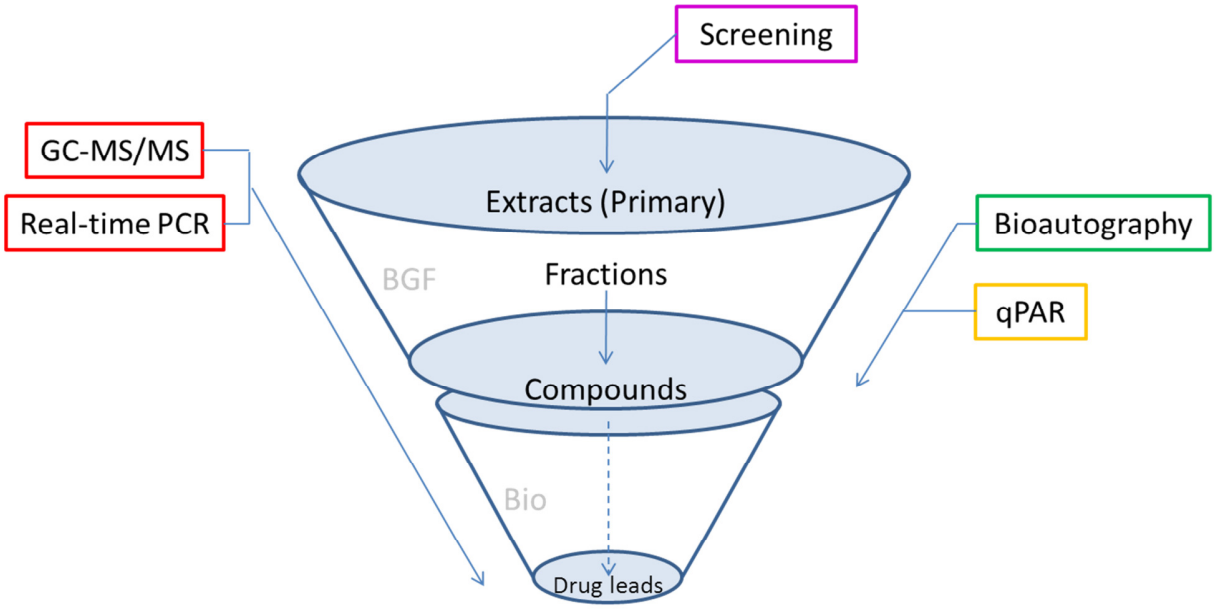

Figure 67. Funnel scheme of summary. BGF=Bioassay-guided fractionation; Bio=Bioavailability studies.

Secondly, this study developed the use of real-time PCR in determining the expression levels of *M. tb*-specific genes as quantitative indicators of viable bacteria counts to compensate for the drawbacks of the GC-MS/MS method, as real-time PCR is capable of detecting the RNA fragments that reflect the viability of *M. tb* when exposed to anti-*M. tb* agents in different sample settings. The expression of three specific and abundantly expressed *M. tb* RNAs, *fbpB*, *icl1*, and 16S rRNA, was quantified from lung tissue of *M. tb* infected gamma-interferon knock-out (GKO) and BALB/c mice after treatment with five anti-*M. tb* agents at three dosage levels. The RNA copy numbers of these gene targets correlated with CFU counts in both models. Levels of one of the RNAs, *icl1*, maintained a superior consistency with CFU and correlated with the doses of anti-*M. tb* agents. This was verified in an *in vivo* efficacy study of ecumicin that

validated *icl1* as a marker gene indicative of CFU level in mice with a high correlation coefficient (see "Section **3.3.5**").

The GC-MS/MS and real-time PCR assays developed for monitoring and quantifying *M. tb* growth in infected mice provide a low-cost, accurate and efficient process for drug efficacy studies compared with the current gold standard for *in vivo* screening for anti-*M. tb* agents, i.e., the CFU method.

9.2 Aim 2: *In vitro* screening of anti-*M. tb* constituents

To determine the anti-*M. tb* activities of the crude extracts, fractions, or isolates from natural resources, phenotypic screening in high throughput settings is widely carried out according to a protocol regime, including A) an initial prioritization of the crude extracts based on the percentage inhibition on *M. tb* growth in inoculated 96-well plates, B) minimum inhibitory concentration (MIC) testing of those that inhibit 90% of *M. tb* growth to verify the bioactivity, C) MIC tracing of bioactive fractionated constituents throughout a bioassay-guided fractionation, D) MIC testing of bioactive constituents against mono-drug resistant, NR, and clinically isolated *M. tb* strains, and E) a cytotoxicity testing against mammalian cells (Vero) to confirm selectivity. Purified compounds that conform to these specific bioactivities and low toxicity criteria will be regarded as potent hit compounds for downstream drug development (**Figure 19**).

As an expedited venue for the bioactivity identification of extracts/fractions before further purification, bioautography following thin layer chromatography (TLC) using a genetically engineered *M. tb* strain enables visualization of *M. tb* growth inhibition by the potentially bioactive constituents in an unpurified state by simply developing a well-defined TLC

and exposing the developed constituents to an interface with a bacterial culture media. Three bioautography methods were introduced: direct contact of the TLC plate with bacterial agar (Contact), submerging into bacterial liquid culture media (Direct), or pouring bacterial culture media onto the surface of TLC plate (Immersion). Constituents that would potentially inhibit the growth of *M. tb* diffuse onto the agar and form a visible inhibition zone on the interface in the luminescence imaging. The bioactive samples are harvested directly from the TLC plate with the help of the TLC-MS interface, and the isolates were manually injected into the mass spectrometer, so that the chemical information of the bioactive constituents can be readily obtained, all in a simple operation.

During bioassay-guided fractionation, the bioactivities can be attributed to a variety of factors. Ideally, the major constituents account for the bioactivities; whereas in many cases, minor but highly active constituents are buried beneath the major ones, complicating the identification of important bioactive constituents. In the case of interactive effects among multiple constituents, more complicated scenarios occur when synergistic or antagonistic effects are involved in enhancing or counteracting the bioactivities of each individual constituent. In order to quantitatively determine the effects of minor constituents on the bioactivity of impurity components, quantitative purity-activity relationship (qPAR) studies give an overall evaluation of the distribution of bioactive constituents in a fractionation procedure in correlation with the purity profiles of those constituents in each fraction. Thus, qPAR provides a perspective in which inactive constituents can be easily dereplicated, active minor constituents can be determined and targeted at an earlier stage of fractionation, and potential synergistic effects are also able to be evaluated to a quantitative endpoint. An example of bioassay-guided

fractionation on potential anti-*M. tb* constituents in the Chinese herbal medicine *Taxillus chinensis* proved the direct relationship between the concentration of (*E*)-phytol determined by GC-MS and the MIC values of a series of countercurrent chromatography (CCC) fractions. By establishing a mathematical model, another minor constituent, (*Z*)-phytol, was identified as an antagonist toward the anti-*M. tb* effect of its configurational isomer. Another qPAR study of the hytramycins in the initial crude fractions verified that the concentration of the major constituents correlated with the overall activity (MICs) of the fractions. As such, qPAR was able to assist in the targeted selection of bioactive fractions for which further purification of the major active constituents is justified.

The three *in vitro* approaches included in the aim of determining anti-*M. tb* constituents in unknown crude extracts or fractions *in vitro* aid in identifying bioactive constituents as the essential guide throughout the bioassay-guided fractionation, and eventually profiling biological and chemical properties of prioritized constituents.

9.3 Aim 3: Isolation of hytramycin and xylamycin

Thirty-five thousand actinomycete extracts were screened for anti-*M. tb* activity, followed by C_{18} cartridge fractionation of 37 prioritized extracts. Based on MICs against replicating and non-replicating *M. tb*, and IC_{50}s against Vero cells to generate selectivity indices, seven fractions from seven different strains were selected for further examination. One strain, ECUM 14046, a *Streptomyces hygroscopicus* strain, when cultured in G.S.S. media and extracted with ethyl acetate, yielded an extract with potent anti-*M. tb* activity and a well-defined chromatographic profile. The presence of two cyclohexapeptides, hytramycins V and I, each containing three unusual piperazic acid moieties, was demonstrated through fractionation by

preparative HPLC and subsequent structural elucidation of two active fractions using 1D- and 2D-NMR and MS methods. ^{1}H iterative full spin analysis (HiFSA) of both hytramycins confirmed that all $J_{H,H}$ and δ_H values are consistent with the proposed structures. The absolute configuration of each amino acid moiety was determined by Marfey's method. The MICs against replicating and, more importantly, non-replicating *M. tb* were tested to confirm that the bioactivities of the isolated compounds fall into the range of those of existing anti-*M. tb* drugs. The compounds maintained their activities against *M. tb* strains that represent the major global clades, as well as H_{37}Rv-isogenic strains that are resistant to individual clinically used anti-*M. tb* drugs.

In another collaborative BGF project, a total of 65,000 actinomycete extracts were screened and prioritized for the isolation of potent anti-*M. tb* principles. The culture supernatant of actinomycete strain, ECUM8412, tentatively identified as *Streptomyces atratus* or *S. sanglieri*, extracted with EtOAc showed 99% inhibition on *M. tb* growth at 10 μg/mL, and was subjected to a purification procedure involving an initial activity enrichment by RP-18 vacuum column chromatography, high speed countercurrent chromatography separation in three solvent systems, and eventually by preparative HPLC purification to yield a group of low polarity constituents. One of the isolates, named as **B14**, was identified by 1D- and 2D- NMR as an analogue of ilamycin, a previously patented anti-*M. tb* cyclic heptapeptide that exhibits high *in vitro* anti-*M. tb* potency under normoxic conditions with an MIC of 0.05 μg/mL measured with MABA, and low activity under hypoxic conditions in LORA. Moreover, the anti-*M. tb* bioactivity was maintained when tested with mono-drug resistant or clinically isolated *M. tb* strains, and when serum proteins were present in the culture media. Unusual amino acids, such

as a nitrotyrosine, an *N*-prenyltryptophan, a cyclized dehydrogenated *N*-methyl-leucine, and a 2-amino-4-hexenoic acid were verified in the molecule.

Two classes of peptides isolated from two batches of actinomycete extract collections were determined to be strongly active antimicrobial agents against drug resistant *M. tb*. The structures of both peptides were elucidated with NMR as well as HR-LC-MS to be cyclic peptides with unusual amino acid residues. Moreover, the activities were verified with a bioautography method on TLC overlay. These molecules represent valuable leads for the design of new anti-*M. tb* drugs.

From the perspective of an ethnopharmaceutical, identification of the activities of a potential drug is a long process of trial and failure; moreover, the chemical composition of an ethnomedicine may not always be fully clarified, which adds difficulty to the biological evaluation of individual constituents. Bioassay-guided drug screening represents a much more efficient approach to specifically target active principles, to identify and correlate the chemical and biological characteristics of the prioritized principles. Although the drug leads from bioassay-guided screening still need to go through *in vivo* potency testing, this approach has the advantage of being target-oriented and high throughput, and provides explicit correlation between the biological activity and chemical composition.

9.3 Future Perspectives

9.3.1 Determination of TBSA in *M. tb* infected mice with GC-MS/MS

This study has proven that the determination of TBSA in TB-infected GKO mouse lung homogenate with GC-MS/MS method can be a promising surrogate method for enumerating

the CFU values. However, one of the drawbacks of this method is the sensitivity of the instrument which still cannot responsively detect the amount TBSA equivalent to bacteria counts lower than that of day 3 after infection (CFU = 1000), although the current GC-MS/MS instrument equipped with a triple quadrupole mass spectrometer can detect analytes at the pictogram (10^{-12} g) level. For this purpose, it would be anticipated to validate the quantitative parameters on an upgraded GC-MS/MS instrument with a new and redesigned ionization source which added an additional extractor lens to provide as much as 10-fold more sensitivity. Alternatively, the latest model of the GC-MS/MS system, Agilent 7000C Triple Quadruple, equipped with the high sensitivity EI extractor ion source, already achieved the limit of detection with smaller than 4 femtogram (10^{-15} g) of the GC standard compound, octafluoronaphthalene (OFN).

Given that GKO mouse is a special model using immunocompromised animals as an inducement for bacterial growth *in vivo*, it would be more practical to utilize the immunocompetent BALB/c mice, where *M. tb* usually grows one or two logs lower in CFU than the GKO mice, for anti-*M. tb* drug screening assays if the sensitivity of the instrument also allows for a much lower limit of detection. The GC-MS/MS upgrade would facilitate detection of *M. tb* not only in infected BALB/c mice where the bacteria colonize less abundantly, but also in animals at the very early post-infection stages. Based on the fact that work with BALB/c mice is more cost effective and these mice have a greater survival rate than the GKO mice, work with BALB/c mice will eventually permit substitution for GKO mice for *in vivo* discovery and screening for anti-*M. tb* principles.

9.3.2 Quantification of gene markers of *M. tb* infected mice with real-time PCR

Although the GC-MS/MS method is more efficient and cheaper, the real-time PCR method serves as an alternative quantitative method for *in vivo* efficacy study with much higher sensitivity and capability of detecting cell viability. In the current study, three gene markers were identified to be abundantly expressed at the RNA level; meanwhile BALB/c mice have been used to verify the sensitivity level that the method can attain. The robustness of selecting *icl1* as the marker for *in vivo M. tb* quantification has been demonstrated. However, correlation between CFU and RNA levels was not significant in the infected mice exposed to anti-*M. tb* drug treatment, such as INH and EMB, partly due to insufficient dose response related to the characteristic mechanisms of action of these drugs. The exploration of new genes that more consistently reflect CFU without strong influence on their expression levels imposed by the drugs during infection would still be a valuable goal for future studies.

In terms of the methodology, real-time PCR sample processing requires dozens of steps, which reduces the overall throughput of such *in vivo* evaluations. In a more efficiency-driven scenario, plate-based high throughput methods are expected to be introduced for RNA extraction, reverse transcription, and real-time PCR quantification, which would allow the sample processing to be completely automated. Currently, the commercially available reagent kits for fast real-time PCR detection in 96- or 384-well plates already include steps of cell or tissue lysis, nucleic acid extraction, and finally PCR, simultaneously. Nonetheless, this method only consumes a small amount of animal tissue to accomplish the equally competitive quantitative analyses of gene profiling. Therefore, applying the plate-based sample preparation

to the real-time PCR would greatly elevate the efficiency of running large batches for drug candidate screening.

9.3.3 Assay development with TLC-bioautography

Although the currently reported methods regarding different interactions between the TLC surfaces loaded with developed crude samples and the bacterial culture layer already provide a fast profiling ability to visualize the antimicrobial activities of constituents, these methods still exhibit a number of conditional drawbacks when applied to molecules with different physiochemical properties. Potential future studies could address how the different classes of molecules are amenable to TLC-bioautography such that the test samples that show well-defined bands on the developed TLC plate yield clearly recognizable inhibition halos in response to those bands with high resolution and definition. This may not only require a better knowledge of the test samples in general, but also the optimization of the bacterial inoculum and the TLC plates as well, as the bioautography profiles that are obtained through interaction between the bacterial culture layer and the compound layer on the TLC plates. One recommended method to prevent sample diffusion from TLC plate to the agar surface is to use cetyl alcohol (1-hexadecanol) as a coating agent between the two interfaces so that the samples are locked within the local area.

As mentioned earlier in the chapter, an interface of TLC plates with LC-MS can be realized by an instrument that takes samples directly from the bands on the developed TLC plate. The interface extracts the constituents with an external solvent pump and recollects the individual extracted constituents for determination of their molecular weights and fragmentation information through direct injection into an LC-MS instrument. If applied to the

ongoing actinomycete-derived anti-TB drug lead discovery studies, this TLC-bioautography-LC-MS system will give a thorough clarification of both the chemical and biological characteristics of each constituent from the crude active principle, and thus provide a prerequisite for a time-saving targeted isolation method.

9.3.4 Anti-*M. tb* drug discovery from Actinomycete extracts

The current workflow of screening a potentially bioactive chemical with novel structural characteristics from an actinomycete or any other extract library follows a funnel-shaped prioritization protocol. At the end of this procedure, only the most active hits should be chosen for the next step of purification while those fractions below the top-tier actives should frequently be abandoned for further pursuit of activities. Although the 90% inhibition rate was defined as a cut-off line for the prioritization of active extracts or fractions for downstream studies, it may be beneficial to further evaluate the deprioritized extracts that showed slightly lower than 90% inhibition, e.g., selecting the top 20% hits in total in an individual batch without considering a cut-off line on percentage inhibition, on *M. tb* growth in the primary screening through the similar bioassay-guided purification and identification, in search of active constituents that are not major constituents.

In this scenario, huge numbers of valuable compounds in small concentrations might be currently neglected, rendering them undetectable. It will be valuable to look for potentially bioactive constituents that are chromatographically buried under the major constituents. Quantitative purity-activity relationship studies will be a useful tool for analyzing the abundance of the individual constituents in relationship to bioactivity so that the characteristics of underlying active constituents can be mathematically determined in advance.

In this thesis, hytramycins and xylamycin were purified as potential anti-*M. tb* drug leads. However, the two hytramycins showed obvious cytotoxicity toward mammalian cells *in vitro* as reflected by the IC_{50} values. Xylamycin showed low toxicity, but due to its fast-killing nature reflected by the strong MABA activity, its *in vivo* activity against non-replicating *M. tb* still remained ambiguous. Directly introducing both peptides in the *in vivo* efficacy studies by means of the established quantitative evaluation methods, i.e., GC-MS/MS and real-time PCR, would more objectively reveal their potencies as well as the *in vivo* bioavailability. In this perspective, a portfolio of additional studies may necessarily accompany the potency evaluation, including an initial toxicity and tolerance monitoring after the oral administration of these peptides, a one-dose plasma pharmacokinetics study to confirm the metabolism and excretion of these peptides through the gastrointestinal and cardiovascular systems and an MIC study with post-dose lung tissue extraction to disclose the distribution parameters of the peptides in the target organs. In summary, the combination of *in vitro* bioassays and *in vivo* efficacy studies in future work would provide a more complete evaluation of these two active peptides for their potential for further development as drug lead molecules.

9.4 Overall Conclusions

Although there are available clinical treatments for TB infection, it still remains an urgent task to explore novel drug leads with unique chemical structures to overcome drug resistance TB. This requires bioactive molecules that act on different bacterial targets, show low cytotoxicity, and exhibit good bioavailability. All procedures involve a huge amount of effort for prioritizing the active principles from existing chemical libraries derived from different sources. In the purification of natural product derived active principles, the complexity and diversity of

crude extracts or fractions can greatly impede the successful biological and chemical identification of individual constituents. In this project, a combination of *in vitro* and *in vivo* screening processes was presented in which newly established methods for *in vivo M. tb* quantification by means of GC-MS/MS and real-time PCR were introduced to facilitate an early-stage screening of potential drug leads in infected animals. At the same time, *in vitro* prioritization methods represented by phenotypic screening, thin layer chromatography aided bioautography, and quantitative purity-activity relationship studies were also utilized in parallel to the bioassay-guided fractionation throughput.

As the anti-*M. tb* drug lead screening projects continued to move forward, two classes of cyclic peptides, the hytramycins and xylamycin, were isolated from two extracts of actinomycete cultures. The structures were elucidated with high resolution LC-MS and 1D/2D-NMR, and the bioactivities were determined by testing the inhibition on the growth of *M. tb* in normoxic or hypoxic conditions, drug resistant or clinically isolated *M. tb*, as well as bacteria other than the mycobacteria. Both classes of cyclic peptides showed strong activity and potentially unique bacterial targets. With these examples of the newly isolated anti-*M. tb* constituents, the reported *in vitro* screening approaches, i.e., qPAR and bioautography, have been validated to be appropriate. The process of anti-*M. tb* drug discovery from natural product resources is facilitated and expedited with the introduction of these approaches.

CITED LITERATURE

1. World Health Organization., *Global tuberculosis control : surveillance, planning, financing : WHO report 2008*. **2008**, Geneva: World Health Organization. 294.

2. Glaziou, P., Floyd K., and Raviglione M., *Global burden and epidemiology of tuberculosis.* Clin Chest Med, **2009**. 30. 621-36.

3. World Health Organization., *10 facts about tuberculosis*. **2013**.

4. Gandhi, N.R., Moll, A., Sturm, A.W., Pawinski, R., Govender, T., Lalloo, U., Zeller, K., Andrews, J., and Friedland, G., *Extensively drug-resistant tuberculosis as a cause of death in patients co-infected with tuberculosis and HIV in a rural area of South Africa.* Lancet, **2006**. 368. 1575-80.

5. Schaaf, H.S., Moll, A.P., and Dheda K., *Multidrug- and extensively drug-resistant tuberculosis in Africa and South America: epidemiology, diagnosis and management in adults and children.* Clin Chest Med, **2009**. 30. 667-83.

6. Bhowruth, V., Alderwick, L.J., Brown, A.K., Bhatt, A., Besra, and G.S., *Tuberculosis: a balanced diet of lipids and carbohydrates.* Biochem Soc Trans, **2008**. 36. 555-65.

7. Rumijowska-Galewicz, A., Korycka-Machała, M., Lisowska, K., and Dziadek, J., *The composition of cell wall skeleton and outermost lipids of* Mycobacterium vaccae *is modified by ethambutol treatment.* Pol J Microbiol, **2008**. 57. 99-104.

8. Daffé, M. and Draper, P., *The envelope layers of mycobacteria with reference to their pathogenicity.* Adv Microb Physiol, **1998**. 39. 131-203.

9. Lee, R.E., Brennan, P.J., and Besra, G.S., Mycobacterium tuberculosis *cell envelope.* Curr Top Microbiol Immunol, **1996**. 215. 1-27.

10. Laval, F., Haites, R., Movahedzadeh, F., Lemassu, A., Wong, C.Y., Stoker, N., Billman-Jacobe, H., and Daffé, M., *Investigating the function of the putative mycolic acid methyltransferase UmaA: divergence between the* Mycobacterium smegmatis *and* Mycobacterium tuberculosis *proteins.* J Biol Chem, **2008**. 283. 1419-27.

11. Barry, C.E., Lee, R.E., Mdluli, K., Sampson, A.E., Schroeder, B.G., Slayden, R.A., and Yuan, Y., *Mycolic acids: structure, biosynthesis and physiological functions.* Prog Lipid Res, **1998**. 37. 143-79.

12. Brennan, P.J. and Nikaido, H., *The envelope of mycobacteria.* Annu Rev Biochem, **1995**. 64. 29-63.

13. Takayama, K., Wang, C., and Besra, G.S., *Pathway to synthesis and processing of mycolic acids in* Mycobacterium tuberculosis*.* Clin Microbiol Rev, **2005**. 18. 81-101.

14. Ortalo-Magné, A., Dupont, M.A., Lemassu, A., Andersen, A.B., Gounon, P., and Daffé, M., *Molecular composition of the outermost capsular material of the tubercle bacillus.* Microbiology, **1995**. 141. 1609-20.

15. Smith, I., Mycobacterium tuberculosis *pathogenesis and molecular determinants of virulence.* Clin Microbiol Rev, **2003**. 16. 463-96.

16. Russell, D.G., Mycobacterium tuberculosis*: here today, and here tomorrow.* Nat Rev Mol Cell Biol, **2001**. 2. 569-77.

17. Wayne, L.G. and Hayes, L.G., *An* in vitro *model for sequential study of shiftdown of* Mycobacterium tuberculosis *through two stages of nonreplicating persistence.* Infect Immun, **1996**. 64. 2062-9.

18. Wayne, L.G., *Dormancy of* Mycobacterium tuberculosis *and latency of disease.* Eur J Clin Microbiol Infect Dis, **1994**. 13. 908-14.

19. McKinney, J.D., Höner zu Bentrup, K., Muñoz-Elías, E.J., Miczak, A., Chen, B., Chan, W.T., Swenson, D., Sacchettini, J.C., Jacobs, W.R., and Russell, D.G., *Persistence of* Mycobacterium tuberculosis *in macrophages and mice requires the glyoxylate shunt enzyme isocitrate lyase.* Nature, **2000**. 406. 735-8.

20. Keeler, E., Perkins, M.D., Small, P., Hanson, C., Reed, S., Cunningham, J., Aledort, J.E., Hillborne, L., Rafael, M.E., Girosi, F., and Dye, C., *Reducing the global burden of tuberculosis: the contribution of improved diagnostics.* Nature, **2006**. 444 Suppl 1. 49-57.

21. Wallis, R.S., Pai, M., Menzies, D., Doherty, T.M., Walzl, G., Perkins, M.D., and Zumla, A., *Biomarkers and diagnostics for tuberculosis: progress, needs, and translation into practice.* Lancet, **2010**. 375. 1920-37.

22. Lange, C. and Mori, T., *Advances in the diagnosis of tuberculosis.* Respirology, **2010**. 15. 220-40.

23. Collins, L. and Franzblau, S.G., *Microplate alamar blue assay versus BACTEC 460 system for high-throughput screening of compounds against* Mycobacterium tuberculosis *and* Mycobacterium avium*.* Antimicrob Agents Chemother, **1997**. 41. 1004-9.

24. Cruciani, M., Scarparo, C., Malena, M., Bosco, O., Serpelloni, G., and Mengoli, C., *Meta-analysis of BACTEC MGIT 960 and BACTEC 460 TB, with or without solid media, for detection of mycobacteria.* J Clin Microbiol, **2004**. 42. 2321-5.

25. Reisner, B.S., Gatson, A.M., and Woods, G.L., *Evaluation of mycobacteria growth indicator tubes for susceptibility testing of* Mycobacterium tuberculosis *to isoniazid and rifampin.* Diagn Microbiol Infect Dis, **1995**. 22. 325-9.

26. Mori, T., *Usefulness of interferon-gamma release assays for diagnosing TB infection and problems with these assays.* J Infect Chemother, **2009**. 15. 143-55.

27. Bartu, V., Havelkova, M., and Kopecka, E., *QuantiFERON-TB Gold in the diagnosis of active tuberculosis.* J Int Med Res, **2008**. 36. 434-7.

28. Pai, M., Zwerling, A., and Menzies, D., *Systematic review: T-cell-based assays for the diagnosis of latent tuberculosis infection: an update.* Ann Intern Med, **2008**. 149. 177-84.

29. Nyendak, M.R., Lewinsohn, D.A., and Lewinsohn, D.M., *New diagnostic methods for tuberculosis.* Curr Opin Infect Dis, **2009**. 22. 174-82.

30. Sarmiento, O.L., Weigle, K.A., Alexander, J., Weber, D.J., and Miller, W.C., *Assessment by meta-analysis of PCR for diagnosis of smear-negative pulmonary tuberculosis.* J Clin Microbiol, **2003**. 41. 3233-40.

31. Flores, L.L., Pai, M., Colford, J.M., and Riley, L.W., *In-house nucleic acid amplification tests for the detection of* Mycobacterium tuberculosis *in sputum specimens: meta-analysis and meta-regression.* BMC Microbiol, **2005**. 5. 55.

32. Pauli, G.F., Case, R.J., Inui, T., Wang, Y., Cho, S., Fischer, N.H., and Franzblau, S.G., *New perspectives on natural products in TB drug research.* Life Sci, **2005**. 78. 485-94.

33. Franzblau, S.G., Witzig, R.S., McLaughlin, J.C., Torres, P., Madico, G., Hernandez, A., Degnan, M.T., Cook, M.B., Quenzer, V.K., Ferguson, R.M., and Gilman, R.H., *Rapid, low-technology MIC determination with clinical* Mycobacterium tuberculosis *isolates by using the microplate Alamar Blue assay.* J Clin Microbiol, **1998**. 36. 362-6.

34. Collins, L.A., Torrero, M.N., and Franzblau, S.G., *Green fluorescent protein reporter microplate assay for high-throughput screening of compounds against* Mycobacterium tuberculosis*.* Antimicrob Agents Chemother, **1998**. 42. 344-7.

35. Changsen, C., Franzblau, S.G., and Palittapongarnpim, P., *Improved green fluorescent protein reporter gene-based microplate screening for antituberculosis compounds by utilizing an acetamidase promoter.* Antimicrob Agents Chemother, **2003**. 47. 3682-7.

36. Cooksey, R.C., Crawford, J.T., Jacobs, W.R., and Shinnick, T.M., *A rapid method for screening antimicrobial agents for activities against a strain of* Mycobacterium tuberculosis *expressing firefly luciferase.* Antimicrob Agents Chemother, **1993**. 37. 1348-52.

37. Arain, T.M., Resconi, A.E., Hickey, M.J., and Stover, C.K., *Bioluminescence screening* in vitro *(Bio-Siv) assays for high-volume antimycobacterial drug discovery.* Antimicrob Agents Chemother, **1996**. 40. 1536-41.

38. Harries, A.D. and Dye, C., *Tuberculosis.* Ann Trop Med Parasitol, **2006**. 100. 415-31.

39. Bastian, I., Rigouts, L., Van Deun, A., and Portaels, F., *Directly observed treatment, short-course strategy and multidrug-resistant tuberculosis: are any modifications required?* Bull World Health Organ, **2000**. 78. 238-51.

40. World Health Organization., *WHO Tuberculosis Programme: Framework for effective Tuberculosis Control.* **1994**.

41. van den Boogaard, J., Kibiki, G.S., Kisanga, E.R., Boeree, M.J., and Aarnoutse, R.E., *New drugs against tuberculosis: problems, progress, and evaluation of agents in clinical development.* Antimicrob Agents Chemother, **2009**. 53. 849-62.

42. Koul, A., Arnoult, E., Lounis, N., Guillemont, J., and Andries, K., *The challenge of new drug discovery for tuberculosis.* Nature, **2011**. 469. 483-90.

43. Palomino, J.C., Ramos, D.F., and da Silva, P.A., *New anti-tuberculosis drugs: strategies, sources and new molecules.* Curr Med Chem, **2009**. 16. 1898-904.

44. Newton, S.M., Lau, C., and Wright, C.W., *A review of antimycobacterial natural products.* Phytother Res, **2000**. 14. 303-22.

45. Copp, B.R., *Antimycobacterial natural products.* Nat Prod Rep, **2003**. 20. 535-57.

46. Copp, B.R. and Pearce, A.N., *Natural product growth inhibitors of* Mycobacterium tuberculosis*.* Nat Prod Rep, **2007**. 24. 278-97.

47. Okunade, A.L., Elvin-Lewis, M.P., and Lewis, W.H., *Natural antimycobacterial metabolites: current status.* Phytochemistry, **2004**. 65. 1017-32.

48. García, A., Bocanegra-García, V., Palma-Nicolás, J.P., and Rivera, G., *Recent advances in antitubercular natural products.* Eur J Med Chem, **2012**. 49C. 1-23.

49. Baltz, R.H., *Marcel Faber Roundtable: is our antibiotic pipeline unproductive because of starvation, constipation or lack of inspiration?* J Ind Microbiol Biotechnol, **2006**. 33. 507-13.

50. Clardy, J., Fischbach, M.A., and Walsh, C.T., *New antibiotics from bacterial natural products.* Nat Biotechnol, **2006**. 24. 1541-50.

51. Nathan, C., *Making space for anti-infective drug discovery.* Cell Host Microbe, **2011**. 9. 343-8.

52. Watve, M.G., Tickoo, R., Jog, M.M., and Bhole, B.D., *How many antibiotics are produced by the genus Streptomyces?* Arch Microbiol, **2001**. 176. 386-90.

53. Larsson, L., Mårdh, P.A., and Odham, G., *Detection of tuberculostearic acid in mycobacteria and nocardiae by gas chromatography and mass spectrometry using selected ion monitoring.* J Chromatogr, **1979**. 163. 221-4.

54. Lambert, M.A., Moss, C.W., Silcox, V.A., and Good, R.C., *Analysis of mycolic acid cleavage products and cellular fatty acids of* Mycobacterium *species by capillary gas chromatography.* J Clin Microbiol, **1986**. 23. 731-6.

55. Anderson, R.J., *Chemical investigation of biologically active lipoids of tubercle bacilli.* Proc Natl Acad Sci U S A, **1929**. 15. 628-33.

56. Collins, M.D., Falsen, E., Akervall, E., Sjöden, B., and Alvarez, A., Corynebacterium kroppenstedtii *sp. nov., a novel corynebacterium that does not contain mycolic acids.* Int J Syst Bacteriol, **1998**. 48. 1449-54.

57. Linos, A., Berekaa, M.M., Steinbüchel, A., Kim, K.K., Sproer, C., and Kroppenstedt, R.M., Gordonia westfalica *sp. nov., a novel rubber-degrading actinomycete.* Int J Syst Evol Microbiol, **2002**. 52. 1133-9.

58. Cha, D., Cheng, D., Liu, M., Zeng, Z., Hu, X., and Guan, W., *Analysis of fatty acids in sputum from patients with pulmonary tuberculosis using gas chromatography-mass spectrometry preceded by solid-phase microextraction and post-derivatization on the fiber.* J Chromatogr A, **2009**. 1216. 1450-7.

59. French, G.L., Chan, C.Y., Cheung, S.W., and Oo, K.T., *Diagnosis of pulmonary tuberculosis by detection of tuberculostearic acid in sputum by using gas chromatography-mass spectrometry with selected ion monitoring.* J Infect Dis, **1987**. 156. 356-62.

60. Kaal, E., Kolk, A.H., Kuijper, S., and Janssen, H.G., *A fast method for the identification of* Mycobacterium tuberculosis *in sputum and cultures based on thermally assisted hydrolysis and methylation followed by gas chromatography-mass spectrometry.* J Chromatogr A, **2009**. 1216. 6319-25.

61. Odham, G., Larsson, L., and Mårdh, P.A., *Demonstration of tuberculostearic acid in sputum from patients with pulmonary tuberculosis by selected ion monitoring.* J Clin Invest, **1979**. 63. 813-9.

62. Brooks, J.B., Daneshvar, M.I., Fast, D.M., and Good, R.C., *Selective procedures for detecting femtomole quantities of tuberculostearic acid in serum and cerebrospinal fluid by frequency-pulsed electron capture gas-liquid chromatography.* J Clin Microbiol, **1987**. 25. 1201-6.

63. Sato, K., Tomioka, H., Akaki, T., and Kawahara, S., *Antimicrobial activities of levofloxacin, clarithromycin, and KRM-1648 against* Mycobacterium tuberculosis *and* Mycobacterium avium *complex replicating within Mono Mac 6 human macrophage and A-549 type II alveolar cell lines.* Int J Antimicrob Agents, **2000**. 16. 25-9.

64. Dhillon, J., Andries, K., Phillips, P.P., and Mitchison, D.A., *Bactericidal activity of the diarylquinoline TMC207 against* Mycobacterium tuberculosis *outside and within cells.* Tuberculosis, **2010**. 90. 301-5.

65. Flynn, J.L., Chan, J., Triebold, K.J., Dalton, D.K., Stewart, T.A., and Bloom, B.R., *An essential role for interferon gamma in resistance to* Mycobacterium tuberculosis *infection.* J Exp Med, **1993**. 178. 2249-54.

66. Cooper, A.M., Dalton, D.K., Stewart, T.A., Griffin, J.P., Russell, D.G., and Orme, I.M., *Disseminated tuberculosis in interferon gamma gene-disrupted mice.* J Exp Med, **1993**. 178. 2243-7.

67. Lenaerts, A.J., Gruppo, V., Brooks, J.V., and Orme, I.M., *Rapid* in vivo *screening of experimental drugs for tuberculosis using gamma interferon gene-disrupted mice.* Antimicrob Agents Chemother, **2003**. 47. 783-5.

68. Lenaerts, A.J., Bitting, C., Woolhiser, L., Gruppo, V., Marietta, K.S., Johnson, C.M., and Orme, I.M., *Evaluation of a 2-pyridone, KRQ-10018, against* Mycobacterium tuberculosis in vitro *and* in vivo*.* Antimicrob Agents Chemother, **2008**. 52. 1513-5.

69. Rullas, J., García, J.I., Beltrán, M., Cardona, P.J., Cáceres, N., García-Bustos, J.F., and Angulo-Barturen, I., *Fast standardized therapeutic-efficacy assay for drug discovery against tuberculosis.* Antimicrob Agents Chemother, **2010**. 54. 2262-4.

70. Ozbek, A. and Aktas, O., *Identification of three strains of Mycobacterium species isolated from clinical samples using fatty acid methyl ester profiling.* J Int Med Res, **2003**. 31. 133-40.

71. Smid, I. and Salfinger, M., *Mycobacterial identification by computer-aided gas-liquid chromatography.* Diagn Microbiol Infect Dis, **1994**. 19. 81-8.

72. Hsu, F.F., Turk, J., Owens, R.M., Rhoades, E.R., and Russell, D.G., *Structural characterization of phosphatidyl-myo-inositol mannosides from* Mycobacterium bovis *Bacillus Calmette Guérin by multiple-stage quadrupole ion-trap mass spectrometry with electrospray ionization. I. PIMs and lyso-PIMs.* J Am Soc Mass Spectrom, **2007**. 18. 466-78.

73. Liu, X., Stocker, B.L., and Seeberger, P.H., *Total synthesis of phosphatidylinositol mannosides of* Mycobacterium tuberculosis*.* J Am Chem Soc, **2006**. 128. 3638-48.

74. Luquin, M., Ausina, V., López Calahorra, F., Belda, F., García Barceló, M., Celma, C., and Prats, G., *Evaluation of practical chromatographic procedures for identification of clinical isolates of mycobacteria.* J Clin Microbiol, **1991**. 29. 120-30.

75. Mayakova, T.I., Kuznetsova, E.E., Kovaleva, M.G., and Plyusnin, S.A., *Gas chromatographic-mass spectrometric study of lipids and rapid diagnosis of* Mycobacterium tuberculosis*.* J Chromatogr B Biomed Appl, **1995**. 672.133-7.

76. Pang, J.A., Chan, H.S., Chan, C.Y., Cheung, S.W., and French, G.L., *A tuberculostearic acid assay in the diagnosis of sputum smear-negative pulmonary tuberculosis. A prospective study of bronchoscopic aspirate and lavage specimens.* Ann Intern Med, **1989**. 111. 650-4.

77. Belanger, A.E., Besra, G.S., Ford, M.E., Mikusová, K., Belisle, J.T., Brennan, P.J., and Inamine, J.M., *The embAB genes of* Mycobacterium avium *encode an arabinosyl transferase involved in cell wall arabinan biosynthesis that is the target for the antimycobacterial drug ethambutol.* Proc Natl Acad Sci U S A, **1996**. 93. 11919-24.

78. Kong, Y., Yao, H., Ren, H., Subbian, S., Cirillo, S.L., Sacchettini, J.C., Rao, J., and Cirillo, J.D., *Imaging tuberculosis with endogenous beta-lactamase reporter enzyme fluorescence in live mice.* Proc Natl Acad Sci U S A, **2010**. 107. 12239-44.

79. Cai, G., Pauli, G.F., Wang, Y., Jaki, B.U., and Franzblau, S.G., *Rapid determination of growth inhibition of* Mycobacterium tuberculosis *by GC-MS/MS quantitation of tuberculostearic acid.* Tuberculosis, **2013**. 93. 322-9.

80. Desjardin, L.E., Chen, Y., Perkins, M.D., Teixeira, L., Cave, M.D., and Eisenach, K.D., *Comparison of the ABI 7700 system (TaqMan) and competitive PCR for quantification of IS6110 DNA in sputum during treatment of tuberculosis.* J Clin Microbiol, **1998**. 36. 1964-8.

81. Hellyer, T.J., DesJardin, L.E., Assaf, M.K., Bates, J.H., Cave, M.D., and Eisenach, K.D., *Specificity of IS6110-based amplification assays for* Mycobacterium tuberculosis *complex.* J Clin Microbiol, **1996**. 34. 2843-6.

82. Hermans, P.W., van Soolingen, D., Dale, J.W., Schuitema, A.R., McAdam, R.A., Catty, D., and van Embden, J.D., *Insertion element IS986 from* Mycobacterium tuberculosis*: a useful tool for diagnosis and epidemiology of tuberculosis.* J Clin Microbiol, **1990**. 28. 2051-8.

83. Thierry, D., Brisson-Noël, A., Vincent-Lévy-Frébault, V., Nguyen, S., Guesdon, J.L., and Gicquel, B., *Characterization of a* Mycobacterium tuberculosis *insertion sequence, IS6110, and its application in diagnosis.* J Clin Microbiol, **1990**. 28. 2668-73.

84. Eisenach, K.D., Sifford, M.D., Cave, M.D., Bates, J.H., and Crawford, J.T., *Detection of* Mycobacterium tuberculosis *in sputum samples using a polymerase chain reaction.* Am Rev Respir Dis, **1991**. 144. 1160-3.

85. Jou, N.T., Yoshimori, R.B., Mason, G.R., Louie, J.S., and Liebling, M.R., *Single-tube, nested, reverse transcriptase PCR for detection of viable* Mycobacterium tuberculosis*.* J Clin Microbiol, **1997**. 35. 1161-5.

86. Wiker, H.G. and Harboe, M., *The antigen 85 complex: a major secretion product of* Mycobacterium tuberculosis*.* Microbiol Rev, **1992**. 56. 648-61.

87. Armitige, L.Y., Jagannath, C., Wanger, A.R., and Norris, S.J., *Disruption of the genes encoding antigen 85A and antigen 85B of* Mycobacterium tuberculosis *H37Rv: effect on growth in culture and in macrophages.* Infect Immun, **2000**. 68. 767-78.

88. De Wit, L., de la Cuvellerie, A., Ooms, J., and Content, J., *Nucleotide sequence of the 32 kDa-protein gene (antigen 85 A) of* Mycobacterium bovis *BCG.* Nucleic Acids Res, **1990**. 18. 3995.

89. Belisle, J.T., Vissa, V.D., Sievert, T., Takayama, K., Brennan, P.J., and Besra, G.S., *Role of the major antigen of* Mycobacterium tuberculosis *in cell wall biogenesis.* Science, **1997**. 276. 1420-2.

90. Fu, L.M. and Fu-Liu, C.S., *The gene expression data of* Mycobacterium tuberculosis *based on Affymetrix gene chips provide insight into regulatory and hypothetical genes.* BMC Microbiol, **2007**. 7. 37.

91. Mdivani, N., Li, H., Akhalaia, M., Gegia, M., Goginashvili, L., Kernodle, D.S., Khechinashvili, G., and Tang, Y.W., *Monitoring therapeutic efficacy by real-time detection of* Mycobacterium tuberculosis *mRNA in sputum.* Clin Chem, **2009**. 55. 1694-700.

92. Li, L., Mahan, C.S., Palaci, M., Horter, L., Loeffelholz, L., Johnson, J.L., Dietze, R., Debanne, S.M., Joloba, M.L., Okwera, A., Boom, W.H., and Eisenach, K.D., *Sputum* Mycobacterium tuberculosis *mRNA as a marker of bacteriologic clearance in response to antituberculosis therapy.* J Clin Microbiol, **2010**. 48. 46-51.

93. Muñoz-Elías, E.J. and McKinney, J.D., Mycobacterium tuberculosis *isocitrate lyases 1 and 2 are jointly required for* in vivo *growth and virulence.* Nat Med, **2005**. 11. 638-44.

94. Moore, D.F., Curry, J.I., Knott, C.A., and Jonas, V., *Amplification of rRNA for assessment of treatment response of pulmonary tuberculosis patients during antimicrobial therapy.* J Clin Microbiol, **1996**. 34. 1745-9.

95. Gamboa, F., Manterola, J.M., Lonca, J., Viñado, B., Matas, L., Giménez, M., Manzano, J.R., Rodrigo, C., Cardona, P.J., Padilla, E., Dominguez, J., and Ausina, V., *Rapid detection of* Mycobacterium tuberculosis *in respiratory specimens, blood and other non-respiratory specimens by amplification of rRNA.* Int J Tuberc Lung Dis, **1997**. 1. 542-55.

96. Desjardin, L.E., Perkins, M.D., Teixeira, L., Cave, M.D., and Eisenach, K.D., *Alkaline decontamination of sputum specimens adversely affects stability of mycobacterial mRNA.* J Clin Microbiol, **1996**. 34. 2435-9.

97. Lachnik, J., Ackermann, B., Bohrssen, A., Maass, S., Diephaus, C., Puncken, A., Stermann, M., and Bange, F.C., *Rapid-cycle PCR and fluorimetry for detection of mycobacteria.* J Clin Microbiol, **2002**. 40. 3364-73.

98. Kraus, G., Cleary, T., Miller, N., Seivright, R., Young, A.K., Spruill, G., and Hnatyszyn, H.J., *Rapid and specific detection of the* Mycobacterium tuberculosis *complex using fluorogenic probes andreal-time PCR.* Mol Cell Probes, **2001**. 15. 375-83.

99. Shi, L., Jung, Y.J., Tyagi, S., Gennaro, M.L., and North, R.J., *Expression of Th1-mediated immunity in mouse lungs induces a* Mycobacterium tuberculosis *transcription pattern characteristic of nonreplicating persistence.* Proc Natl Acad Sci U S A, **2003**. 100. 241-6.

100. Porcher, C., Malinge, M.C., Picat, C., and Grandchamp, B., *A simplified method for determination of specific DNA or RNA copy number using quantitative PCR and an automatic DNA sequencer.* Biotechniques, **1992**. 13. 106-14.

101. VanGuilder, H.D., Vrana, K.E., and Freeman, W.M., *Twenty-five years of quantitative PCR for gene expression analysis.* Biotechniques, **2008**. 44. 619-26.

102. Mikula, M., Dzwonek, A., Jagusztyn-Krynicka, K., and Ostrowski, J., *Quantitative detection for low levels of* Helicobacter pylori *infection in experimentally infected mice by real-time PCR.* J Microbiol Methods, **2003**. 55. 351-9.

103. Näslund, J., Lagerqvist, N., Lundkvist, A., Evander, M., Ahlm, C., and Bucht, G., *Kinetics of Rift Valley Fever Virus in experimentally infected mice using quantitative real-time RT-PCR.* J Virol Methods, **2008**. 151. 277-82.

104. Morton, C.O., Clemons, K.V., Springer, J., Mueller, J.G., Rogers, T.R., Stevens, D.A., Kurzai, O., Einsele, H., and Loeffler, J., *Real-time PCR and quantitative culture for monitoring of experimental* Aspergillus fumigatus *intracranial infection in neutropenic mice.* J Med Microbiol, **2011**. 60. 913-9.

105. Tester, A.M., Sharp, J.A., Dhanesuan, N., Waltham, M., and Thompson, E.W., *Correlation between extent of osteolytic damage and metastatic burden of human breast cancer metastasis in nude mice: real-time PCR quantitation.* Clin Exp Metastasis, **2002**. 19. 377-83.

106. Broccolo, F., Scarpellini, P., Locatelli, G., Zingale, A., Brambilla, A.M., Cichero, P., Sechi, L.A., Lazzarin, A., Lusso, P., and Malnati, M.S., *Rapid diagnosis of mycobacterial infections and quantitation of* Mycobacterium tuberculosis *load by two real-time calibrated PCR assays.* J Clin Microbiol, **2003**. 41. 4565-72.

107. Eishi, Y., Suga, M., Ishige, I., Kobayashi, D., Yamada, T., Takemura, T., Takizawa, T., Koike, M., Kudoh, S., Costabel, U., Guzman, J., Rizzato, G., Gambacorta, M., du Bois, R., Nicholson, A.G., Sharma, O.P., and Ando, M., *Quantitative analysis of mycobacterial and propionibacterial DNA in lymph nodes of Japanese and European patients with sarcoidosis.* J Clin Microbiol, **2002**. 40. 198-204.

108. Clarridge, J.E., *Impact of 16S rRNA gene sequence analysis for identification of bacteria on clinical microbiology and infectious diseases.* Clin Microbiol Rev, **2004**. 17. 840-62, table of contents.

109. Tortoli, E., *Impact of genotypic studies on mycobacterial taxonomy: the new mycobacteria of the 1990s.* Clin Microbiol Rev, **2003**. 16. 319-54.

110. Singh, U.B., Rana, T., Kaushik, A., Porwal, C., and Makkar, N., *Day zero quantitative mRNA analysis as a prognostic marker in pulmonary tuberculosis category II patients on treatment.* Clin Microbiol Infect, **2012**. 18. E473-81.

111. Huygen, K., Palfliet, K., Jurion, F., Hilgers, J., ten Berg, R., Van Vooren, J.P., and De Bruyn, J., *H-2-linked control of* in vitro *gamma interferon production in response to a 32-kilodalton antigen (P32) of* Mycobacterium bovis *bacillus Calmette-Guérin.* Infect Immun, **1988**. 56. 3196-200.

112. Desjardin, L.E., Hayes, L.G., Sohaskey, C.D., Wayne, L.G., and Eisenach, K.D., *Microaerophilic induction of the alpha-crystallin chaperone protein homologue (hspX) mRNA of* Mycobacterium tuberculosis*.* J Bacteriol, **2001**. 183. 5311-6.

113. Timm, J., Post, F.A., Bekker, L.G., Walther, G.B., Wainwright, H.C., Manganelli, R., Chan, W.T., Tsenova, L., Gold, B., Smith, I., Kaplan, G., and McKinney, J.D., *Differential expression of iron-, carbon-, and oxygen-responsive mycobacterial genes in the lungs of chronically infected mice and tuberculosis patients.* Proc Natl Acad Sci U S A, **2003**. 100. 14321-6.

114. Campbell, E.A., Korzheva, N., Mustaev, A., Murakami, K., Nair, S., Goldfarb, A., and Darst, S.A., *Structural mechanism for rifampicin inhibition of bacterial rna polymerase.* Cell, **2001**. 104. 901-12.

115. Cho, S.H., Warit, S., Wan, B., Hwang, C.H., Pauli, G.F., and Franzblau, S.G., *Low-oxygen-recovery assay for high-throughput screening of compounds against nonreplicating* Mycobacterium tuberculosis*.* Antimicrob Agents Chemother, **2007**. 51. 1380-5.

116. Filliol, I., Motiwala, A.S., Cavatore, M., Qi, W., Hazbón, M.H., Bobadilla del Valle, M., Fyfe, J., García-García, L., Rastogi, N., Sola, C., Zozio, T., Guerrero, M.I., León, C.I., Crabtree, J., Angiuoli, S., Eisenach, K.D., Durmaz, R., Joloba, M.L., Rendón, A., Sifuentes-Osornio, J., Ponce de León, A., Cave, M.D., Fleischmann, R., Whittam, T.S., and Alland, D., *Global phylogeny of* Mycobacterium tuberculosis *based on single nucleotide polymorphism (SNP) analysis: insights into tuberculosis evolution, phylogenetic accuracy of other DNA fingerprinting systems, and recommendations for a minimal standard SNP set.* J Bacteriol, **2006**. 188. 759-72.

117. Gagneux, S. and Small, P.M., *Global phylogeography of* Mycobacterium tuberculosis *and implications for tuberculosis product development.* Lancet Infect Dis, **2007**. 7. 328-37.

118. Falzari, K., Zhu, Z., Pan, D., Liu, H., Hongmanee, P., and Franzblau, S.G., In vitro *and* in vivo *activities of macrolide derivatives against* Mycobacterium tuberculosis*.* Antimicrob Agents Chemother, **2005**. 49. 1447-54.

119. Deng, S., Wang, Y., Inui, T., Chen, S.N., Farnsworth , N.R., Cho, S., Franzblau, S.G., and Pauli, G.F., *Anti-TB polyynes from the roots of* Angelica sinensis*.* Phytotherapy Research, **2008**. 22. 878-882.

120. Betina, V., *Bioautography in paper and thin-layer chromatography and its scope in the antibiotic field.* J Chromatogr, **1973**. 78. 41-51.

121. Grzelak, E.M., Majer-Dziedzic, B., and Choma, I.M., *Development of a novel direct bioautography-thin-layer chromatography test: optimization of growth conditions for gram-negative bacteria,* Escherichia coli*.* J AOAC Int, **2011**. 94. 1567-72.

122. Choma, I.M. and Grzelak, E.M., *Bioautography detection in thin-layer chromatography.* J Chromatogr A, **2011**. 1218. 2684-91.

123. Ramirez, A., Gutiérrez, R., Diaz, G., González, C., Pérez, N., Vega, S., and Noa, M., *High-performance thin-layer chromatography-bioautography for multiple antibiotic residues in cow's milk.* J Chromatogr B Analyt Technol Biomed Life Sci, **2003**. 784. 315-22.

124. Hamburger, M.O. and Cordell, G.A., *A direct bioautographic TLC assay for compounds possessing antibacterial activity.* J Nat Prod, **1987**. 50. 19-22.

125. Poole, C.F., *Thin-layer chromatography: challenges and opportunities.* J Chromatogr A, **2003**. 1000. 963-84.

126. Rios, J.L., Recio, M.C., and Villar, A., *Screening methods for natural products with antimicrobial activity: a review of the literature.* J Ethnopharmacol, **1988**. 23. 127-49.

127. Marston, A., *Thin-layer chromatography with biological detection in phytochemistry.* J Chromatogr A, **2011**. 1218. 2676-83.

128. Meyers, E. and Erickson, R.C., *Bioautography of antibiotics on thin layer chromatograms.* J Chromatogr, **1967**. 26. 531-2.

129. Móricz, A.M., Szarka, S., Ott, P.G., Héthelyi, E.B., Szoke, E., and Tyihák, E., *Separation and identification of antibacterial chamomile components using OPLC, bioautography and GC-MS.* Med Chem, **2012**. 8. 85-94.

130. Francis, K.P., Joh, D., Bellinger-Kawahara, C., Hawkinson, M.J., Purchio, T.F., and Contag, P.R., *Monitoring bioluminescent* Staphylococcus aureus *infections in living mice using a novel luxABCDE construct.* Infect Immun, **2000**. 68. 3594-600.

131. Sambandamurthy, V.K., Wang, X., Chen, B., Russell, R.G., Derrick, S., Collins, F.M., Morris, S.L., and Jacobs, W.R., *A pantothenate auxotroph of* Mycobacterium tuberculosis *is highly attenuated and protects mice against tuberculosis.* Nat Med, **2002**. 8. 1171-4.

132. Meyers, E. and Smith, D.A., *Bioautography of antibiotic spread-layer chromatograms.* J Chromatogr, **1964**. 13. 129-32.

133. Alpmann, A. and Morlock, G., *Improved online coupling of planar chromatography with electrospray mass spectrometry: extraction of zones from glass plates.* Anal Bioanal Chem, **2006**. 386. 1543-51.

134. Luftmann, H., Aranda, M., and Morlock, G.E., *Automated interface for hyphenation of planar chromatography with mass spectrometry.* Rapid Commun Mass Spectrom, **2007**. 21. 3772-6.

135. Morlock, G. and Ueda, Y., *New coupling of planar chromatography with direct analysis in real time mass spectrometry.* J Chromatogr A, **2007**. 1143. 243-51.

136. Inui, T., Wang, Y., Pro, S.M., Franzblau, S.G., and Pauli, G.F., *Unbiased evaluation of bioactive secondary metabolites in complex matrices.* Fitoterapia, **2012**. 83. 1218-25.

137. Qiu, F., Imai, A., McAlpine, J.B., Lankin, D.C., Burton, I., Karakach, T., Farnsworth, N.R., Chen, S.N., and Pauli, G.F., *Dereplication, residual complexity, and rational naming: the case of the* Actaea *triterpenes.* J Nat Prod, **2012**. 75. 432-43.

138. Jaki, B.U., Franzblau, S.G., Chadwick, L., Lankin, D.C., Wang, Y., Zhang, F, and Pauli, G.F., *Purity Activity-Relationships of Natural Products: The Case of Anti-TB Active Ursolic Acid.* J Nat Prod, **2008**. 71. 1742-1748.

139. Tian, W.X., Li, L.C., Wu, X.D., and Chen, C.C., *Weight reduction by Chinese medicinal herbs may be related to inhibition of fatty acid synthase.* Life Sci, **2004**. 74. 2389-99.

140. Wang, Y., Deng, M., Zhang, S.Y., Zhou, Z.K., and Tian, W.X., *Parasitic loranthus from Loranthaceae rather than Viscaceae potently inhibits fatty acid synthase and reduces body weight in mice.* J Ethnopharmacol, **2008**. 118. 473-8.

141. Wang, Y., Zhang, S.Y., Ma, X.F., and Tian, W.X., *Potent inhibition of fatty acid synthase by parasitic loranthus [*Taxillus chinensis *(dc.) danser] and its constituent avicularin.* J Enzyme Inhib Med Chem, **2006**. 21. 87-93.

142. Bhatt, A., Molle, V., Besra, G.S., Jacobs, W.R., and Kremer, L., *The* Mycobacterium tuberculosis *FAS-II condensing enzymes: their role in mycolic acid biosynthesis, acid-fastness, pathogenesis and in future drug development.* Mol Microbiol, **2007**. 64. 1442-54.

143. Saikia, D., Parihar, S., Chanda, D., Ojha, S., Kumar, J.K., Chanotiya, C.S., Shanker, K., and Negi, A.S., *Antitubercular potential of some semisynthetic analogues of phytol.* Bioorg Med Chem Lett, **2010**. 20. 508-12.

144. Rajab, M.S., Cantrell, C.L., Franzblau, S.G., and Fischer, N.H., *Antimycobacterial activity of (E)-phytol and derivatives: a preliminary structure-activity study.* Planta Med, **1998**. 64. 2-4.

145. Saludes, J.P., Garson, M.J., Franzblau, S.G., and Aguinaldo, A.M., *Antitubercular constituents from the hexane fraction of* Morinda citrifolia *Linn. (Rubiaceae).* Phytother Res, **2002**. 16. 683-5.

146. Napolitano, J.G., Gödecke, T., Rodríguez-Brasco, M.F., Jaki, B.U., Chen, S.N., Lankin, D.C., and Pauli, G.F., *The tandem of full spin analysis and qHNMR for the quality control of botanicals exemplified with* Ginkgo biloba*.* J Nat Prod, **2012**. 75. 238-48.

147. Bhushan, R. and Brückner, H., *Marfey's reagent for chiral amino acid analysis: a review.* Amino Acids, **2004**. 27. 231-47.

148. Fujii, K., Ikai, Y., Mayumi, T., Oka, H., Suzuki, M., and Harada, K., *A Nonempirical Method Using LC/MS for Determination of the Absolute Configuration of Constituent Amino Acids in a Peptide: Elucidation of Limitations of Marfey's Method and of Its Separation Mechanism*, Anal Chem, **1997**. 3346-3352.

149. Williams, D.E., Dalisay, D.S., Patrick, B.O., Matainaho, T., Andrusiak, K., Deshpande, R., Myers, C.L., Piotrowski, J.S., Boone, C., Yoshida, M., and Andersen, R.J., *Padanamides A and B, highly modified linear tetrapeptides produced in culture by a* Streptomyces *sp. isolated from a marine sediment.* Org Lett, **2011**. 13. 3936-9.

150. Kozone, I., Izumikawa, M., Motohashi, K., Nagai, A., Yoshida, M., Doi, T., Takagi, M., and Shin-ya, K., *Isolation of New Hexapeptides—JBIR-39 and JBIR-40—from a Marine Sponge-Derived* Streptomyces *sp. Sp080513SC-24*, **2011**: J Marine Sci Res Development.

151. Lang, G., Mitova, M.I., Cole, A.L., Din, L.B., Vikineswary, S., Abdullah, N., Blunt, J.W., and Munro, M.H., *Pterulamides I-VI, linear peptides from a Malaysian Pterula sp.* J Nat Prod, **2006**. 69. 1389-93.

152. Ji, Z., Wei, S., Fan, L., and Wu, W., *Three novel cyclic hexapeptides from* Streptomyces alboflavus *313 and their antibacterial activity.* Eur J Med Chem, **2012**. 50. 296-303.

153. Claridge, T.D. and Pérez-Victoria, I., *Enhanced 13C resolution in semi-selective HMBC: a band-selective, constant-time HMBC for complex organic structure elucidation by NMR.* Org Biomol Chem, **2003**. 1. 3632-4.

154. Laatikainen, R., Niemitz, M., Malaisse, W.J., Biesemans, M., and Willem, R., *A computational strategy for the deconvolution of NMR spectra with multiplet structures and constraints: analysis of overlapping 13C-2H multiplets of 13C enriched metabolites from cell suspensions incubated in deuterated media.* Magn Reson Med, **1996**. 36. 359-65.

155. Napolitano, J.G., Lankin, D.C., Chen, S.N., and Pauli, G.F., *Complete 1H NMR spectral analysis of ten chemical markers of Ginkgo biloba.* Magn Reson Chem, **2012**. 50. 569-75.

156. Reyrat, J.M. and Kahn, D., Mycobacterium smegmatis*: an absurd model for tuberculosis?* Trends Microbiol, **2001**. 9. 472-4.

157. Oelke, A.J., France, D.J., Hofmann, T., Wuitschik, G., and Ley, S.V., *Piperazic acid-containing natural products: isolation, biological relevance and total synthesis.* Nat Prod Rep, **2011**. 28. 1445-71.

158. Lam, K.S., Hesler, G.A., Mattei, J.M., Mamber, S.W., Forenza, S., and Tomita, K., *Himastatin, a new antitumor antibiotic from* Streptomyces hygroscopicus*. I. Taxonomy of producing organism, fermentation and biological activity.* J Antibiot, **1990**. 43. 956-60.

159. Leet, J.E., Schroeder, D.R., Golik, J., Matson, J.A., Doyle, T.W., Lam, K.S., Hill, S.E., Lee, M.S., Whitney, J.L., and Krishnan, B.S., *Himastatin, a new antitumor antibiotic from* Streptomyces hygroscopicus*. III. Structural elucidation.* J Antibiot, **1996**. 49. 299-311.

160. Leet, J.E., Schroeder, D.R., Krishnan, B.S., and Matson, J.A., *Himastatin, a new antitumor antibiotic from* Streptomyces hygroscopicus*. II. Isolation and characterization.* J Antibiot, **1990**. 43. 961-6.

161. Umezawa, K., Ikeda, Y., Uchihata, Y., Naganawa, H., and Kondo, S., *Chloptosin, an apoptosis-inducing dimeric cyclohexapeptide produced by* Streptomyces*.* J Org Chem, **2000**. 65. 459-63.

162. Miller, E.D., Kauffman, C.A., Jensen, P.R., and Fenical, W., *Piperazimycins: cytotoxic hexadepsipeptides from a marine-derived bacterium of the genus* Streptomyces*.* J Org Chem, **2007**. 72. 323-30.

163. Guo, Z., Shen, L., Ji, Z., Zhang, J., Huang, L., and Wu, W., *NW-G01, a novel cyclic hexadepsipeptide antibiotic, produced by* Streptomyces alboflavus *313: I. Taxonomy, fermentation, isolation, physicochemical properties and antibacterial activities.* J Antibiot, **2009**. 62. 201-5.

164. Guo, Z., Ji, Z., Zhang, J., Deng, J., Shen, L., Liu, W., and Wu, W., *NW-G01, a novel cyclic hexapeptide antibiotic, produced by* Streptomyces alboflavus *313: II. Structural elucidation.* J Antibiot, **2010**. 63. 231-5.

165. Guo, Z., Shen, L., Zhang, J., Xin, H., Liu, W., Ji, Z., and Wu, W., *NW-G03, a related cyclic hexapeptide compound of NW-G01, produced by* Streptomyces alboflavus *313.* J Antibiot, **2011**. 64. 789-94.

166. Wei, S., Fan, L., Wu, W., and Ji, Z., *Two piperazic acid-containing cyclic hexapeptides from Streptomyces alboflavus 313.* Amino Acids, **2012**. 43. 2191-8.

167. Huang, X., Roemer, E., Sattler, I., Moellmann, U., Christner, A., and Grabley, S., *Lydiamycins A-D: cyclodepsipetides with antimycobacterial properties.* Angew Chem Int Ed Engl, **2006**. 45. 3067-72.

168. Isshiki, K., Sawa, T., Naganawa, H., Koizumi, Y., Matsuda, N., Hamada, M., Takeuchi, T., Iijima, M., Osono, M., and Masuda, T., *Depsidomycin, a new immunomodulating antibiotic.* J Antibiot, **1990**. 43. 1195-8.

169. Nguyen, L. and Thompson, C.J., *Foundations of antibiotic resistance in bacterial physiology: the mycobacterial paradigm.* Trends Microbiol, **2006**. 14. 304-12.

170. Waksman, S.A., Schatz, A., and Reynolds, D.M., *Production of antibiotic substances by actinomycetes.* Ann N Y Acad Sci, **2010**. 1213. 112-24.

171. Pauli, G.F., Pro, S.M., and Friesen, J.B., *Countercurrent separation of natural products.* J Nat Prod, **2008**. 71. 1489-508.

172. Inui, T., Wang, Y., Deng, S., Smith, D.C., Franzblau, S.G., and Pauli, G.F., *Counter-current chromatography based analysis of synergy in an anti-tuberculosis ethnobotanical.* J Chromatogr A, **2007**. 1151. 211-5.

173. Friesen, J.B. and Pauli, G.F., *GUESSmix-guided optimization of elution-extrusion counter-current separations.* J Chromatogr A, **2009**. 1216. 4225-31.

174. Friesen, J.B. and Pauli, G.F., *G.U.E.S.S.--A generally useful estimations of solvent systems in CCC.* J Liq Chromatogr Related Technol, **2005**. 28. 2777-806.

175. Berthod, A., Friesen, J.B., Inui, T., and Pauli, G.F., *Elution-extrusion countercurrent chromatography: theory and concepts in metabolic analysis.* Analytical Chemistry, **2007**. 79. 3371-82.

176. Friesen, J.B. and Pauli, G.F., *Performance characteristics of countercurrent separation in analysis of natural products of agricultural significance.* J Agric Food Chem, **2008**. 56. 19-28.

177. Cone, E.J., Buchwald, W.F., and Darwin, W.D., *Analytical controls in drug metabolic studies. II. Artifact formation during chloroform extraction of drugs and metabolites with amine substituents.* Drug Metab Dispos, **1982**. 10. 561-7.

178. Parker, R.E. and Isaacs, N.S., *Mechanisms of epoixde reactions*. Chem Rev, **1959**. 737-799.

179. Takita, T., Nagnawa, H., Maeda, K., and Umezawa, H., *A new amino acid from ilamycin B1 and the structure of ilamycin B1.* J Antibiot, **1964**. 17. 90-1.

180. Takita, T., Nagnawa, H., Maeda, K., and Umezawa, H., *The structures of ilamycin and ilamycin B2.* J Antibiot, **1964**. 17. 129-31.

181. Takita, T., Ohi, K., Okami, Y., Maeda, K., and Umezawa, H., *New antibiotics, ilamycins.* J Antibiot, **1962**. 15. 46-8.

182. Cary, L.W., Takita, T., and Ohnishi, M., *A study of the secondary structure of ilamycin B(1) by 300 MHz proton magnetic resonance.* FEBS Lett, **1971**. 17. 145-148.

183. Iitaka, Y., *An X-ray Study of Ilamycin B1, a Cyclic Heptapeptide Antibiotic.* Acta Cryst, **1974**. 2817.

184. Andjelic, C.D., Planelles, V., and Barrows, L.R., *Characterizing the anti-HIV activity of papuamide A.* Mar Drugs, **2008**. 6. 528-49.

185. Craik, D.J., *Chemistry. Seamless proteins tie up their loose ends.* Science, **2006**. 311. 1563-4.

186. Eli Lilly and Company, *Rufomycin Derivatives Usefule as Antibiotics*. World Intellectual Property Organization, **2000**. 1-92.

APPENDICES

Appendix A
Spectra and chromatograms of hytramycins V (**1**) and I (**2**)

Appendix B
Spectra and chromatograms of xylamycin (**3**)

Appendix C
^{1}H NMR HiFSA profile of hytramycin V (**1**) in the PERCH .PMS file format (MeOH-d_4)

Appendix D
^{1}H NMR HiFSA profile of hytramycin I (**2**) in the PERCH .PMS file format (MeOH-d_4)

Appendix E
^{1}H NMR HiFSA profile of xylamycin (**3**) in the PERCH .PMS file format (MeOH-d_4)

Appendix F
Details of the culture media

Appendix G
License agreement of publications

Appendix A. Spectra and chromatograms of hytramycins V (1) and I (2)

Figure A-1. Accurate ESI-IT-TOF mass spectra (showing ions of $[M+H]^+$ and $[M+Na]^+$) of 1 (A) and 2 (B)

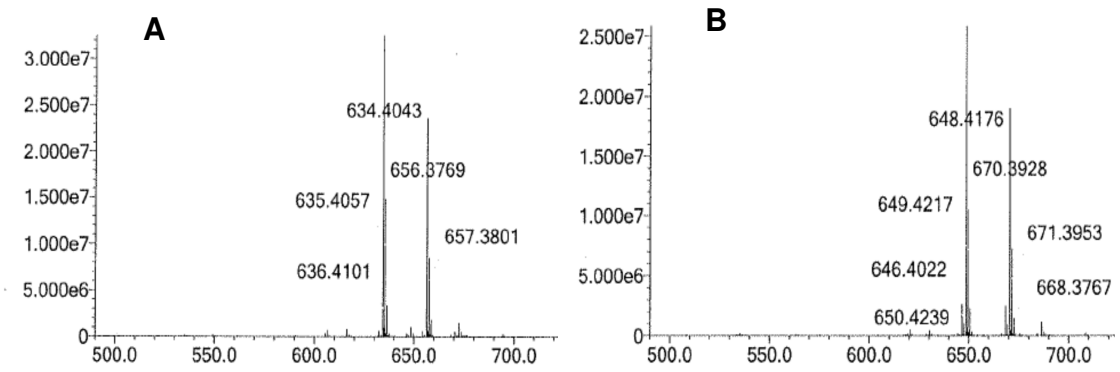

Appendix A (continued)

Figure A-2. MS/MS spectra and key fragmentation patterns of hytramycin V (1), (A and C), and hytramycin I (2), (B and D). A=*N*MeAla; V=Val; I=Ile; L=Leu; Pip=piperazic acid [a]

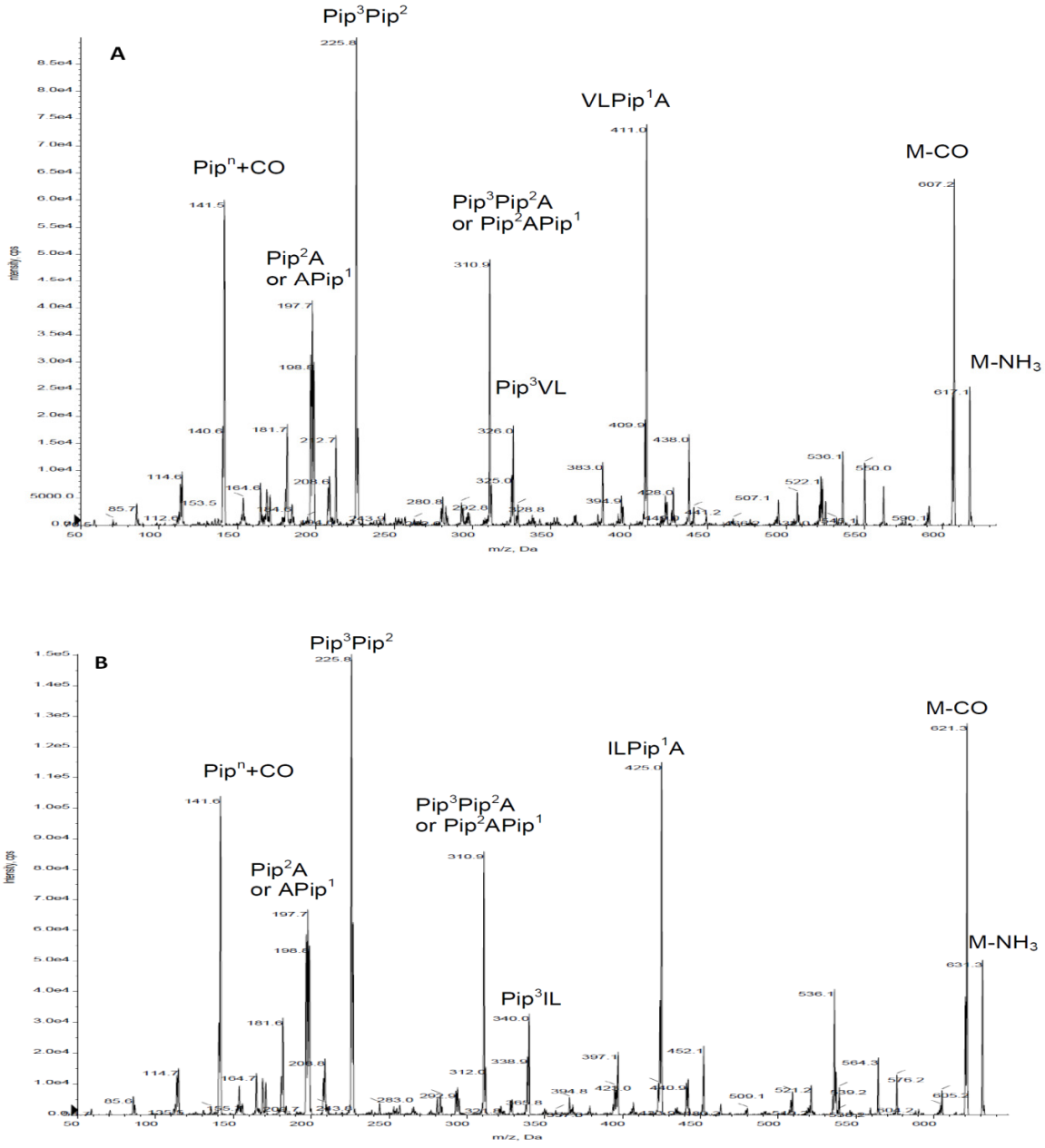

Appendix A (continued)

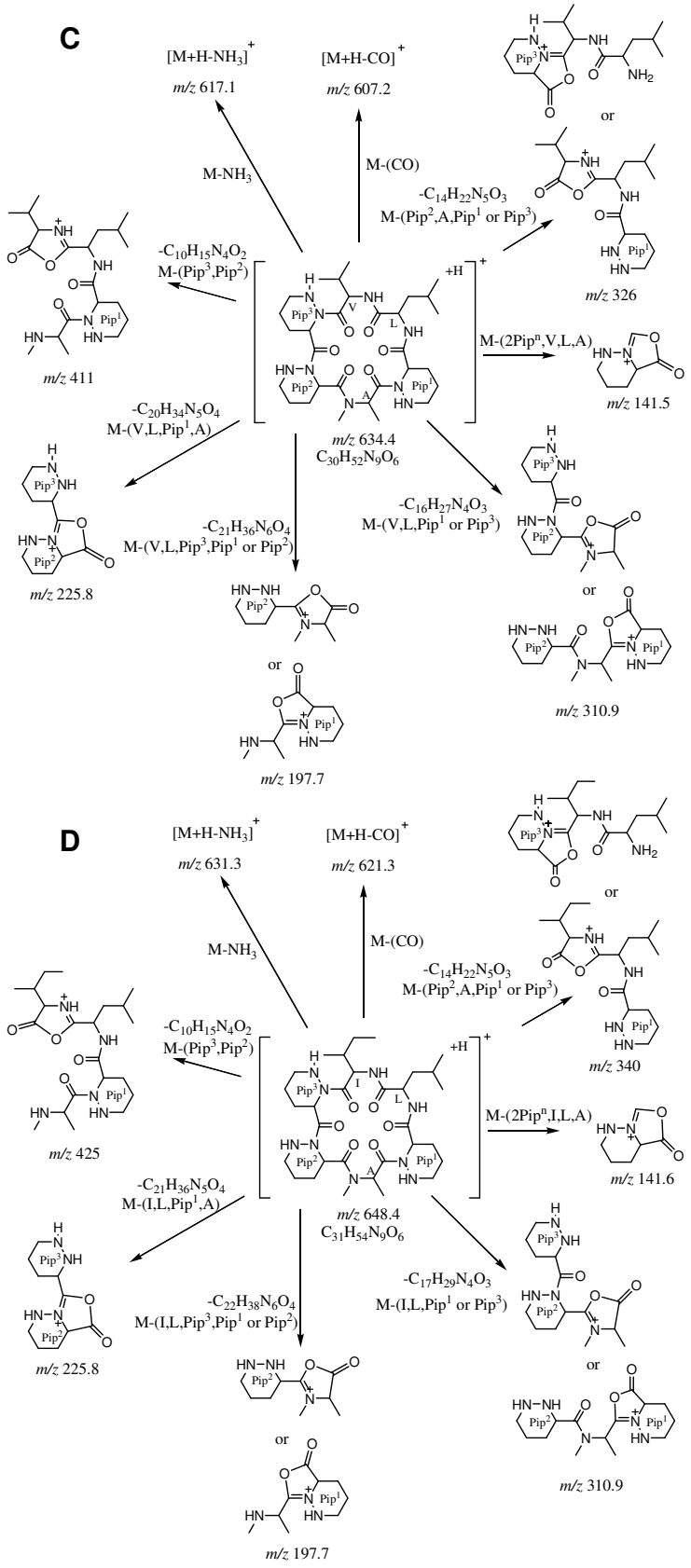

Appendix A (continued)

[a] The fragmentation mass spectra of both **1** and **2** share common fragments, such as a Pip^3Pip^2 base peak at *m/z* 225.8, a Pip^n+CO peak at *m/z* 141.5, a Pip^3Pip^2A or Pip^2APip^1 peak at *m/z* 310.9, and a Pip^2A or $APip^1$ peak at *m/z* 197.7, where the uncertainty of fragmentation loci are caused by the identical compositions of multiple Pip moieties in the molecules. The differences between the two molecules can be reflected by the following observations: the $VLPip^1A$ fragment at *m/z* 411.0, the Pip^3VL fragment at *m/z* 326.0, the M-CO peak at *m/z* 607.2, and the M-NH_3 peak at *m/z* 617.1 for **1**. In contrast, **2** showed the $ILPip^1A$ fragment at *m/z* 425.0, the Pip^3IL fragment at *m/z* 340.0, the M-CO peak at *m/z* 621.3, and the M-NH_3 peak at *m/z* 631.3.

Figure A-3. IR spectra of hytramycin V (1), (top), and hytramycin I (2), (bottom)

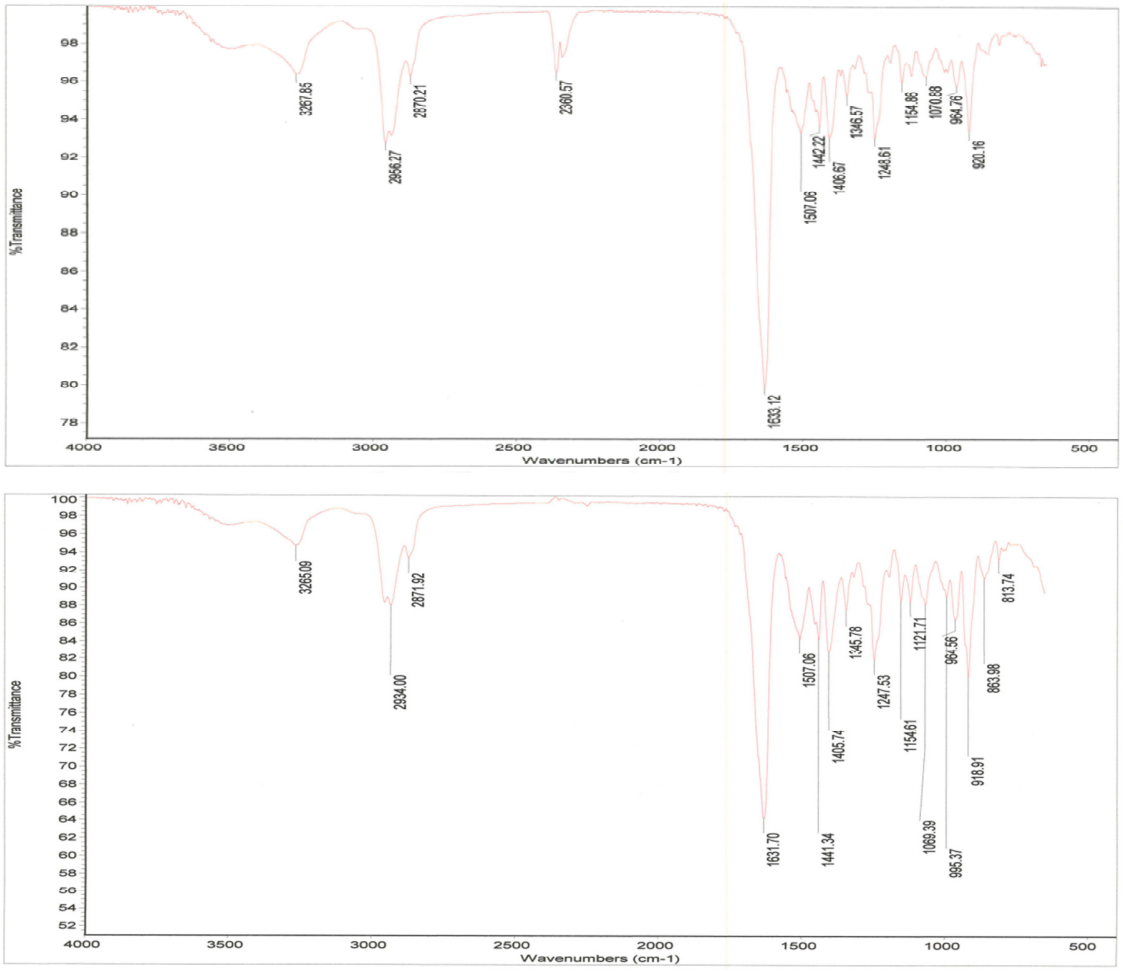

Appendix A (continued)

Figure A-4. COSY spectrum of hytramycin V (1), (400 MHz, MeOH-d_4)

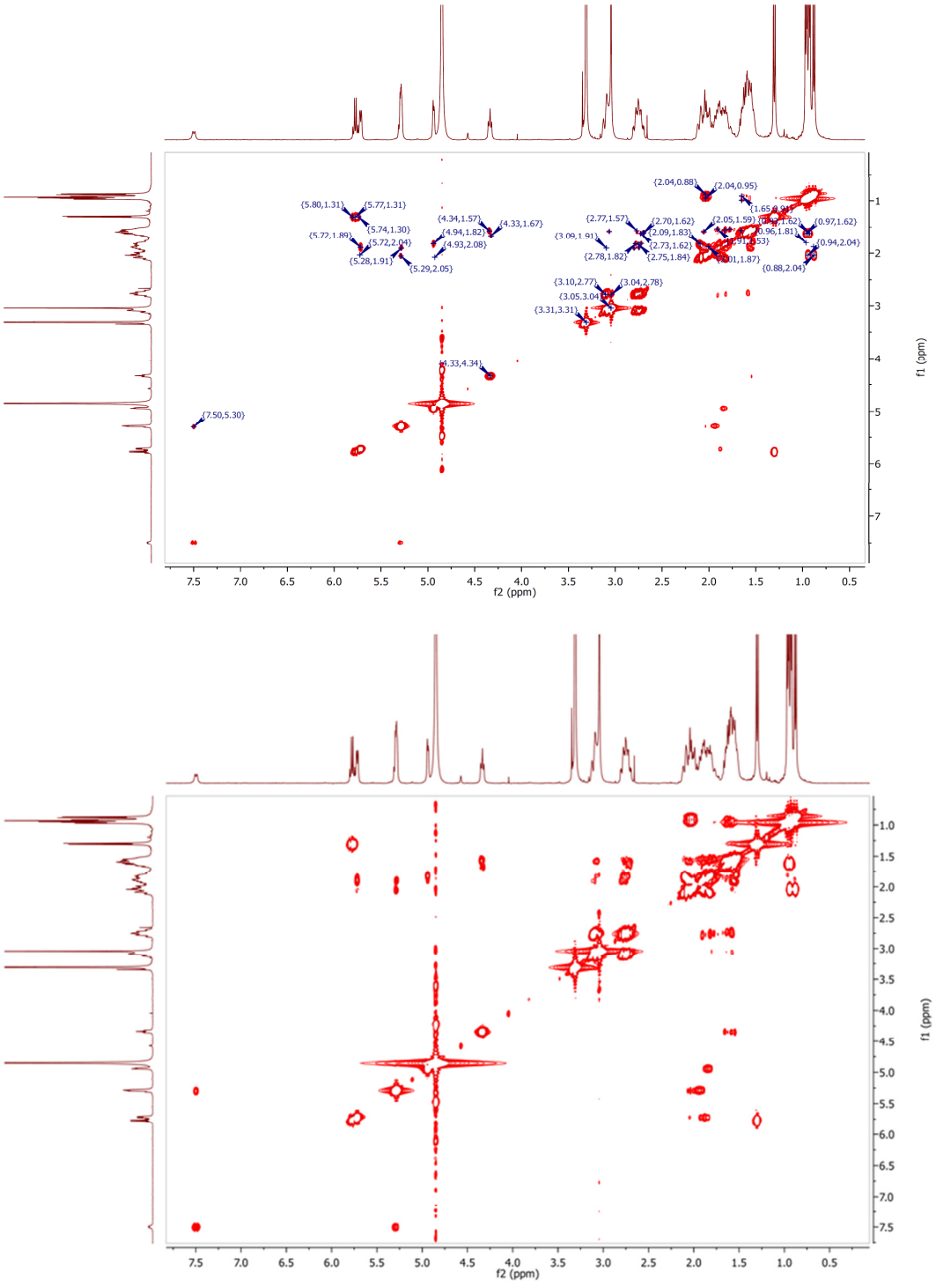

Appendix A (continued)

Figure A-5. HSQC spectrum of hytramycin V (1) (400 MHz, MeOH-d_4)

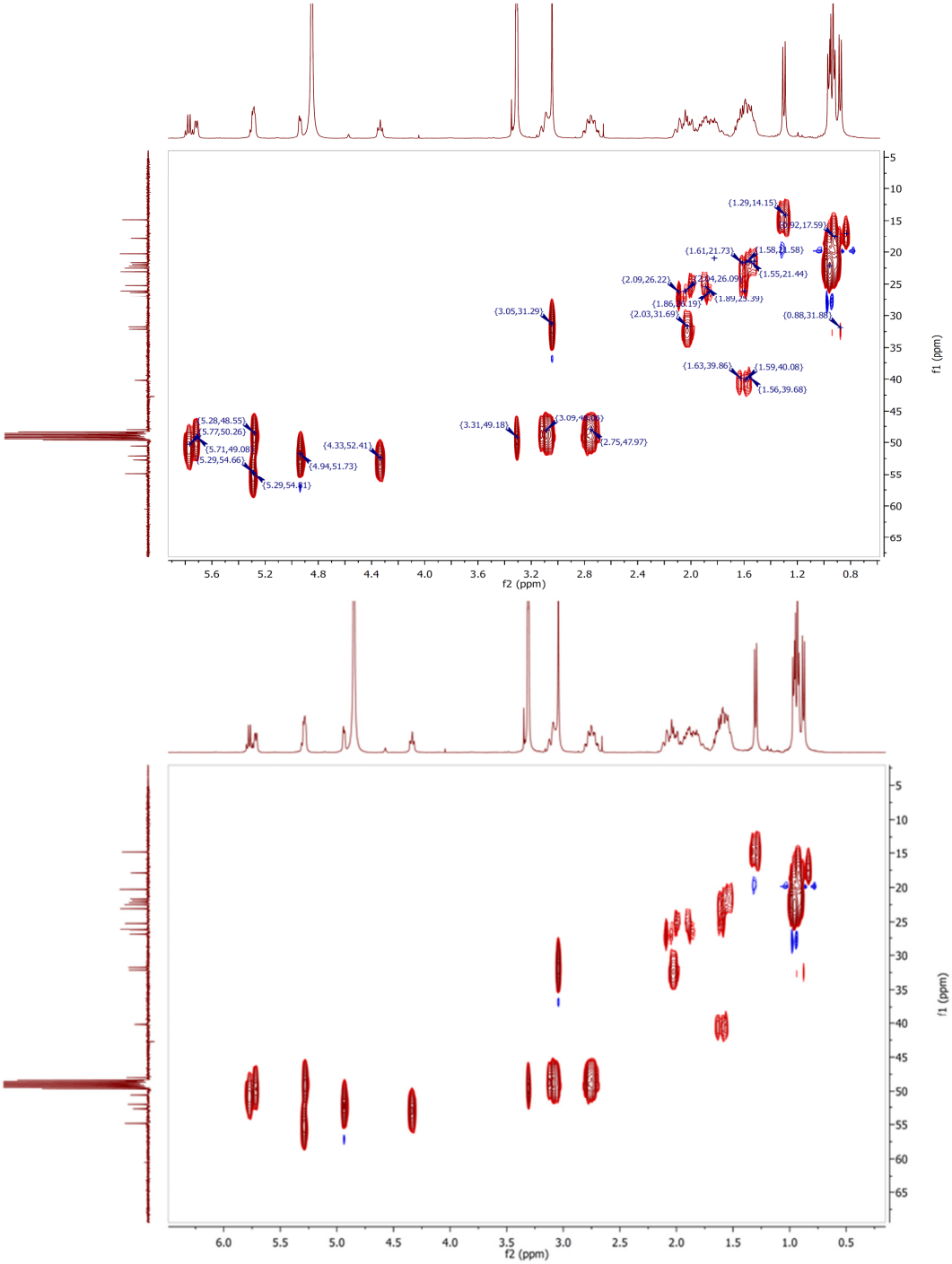

Appendix A (continued)

Figure A-6. HMBC spectrum of hytramycin V (1), (400 MHz, MeOH-d_4)

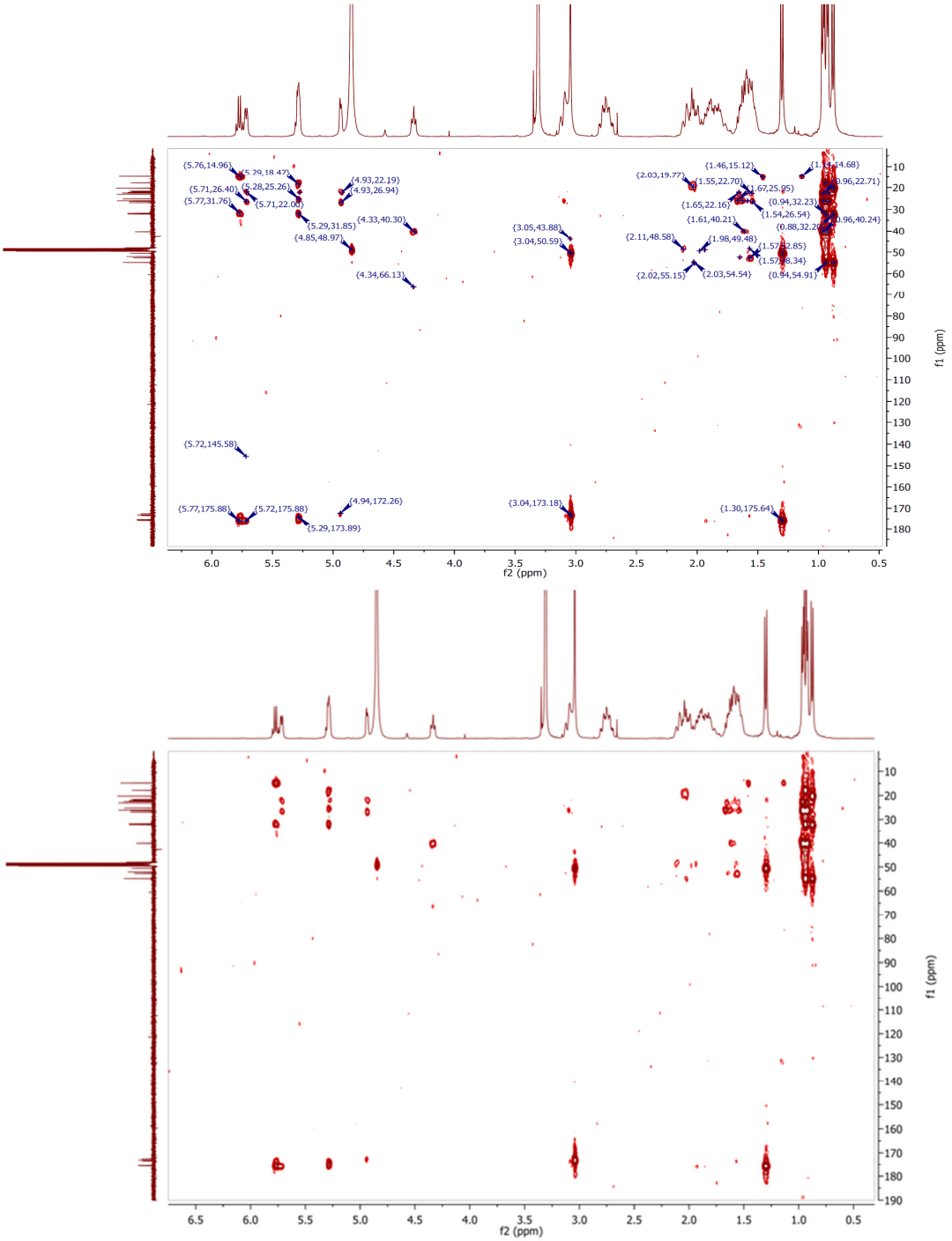

Appendix A (continued)

Figure A-7. TOCSY spectrum of hytramycin V (1) (400 MHz, MeOH-d_4)

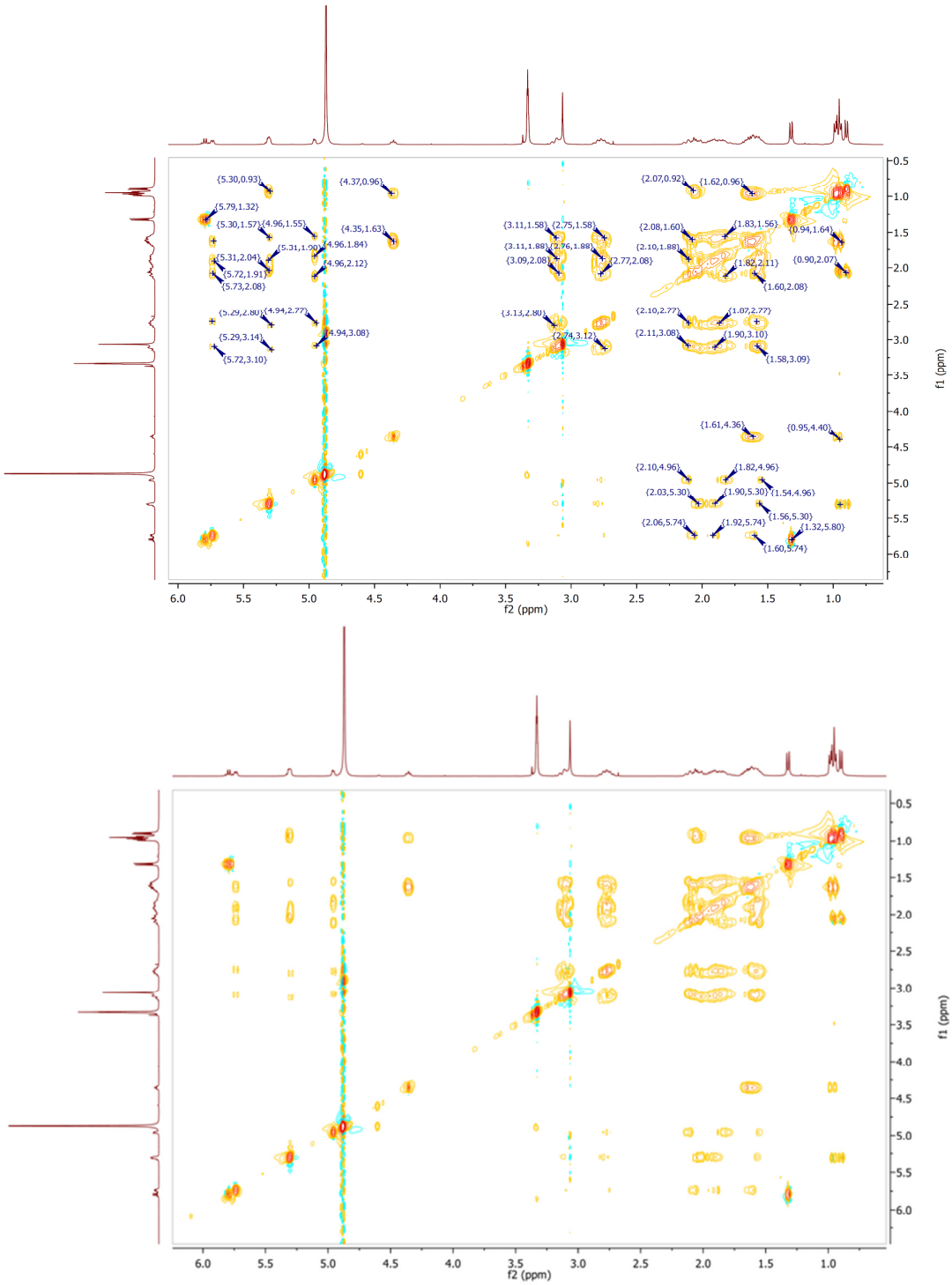

Appendix A (continued)

Figure A-8. NOESY spectrum of hytramycin V (1), (400 MHz, MeOH-d_4)

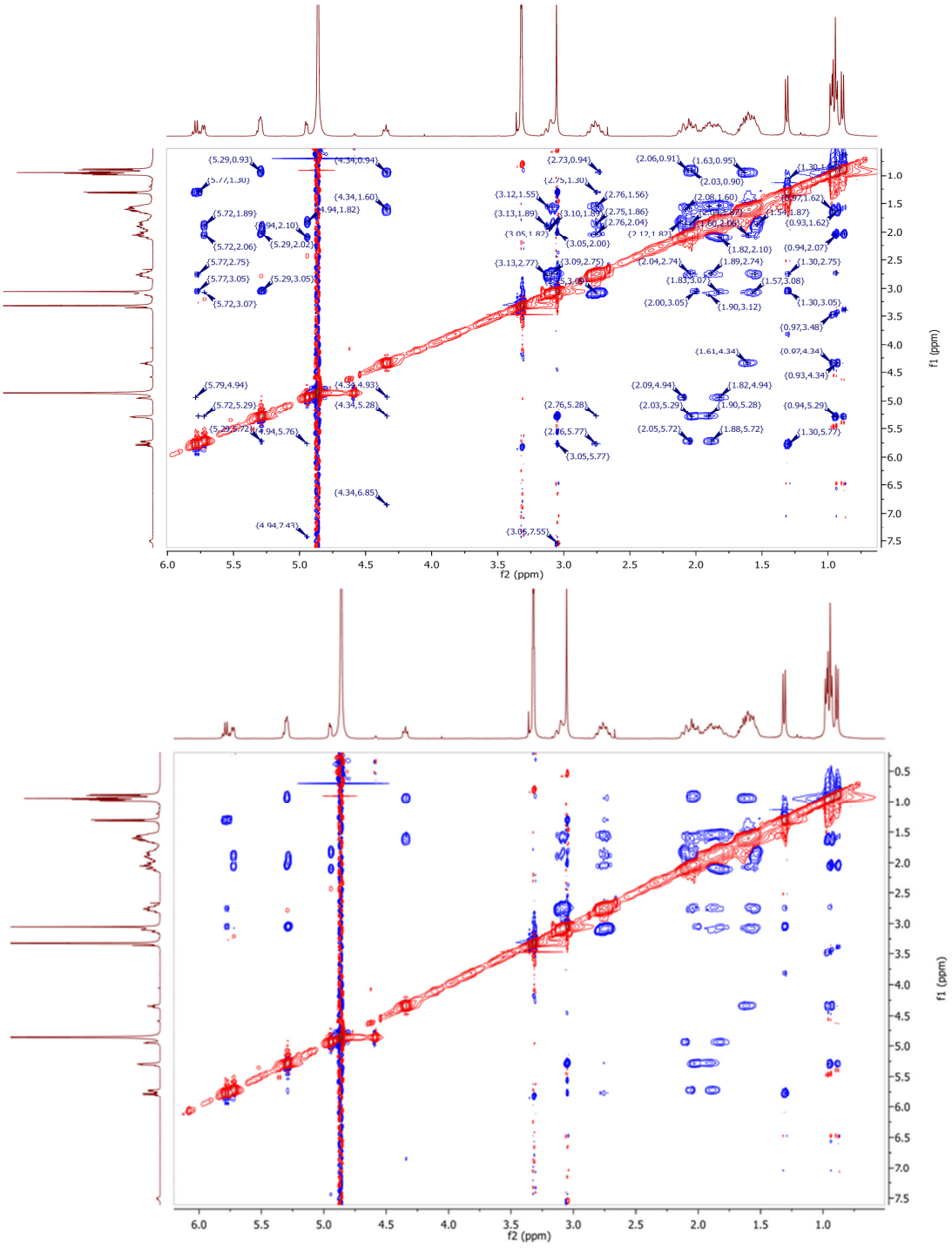

Appendix A (continued)

Figure A-9. ^{1}H NMR expansion spectra of hytramycin I (2), (400 MHz, MeOH-d_4)

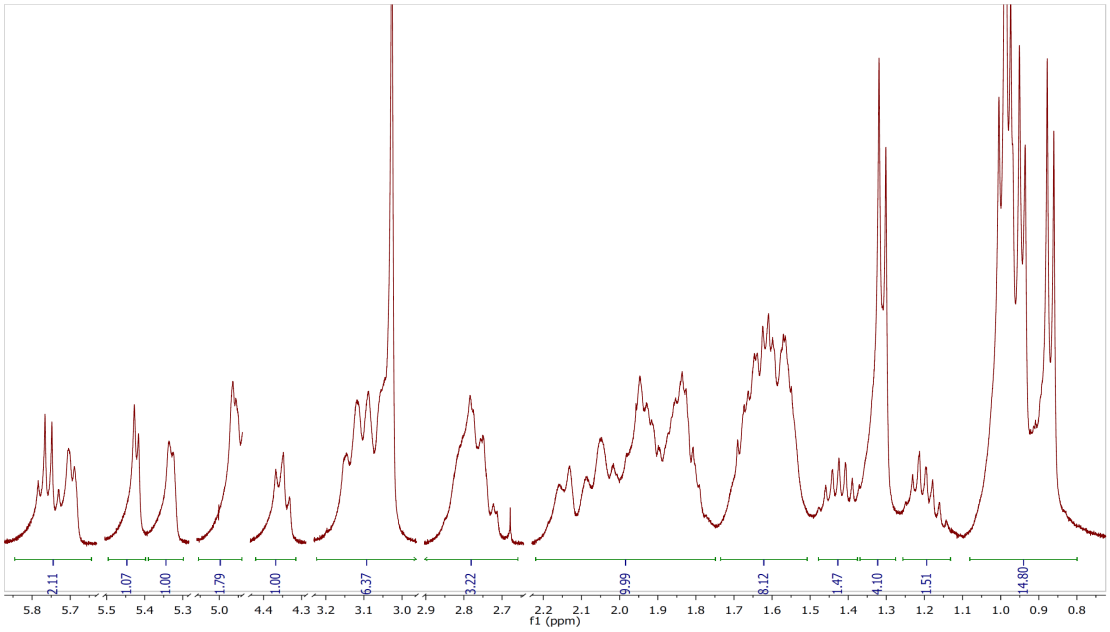

Appendix A (continued)

Figure A-10. COSY spectrum of hytramycin I (2), (400 MHz, MeOH-d_4)

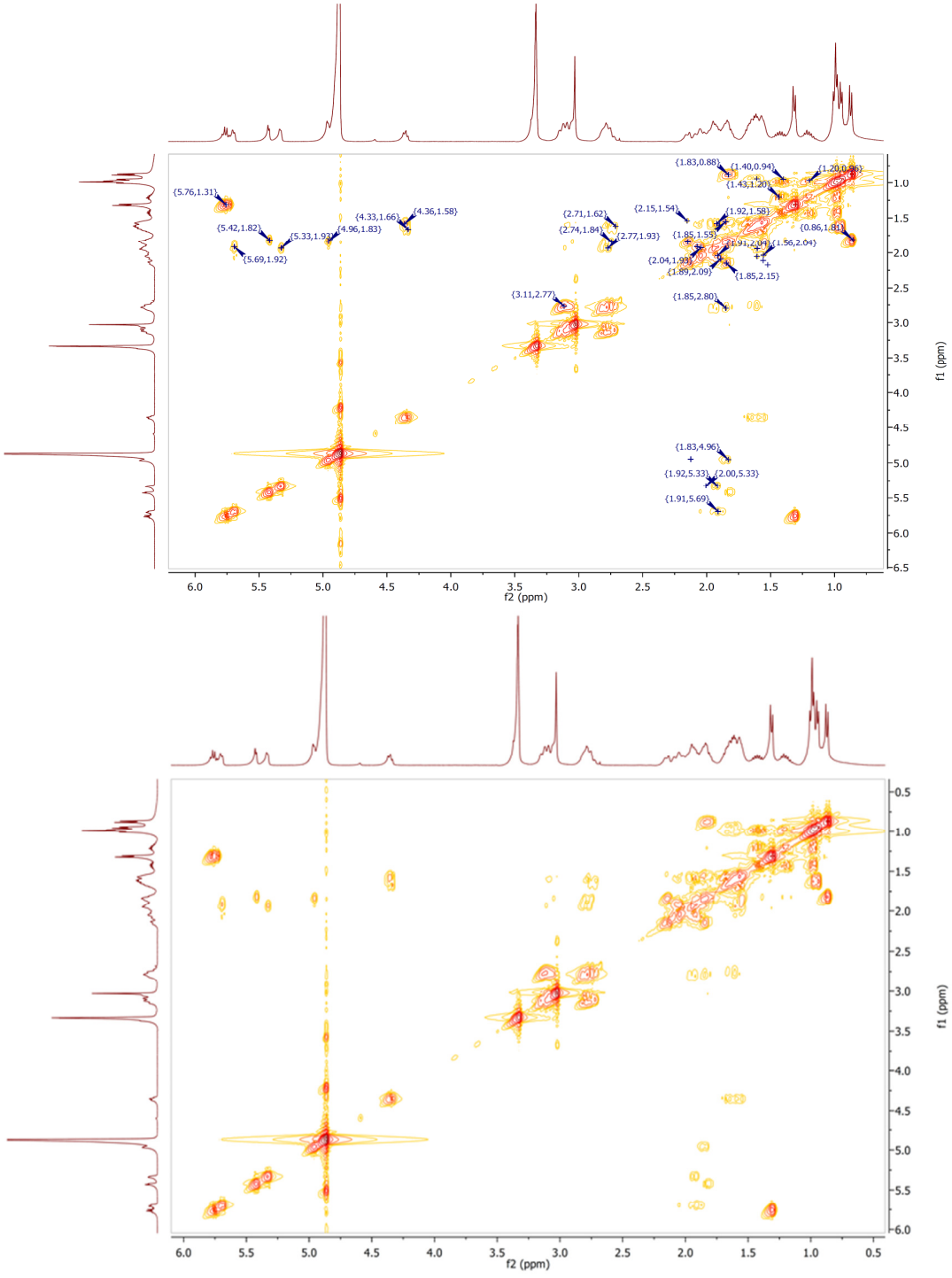

Appendix A (continued)

Figure A-11. HSQC spectrum of hytramycin I (2), [400 MHz, MeOH-d_4, vertical axis showing ^{13}C NMR spectrum of hytramycin V (1)]

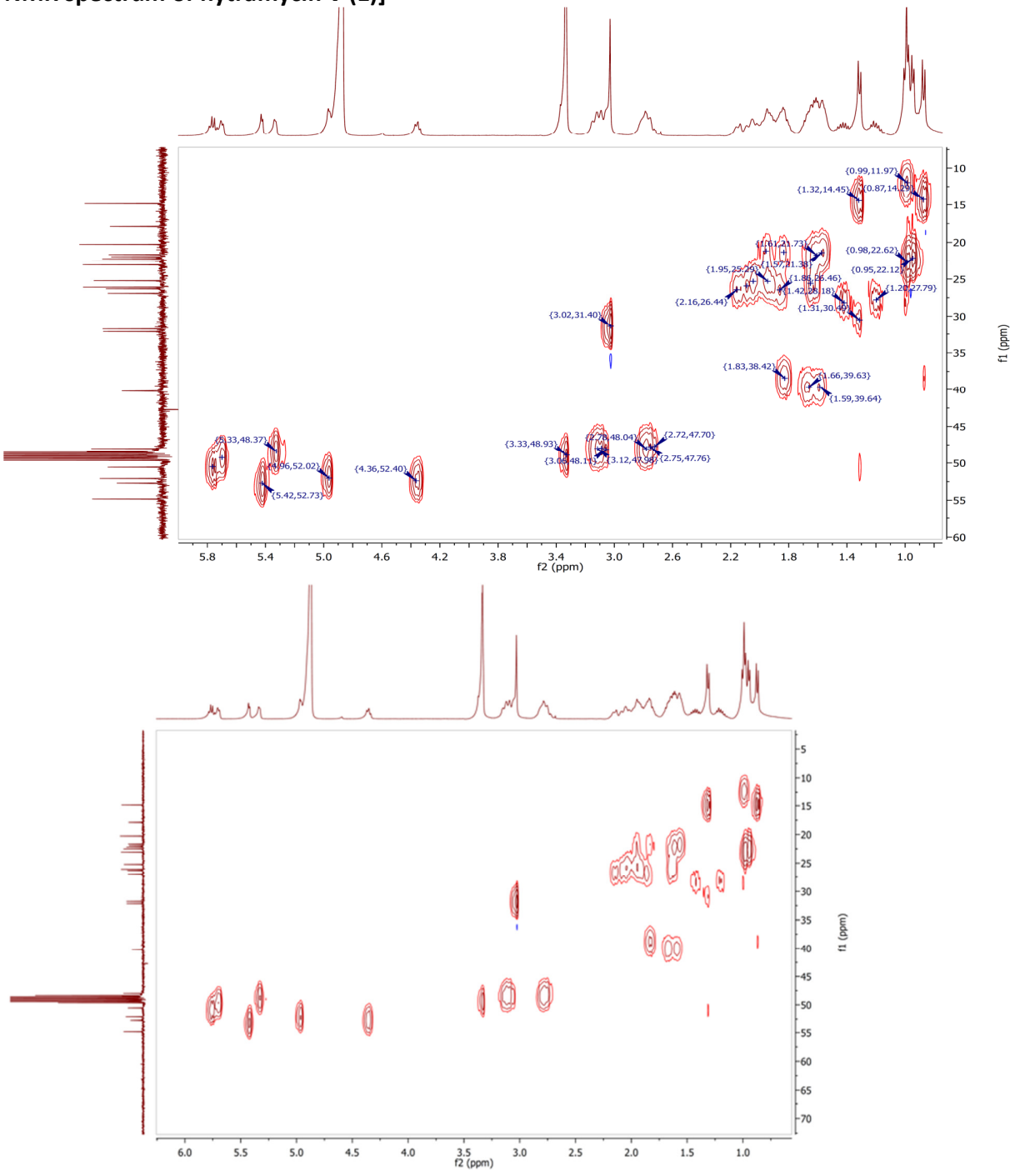

Appendix A (continued)

Figure A-12. HMBC spectrum of hytramycin I (2), [400 MHz, MeOH-d_4, vertical axis showing ^{13}C NMR spectrum of hytramycin V (1)]

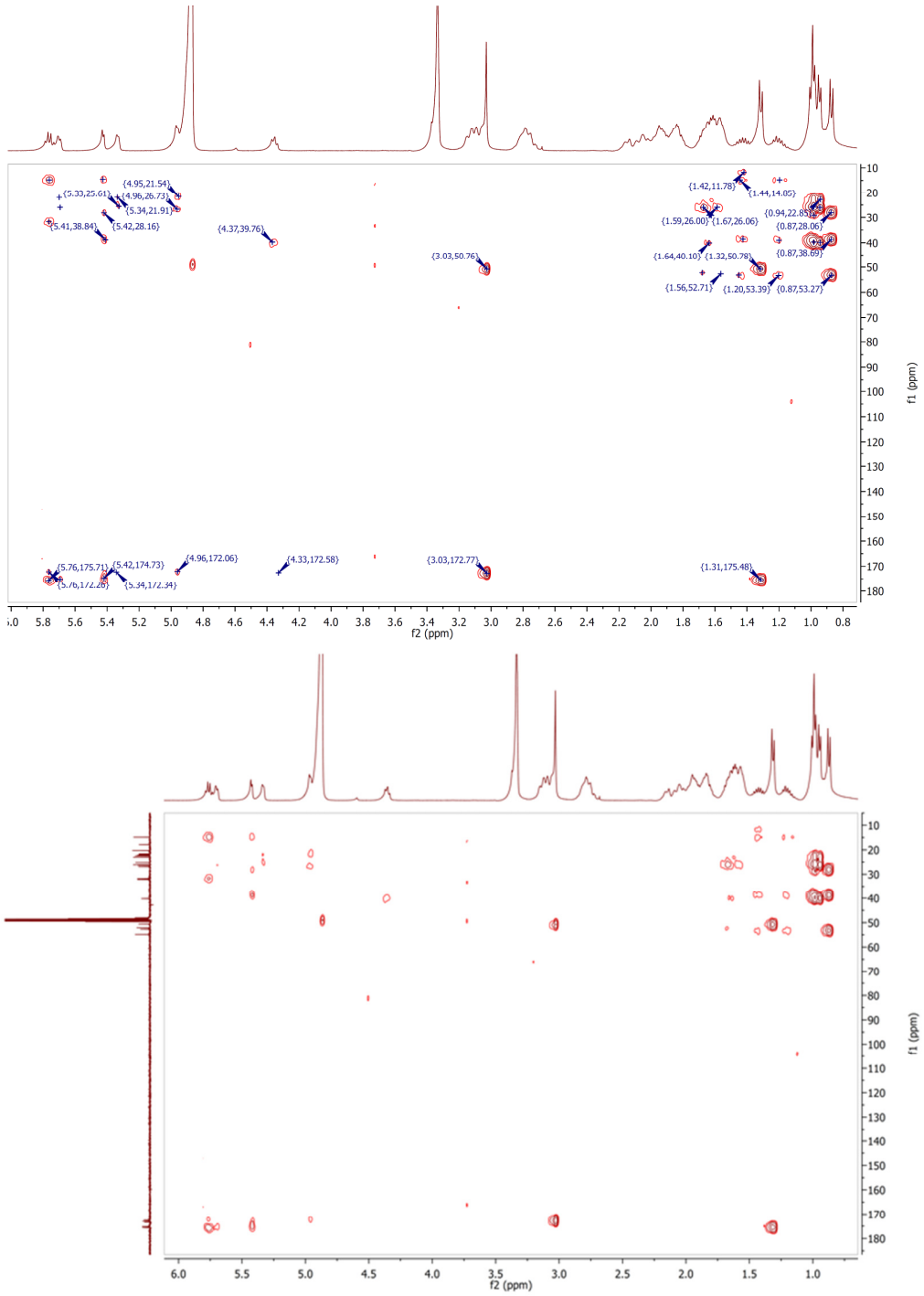

Appendix A (continued)

Figure A-13. ^{13}C NMR spectrum of hytramycin I (2), (100 MHz, DMSO-d_6)

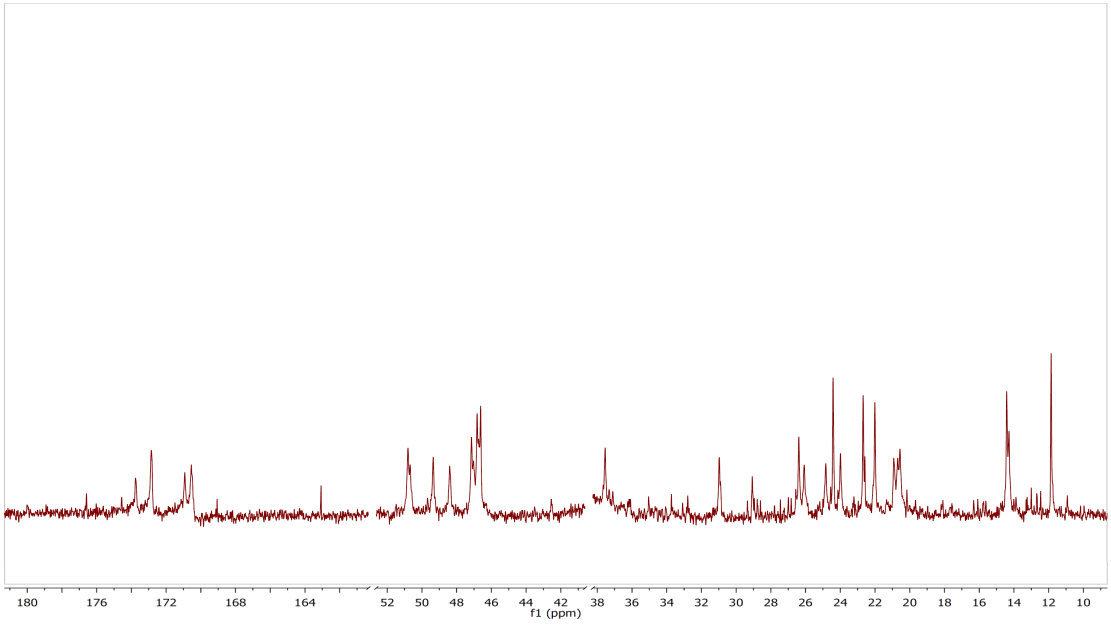

Appendix B. Spectra and chromatograms of xylamycin (3)

Figure B-1. UV (upper) and IR (lower) spectra of B14 (3)

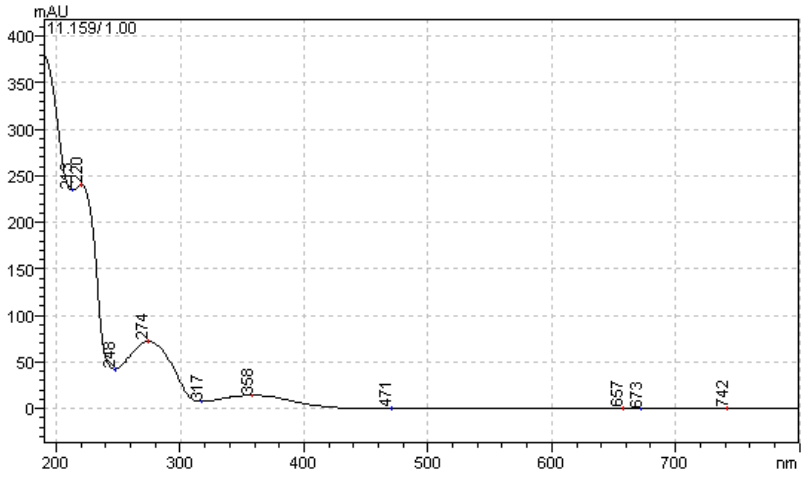

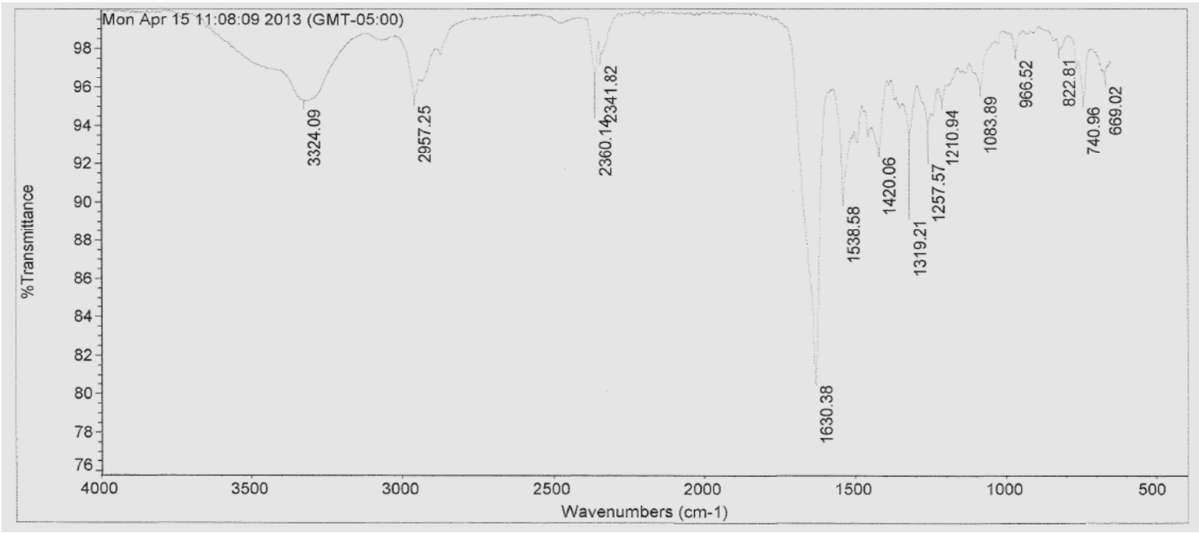

Appendix B (continued)

Figure B-2. Accurate ESI-IT-TOF mass spectra of B14 (3), ([M+H]$^+$)

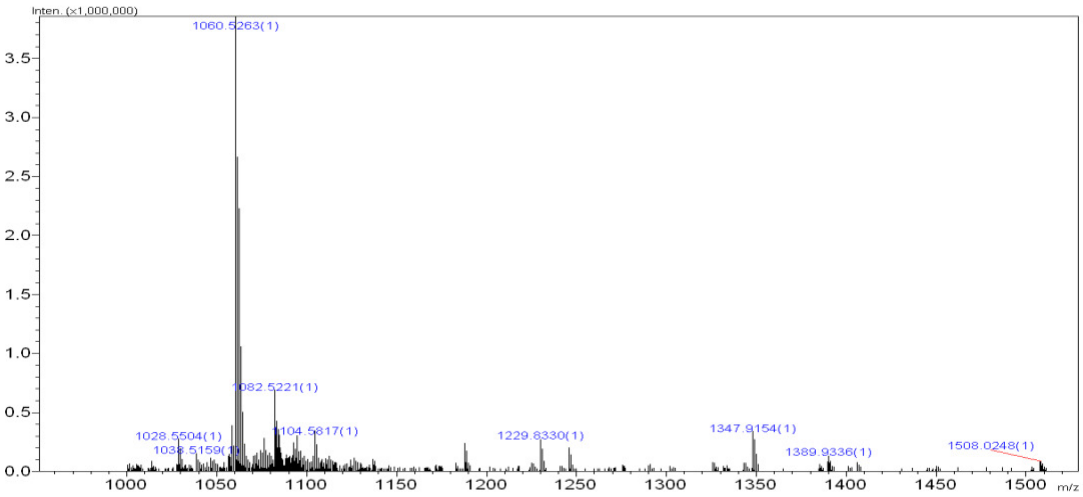

Figure B-3. COSY spectrum of B14 (3) and expansions (600 MHz, MeOH-d_4)

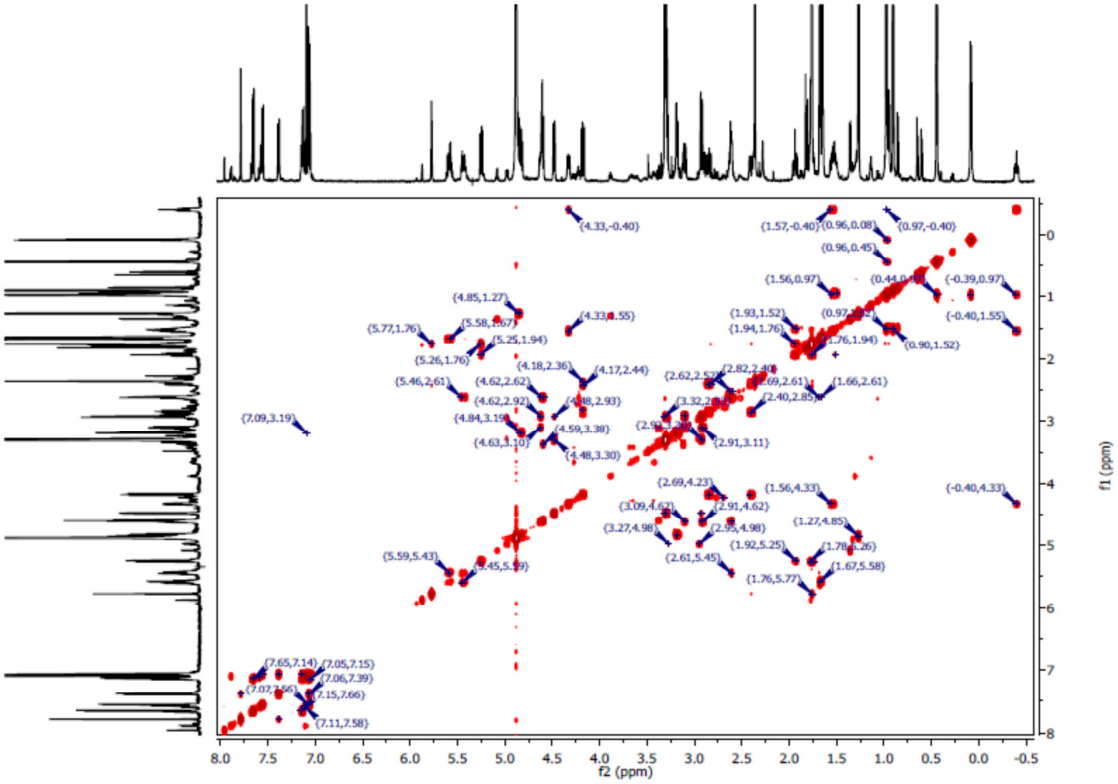

Appendix B (continued)

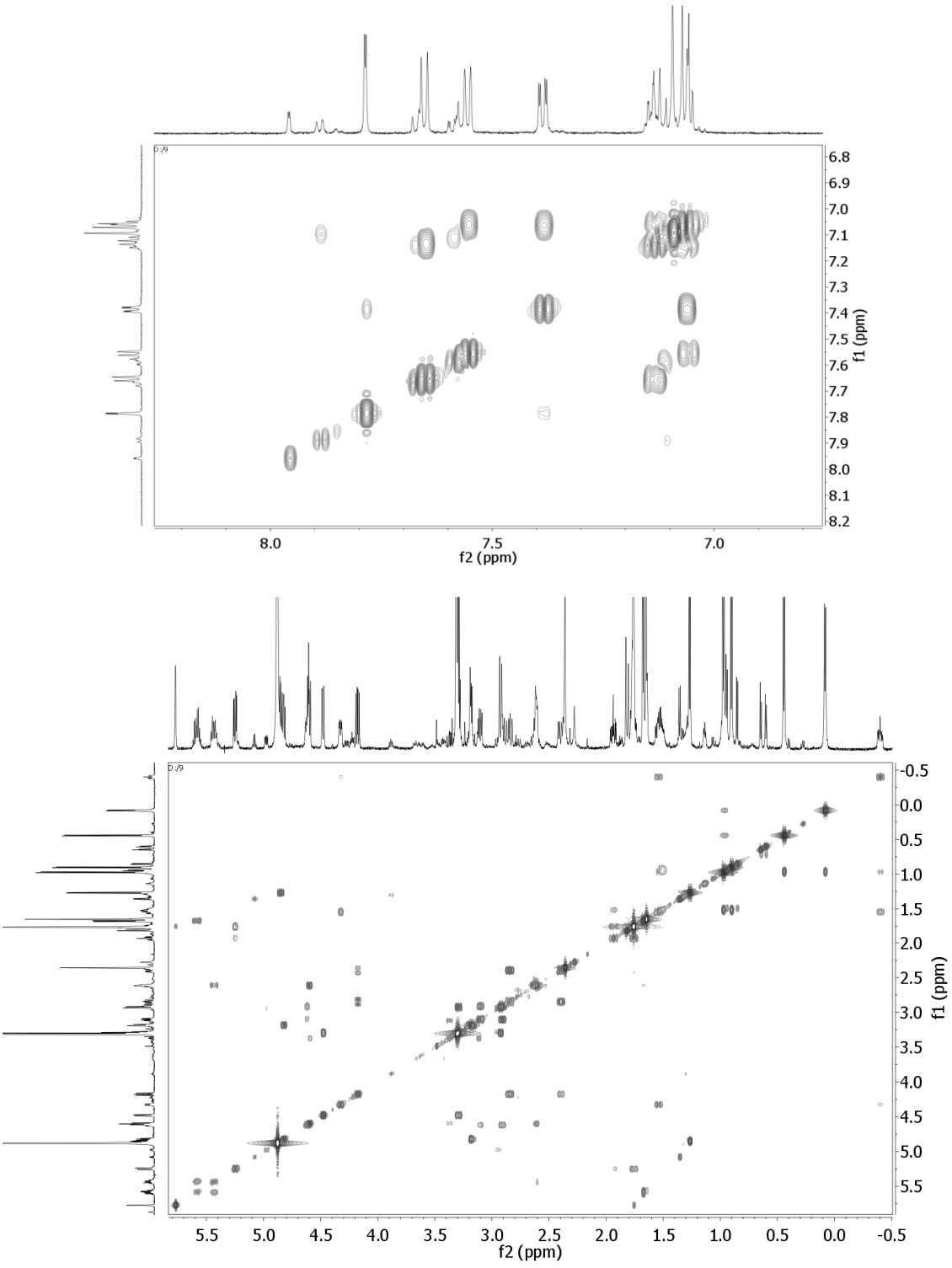

Appendix B (continued)

Figure B-4. ^{13}C spectrum of B14 (3), (400 MHz, MeOH-d_4)

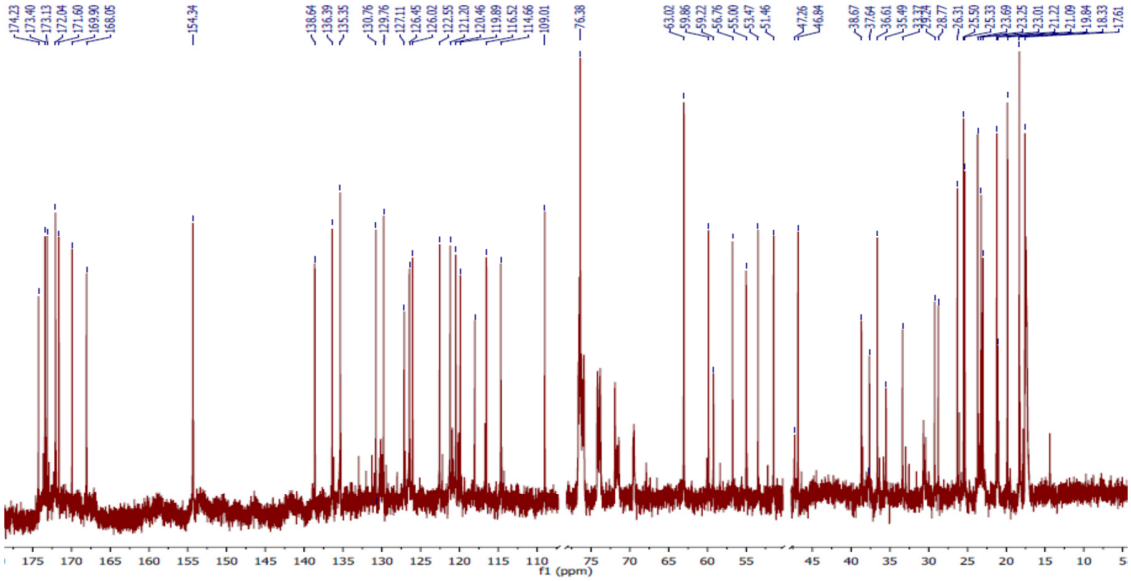

Figure B-5. HSQC spectrum of B14 (3) and expansions (600 MHz, MeOH-d_4)

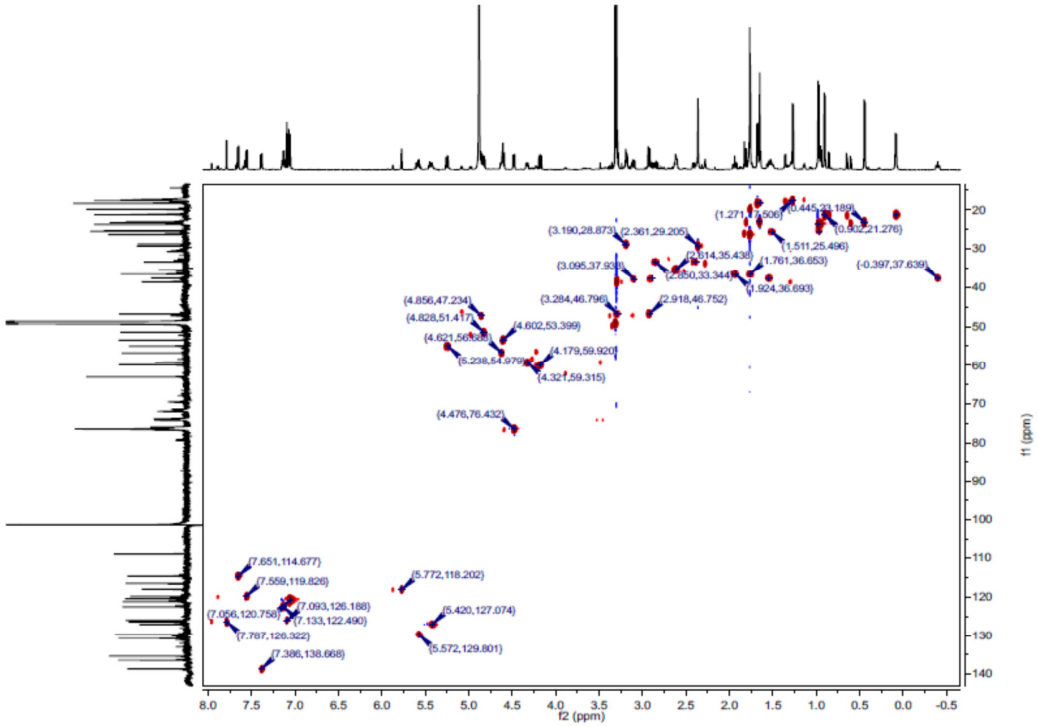

Appendix B (continued)

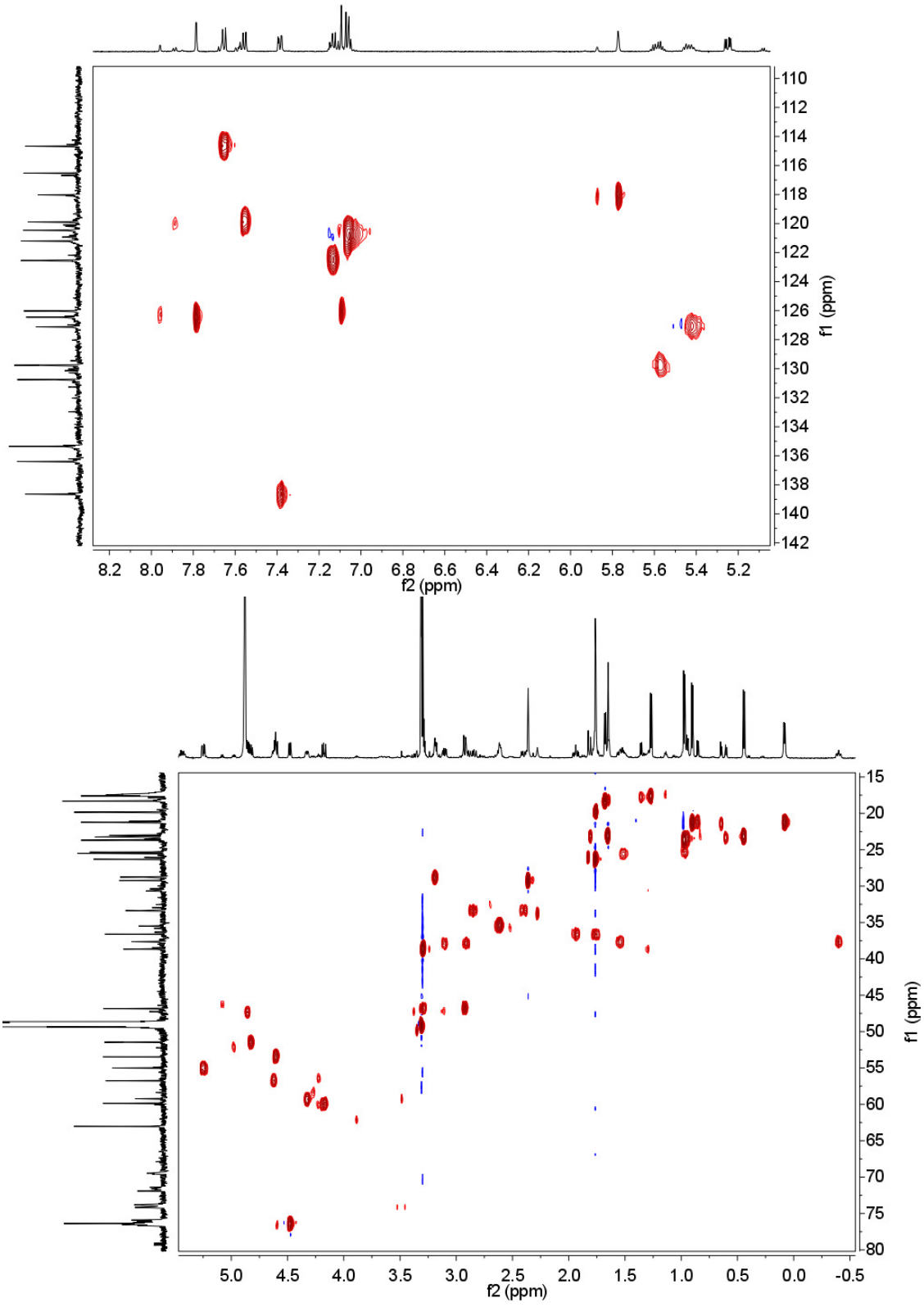

Appendix B (continued)

Figure B-6. HMBC spectrum of B14 (3) and expansions (600 MHz, MeOH-d_4)

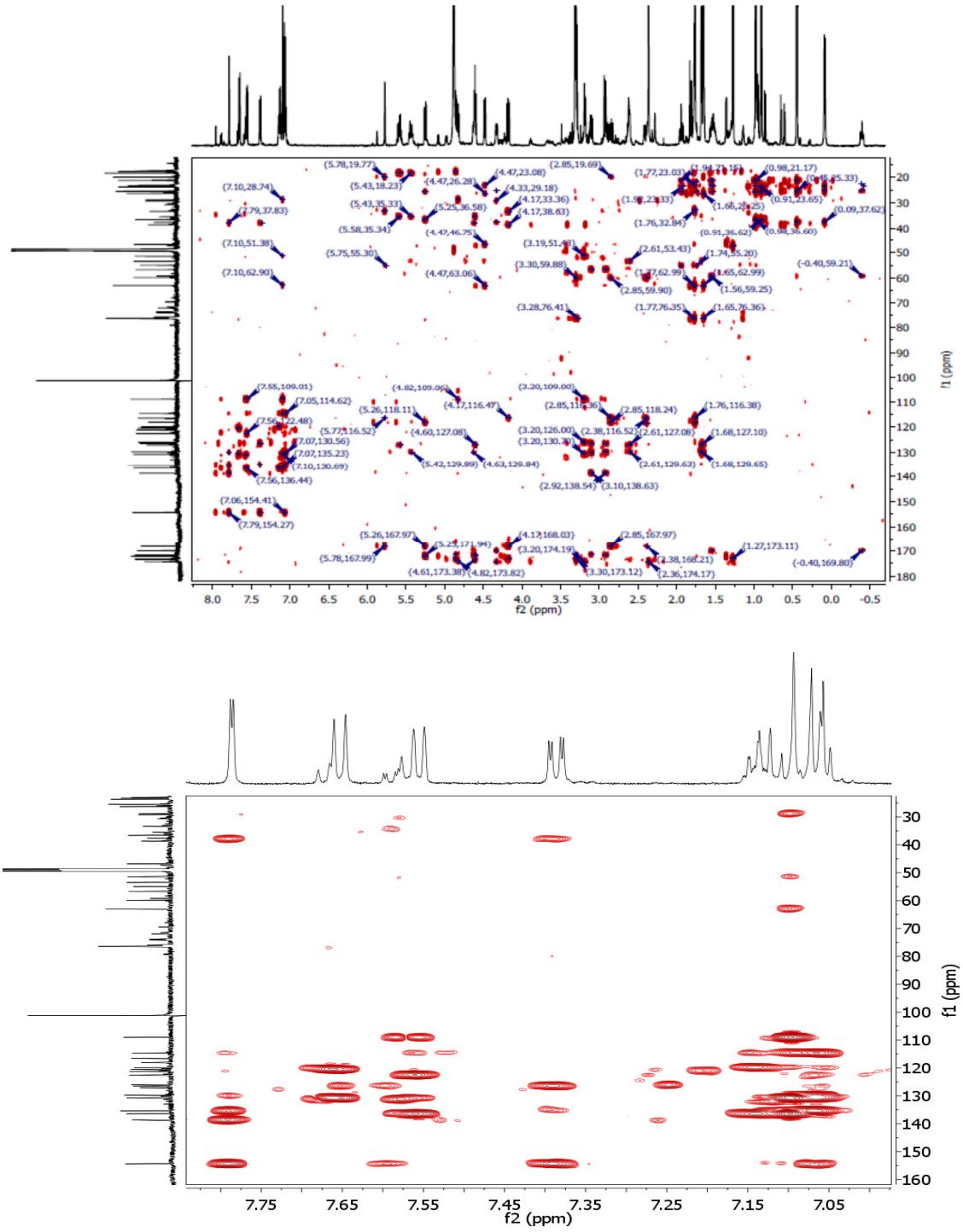

Appendix B (continued)

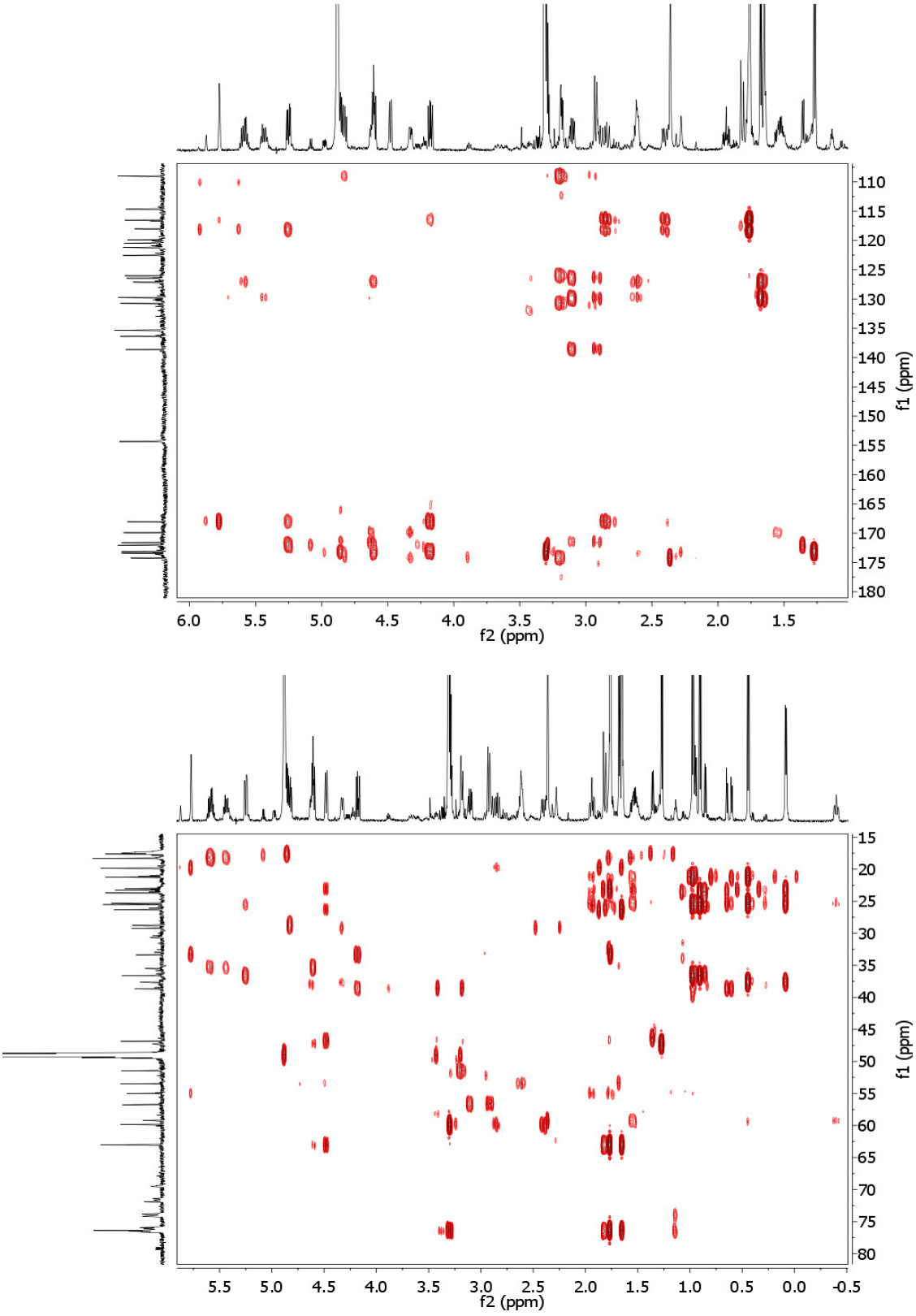

Appendix C. ^{1}H NMR HiFSA profile of hytramycin V (1) in the PERCH .PMS file format (MeOH-d_4)

```
* NEW: the lines beginning by * are comment lines !
* To keep all the chemical shifts fixed during iteration
* replace "CHEMICAL SHIFTS(HZ):" by "..SHIFTS(HZ): fixed"
* The couplings can be fixed in the same way

NMR-data: C:\Users\jgnapo_2\Desktop\gcai_P1\p1
#$? Date 29.10.2012;  Time 12: 2:10     p1.4th

CHEMICAL SHIFTS(PPM):
PROTON    2*SPIN= 1 SPECIES=1H    POPULATION(Y)=   1.00000
 H1  / 1    5.290742  1*1*1  STAT=Y  PRED= 4.099 RANGE= 1.160 WIDTH(Y)= 2.857 RESP(Y)= 0.4944 HSQC= C1
 H4  / 1    4.337917  1*1*1  STAT=Y  PRED= 4.428 RANGE= 1.490 WIDTH(Y)= 3.152 RESP(Y)= 0.4744 HSQC= C4
 H7  / 1    4.937217  1*1*1  STAT=Y  PRED= 4.399 RANGE= 0.840 WIDTH(Y)= 2.883 RESP(Y)= 0.5379 HSQC= C7
 H10 / 1    5.775068  1*1*1  STAT=Y  PRED= 4.337 RANGE= 1.010 WIDTH(Y)= 2.052 RESP(Y)= 0.5011 HSQC= C10
 H13 / 1    5.280657  1*1*1  STAT=Y  PRED= 4.381 RANGE= 0.975 WIDTH(Y)= 3.597 RESP(Y)= 0.4938 HSQC= C13
 H16 / 1    5.721390  1*1*1  STAT=Y  PRED= 3.979 RANGE= 0.620 WIDTH(Y)= 3.636 RESP(Y)= 0.4919 HSQC= C16
 H19 / 1    2.056042  1*1*1  STAT=Y  PRED= 2.217 RANGE= 0.520 WIDTH(Y)= 2.664 RESP(Y)= 0.3713 HSQC= C19
 H20 / 1    0.877195  1*1*3  STAT=Y  PRED= 1.092 RANGE= 0.232 WIDTH(Y)= 2.339 RESP(Y)= 0.5243 HSQC= C20
 H21 / 1    0.939996  1*1*3  STAT=Y  PRED= 1.114 RANGE= 0.187 WIDTH(Y)= 1.893 RESP(Y)= 0.5235 HSQC= C21
 H22A/ 1    1.641323  1*1*1  STAT=Y  PRED= 1.927 RANGE= 0.567 WIDTH(Y)= 1.895 RESP(Y)= 0.2267 HSQC= C22
 H22B/ 1    1.596955  1*1*1  STAT=Y  PRED= 1.689 RANGE= 0.607 WIDTH(Y)= 0.952 RESP(Y)= 0.2519 HSQC= C22
 H23 / 1    1.565212  1*1*1  STAT=Y  PRED= 1.654 RANGE= 0.237 WIDTH(Y)= 3.836 RESP(Y)= 0.4933 HSQC= C23
 H24 / 1    0.925231  1*1*3  STAT=Y  PRED= 0.925 RANGE= 0.150 WIDTH(Y)= 1.722 RESP(Y)= 0.5056 HSQC= C24
 H25 / 1    0.965224  1*1*3  STAT=Y  PRED= 0.945 RANGE= 0.150 WIDTH(Y)= 1.697 RESP(Y)= 0.5205 HSQC= C25
 H26A/ 1    2.096810  1*1*1  STAT=Y  PRED= 2.069 RANGE= 0.540 WIDTH(Y)= 2.132 RESP(Y)= 0.4756 HSQC= C26
 H26B/ 1    1.860558  1*1*1  STAT=Y  PRED= 1.791 RANGE= 0.527 WIDTH(Y)= 4.350 RESP(Y)= 0.6059 HSQC= C26
 H27A/ 1    1.579215  1*1*1  STAT=Y  PRED= 1.407 RANGE= 0.675 WIDTH(Y)= 2.093 RESP(Y)= 0.5589 HSQC= C27
 H27B/ 1    1.630278  1*1*1  STAT=Y  PRED= 1.666 RANGE= 0.555 WIDTH(Y)= 2.331 RESP(Y)= 1.0000 HSQC= C27
 H28A/ 1    2.727378  1*1*1  STAT=Y  PRED= 3.162 RANGE= 0.527 WIDTH(Y)= 2.014 RESP(Y)= 0.4825 HSQC= C28
 H28B/ 1    3.070876  1*1*1  STAT=Y  PRED= 2.664 RANGE= 0.430 WIDTH(Y)= 2.497 RESP(Y)= 0.2432 HSQC= C28
 H30 / 1    1.302513  1*1*3  STAT=Y  PRED= 1.441 RANGE= 0.272 WIDTH(Y)= 2.493 RESP(Y)= 0.5154 HSQC= C30
 H31 / 1    3.047984  1*1*3  STAT=Y  PRED= 3.064 RANGE= 0.415 WIDTH(Y)= 2.017 RESP(Y)= 0.5113 HSQC= C31
 H32A/ 1    2.001474  1*1*1  STAT=Y  PRED= 2.157 RANGE= 0.535 WIDTH(Y)= 0.851 RESP(Y)= 0.2967 HSQC= C32
 H32B/ 1    1.930903  1*1*1  STAT=Y  PRED= 1.649 RANGE= 0.585 WIDTH(Y)= 4.563 RESP(Y)= 0.5084 HSQC= C32
 H34A/ 1    2.774459  1*1*1  STAT=Y  PRED= 2.651 RANGE= 0.397 WIDTH(Y)= 2.668 RESP(Y)= 0.4711 HSQC= C34
 H34B/ 1    3.107020  1*1*1  STAT=Y  PRED= 3.202 RANGE= 0.437 WIDTH(Y)= 4.224 RESP(Y)= 0.4729 HSQC= C34
 H35A/ 1    1.835198  1*1*1  STAT=Y  PRED= 1.728 RANGE= 0.572 WIDTH(Y)= 2.032 RESP(Y)= 0.3571 HSQC= C35
 H35B/ 1    1.535072  1*1*1  STAT=Y  PRED= 1.713 RANGE= 0.707 WIDTH(Y)= 1.217 RESP(Y)= 0.1545 HSQC= C35
 H37A/ 1    2.033460  1*1*1  STAT=Y  PRED= 1.893 RANGE= 0.600 WIDTH(Y)= 2.825 RESP(Y)= 0.7952 HSQC= C37
 H37B/ 1    1.887869  1*1*1  STAT=Y  PRED= 1.811 RANGE= 0.560 WIDTH(Y)= 3.252 RESP(Y)= 0.5150 HSQC= C37
 H38A/ 1    2.750544  1*1*1  STAT=Y  PRED= 2.424 RANGE= 0.502 WIDTH(Y)= 2.939 RESP(Y)= 0.5177 HSQC= C38
 H38B/ 1    3.069465  1*1*1  STAT=Y  PRED= 2.949 RANGE= 0.302 WIDTH(Y)= 4.205 RESP(Y)= 0.7504 HSQC= C38
 H39A/ 1    1.792834  1*1*1  STAT=Y  PRED= 1.606 RANGE= 0.562 WIDTH(Y)= 3.480 RESP(Y)= 0.5436 HSQC= C39
 H39B/ 1    1.543038  1*1*1  STAT=Y  PRED= 1.689 RANGE= 0.435 WIDTH(Y)= 2.366 RESP(Y)= 0.9266 HSQC= C39

COUPLING CONSTANTS(HZ):
 J46_54     5.8322   J H1   H19    STAT=Y  PRED= 2.850 RANGE= 7.800
```

Appendix C (continued)

J48_61 8.4061 J H4 H22A STAT=Y PRED= 11.830 RANGE= 8.390
J48_62 6.6932 J H4 H22B STAT=Y PRED= 3.800 RANGE= 10.800
J50_70 1.8459 J H7 H26A STAT=Y PRED= 7.570 RANGE= 5.600
J50_71 5.4479 J H7 H26B STAT=Y PRED= 10.890 RANGE= 4.400
J51_77 7.2406 J H10 H30 STAT=Y PRED= 7.260 RANGE= 0.890
J52_83 1.7574 J H13 H32A STAT=Y PRED= 10.690 RANGE= 4.000
J52_84 6.1821 J H13 H32B STAT=Y PRED= 2.790 RANGE= 4.400
J53_91 1.7121 J H16 H37A STAT=Y PRED= 12.690 RANGE= 4.000
J53_92 6.6860 J H16 H37B STAT=Y PRED= 4.740 RANGE= 6.000
J54_55 6.8353 J H19 H20 STAT=Y PRED= 6.640 RANGE= 0.200
J54_58 6.8034 J H19 H21 STAT=Y PRED= 6.640 RANGE= 0.200
J61_62 -7.5475 J H22A H22B STAT=Y PRED= -14.720 RANGE= 1.600
J61_63 4.1758 J H22A H23 STAT=Y PRED= 7.090 RANGE= 6.400
J62_63 13.5659 J H22B H23 STAT=Y PRED= 7.290 RANGE= 6.400
J63_64 6.5427 J H23 H24 STAT=Y PRED= 6.640 RANGE= 0.200
J63_67 6.6018 J H23 H25 STAT=Y PRED= 6.640 RANGE= 0.200
J70_71 -13.7044 J H26A H26B STAT=Y PRED= -13.120 RANGE= 1.600
J70_72 1.8156 J H26A H27A STAT=Y PRED= 2.960 RANGE= 2.800
J70_73 4.7027 J H26A H27B STAT=Y PRED= 3.140 RANGE= 3.800
J70_74 3.5321 J H26A H28A STAT=Y PRED= 2.780 RANGE= 2.250
J71_72 2.8173 J H26B H27A STAT=Y PRED= 13.090 RANGE= 2.560
J71_73 5.6723 J H26B H27B STAT=Y PRED= 3.430 RANGE= 3.800
J72_73 -17.3494 J H27A H27B STAT=Y PRED= -13.130 RANGE= 1.500
J72_74 0.2176 J H27A H28A STAT=Y PRED= 3.870 RANGE= 5.690
J72_75 4.4271 J H27A H28B STAT=Y PRED= 11.910 RANGE= 3.900
J73_74 12.1464 J H27B H28A STAT=Y PRED= 2.110 RANGE= 4.500
J73_75 1.5943 J H27B H28B STAT=Y PRED= 3.660 RANGE= 5.690
J74_75 -13.3597 J H28A H28B STAT=Y PRED= -11.520 RANGE= 3.320
J83_84 -12.2227 J H32A H32B STAT=Y PRED= -13.090 RANGE= 1.600
J83_87 0.8315 J H32A H34B STAT=Y PRED= 1.630 RANGE= 1.650
J83_88 3.2357 J H32A H35A STAT=Y PRED= 0.680 RANGE= 3.000
J83_89 1.0202 J H32A H35B STAT=Y PRED= 8.090 RANGE= 3.800
J84_88 4.9475 J H32B H35A STAT=Y PRED= 8.480 RANGE= 3.800
J84_89 12.9806 J H32B H35B STAT=Y PRED= 9.220 RANGE= 3.800
J86_87 -13.5943 J H34A H34B STAT=Y PRED= -11.670 RANGE= 3.320
J86_88 3.0146 J H34A H35A STAT=Y PRED= 2.660 RANGE= 4.190
J86_89 11.8190 J H34A H35B STAT=Y PRED= 12.090 RANGE= 3.900
J87_88 1.7351 J H34B H35A STAT=Y PRED= 2.680 RANGE= 4.190
J87_89 3.1247 J H34B H35B STAT=Y PRED= 3.430 RANGE= 5.690
J88_89 -14.5760 J H35A H35B STAT=Y PRED= -13.060 RANGE= 1.500
J91_92 -13.6666 J H37A H37B STAT=Y PRED= -13.120 RANGE= 1.600
J91_95 9.8700 J H37A H39A STAT=Y PRED= 2.310 RANGE= 3.200
J91_96 16.5640 J H37A H39B STAT=Y PRED= 10.880 RANGE= 2.800
J92_95 5.0505 J H37B H39A STAT=Y PRED= 10.890 RANGE= 2.800
J92_96 5.8469 J H37B H39B STAT=Y PRED= 4.480 RANGE= 4.000
J93_94 -11.5872 J H38A H38B STAT=Y PRED= -11.610 RANGE= 3.320
J93_95 13.1099 J H38A H39A STAT=Y PRED= 4.220 RANGE= 6.000
J93_96 3.1746 J H38A H39B STAT=Y PRED= 11.460 RANGE= 4.190
J94_95 14.2728 J H38B H39A STAT=Y PRED= 1.690 RANGE= 4.500
J94_96 1.9015 J H38B H39B STAT=Y PRED= 4.980 RANGE= 5.690
J95_96 -12.0052 J H39A H39B STAT=Y PRED= -13.040 RANGE= 1.500

Appendix C (continued)

CONTROL PARAMETERS:
Solvent = none (def. 99% enriched)
1.000 = Concentration (vol%, def=1.0%)
0.00100000 = Minimum line-intensity
0.00100000 = Diagonalization criterium (not in use)
8.00703139 = Left frequency (ppm)
-0.19766268 = Right frequency (ppm)
0.000 = Acquisition time (s, for QMTLS)
1.264 = Line-width (for modes D, P & T, 0=use defaults)
0.068609924 = Data-point resolution (Hz)
22.422 = GAUSSIAN (%, 0=use default from INF)
0.048 = Dispersion contribution (%, 0=use default from INF)
0.00000000 = Decoupling frequency (for DORES)

CONSTRAINTS (in equations X0 = 1.0)...use no empty lines
EQUAL H22B = H39B
IGNORE(HZ): 2946.272 to 2911.284
IGNORE(HZ): 2058.892 to 1953.362
IGNORE(HZ): 1599.970 to 1592.718
IGNORE(HZ): 2805.321 to 2715.235
IGNORE(HZ): 738.589 to 636.820

END of FILE

Appendix D. ^{1}H NMR HiFSA profile of hytramycin I (2) in the PERCH .PMS file format (MeOH-d_4)

```
* NEW: the lines beginning by * are comment lines !
* To keep all the chemical shifts fixed during iteration
* replace "CHEMICAL SHIFTS(HZ):" by "..SHIFTS(HZ): fixed"
* The couplings can be fixed in the same way

NMR-data: C:\Users\jgnapo_2\Desktop\gcai_P1\p1
#$? Date  2. 2.2013;  Time 22:10:14     perch.5th

CHEMICAL SHIFTS(PPM):
PROTON    2*SPIN= 1 SPECIES=1H    POPULATION(Y)=   1.00000
 H1  / 1    5.401352  1*1*1  STAT=Y  PRED= 4.099 RANGE= 1.160 WIDTH(Y)= 2.057 RESP(Y)= 0.4940 HSQC= C1
 H4  / 1    4.329179  1*1*1  STAT=Y  PRED= 4.428 RANGE= 1.490 WIDTH(Y)= 2.057 RESP(Y)= 0.5212 HSQC= C4
 H7  / 1    4.938460  1*1*1  STAT=Y  PRED= 4.399 RANGE= 0.840 WIDTH(Y)= 2.057 RESP(Y)= 0.8220 HSQC= C7
 H10 / 1    5.736679  1*1*1  STAT=Y  PRED= 4.337 RANGE= 1.010 WIDTH(Y)= 2.057 RESP(Y)= 0.5819 HSQC= C10
 H13 / 1    5.309348  1*1*1  STAT=Y  PRED= 4.381 RANGE= 0.975 WIDTH(Y)= 2.057 RESP(Y)= 0.5136 HSQC= C13
 H16 / 1    5.674814  1*1*1  STAT=Y  PRED= 3.979 RANGE= 0.620 WIDTH(Y)= 2.057 RESP(Y)= 0.5267 HSQC= C16
 H19 / 1    1.996941  1*1*1  STAT=Y  PRED= 2.217 RANGE= 0.520 WIDTH(Y)= 2.057 RESP(Y)= 0.6182 HSQC= C19
 H17A/ 1    1.402181  1*1*1  STAT=Y  PRED= 2.217 RANGE= 0.520 WIDTH(Y)= 2.057 RESP(Y)= 0.6294 HSQC= C19
 H17B/ 1    1.194159  1*1*1  STAT=Y  PRED= 2.217 RANGE= 0.520 WIDTH(Y)= 2.057 RESP(Y)= 0.6359 HSQC= C19
 H20 / 1    0.966698  1*1*3  STAT=Y  PRED= 1.092 RANGE= 0.230 WIDTH(Y)= 2.057 RESP(Y)= 0.7587 HSQC= C20
 H21 / 1    0.849012  1*1*3  STAT=Y  PRED= 1.114 RANGE= 0.185 WIDTH(Y)= 2.057 RESP(Y)= 0.5542 HSQC= C21
 H22A/ 1    1.624906  1*1*1  STAT=Y  PRED= 1.927 RANGE= 0.565 WIDTH(Y)= 2.057 RESP(Y)= 0.8750 HSQC= C22
 H22B/ 1    1.531107  1*1*1  STAT=Y  PRED= 1.689 RANGE= 0.605 WIDTH(Y)= 2.057 RESP(Y)= 0.3820 HSQC= C22
 H23 / 1    1.600790  1*1*1  STAT=Y  PRED= 1.654 RANGE= 0.235 WIDTH(Y)= 2.057 RESP(Y)= 0.2730 HSQC= C23
 H24 / 1    0.922961  1*1*3  STAT=Y  PRED= 0.925 RANGE= 0.150 WIDTH(Y)= 2.057 RESP(Y)= 0.6675 HSQC= C24
 H25 / 1    0.961280  1*1*3  STAT=Y  PRED= 0.945 RANGE= 0.150 WIDTH(Y)= 2.057 RESP(Y)= 0.5021 HSQC= C25
 H26A/ 1    2.123691  1*1*1  STAT=Y  PRED= 2.069 RANGE= 0.540 WIDTH(Y)= 2.057 RESP(Y)= 0.5044 HSQC= C26
 H26B/ 1    1.824181  1*1*1  STAT=Y  PRED= 1.791 RANGE= 0.525 WIDTH(Y)= 2.057 RESP(Y)= 0.3583 HSQC= C26
 H27A/ 1    1.652248  1*1*1  STAT=Y  PRED= 1.407 RANGE= 0.675 WIDTH(Y)= 2.057 RESP(Y)= 0.8087 HSQC= C27
 H27B/ 1    1.572935  1*1*1  STAT=Y  PRED= 1.666 RANGE= 0.555 WIDTH(Y)= 2.057 RESP(Y)= 0.8942 HSQC= C27
 H28A/ 1    3.054884  1*1*1  STAT=Y  PRED= 3.162 RANGE= 0.525 WIDTH(Y)= 2.057 RESP(Y)= 0.9117 HSQC= C28
 H28B/ 1    2.733035  1*1*1  STAT=Y  PRED= 2.664 RANGE= 0.430 WIDTH(Y)= 2.057 RESP(Y)= 0.6369 HSQC= C28
 H30 / 1    1.290081  1*1*3  STAT=Y  PRED= 1.441 RANGE= 0.270 WIDTH(Y)= 2.057 RESP(Y)= 0.6061 HSQC= C30
 H31 / 1    3.006256  1*1*3  STAT=Y  PRED= 3.064 RANGE= 0.415 WIDTH(Y)= 2.057 RESP(Y)= 0.5274 HSQC= C31
 H32A/ 1    1.940424  1*1*1  STAT=Y  PRED= 2.157 RANGE= 0.535 WIDTH(Y)= 2.057 RESP(Y)= 0.4974 HSQC= C32
 H32B/ 1    1.889029  1*1*1  STAT=Y  PRED= 1.649 RANGE= 0.585 WIDTH(Y)= 2.057 RESP(Y)= 0.4296 HSQC= C32
 H34A/ 1    2.776366  1*1*1  STAT=Y  PRED= 2.651 RANGE= 0.395 WIDTH(Y)= 2.057 RESP(Y)= 0.3615 HSQC= C34
 H34B/ 1    3.111737  1*1*1  STAT=Y  PRED= 3.202 RANGE= 0.435 WIDTH(Y)= 2.057 RESP(Y)= 0.8023 HSQC= C34
 H35A/ 1    1.817693  1*1*1  STAT=Y  PRED= 1.728 RANGE= 0.570 WIDTH(Y)= 2.057 RESP(Y)= 0.6742 HSQC= C35
 H35B/ 1    1.532509  1*1*1  STAT=Y  PRED= 1.713 RANGE= 0.705 WIDTH(Y)= 2.057 RESP(Y)= 1.0000 HSQC= C35
 H37A/ 1    1.907134  1*1*1  STAT=Y  PRED= 1.893 RANGE= 0.600 WIDTH(Y)= 2.057 RESP(Y)= 0.9704 HSQC= C37
 H37B/ 1    2.046178  1*1*1  STAT=Y  PRED= 1.811 RANGE= 0.560 WIDTH(Y)= 2.057 RESP(Y)= 0.6448 HSQC= C37
 H38A/ 1    3.045500  1*1*1  STAT=Y  PRED= 2.424 RANGE= 0.500 WIDTH(Y)= 2.057 RESP(Y)= 0.3721 HSQC= C38
 H38B/ 1    2.756802  1*1*1  STAT=Y  PRED= 2.949 RANGE= 0.300 WIDTH(Y)= 2.057 RESP(Y)= 0.7434 HSQC= C38
 H39A/ 1    1.794705  1*1*1  STAT=Y  PRED= 1.606 RANGE= 0.560 WIDTH(Y)= 2.057 RESP(Y)= 0.8844 HSQC= C39
 H39B/ 1    1.553992  1*1*1  STAT=Y  PRED= 1.689 RANGE= 0.435 WIDTH(Y)= 2.057 RESP(Y)= 0.3980 HSQC= C39
```

Appendix D (continued)

COUPLING CONSTANTS(HZ):

```
J46_54     4.4681   J H1   H19    STAT=Y  PRED= 2.850 RANGE= 7.800
J48_61     6.6488   J H4   H22A   STAT=Y  PRED= 11.830 RANGE= 8.390
J48_62     8.5233   J H4   H22B   STAT=Y  PRED= 3.800 RANGE= 10.800
J50_70     2.5597   J H7   H26A   STAT=Y  PRED= 7.570 RANGE= 5.600
J50_71     5.7939   J H7   H26B   STAT=Y  PRED= 10.890 RANGE= 4.400
J51_77     7.0729   J H10  H30    STAT=Y  PRED= 7.260 RANGE= 0.890
J52_83     1.7734   J H13  H32A   STAT=Y  PRED= 10.690 RANGE= 4.000
J52_84     5.8405   J H13  H32B   STAT=Y  PRED= 2.790 RANGE= 4.400
J53_91     6.9815   J H16  H37A   STAT=Y  PRED= 12.690 RANGE= 4.000
J53_92     2.4934   J H16  H37B   STAT=Y  PRED= 4.740 RANGE= 6.000
J1         6.1049   J H19  H17A   STAT=Y  PRED= 6.640 RANGE= 0.200
J2         8.2962   J H19  H17B   STAT=Y  PRED= 6.640 RANGE= 0.200
J54_58     6.9336   J H19  H21    STAT=Y  PRED= 6.640 RANGE= 0.200
J3       -14.0169   J H17A H17B   STAT=Y  PRED= 6.640 RANGE= 0.200
J4         7.4078   J H17A H20    STAT=Y  PRED= 6.640 RANGE= 0.200
J5         7.3592   J H17B H20    STAT=Y  PRED= 6.640 RANGE= 0.200
J61_62   -12.1285   J H22A H22B   STAT=Y  PRED= -14.720 RANGE= 1.600
J61_63     5.4626   J H22A H23    STAT=Y  PRED= 7.090 RANGE= 6.400
J62_63     4.2073   J H22B H23    STAT=Y  PRED= 7.290 RANGE= 6.400
J63_64     6.4743   J H23  H24    STAT=Y  PRED= 6.640 RANGE= 0.200
J63_67     6.5091   J H23  H25    STAT=Y  PRED= 6.640 RANGE= 0.200
J70_71   -11.5234   J H26A H26B   STAT=Y  PRED= -13.120 RANGE= 1.600
J70_72     4.7669   J H26A H27A   STAT=Y  PRED= 3.560 RANGE= 4.000
J70_73     0.9399   J H26A H27B   STAT=Y  PRED= 2.740 RANGE= 3.000
J70_74     2.7717   J H26A H28A   STAT=Y  PRED= 2.650 RANGE= 2.250
J71_72    12.0329   J H26B H27A   STAT=Y  PRED= 12.730 RANGE= 2.800
J71_73     1.7447   J H26B H27B   STAT=Y  PRED= 4.040 RANGE= 4.000
J72_73   -14.2164   J H27A H27B   STAT=Y  PRED= -13.120 RANGE= 1.500
J72_74     6.1086   J H27A H28A   STAT=Y  PRED= 3.940 RANGE= 5.690
J72_75    13.6586   J H27A H28B   STAT=Y  PRED= 11.850 RANGE= 4.190
J73_74     4.3027   J H27B H28A   STAT=Y  PRED= 2.120 RANGE= 4.500
J73_75     3.0122   J H27B H28B   STAT=Y  PRED= 3.670 RANGE= 6.000
J74_75   -14.2827   J H28A H28B   STAT=Y  PRED= -11.520 RANGE= 3.320
J83_84   -13.1205   J H32A H32B   STAT=Y  PRED= -13.090 RANGE= 1.600
J83_87     1.4366   J H32A H34B   STAT=Y  PRED= 2.180 RANGE= 1.950
J83_88     2.1153   J H32A H35A   STAT=Y  PRED= 1.590 RANGE= 3.200
J83_89     3.9072   J H32A H35B   STAT=Y  PRED= 5.910 RANGE= 4.000
J84_88     6.6315   J H32B H35A   STAT=Y  PRED= 6.420 RANGE= 4.000
J84_89    10.0593   J H32B H35B   STAT=Y  PRED= 11.000 RANGE= 3.000
J86_87   -11.6894   J H34A H34B   STAT=Y  PRED= -11.580 RANGE= 3.320
J86_88     3.3415   J H34A H35A   STAT=Y  PRED= 2.840 RANGE= 4.190
J86_89    10.4294   J H34A H35B   STAT=Y  PRED= 12.090 RANGE= 3.900
J87_88     4.6973   J H34B H35A   STAT=Y  PRED= 2.630 RANGE= 4.190
J87_89     2.4655   J H34B H35B   STAT=Y  PRED= 3.340 RANGE= 5.690
J88_89   -11.1615   J H35A H35B   STAT=Y  PRED= -13.090 RANGE= 1.500
J91_92   -13.7170   J H37A H37B   STAT=Y  PRED= -13.150 RANGE= 1.600
J91_95    14.8245   J H37A H39A   STAT=Y  PRED= 12.820 RANGE= 2.800
J91_96     4.2983   J H37A H39B   STAT=Y  PRED= 3.830 RANGE= 3.800
J92_93     1.3476   J H37B H38A   STAT=Y  PRED= 2.100 RANGE= 1.790
J92_95     5.7823   J H37B H39A   STAT=Y  PRED= 3.680 RANGE= 4.000
J92_96     2.5923   J H37B H39B   STAT=Y  PRED= 2.730 RANGE= 3.000
```

Appendix D (continued)

```
 J93_94   -15.4223   J H38A H38B   STAT=Y  PRED= -11.470 RANGE= 3.320
 J93_95     2.7112   J H38A H39A   STAT=Y  PRED= 5.190 RANGE= 6.000
 J93_96     1.7274   J H38A H39B   STAT=Y  PRED= 1.750 RANGE= 4.800
 J94_95    13.0015   J H38B H39A   STAT=Y  PRED= 10.780 RANGE= 4.500
 J94_96     3.6263   J H38B H39B   STAT=Y  PRED= 5.070 RANGE= 6.000
 J95_96   -14.1390   J H39A H39B   STAT=Y  PRED= -13.110 RANGE= 1.500

CONTROL PARAMETERS:
      Solvent =  none (def. 99% enriched)
        1.000 =  Concentration (vol%, def=1.0%)
   0.00100000 =  Minimum line-intensity
   0.00100000 =  Diagonalization criterium (not in use)
   8.00703139 =  Left frequency (ppm)
  -0.19766267 =  Right frequency (ppm)
        0.000 =  Acquisition time (s, for QMTLS)
        2.057 =  Line-width (for modes D, P & T, 0=use defaults)
  0.030566717 =  Data-point resolution (Hz)
     -101.595 =  GAUSSIAN (%, 0=use default from INF)
       17.541 =  Dispersion contribution (%, 0=use default from INF)
   0.00000000 =  Decoupling frequency (for DORES)

CONSTRAINTS (in equations X0 = 1.0)...use no empty lines
 EQUAL H22B     = H39B
 IGNORE(HZ):  2946.272 to  2911.284
 IGNORE(HZ):  2805.321 to  2715.235
 IGNORE(HZ):  1404.419 to  1282.755
 IGNORE(HZ):  1877.337 to  1790.995
 IGNORE(HZ):  1068.017 to  1057.968
 IGNORE(HZ):   362.173 to   348.045
 IGNORE(HZ):   422.905 to   398.741
 IGNORE(HZ):   541.686 to   524.499
 IGNORE(HZ):  1970.707 to  1922.823

END of FILE
```

Appendix E. ^{1}H NMR HiFSA profile of xylamycin (3) in the PERCH .PMS file format (MeOH-d_4)

* NEW: the lines beginning by * are comment lines !
* To keep all the chemical shifts fixed during iteration
* replace "CHEMICAL SHIFTS(HZ):" by "..SHIFTS(HZ): fixed"
* The couplings can be fixed in the same way

NMR-data: E:\Test\Perch\perch
#$œ Date 31.12.2013; Time 16:54:34   perch.pms

CHEMICAL SHIFTS(PPM):
PROTON 2*SPIN= 1 SPECIES=1H POPULATION(Y)= 1.00000
H1 / 1 5.772000 1*1*1 STAT=Y PRED= 6.429 RANGE= 0.307 WIDTH(Y)= 2.432 RESP(Y)= 0.1076 HSQC= C1
H3A / 1 2.850851 1*1*1 STAT=Y PRED= 3.079 RANGE= 0.439 WIDTH(Y)= 1.899 RESP(Y)= 0.0969 HSQC= C3
H3B / 1 2.399019 1*1*1 STAT=Y PRED= 2.328 RANGE= 0.429 WIDTH(Y)= 2.324 RESP(Y)= 0.0972 HSQC= C3
H4 / 1 4.177919 1*1*1 STAT=Y PRED= 5.342 RANGE= 0.787 WIDTH(Y)= 1.301 RESP(Y)= 0.0938 HSQC= C4
H7 / 1 1.765887 1*1*3 STAT=Y PRED= 1.867 RANGE= 0.238 WIDTH(Y)= 1.664 RESP(Y)= 0.1089 HSQC= C2B
H9 / 1 5.251617 1*1*1 STAT=Y PRED= 4.369 RANGE= 0.769 WIDTH(Y)= 1.726 RESP(Y)= 0.1105 HSQC= C8
H11A/ 1 1.937574 1*1*1 STAT=Y PRED= 2.543 RANGE= 0.459 WIDTH(Y)= 1.521 RESP(Y)= 0.0890 HSQC= C10
H11B/ 1 1.759994 1*1*1 STAT=Y PRED= 2.166 RANGE= 0.408 WIDTH(Y)= 2.329 RESP(Y)= 0.3374 HSQC= C10
H12 / 1 1.514261 1*1*1 STAT=Y PRED= 1.723 RANGE= 0.369 WIDTH(Y)= 2.267 RESP(Y)= 0.1067 HSQC= C11A
H13 / 1 0.903494 1*1*3 STAT=Y PRED= 0.942 RANGE= 0.149 WIDTH(Y)= 1.577 RESP(Y)= 0.1109 HSQC= C11BA
H14 / 1 0.974353 1*1*3 STAT=Y PRED= 0.843 RANGE= 0.229 WIDTH(Y)= 1.701 RESP(Y)= 0.1299 HSQC= C11BB
H16 / 1 4.614962 1*1*1 STAT=Y PRED= 4.369 RANGE= 1.039 WIDTH(Y)= 0.733 RESP(Y)= 0.0493 HSQC= C13
H17 / 1 3.299898 1*1*3 STAT=Y PRED= 3.142 RANGE= 0.398 WIDTH(Y)= 1.431 RESP(Y)= 0.1011 HSQC= C7
H20A/ 1 2.624115 1*1*1 STAT=Y PRED= 3.181 RANGE= 0.309 WIDTH(Y)= 3.269 RESP(Y)= 0.1851 HSQC= C16
H20B/ 1 2.590933 1*1*1 STAT=Y PRED= 3.289 RANGE= 0.309 WIDTH(Y)= 1.688 RESP(Y)= 0.0189 HSQC= C16
H21 / 1 5.438222 1*1*1 STAT=Y PRED= 5.358 RANGE= 0.659 WIDTH(Y)= 2.966 RESP(Y)= 0.1131 HSQC= C17
H22 / 1 5.588930 1*1*1 STAT=Y PRED= 5.352 RANGE= 0.389 WIDTH(Y)= 2.190 RESP(Y)= 0.1176 HSQC= C18A
H23 / 1 1.676625 1*1*3 STAT=Y PRED= 1.693 RANGE= 0.149 WIDTH(Y)= 2.237 RESP(Y)= 0.1191 HSQC= C18B
H25 / 1 4.825010 1*1*1 STAT=Y PRED= 4.660 RANGE= 1.519 WIDTH(Y)= 4.223 RESP(Y)= 0.3145 HSQC= C20
H28A/ 1 3.188228 1*1*1 STAT=Y PRED= 2.969 RANGE= 0.507 WIDTH(Y)= 2.538 RESP(Y)= 0.5318 HSQC= C23
H28B/ 1 3.168661 1*1*1 STAT=Y PRED= 2.969 RANGE= 0.447 WIDTH(Y)= 2.817 RESP(Y)= 1.0000 HSQC= C23
H33 / 1 7.094297 1*1*1 STAT=Y PRED= 6.627 RANGE= 0.149 WIDTH(Y)= 1.986 RESP(Y)= 0.1242 HSQC= C28
H34 / 1 7.557638 1*1*1 STAT=Y PRED= 7.860 RANGE= 0.319 WIDTH(Y)= 1.164 RESP(Y)= 0.1081 HSQC= C29
H35 / 1 7.064148 1*1*1 STAT=Y PRED= 7.061 RANGE= 0.238 WIDTH(Y)= 0.983 RESP(Y)= 0.0882 HSQC= C30
H36 / 1 7.137938 1*1*1 STAT=Y PRED= 7.106 RANGE= 0.339 WIDTH(Y)= 1.677 RESP(Y)= 0.1367 HSQC= C31
H37 / 1 7.655160 1*1*1 STAT=Y PRED= 7.233 RANGE= 0.219 WIDTH(Y)= 1.385 RESP(Y)= 0.1171 HSQC= C32
H39 / 1 1.650088 1*1*3 STAT=Y PRED= 1.649 RANGE= 0.629 WIDTH(Y)= 2.749 RESP(Y)= 0.1254 HSQC= C33BA
H40 / 1 4.481902 1*1*1 STAT=Y PRED= 5.006 RANGE= 0.379 WIDTH(Y)= 1.645 RESP(Y)= 0.1061 HSQC= C34
H41A/ 1 3.292845 1*1*1 STAT=Y PRED= 3.808 RANGE= 0.546 WIDTH(Y)= 1.825 RESP(Y)= 0.1927 HSQC= C35
H41B/ 1 2.922900 1*1*1 STAT=Y PRED= 4.174 RANGE= 0.439 WIDTH(Y)= 1.822 RESP(Y)= 0.0008 HSQC= C35
H43 / 1 1.759715 1*1*3 STAT=Y PRED= 1.788 RANGE= 0.669 WIDTH(Y)= 3.046 RESP(Y)= 0.0900 HSQC= C33BB
H44 / 1 2.360767 1*1*3 STAT=Y PRED= 2.664 RANGE= 1.019 WIDTH(Y)= 5.915 RESP(Y)= 0.0984 HSQC= C22
H45 / 1 4.326838 1*1*1 STAT=Y PRED= 5.302 RANGE= 1.516 WIDTH(Y)= 2.807 RESP(Y)= 0.0736 HSQC= C36
H47A/ 1 -0.407540 1*1*1 STAT=Y PRED= 1.503 RANGE= 0.509 WIDTH(Y)= 2.867 RESP(Y)= 0.0926 HSQC= C38
H47B/ 1 1.543590 1*1*1 STAT=Y PRED= 1.747 RANGE= 0.638 WIDTH(Y)= 2.100 RESP(Y)= 0.1105 HSQC= C38
H48 / 1 0.950136 1*1*1 STAT=Y PRED= 1.762 RANGE= 0.619 WIDTH(Y)= 3.138 RESP(Y)= 0.1170 HSQC= C39A
H49 / 1 0.079049 1*1*3 STAT=Y PRED= 0.942 RANGE= 0.149 WIDTH(Y)= 5.359 RESP(Y)= 0.0972 HSQC= C39BA
H50 / 1 0.441425 1*1*3 STAT=Y PRED= 1.153 RANGE= 0.229 WIDTH(Y)= 1.660 RESP(Y)= 0.1036 HSQC= C39BB
H52 / 1 4.616655 1*1*1 STAT=Y PRED= 4.499 RANGE= 0.989 WIDTH(Y)= 1.600 RESP(Y)= 0.0492 HSQC= C41

Appendix E (continued)

H54A/ 1 3.105780 1*1*1 STAT=Y PRED= 2.814 RANGE= 0.469 WIDTH(Y)= 3.373 RESP(Y)= 0.1093 HSQC= C43
H54B/ 1 2.916402 1*1*1 STAT=Y PRED= 3.099 RANGE= 0.339 WIDTH(Y)= 3.029 RESP(Y)= 0.2040 HSQC= C43
H56 / 1 7.786637 1*1*1 STAT=Y PRED= 7.213 RANGE= 0.239 WIDTH(Y)= 1.588 RESP(Y)= 0.1151 HSQC= C45
H59 / 1 7.069303 1*1*1 STAT=Y PRED= 6.983 RANGE= 0.536 WIDTH(Y)= 1.357 RESP(Y)= 0.1344 HSQC= C48
H60 / 1 7.390832 1*1*1 STAT=Y PRED= 7.405 RANGE= 0.419 WIDTH(Y)= 1.429 RESP(Y)= 0.1081 HSQC= C49
H62 / 1 4.855253 1*1*1 STAT=Y PRED= 4.815 RANGE= 0.989 WIDTH(Y)= 3.934 RESP(Y)= 0.4159 HSQC= C50A
H64 / 1 1.269485 1*1*3 STAT=Y PRED= 1.418 RANGE= 0.347 WIDTH(Y)= 2.175 RESP(Y)= 0.1045 HSQC= C50B

COUPLING CONSTANTS(HZ):
J76_77 1.3526 J H1 H3A STAT=Y PRED= -2.990 RANGE= 1.600
J47 2.0878 J H1 H3B STAT=Y
J76_80 0.0000 J H1 H7 STAT=N PRED= -1.650 RANGE= 1.000
J77_78 18.4337 J H3A H3B STAT=Y PRED= -15.320 RANGE= 2.560
J77_79 11.3655 J H3A H4 STAT=Y PRED= 12.430 RANGE= 4.000
J77_80 0.4486 J H3A H7 STAT=Y PRED= -0.800 RANGE= 1.000
J78_79 7.5281 J H3B H4 STAT=Y PRED= 6.780 RANGE= 5.190
J78_80 0.3772 J H3B H7 STAT=Y PRED= -0.800 RANGE= 1.000
J83_84 4.3124 J H9 H11A STAT=Y PRED= 14.260 RANGE= 4.000
J83_85 11.9733 J H9 H11B STAT=Y PRED= 2.830 RANGE= 4.000
J84_85 14.1978 J H11A H11B STAT=Y PRED= -14.550 RANGE= 1.600
J84_86 10.6140 J H11A H12 STAT=Y PRED= 9.730 RANGE= 3.400
J85_86 0.7509 J H11B H12 STAT=Y PRED= 7.730 RANGE= 3.400
J49 0.0000 J H11B H13 STAT=N
J86_87 6.5672 J H12 H13 STAT=Y PRED= 6.640 RANGE= 0.200
J86_90 6.6868 J H12 H14 STAT=Y PRED= 6.640 RANGE= 0.200
J94_98 9.7112 J H16 H20A STAT=Y PRED= 13.380 RANGE= 6.000
J94_99 5.0126 J H16 H20B STAT=Y PRED= 1.900 RANGE= 6.000
J98_99 14.2576 J H20A H20B STAT=Y PRED= -16.700 RANGE= 2.400
J98_100 7.3536 J H20A H21 STAT=Y PRED= 7.260 RANGE= 4.000
J48 0.6444 J H20A H22 STAT=Y
J98_102 0.0000 J H20A H23 STAT=N PRED= 0.650 RANGE= 0.850
J99_100 6.4149 J H20B H21 STAT=Y PRED= 9.510 RANGE= 4.000
J99_101 0.8847 J H20B H22 STAT=Y PRED= -1.110 RANGE= 1.280
J99_102 0.0000 J H20B H23 STAT=N PRED= 0.650 RANGE= 0.850
J100_101 15.1846 J H21 H22 STAT=Y PRED= 17.200 RANGE= 2.000
J100_102 1.5062 J H21 H23 STAT=Y PRED= -1.650 RANGE= 1.000
J101_102 6.4492 J H22 H23 STAT=Y PRED= 6.600 RANGE= 1.000
J106_107 10.1000 J H25 H28A STAT=Y PRED= 1.780 RANGE= 6.000
J106_108 6.2000 J H25 H28B STAT=Y PRED= 13.540 RANGE= 6.000
J107_108 15.9674 J H28A H28B STAT=Y PRED= -16.750 RANGE= 2.560
J109_110 0.0000 J H33 H34 STAT=N PRED= -0.300 RANGE= 0.500
J109_113 0.0000 J H33 H37 STAT=N PRED= -0.300 RANGE= 0.500
J110_111 7.9123 J H34 H35 STAT=Y PRED= 7.460 RANGE= 0.460
J110_112 1.2170 J H34 H36 STAT=Y PRED= 1.370 RANGE= 1.400
J110_113 0.6735 J H34 H37 STAT=Y PRED= 0.530 RANGE= 0.750
J111_112 6.9141 J H35 H36 STAT=Y PRED= 7.110 RANGE= 0.320
J111_113 0.7014 J H35 H37 STAT=Y PRED= 1.310 RANGE= 1.400
J112_113 8.4791 J H36 H37 STAT=Y PRED= 8.290 RANGE= 0.800
J117_118 2.1761 J H40 H41A STAT=Y PRED= 1.570 RANGE= 4.000
J117_119 9.7130 J H40 H41B STAT=Y PRED= 10.710 RANGE= 4.000
J118_119 9.5795 J H41A H41B STAT=Y PRED= -15.350 RANGE= 2.200
J127_128 3.9856 J H45 H47A STAT=Y PRED= 4.800 RANGE= 5.190

Appendix E (continued)

```
 J127_129   10.7247   J H45  H47B   STAT=Y  PRED= 13.900 RANGE= 4.000
 J128_129   13.0542   J H47A H47B   STAT=Y  PRED= -14.730 RANGE= 1.600
 J128_130    8.6330   J H47A H48    STAT=Y  PRED= 13.140 RANGE= 2.560
 J129_130    4.9927   J H47B H48    STAT=Y  PRED= 3.470 RANGE= 3.400
 J130_131    6.6037   J H48  H49    STAT=Y  PRED= 6.640 RANGE= 0.200
 J130_134    6.6634   J H48  H50    STAT=Y  PRED= 6.640 RANGE= 0.200
 J138_139    5.8201   J H52  H54A   STAT=Y  PRED= 1.730 RANGE= 6.000
 J138_140   10.7702   J H52  H54B   STAT=Y  PRED= 12.980 RANGE= 6.000
 J139_140   13.2508   J H54A H54B   STAT=Y  PRED= -16.900 RANGE= 2.560
 J140_141    0.0000   J H54B H56    STAT=N  PRED= -0.750 RANGE= 0.400
 J140_143    0.0000   J H54B H60    STAT=N  PRED= -0.750 RANGE= 0.400
 J141_142    0.0000   J H56  H59    STAT=N  PRED= 0.430 RANGE= 0.640
 J141_143    2.2184   J H56  H60    STAT=Y  PRED= 2.030 RANGE= 1.600
 J142_143    8.5370   J H59  H60    STAT=Y  PRED= 8.090 RANGE= 0.890
 J145_147    6.6511   J H62  H64    STAT=Y  PRED= 7.260 RANGE= 1.350

CONTROL PARAMETERS:
      Solvent =  none (def. 99% enriched)
        1.000 =  Concentration (vol%, def=1.0%)
   0.00100000 =  Minimum line-intensity
   0.00100000 =  Diagonalization criterium (not in use)
  19.93156550 =  Left frequency (ppm)
 -10.18199279 =  Right frequency (ppm)
        0.000 =  Acquisition time (s, for QMTLS)
        0.733 =  Line-width (for modes D, P & T, 0=use defaults)
  0.103379726 =  Data-point resolution (Hz)
       12.706 =  GAUSSIAN (%, 0=use default from INF)
       -8.874 =  Dispersion contribution (%, 0=use default from INF)
   0.00000000 =  Decoupling frequency (for DORES)

CONSTRAINTS (in equations X0 = 1.0)...use no empty lines
 EQUAL H9      = H16
 EQUAL H13     = H49
 EQUAL H28A    = H28B
 EQUAL H20A    = H20B
 EQUAL H11B    = H43
 IGNORE(HZ):  4417.583 to  4388.524
 IGNORE(HZ):  7766.144 to  7063.933
 IGNORE(HZ):  5556.027 to  5245.576
 IGNORE(HZ):  4636.878 to  4461.150
 IGNORE(HZ):  1081.757 to   928.558
 IGNORE(HZ):  2095.575 to  1919.847
 IGNORE(HZ):  2523.632 to  2397.468
 IGNORE(HZ):  6956.134 to  6900.947
 IGNORE(HZ):  6843.753 to  6812.648
 IGNORE(HZ):  6412.459 to  6389.047
 IGNORE(HZ):  6344.897 to  6318.809
 IGNORE(HZ):  2676.074 to  2650.394
 IGNORE(HZ):  2283.647 to  2240.312
 IGNORE(HZ):  1821.603 to  1807.961
 IGNORE(HZ):  1712.462 to  1616.964
 IGNORE(HZ):   783.158 to   418.819
```

Appendix E (continued)

IGNORE(HZ): 384.713 to 228.224
IGNORE(HZ): 1837.859 to 1832.475
IGNORE(HZ): 3969.434 to 3945.171
IGNORE(HZ): 4158.688 to 4147.770
IGNORE(HZ): 4186.555 to 4149.834
IGNORE(HZ): 1479.808 to 1470.853
IGNORE(HZ): 1325.507 to 1153.985
IGNORE(HZ): 1129.703 to 887.919
IGNORE(HZ): 3868.635 to 3786.911
IGNORE(HZ): 3737.667 to 3000.050
IGNORE(HZ): 2986.045 to 2975.966
IGNORE(HZ): 4197.288 to 4131.030
IGNORE(HZ): 2987.864 to 2974.147
IGNORE(HZ): 4434.509 to 4385.305
IGNORE(HZ): 1575.732 to 1522.291
IGNORE(HZ): 2903.405 to 2880.973
IGNORE(HZ): 3005.077 to 2973.347
IGNORE(HZ): 2926.928 to 2899.018
IGNORE(HZ): 2952.627 to 2940.525
IGNORE(HZ): 2766.834 to 2649.013
IGNORE(HZ): 2097.612 to 1879.251
IGNORE(HZ): 2099.265 to 1766.130
IGNORE(HZ): 4711.380 to 4464.346
IGNORE(HZ): 2314.538 to 2179.851
IGNORE(HZ): 1456.931 to 1409.498
IGNORE(HZ): 860.712 to 844.341
IGNORE(HZ): -497.270 to -541.975

END of FILE

Appendix F. Details of the culture media

G.S.S. medium (rich medium)

Soluble starch	10 g
Glucose	20 g
Soybean meal	20 g
Beef extract	1 g
Yeast extract	4 g
NaCl	2 g
K_2HPO_4	0.25 g
$CaCO_3$	2 g
D.W.	1 L
pH 7.2	

Bennett's medium (general actinomycetes medium)

Glucose	10 g
Yeast extract	1 g
Bacto-peptone	2 g
Beef extract	1 g
D.W.	1 L

DYC medium (minimal medium)

Dextrin	25 g
Dry yeast	12 g
CSL	20 g
NaBr	1 g
$CoCl_2$	1 g
D.W.	1 L
pH 7.0	

Appendix G. License agreement of publications

ELSEVIER LICENSE
TERMS AND CONDITIONS

Oct 19, 2013

This is a License Agreement between Geping Cai ("You") and Elsevier ("Elsevier") provided by Copyright Clearance Center ("CCC"). The license consists of your order details, the terms and conditions provided by Elsevier, and the payment terms and conditions.

All payments must be made in full to CCC. For payment instructions, please see information listed at the bottom of this form.

Supplier	Elsevier Limited The Boulevard,Langford Lane Kidlington,Oxford,OX5 1GB,UK
Registered Company Number	1982084
Customer name	Geping Cai
Customer address	833 S Wood St CHICAGO, IL 60612
License number	3252581035773
License date	Oct 19, 2013
Licensed content publisher	Elsevier
Licensed content publication	Tuberculosis
Licensed content title	Rapid determination of growth inhibition of *Mycobacterium tuberculosis* by GC–MS/MS quantitation of tuberculostearic acid
Licensed content author	Geping Cai, Guido F. Pauli, Yuehong Wang, Birgit U. Jaki, Scott G. Franzblau
Licensed content date	May 2013
Licensed content volume number	93
Licensed content issue number	3
Number of pages	8
Start Page	322
End Page	329

Appendix G (continued)

Type of Use	reuse in a thesis/dissertation
Portion	full article
Format	both print and electronic
Are you the author of this Elsevier article?	Yes
Will you be translating?	No
Order reference number	
Title of your thesis/dissertation	CLOSING THE GAP BETWEEN IN VITRO AND IN VIVO PARAMETERS FOR TB DRUG DISCOVERY
Expected completion date	Dec 2013
Estimated size (number of pages)	230
Elsevier VAT number	GB 494 6272 12
Permissions price	0.00 USD
VAT/Local Sales Tax	0.0 USD / 0.0 GBP
Total	0.00 USD
Terms and Conditions	

Appendix G (continued)

Copyright Clearance Center RightsLink®

Home | Account Info | Help

ACS Publications High quality. High impact.

Title: Hytramycins V and I, Anti-Mycobacterium tuberculosis Hexapeptides from a Streptomyces hygroscopicus Strain

Author: Geping Cai, José G. Napolitano, James B. McAlpine, Yuehong Wang, Birgit U. Jaki, Joo-Won Suh, Seung Hwan Yang, In-Ae Lee, Scott G. Franzblau, Guido F. Pauli, and Sanghyun Cho

Publication: Journal of Natural Products

Publisher: American Chemical Society

Date: Nov 1, 2013

Copyright © 2013, American Chemical Society

Logged in as:
Geping Cai
Account #:
3000709321

LOGOUT

PERMISSION/LICENSE IS GRANTED FOR YOUR ORDER AT NO CHARGE

This type of permission/license, instead of the standard Terms & Conditions, is sent to you because no fee is being charged for your order. Please note the following:

- Permission is granted for your request in both print and electronic formats, and translations.
- If figures and/or tables were requested, they may be adapted or used in part.
- Please print this page for your records and send a copy of it to your publisher/graduate school.
- Appropriate credit for the requested material should be given as follows: "Reprinted (adapted) with permission from (COMPLETE REFERENCE CITATION). Copyright (YEAR) American Chemical Society." Insert appropriate information in place of the capitalized words.
- One-time permission is granted only for the use specified in your request. No additional uses are granted (such as derivative works or other editions). For any other uses, please submit a new request.

BACK | CLOSE WINDOW

Copyright © 2013 Copyright Clearance Center, Inc. All Rights Reserved. Privacy statement.
Comments? We would like to hear from you. E-mail us at customercare@copyright.com

VITA

NAME:	Geping Cai
EDUCATION:	Ph.D. Pharmacognosy, University of Illinois at Chicago, Chicago, IL, 2013 M.S. Pharmacognosy, Fudan University, Shanghai, China, 2008 B.S. Pharmacology, Fudan University, Shanghai, China, 2005
TEACHING EXPERIENCE:	Teaching assistant, College of Pharmacy, University of Illinois at Chicago PHAR 406 Principles of Drug Action and Therapeutics VI, Fall 2008 PHAR 408 Principles of Drug Action and Therapeutics VIII, Spring 2009 PHAR 401 Principles of Drug Action and Therapeutics I, Fall 2009 PHAR 404 Principles of Drug Action and Therapeutics IV, Spring 2010 PHAR 401 Principles of Drug Action and Therapeutics I, Fall 2010 PHAR 404 Principles of Drug Action and Therapeutics IV, Spring 2011 Teaching assistant, School of Life Sciences, Fudan University General Biology Experiments, Spring 2007
RESEARCH EXPERIENCE:	Research assistant, University of Illinois at Chicago, 2009-2013 Research assistant, Fudan University, 2006-2008
INTERNSHIP:	Gilead Sciences Inc., Foster City, CA, 2013.06-2013.08
HONORS:	Myron Goldsmith Scholarship, University of Illinois at Chicago, 2013 W.E. van Doren Scholarship, University of Illinois at Chicago, 2012 People's Scholarship, Fudan University, 2004 & 2005
PROFESSIONAL MEMBERSHIPS:	American Society for Mass Spectrometry (ASMS) American Society of Pharmacognosy (ASP) American Association of Pharmaceutical Scientists (AAPS)
PUBLICATIONS:	· Geping Cai, Guido F. Pauli, Yuehong Wang, Birgit U. Jaki, and Scott G. Franzblau. Rapid Determination of Growth Inhibition of *Mycobacterium tuberculosis* by GC-MS/MS Quantitation of Tuberculostearic Acid. *Tuberculosis* (Edinburgh). **2013**. 93 (3): 322-329. [permission: Appendix F] · Geping Cai, José G. Napolitano, James B. McAlpine, Sanghyun Cho, Yuehong Wang, Birgit U. Jaki, Joo-Won Suh, Seung Hwan Yang, In-Ae Lee, Guido F. Pauli, Scott G. Franzblau. Hytramycin-V and -I, Novel Anti-tuberculosis Hexapeptides from a *Streptomyces hygroscopicus* strain.

Journal of Natural Products. **2013**. 76 (11): 2009-2018. [permission: Appendix F]

· Geping Cai, Yuehong Wang, Sanghyun Cho, Guido F. Pauli, Scott G. Franzblau. Fast *Mycobacterium tuberculosis* quantitation for *in vivo* anti-*M. tb* drug screening using real-time PCR method. (in preparation)

· Feng Qiu, Geping Cai, Birgit U. Jaki, David C. Lankin, Scott G. Franzblau, Guido F. Pauli. Quantitative Purity–Activity Relationships of Natural Products: The Case of Anti-*M. tb* Active Triterpenes from *Oplopanax horridus*. *Journal of Natural Products*. **2013**. 76 (3): 413-419.

· Shi-hui Dong, Geping Cai, José G. Napolitano, Dejan Nikolić, David C. Lankin, James B. McAlpine, Richard B. van Breemen, Djaja D. Soejarto, Guido F. Pauli, Shao-Nong Chen. Lipidated Steroid Saponins from *Dioscorea villosa* (wild yam). *Fitoterapia*. **2013**. 91: 113-124.

· Cai Geping, Guo Yanhong, Yao Hui, Chen Shilin, Zhou Tongshui. Impacts of cycocel and gibberellin on the biomass and flavonoid production in *Scutellaria baicalensis* Georgi. *Chinese Agricultural Science Bulletin*. **2008**. 24 (07): 213-217.

PRESENTATIONS:

· Geping Cai, José G. Napolitano, James B. McAlpine, Sanghyun Cho, Yuehong Wang, Brian T. Murphy, Birgit U. Jaki, Joo-Won. Suh, Seung Hwan. Yang, In-Ae Lee, Guido F. Pauli, Scott G. Franzblau. Isolation of Novel Anti-*M. tb* Cyclopeptides from Actinomycetes. International Congress on Natural Products Research (ICNPR). New York City, NY, Jul 2012;
2012 American Association of Pharmaceutical Scientists (AAPS) Annual Meeting and Exposition. Chicago, IL, Oct 2012 (Encore poster)

· Geping Cai, Guido F. Pauli, Yuehong Wang, Baojie Wan, Marcelle Hon, Birgit U. Jaki, Scott G. Franzblau. Rapid Determination of Growth Inhibition of *Mycobacterium tuberculosis* in Mice by GC-MS/MS Quantitation of Tuberculostearic Acid. 49th Annual Departmental MIKI Meeting, Lawrence, KS, Apr 2011;
The 111th General Meeting of American Society of Microbiology (ASM), New Orleans, LA, May 2011

· Geping Cai, Birgit U. Jaki, Guido F. Pauli and Scott G. Franzblau. Lipid Biomarker for the Profiling of Anti-tuberculosis Drug Leads. The 51st ASP (The American Society of Pharmacognosy) Conference, St. Petersburg Beach, FL, Jul 2010

· Geping Cai, Guido F. Pauli and Scott G. Franzblau. GC-MS/MS Measurement of Tuberculostearic Acid (TBSA) for Rapid Quantitation of *Mycobacterium Tuberculosis* in Experimental Infections. The 58th ASMS Conference on Mass Spectrometry and Allied Topics, Salt Lake City, UT, May 2010

· Chang-Hwa Hwang, James B. McAlpine, Geping Cai, Sang-Hyun Cho, Mary Choules, Wei Gao, David C. Lankin, José G. Napolitano, Joo-Won Suh, Seung Hwan Yang, Jinhua Cheng, Jinyong Kim, Guido F. Pauli, Scott G. Franzblau, and Birgit U. Jaki. Bioautography for Rapid Detection, Isolation, and Identification of Anti-tuberculosis Leads. The 54th ASP Conference, St. Louis, MO, July 2013

· Birgit U. Jaki, René F. Ramos Alvarenga, Geping Cai, Marcelle Hon, David C. Lankin, Baojie Wan, Yuehong Wang, Guido F. Pauli, and Scott G. Franzblau. Essential Oils for Extensively Drug Resistant Tuberculosis (XDR-TB). The 50th ASP Conference, Honolulu, HI, June 2009